

A STUDY OF RESIDUAL SHEAR STRENGTH OF NAMURIAN
SHALE IN RESPECT OF SLOPES IN NORTH DERBYSHIRE.

THANOON H. AL-DABBAGH

Thesis submitted in fulfilment of the requirements for the
Degree of PH.D.

Department of Geology
University of Sheffield

June 1985

WAS 1916
1916
1916

TO MY PARENTS...WITH LOVE

SUMMARY

This study deals with the classification and stability of number of landslips in North Derbyshire. The engineering properties of materials controlling stability are investigated with particular reference to residual shear strength. The topography of the study area comprises a series of valleys eroded into Carboniferous (Namurian) sandstones and shales. Landslippage occurs on valley sides where thick units of sandstone overlie comparatively weaker shale.

Geomorphological studies using aerial photographs, topographic maps and field observations have served as primary data for establishing the style and geometry of movement together with the present day stability condition. The landslide at Mam Tor has been given special attention in view of its present instability. Two boreholes were drilled in which piezometers were installed and movements have been monitored using EDM equipment. The stability of each landslide was analysed in terms of a factor of safety against movement for both first time, and subsequent movements, using the limit equilibrium method.

An extensive investigation of the engineering properties of the mudrocks involved in the landslides has been carried out. These studies include determination of remoulded residual shear strength, grading, composition, and index properties of samples from boreholes, the quarry at Hope Valley Cement Works and surface outcrops. Both the ring shear and shear box apparatuses were employed and besides test method and sample pretreatment, other causes of variation of residual shear strength have been investigated. These include normal effective stress value, loading sequence, rate of displacement as well as sample composition, grading and classification.

It is concluded that ring shear tests give lower residual shear strength values than the shear box method. Also shale disaggregated by tumbling in water produces a lower residual shear strength values than crushed

material. It would appear that in conventional tests on indurated shale a high proportion of clay aggregations remain intact even when sheared.

The study indicates that the mobilized shear strength in the field is little higher than the laboratory ring shear one for thoroughly disaggregated shale. However, it suggested that standard preparation methods and shear box tests yield erroneously high residual shear strength for the indurated shale studied.

ACKNOWLEDGEMENTS

Thanks are expressed mainly to the academic, technical and office staff and fellow post-graduate students of the Department of Geology of the University of Sheffield. In addition, the financial support provided by the Ministry of Higher Education and Scientific Research of Iraq and Mosul University is gratefully acknowledged.

Particular gratitude is expressed to my supervisor Dr. John Cripps for his help, advice and criticism throughout this work. Dr. Helen Steward, Miss Gill Thompson, Mr. Gordon Fiander, Mr. Graham Mulhearn, Mr. Paul Higham and Mr. Steve Ellin are thanked for their assistance with surveying and drilling work at Mam Tor. In addition, Mr. Ken Fenwick is thanked for applying his workshop skills to the manufacture and maintenance of the equipment used during the research.

Thanks are expressed to Mr. Dai Thompson of the Department of Civil and Structural Engineering for his considerable time and patience in respect of surveying work and aerial photograph interpretation. I am also grateful to the Department of Civil and Structural Engineering for the use of the Surveying equipment.

Valuable training in geomorphological mapping under the helpful guidance of Professor R. Walters and Mr. R. Brown of the Department of Geography is also gratefully acknowledged. I also wish to thank Mrs. Shatha Abdulmajid for assistance with statistical analysis of data.

I am grateful to my parents, my brother Dr. Raidh Al-Dabbagh and a number of friends for their encouragement, understanding and support. Thanks are also expressed to Mrs. June Marriott for her patience and understanding during the preparation of this thesis.

Finally, I wish to express my gratitude to Mrs. M. Roberts who undertook the painstaking task of typing this thesis.

CONTENTS

	Page
LIST OF TABLES	
LIST OF FIGURES	
LIST OF PLATES	
CHAPTER 1 INTRODUCTION	1
1.1 Objective of Study	1
1.2 Landslip Activity	2
1.3 Shear Strength	4
1.4 Field Work	4
1.5 Analysis of Stability	5
CHAPTER 2 THE STUDY AREA	7
2.1 Location	7
2.2 Topography	7
2.3 Geological Conditions	8
2.3.1 Eyam Limestone	10
2.3.2 Edale Shale	10
2.3.3 Mam Tor Beds	11
2.3.4 Shale Grit	12
2.3.5 Grindslow Shales	14
2.3.6 Kinderscout Grit	15
2.4 Glacial and Periglacial Activity	16
2.5 Concluding Remarks	18
CHAPTER 3 PREPARATION OF GEOMORPHOLOGICAL MAPS AND FIELD WORK AT MAM TOR.	19
3.1 Geomorphological Mapping	19
3.2 Boreholes at Mam Tor	21
3.2.1 Drilling of Boreholes	21
3.2.2 Core Description	23
3.2.3 Installation of Piezometers	37

	Page
3.3 Measurement of Movement at Mam Tor	39
3.3.1 Surveying	40
3.3.2 Calculation of Data	41
3.3.3 Presentation of Data	42
 CHAPTER 4 SHEAR STRENGTH PARAMETERS OF SOILS	 43
4.1 Introduction	43
4.1.1 Mohr-Coulomb Failure Criterion	45
4.1.2 Peak and Residual Shear Strength	46
4.1.3 Determination of Shear Strength	49
4.1.4 Determination of Residual Shear Strength	53
4.2 Variation in Residual Shear Strength	56
4.2.1 Lithological Effects	56
4.2.1.1 Conclusion	61
4.2.2 Type of Specimen	61
4.2.3 Type of Test	65
4.2.4 Test Conditions	68
4.3 Conclusion	70
 CHAPTER 5 RESIDUAL SHEAR STRENGTH TESTS	 72
5.1 Introduction	72
5.2 Sample Preparation	75
5.3 Experimental Procedure	76
5.3.1 Index Properties	76
5.3.2 Grading	76
5.3.3 Composition	77
5.4 Residual Shear Strength	77
5.4.1 Ring Shear	77
5.4.2 Shear Box	80
5.4.3 Presentation of the Results	82
5.5 Test Results and Discussion	83

	Page
5.5.1 Classification and composition	83
5.5.2 Ring Shear	85
5.5.3 Shear Box	85
5.5.4 Variation in Residual Shear Strength Value	86
5.5.5 Failure Envelopes for Residual Condition	89
5.5.6 Statistical Analysis	91
5.6 Relationship Between (ϕ_{rr}' , c_{rr}') and other Engineering Properties	92
5.6.1 Grading and Composition	92
5.6.2 Classification and Water Content	95
5.6.3 Relation of c_{rr}' and Enginee- ring properties	97
5.6.4 Remoulded Peak Shear Strength	97
5.7 Conclusion	98
 CHAPTER 6 STABILITY OF SLOPES	 101
6.1 Introduction	101
6.1.1 Purpose and Philosophy	101
6.1.2 Classification	101
6.1.3 Factors contributing to slope Failure	107
6.2 Stability Analysis	109
6.2.1 Effective and Total Stress Conditions	111
6.2.2 Limit Equilibrium Analysis	112
6.3 Location of Slip Surface	114
6.4 Determination of Factor of Safety	115
6.4.1 Infinite Slope-Planer Slide	116
6.4.2 Finite Slope - Rotational Slide.	118
6.5 Summary	120
 CHAPTER 7 MORPHOLOGY AND MAIN FEATURES OF LANDSLIPS IN THE STUDY AREA	 123

	Page
7.1 Introduction	123
7.2 Mam Tor	125
7.2.1 Morphology	126
7.2.2 Movement at Mam Tor	129
7.3 Rushup Edge	131
7.4 Cold Side	132
7.5 Back Tor	134
7.6 Burr Tor	136
7.7 Bretton Clough	137
7.8 Alport Castles	140
7.9 Rowlee Pasture	143
7.10 Cowms Moor	145
7.11 Kinder Scout	147
7.12 Conclusion	149
 CHAPTER 8 STABILITY ANALYSIS FOR LANDSLIPS STUDIED	 151
8.1 Introduction	151
8.2 Information Required for the Analysis of Stability	151
8.3 Stability Analyses for Rotational Movement	154
8.4 Stability Analyses for Translational Movement.	156
8.5 Volumetric Changes	156
8.6 Sources of Error	157
8.7 Results of Stability Analyses	157
8.8 Summary and Discussion	170
8.9 Conclusion	174
 CHAPTER 9 CONCLUSION	 176
9.1 General Conclusion	176
9.2 Suggested Further Research	180
 APPENDIX A CALIBRATION AND CALCULATION FOR SHEARING TEST	 183

	Page
A.1 Calibration of Proving Rings	183
A.2 Calculation of Shear Stress	183
A.3 Calculation of Shearing Rate	184
A.4 Calculation of Load used in Apparatus.	185
APPENDIX B COMPUTER PROGRAM FOR CALCULATING AND PLOTTING RING SHEAR TEST RESULTS	187
APPENDIX C X-RAY DIFFRACTION TECHNIQUES	188
C.1 Introduction	188
C.1.1 Mineral Identification Technique.	189
C.2 XRD Results	191
C.2.1 Whole Rock Sample	191
C.2.2 $< 2 \mu\text{m}$ Clay Fraction	192
C.3 Semi-quantitative Estimation of Clay Minerals.	193
APPENDIX D STATISTICAL ANALYSIS	195
D.1 Introduction	195
D.1.1 Test Procedure	195
APPENDIX E DETERMINATION OF THE HEIGHT OF BACK SCARPS FROM AERIAL PHOTOGRAPHS.	205
REFERENCES	107

LIST OF TABLES

Table No.		Following or in page
3.1	Ordnance Survey maps used in study.	20
3.2	Details of aerial photographs used for geomorphological mapping.	20
3.3	Detail of the Eldi 3 EDM and TH 2 Theodolite used in the survey at Mam Tor.	40
4.1	Shear strength parameter for drained shear box test on of Oxford Clay (After Parry, 1972).	62
4.2	The effect of method of processing on the residual shear strength of Strawn Shale and Dawson Shale (After Townsend and Gilbert, 1976).	64
4.3	Effect of equipment type on the residual shear strength of London Clay.	67
5.1	Source and description of samples used in analysis .	72
5.2	Sample numbering and preparation techniques.	83
5.3	Results of Atterberge limits grading, mineralogy, organic-carbon, soluble carbonate clay/quartz ratio and activity determinations.	83
5.4	Clay mineral abundances expressed as percentages (< 2 micron clay fraction) and the ratio of clay mineral abundances expressed as a percentage of the clay size fraction.	84

Table No.		Following or in page
5.5	Residual shear stress values, normal stress values and shear stress: normal stress ratio for ring shear test on remoulded tumbled samples.	86
5.6	Residual shear stress values, normal stress values and shear stress: normal stress ratio for ring shear tests on remoulded crushed samples of Edale Shale from Hope Valley Cement Works.	86
5.7	Residual shear stress values, normal stress values and shear stress: normal stress ratio for ring shear tests on remoulded crushed sieved Edale Shale from Hope Valley Cement Works.	86
5.8	Residual shear stress values, normal stress values, and shear stress: normal stress ratio for shear box test on remoulded tumbled and crushed samples.	87
5.9	The effect of rate of displacement or residual shear strength for ring shear tests on remoulded tumbled sample.	88
5.10	The effect of rate of displacement on the residual shear strength for ring shear tests on remoulded crushed sample.	88
5.11	Strength values for ring shear and shear box tests on tumbled, crushed, crushed and sieved remoulded samples.	89
5.12	Initial and final moisture contents of ring shear apparatus.	96

Table No.		Following or in page
5.13	Initial and final moisture content of shear box samples.	96
5.14	Remoulded peak shear stress values, normal stress values for ring shear tests on remoulded tumbled samples.	98
5.15	Peak shear strength values for ring shear test on tumbled remoulded samples.	98
6.1	Abbreviated classification of slope movement (After Varnes, 1978).	101
6.2	Hutchinson's (1968) classification of mass movement.	102
7.1	The observation and measurements data presented on the maps (Figs. 7.6 to 7.15)	124
7.2	Symbols used for the interpretations of geomorphological maps.	- 125
7.3	Results of EDM survey at Mam Tor.	129
7.4	Average rates of movement at Mam Tor landslip between Oct. 1981 and May 1983.	130
8.1	Summary of instability in North Derbyshire.	151
8.2	Typical value of strength parameter ϕ' (After Polish Code PN-59/B - 03020, 1959)	154

Table No.		Following or in page
8.3	Residual friction angle of sandstone (After Barton, 1973).	154
8.4	Volumetric changes for zones of depletion and accumulation of the landslips studied.	157
8.5	Shear strength used in the analysis .	157
8.6	The effect of water table, shear strength of shale and sandstone used in the stability analysis.	173
A.1	Calibration factors for proving rings used in the ring shear and shear box apparatus.	183
C.1	Schultz (1960) "Kaolinite crystallinity" for $< 2 \mu$ micron clay fraction.	194
D.1a	Statistical analysis of residual shear strength values for ring shear and shear box.	198
D.1b	Two-way ANOVA analysis.	198
D.2a	Statistical analysis of cohesion intercept values for ring shear and shear box.	200
D.2b	Two-way ANOVA analysis.	200
D.3a	Statistical analysis of residual shear strength values for shear box.	201
D.3b	Two-way ANOVA analysis.	201

Table No.		Following or in page
D.4a	Statistical analysis of residual shear strength values for ring shear.	202
D.4b	Two-way ANOVA analysis.	203
D.5a	Statistical analysis of residual shear strength values for ring shear.	203
D.5b	Two-way ANOVA analysis.	204

LIST OF FIGURES

Figure No.		Following page
2.1	Location map for landslips studied.	7
2.2	Geological map of North Derbyshire (After Geological Survey Sheet '99').	8
2.3	Generalized Section of stratigraphy at North Derbyshire (After Stevenson and Gaunt, 1971).	10
3.1A	Core description of Borehole 1 at Mam Tor main unit.	22
3.1B	Core description of Borehole 1a at Mam Tor main unit.	22
3.2	Core description of Borehole 2 at Mam Tor toe.	22
3.3	Installation of piezometer.	38
3.4	Modification to piezometer.	38
3.5	Location of survey points at Mam Tor.	39
3.6	The coordination of the horizontal angle for the location of stations and mea- surement of the amount of movement.	42
4.1	Types of soil.	43
4.2	Shear stress deformation and normal stress relationship for typical soil.	43

Figure No.		Following page
4.3	Stress acting on soil sample in triaxial compression test (After Jumikis, 1965).	45
4.4	Mohr's stress circle.	45
4.5	Stress strain relationship for typical soil and for an elastic perfectly plastic model soil (After Scott, 1980).	46
4.6	Typical shear stress-shear strain and shear-effective normal stress relationships.	46
4.7	Triaxial apparatus.	49
4.8	Typical triaxial test results.	49
4.9	Schematic diagram of shear box apparatus.	50
4.10	Vaneshear test apparatus.	50
4.11	Ring shear test sample.	52
4.12	Residual shear strength and clay size fraction of U.K. mudrocks (After Cripps and Taylor, 1981).	56
4.13	Residual strength: correlations with clay fraction (After Lupini <u>et al</u> , 1981).	56
4.14	Type of grains and the characteristic of shear plane.	56
4.15	Residual strength: correlations with plasticity index (After Lupini <u>et al</u> 1981).	58

Figure No.		Following page
4.16	Relationship between residual friction angle and plasticity (After Mitchell 1976 and Deere, 1974).	58
4.17	Quartz: clay minerals ratio (logarithmic) plotted against residual ϕ_r' (c' assumed zero) (After Spears and Taylor, 1972).	59
4.18	Influence of clay minerals on residual shear strength all mineralogical data from the same XRD machine and ϕ_r' values from the same reversing (After Cripps and Taylor, 1981).	59
4.19	Geometrical component due to the undulating shear surface. A. Upper and lower half match each other. Lower shear strength. B. Upper and lower half not match each other. Higher shear strength.	66
4.20	Idealized expression of the three components of shear stress measured in the repeated direct shear test. (After Heley and MacIver, 1971).	66
4.21	Effects of loading sequence and value of effective normal stress on residual shear strength value. (After Bishop <u>et al</u> , 1971).	69
5.1	Ring shear apparatus.	78
5.2	Bridge arrangement filled to 100mm square shear box.	80

Figure No.		Following page
5.3	Plasticity chart for samples used in shear strength tests.	83
5.4	Effect of clay fraction on liquid limit and plasticity index.	83
5.5A	Grain size analysis for tumbled samples.	84
5.5B	Grain size analysis for tumbled samples.	84
5.6	Shear stress-displacement and displacement vertical thickness relationship for ring shear tests on tumbled remoulded samples.	85
5.7	Shear stress-displacement and vertical thickness relationship for ring shear test on remoulded crushed and crushed sieved samples.	85
5.8	Shear stress-displacement and displacement-vertical thickness relationships for shear box tests on remoulded tumbled and crushed sieved samples.	85
5.9	Variation of residual shear stress ratio with normal effective stress for ring shear tests on remoulded tumbled samples.	87
5.10	Variation of residual shear stress ratio with normal effective stress for ring shear tests on remoulded crushed and crushed sieved samples.	87

Figure No.		Following page
5.11	Variation of residual shear stress ratio with normal effective stress for shear box tests on remoulded tumbled and crushed sieved samples.	87
5.12A	Effect of rate of strain on residual shear stress and vertical thickness of remoulded tumbled sample.	88
5.12B	Effect of rate of strain on residual shear stress and vertical thickness of remoulded crushed sample.	88
5.13	Effect of rate of strain on tumbled sample.	89
5.14	Effect of rate of strain on crushed sample.	89
5.15	Residual shear stress-normal effective stress relationship for ring shear test on remoulded tumbled samples.	89
5.16	Residual shear stress-normal effective stress relationship for ring shear tests on remoulded crushed samples.	89
5.17	Residual shear stress-normal effective stress relationship for shear box tests on remoulded tumbled and crushed sieved samples.	89
5.18	Relationship between clay fraction and residual shear strength for ring shear tests on remoulded tumbled samples.	93
5.19	Relationship between quartz and residual shear strength for ring shear test on remoulded tumbled samples.	93

Figure No.		Following page
5.20	Comparison between published and present relationship between residual shear strength and ratio of clay minerals to detrital minerals.	94
5.21	Relationship between residual shear strength for ring shear tests on tumbled samples and amount of clay.	95
5.22	Relationship between residual shear strength for ring shear tests on remoulded tumbled samples and clay minerals: quartz ratio.	95
5.23	Relationship between residual shear strength for ring shear tests on remoulded tumbled samples and liquid limit or plasticity index.	95
5.24	Published and present relationships between residual shear strength and plasticity index.	95
5.25A	Relationship between residual shear strength for ring shear tests on remoulded tumbled samples and final moisture content.	95
5.25B	Relationship between residual shear strength for shear box tests on remoulded tumbled samples and final moisture content.	96
5.26	Relationship between remoulded residual shear strength for ring shear tests on remoulded tumbled samples and amount of organic carbon.	96

Figure No.		Following page
5.27	The relationship between c_{rr}' and various engineering properties for remoulded tumbled ring shear tests.	97
5.28	Displacement shear stress curves fore ring shear test on remoulded tumbled samples.	98
5.29	Remoulded peak shear stress-normal effective stress relationship for ring shear test on remoulded tumbled samples.	98
6.1	Landslide properties (After Skempton, 1953a and b).	103
6.2	Some basic types of mass movement, multiple and complex landslides in clay slopes. (After Skempton and Hutchinson, 1969).	103
6.3	Forces in planer slide analysis.	116
6.4	Forces acting on single slice in sliding mass.	118
7.1	Schematic plan view of a slide.	123
7.2	Main features of rotational slide. (After Varnes, 1978).	123
7.3	Geomorphological map of Mam Tor landslip.	126
7.4	Mam Tor landslip showing the main damage and the heave area.	128

Figure No.		Following page
7.5	Results of surveying at Mam Tor.	129
7.6	Histogram of monthly rainfall for Edale Mill and Hope Cement Works, Years, 1981, 1982 and 1983.	130
7.7	Geomorphological map of Rushup Edge landslip.	131
7.8	Geomorphological map of Cold Side landslip.	133
7.9	Geomorphological map of Back Tor landslip.	134
7.10	Geomorphological map of Burr Tor landslip.	136
7.11	Geomorphological map of Bretton Clough landslip.	137
7.11A	Sketch, showing regional subdivisions of Bretton Clough landslip to which reference is made in the text.	137
7.12	Geomorphological map of Alport Castles landslip.	140
7.12A	Sketch showing regional subdivisions of Alport Castles landslip to which reference is made in the text.	141
7.13	Geomorphological map of Rowlee Pasture landslip.	143
7.13A	Sketch showing regional subdivisions of Rowlee Pasture landslip to which reference is made in the text.	143

Figure No.		Following page
7.14	Geomorphological map of Cowms Moor landslip.	145
7.15	Geomorphological map of Kinder Scout landslips.	147
7.16	Areas of instability and the possible directions of movement at Kinder Scout.	147
7.17	Possible evolution of landslip.	149
8.1	Critical state for drained shear tests on ideal clay (After Skempton, 1970).	153
8.2	Method of calculating stability.	154
8.3	Sketch of typical features of landslip.	156
8.4	Piezometers readings at Boreholes 1 and 2 (Mam Tor).	156
8.5	Stability analysis for Mam Tor landslip.	158
8.6	Stability analysis for Rushup Edge landslip.	160
8.7	Stability analysis for Cold Side landslip.	161
8.8	Stability analysis for Back Tor landslip.	162
8.9	Stability analysis for Burr Tor landslip.	163
8.10	Stability analysis for Bretton Clough landslip.	163

Figure No.		Following page
8.11	Stability analysis for Alport Castles landslip.	165
8.12	Stability analysis for Rowlee Pasture landslip.	166
8.13	Stability analysis for Cowms Moor landslip.	167
8.14	Stability analysis for Kinder Scout landslips.	169
9.1	Field residual shear strength.	176
A.1	Calibration curve of proving rings for ring shear apparatus.	183
A.2	Calibration curve of proving ring for shear box apparatus.	183
B.1	Computer program for calculating and plotting ring shear test results.	187
C.1	Centrifuging time for particle size separation at various temperatures.	190
C.2	X-ray diffractogram of smear mount of whole rock.	191
C.3	X-ray diffraction of orientated smear mounts of the $\leq 2 \mu m$ clay fraction after different treatments.	192

LIST OF PLATES

Plate No.		Following page
3.1	The Drilling Machine used for drilling Boreholes at Mam Tor.	21
3.2	Unweathered Edale Shale from between 25.9 and 27.4m (85-90ft.) in Borehole 1, at Mam Tor.	31
3.3	Unweathered Edale Shale from Borehole 1, depth 25.9 to 27.4m. (85-90ft.), note the pyrite crystal and jointing.	32
3.4	Gypsum in fractures in Edale Shale from depth of 25.9m. (85ft.) in Borehole 1.	32
3.5	Borehole 2 material from a depth of 15.8 to 20.4m. (52-67ft.).	37
3.6	Measuring the elevation of the water table at Mam Tor.	37
3.7	Eldi 3 EDM and TH 2 theodolite equipment used in the survey at Mam Tor.	40
5.1	Bromhead ring shear apparatus.	78
5.2	Shear box apparatus.	80
5.3	Slickensided shear surface-ring shear test on sample MTBH.	85
5.4	Slickensided shear surface-ring shear test on sample CS.	85
5.5	Slickensided shear surface-shear box test on sample SK.	86

Plate No.		Following page
5.6	Slickensided shear surface-shear box test on sample CW1CP200	86
5.7	Slickensided shear surface-shear box test on sample CW1.	86
5.8	Slickensided shear surface-shear box test on sample MTBH.	86
5.9	Slickensided shear surface-shear box test on sample MT5	86
5.10	Slickensided shear surface-shear box test on sample AC.	86
5.11	Slickensided shear surface-shear box test on sample RP.	86
7.1	Aerial photographs of Mam Tor landslip.	126
7.2	General view of Mam Tor landslip looking in a southerly direction. Note the contrast in the character of the ground surface between the toe and other parts of the landslip. August 1983.	126
7.3	Landslip at Mam Tor. Main scarp. Main scarp 'A' viewed in a westerly direction with minor scarps B, C and D on the southern flank of the landslip. Note: downward movement of road surface 'E'.	126
7.4	Slickensided, back scarp surface at Mam Tor.	127
7.5	Damage at the upper road at Mam Tor.	

Plate No.		Following page
	Note that: successive layers of road surfacing material have been applied in an attempt to maintain the road. French drains on main unit of Mam Tor landslip 'F'.	127
7.6	Damage of the upper road at Mam Tor. Note that: the recent instability has caused a downward movement with lateral displacement.	128
7.7	Minor scarp at little Mam Tor 'A'.	128
7.8	Hummocky ground at the foot of main unit. Recent downward movement of lower southern edge of the road in January 1983.	128
7.9	Heave movement at northern part, lower road.	128
7.10	Blacketlay Barn before March 1983.	129
7.11	Destruction of Blacketlay Barn March 1983. Note convex character of toe.	129
7.12	Aerial photograph of Rushup Edge landslip.	131
7.13	Main scarp and main unit landslip at Rushup Edge.	131
7.14	Toe of landslip at Rushup Edge. Note the presence of marshy areas.	131

Plate No.		Following page
7.15	The convex margin of the toe of the landslip at Rushup Edge.	132
7.16	Aerial photograph of Cold Side land- slip.	133
7.17	General view of Cold Side landslip. Note the vegetated character and change in direction of the minor scarp.	133
7.18	East-west part of the main scarp of the landslip at Cold Side.	133
7.19	Minor scarps in the landslip at Cold Side, note that there are mostly grass covered.	133
7.20	The toe of Cold Side landslip. Note the presence of marshy areas.	133
7.21	Aerial photograph of Back Tor landslip.	134
7.22	General view of Back Tor landslip. Note the steep exposure of Shale Grit and Mam Tor beds in the back-scarp.	134
7.23	Eastern side of the main scarp of the landslip at Back Tor.	134
7.24	Western side of the main scarp of Back Tor landslip. Part of the main unit shows the hummocky ground with sand- tone blocks below the main scarp.	134
7.25	Minor scarp at foot of the main unit of Back Tor landslip.	135

Plate No.		Following page
7.26	Part of the foot and toe of the landslide at Back Tor. Note the gentle slope of toe.	135
7.27	Aerial photograph of Burr Tor landslide.	136
7.28	General view of landslide at Burr Tor. Note the main scarp behind the belt of trees.	136
7.29	Main scarp of the landslide at Burr Tor. Note the steep exposure of sandstone of Shale Grit and hummocky ground at the main unit.	136
7.30	Aerial photograph of Bretton Clough landslide.	137
7.31	Western part of the landslide at Bretton Clough. Note ridged ground.	138
7.32	Eastern landslide at Bretton Clough - general view.	138
7.33	Part of the toe in the eastern part of landslide at Bretton Clough - note the gentle slope towards the river.	139
7.34	Minor scarp on the eastern side of Bretton Clough with evidence of recent instability.	139
7.35	Aerial photograph of Alport Castles landslide.	140

Plate No.		Following page
7.36	General view of the landslip at Alport Castles.	140
7.37	The Crown of Alport Castles landslip. Note the trenches contain peat.	140
7.38	Main scarp of landslip at Alport Castles showing a recent rockfall. Note the detached of block of the main unit.	140
7.39	The main sacrp at the southern side of Alport Castles landslip. Note the hummocky ground of the main unit.	140
7.40	Scree formed by distribution of sandstone blocks in the main unit of landslip at Alport Castles with a detached block due to secondary movement. Note Back scarp of sandstone and shale beds of Shale Grit formation.	141
7.41	Part of the main unit of the landslip shows a block of 250m by 75m wide at Alport Castles landslip.	141
7.42	Northern side of the main unit of the landslip at Alport Castles. Note the ponding of water.	141
7.43	Part of the toe at landslip of Alport Castles forming minor scarp along flank of river Alport.	141
7.44	Recent rockfall in the main scarp at Alport Castles. August 1982. Scales 1cm = 0.5m.	143

Plate No.		Following page
7.45	Aerial photograph of Rowlee Pasture landslip.	143
7.46	Part of the main scarp (A) of landslip at Rowlee Pasture. Main unit and foot are highly vegetated. Note part of the toe forming minor scarp (B).	144
7.47	Repairs to the A57 road due to movements of the landslip at Rowlee Pasture.	144
7.48	Gabbion wall to protect the toe of the landslip at Rowlee Pasture.	145
7.49	Concrete wall to protect the toe of the landslip at Rowlee Pasture.	145
7.50	The Gabbion protection has not entirely prevented movement of toe of the Rowlee Pasture landslip.	145
7.51	Aerial photograph of Cowms Moor landslips.	145
7.52	Main scarp and main unit of landslip at Cowms Moor. Note the exposure of sandstone of Shale Grit formation in the main scarp at 'A' and the fallen sandstone block in the main unit at 'B'.	146
7.53	Hummocky ground in the main unit of landslip at Cowms Moor.	146
7.54	The main unit of the lower slip at Cowms Moor. Note the NW-SE ridges and hallows.	146

Plate No.		Following page
7.55	Aerial photograph of Kinder Scout landslips.	147
7.56	Main scarps in the NW part of landslip at Kinder Scout (A) and exposure of coarse feldspathic sandstone at the crown (B).	148
7.57	Crown of landslips at Kinder Scout showing the surface drainage.	148
7.58	The landslip in the SW part of Kinder Scout. Note exposure of sandstone at the crown and the ponding water.	148
7.59	Kinder Scout sandstone cliff forming part of NW Main scarp.	148

CHAPTER 1

INTRODUCTION

1.1 Objectives of Study.

Little previous work regarding landslip in North Derbyshire has been carried out, and few references occur in the literature to extensive and interesting land instability phenomena in this area. Related studies include work by Franks and Johnson (1964) in which landslips are dated using pollen analysis techniques. Bass (1954) reports on geomorphological studies of the characteristics and origin of some landslips in North Derbyshire. Carson and Petley (1970) have made a generalized study of slope angles and their relation to shear strength in the denudation of the landscape in the Derwent Valley. Later work by Vear (1981) concerns the geochemistry of water seepages in the vicinity of the landslip at Mam Tor. From this research it was concluded that chemical weathering of Edale Shale produces large quantities of sulphuric acid which may react with soil and groundwater constituents including carbonates. It is also implied that clay minerals may also be affected. In another study by Steward (1984) attempts were made to link the chemical composition of porewaters to changes in residual shear strength and other geotechnical properties of Edale Shale. Measurements of the drained residual shear strength of Edale Shale from an outcrop at Mam Tor are also reported by Lupini et al (1981), who carried out a wider study of the residual shear strength characteristics of various soils and rocks. Although a few authors have studied the geomorphological features of some landslips, work has been restricted to slopes in Edale Shale at Mam Tor. No attempts to link the geomorphological features of the many landslips which occur in North Derbyshire with the engineering properties of the materials concerned have been published.

In order to do this the stability of individual landslips will be analysed using standard limiting

equilibrium techniques. Hence, it is necessary to establish the style and geometry of instability together with the controlling shear strength parameters. of particular interest is the value of residual shear strength (ϕ_r') which can be determined by carrying out laboratory tests. From the analysis of landslips it is possible to back figure the shear strength mobilized during landslide activity and this can be compared with the laboratory value.

This research can therefore be divided into two main related aspects:-

- i. The classification of land instability and the determination of geometry of landslips in the study area.
- ii. The determination of the engineering characteristics of the material concerned. Of particular interest are the parameters controlling the initial instability together with those relevant to subsequent failure. The opportunity arises to compare laboratory determined values with those operating in the field.

1.2 Landslip Activity.

Stability of natural slopes is controlled by forces acting within and on the soil mass. Thus two types of force are considered, body forces due to the weight of material and external forces applied to the soil mass. Landslips occur in response to situations in which combinations of stresses are sufficient to overcome the strength mobilized within the rock or soil mass.

Landslips have been a source of interest since ancient times and, in addition, many studies have been conducted in response to major disasters. Landslips are characterized by a host of observable features which can be related to the kind of material in which the slide occurs as well as to the amount and direction of motion. Certain workers, including for example Terzaghi (1950) and Hutchinson (1968), have studied the actual mechanism

which causes landslip movement and investigated the possibility of predicting the occurrence of instability of particular locations. Much of the research on landslips has been carried out within the discipline of Civil Engineering with the emphasis on the prevention of damage to engineering structures. However, early work dealing with geological and geomorphological aspects of landslips is presented by Sharp (1938 reprinted 1960). Thus landslippage may be regarded as a process of landscape development of relevance to geographical studies and also a fuller understanding of the behaviour of natural materials may be gained only by reference to important geological structures and processes. Piteau (1970) points out for instance that bedding and joint structures can exert strong controls over landslip processes. In addition he notes that weathering products often accumulate in joints so that stability which depends on the shear strength of this material is controlled by the geological degradation process and the attitude and incidence of discontinuities.

Many authors, including for example Bromhead (1984) Skempton and Hutchinson (1969) and Bishop (1955), consider the stability of landslides in terms of limiting equilibrium. For this a factor of safety (F) is defined as the ratio of forces inhibiting movement to those causing it. Thus for values of F greater than unity a stable condition should obtain whereas, if F is less than this, then the slope will be subjected to instability. In most soil masses which are not subjected to external forces, the resisting forces arise from the shear strength mobilized within the soil mass and also gravitational forces. Forces promoting instability are due to the weight of the soil mass. Bromhead (1984) has suggested that a useful alternative definition for factor of safety would be to take it as the amount by which the shear strength has to be factored in order to bring the resisting forces into equilibrium with the destabilizing forces. Limit equilibrium analysis of the instability conditions of

slopes can be carried out by considering the soil mass liable to fail as a whole, or by dividing it up into a number of parts. However, a more detailed discussion of these aspects and the controls of stability will be included in Chapter 6.

1.3 Shear Strength.

For reasons which are discussed in Chapter 8, the value shear strength used in the analysis of first time sliding is the remoulded peak value. However, the post-initial failure is controlled by residual shear strength, or a near value. It is apparent that a strength reduction occurs in soils both before initial failure and after this to a minimum shear strength. There exists much discussion in the literature regarding the concept and measurement of residual shear strength. Those aspects are considered in Chapter 4 together a review of the relationship of this parameter to other soil properties. Experimental work carried out and during this research in which the effects of changes in normal effective stress, grain size and mineralogy of the material being tested as well as the rate of strain used during the determination together with other causes of variation are the subject of Chapter 5. This chapter also includes discussion of the results of this work. In addition, other determinations including the measurement of the peak remoulded strength of a number of shales are also included.

1.4 Field Work.

Extensive field studies form an important aspect of this research. Geomorphological mapping is used to establish the geometry of a number of landslips in North Derbyshire. In addition to establishing the stability condition, the usefulness of this technique in landslide studies is also demonstrated. The opportunity is taken

of comparing the residual shear strength obtained by laboratory methods described in Chapter 5 with that apparently mobilized in active and non-active slips. The particular geographical and geological situation of study area is discussed in Chapter 2. The techniques used in the preparation of the geomorphological maps forms part of Chapter 3 while the implications of the geomorphological features in terms of land instability are discussed in Chapter 7.

The landslip at Mam Tor has received special attention during this work. Movements have been monitored over a period of time and with other investigations including the drilling of two boreholes, and measurement of ground water levels with piezometers have been carried out. Hence it is possible to use this landslip to calibrate the geomorphological interpretation and also test the methods of analysis used. The method employed for the monitoring of movements and also of drilling, installation of piezometers and the description of core are covered in Chapter 3. The result of measurements of landslip movement at Mam Tor together with the discussion of the geomorphological features are included in Chapter 7. Since variations in groundwater levels are of most relevance to the analysis of slope instability these determination are presented in Chapter 8.

1.5 Analysis of Stability.

The stability condition of various landslips in the area of interest is carried out with respect of their present post-failure condition and also for initial instability. It is argued in Chapter 8 that since the slip surface for the initial instability will also apply in the case of subsequent movement, locating this surface by carrying out trial stability analyses, yields useful information regarding the geometry of later instability. This can be incorporated with the geomorphological observations into the prediction of the present day

stability condition. Hence, from observation of stability of the relevant landslips in the field a mobilized shear stress value can be deduced. A comparison between this value and one obtained by laboratory tests forms a major part of Chapter 8.

CHAPTER 2

THE STUDY AREA

2.1 Location

The study area occupies an approximately rectangular piece of ground about 8.5 km wide by 20 km long, within the North Derbyshire Pennines. As shown in Fig. 2.1, it stretches from Kinder Reservoir in the Northwest to Eyam Moor in the Southeast, and from Derwent Reservoir in the Northeast to Rushup Edge in the Southwest. Within this area, many landslips are present, of which the ones studied are included in Fig. 2.1.

2.2 Topography

The topography or landform in North Derbyshire is variable between steep slopes, deep valleys and plateaux. Kinder Scout plateau which lies approximately 610 m (2000 ft.) above ordnance datum forms the highest part of the area while valley floors range in elevation between about 150 m and 180 m. (500-600 ft.). Over much of the area, landform is strongly controlled by rock type although field observations discussed in Chapter 7 show that there is nevertheless also a marked dependence upon physical and chemical properties and geological structure. Although in general, rocks of any kind have the same characteristics when exposed to the same kind of degradation processes and hence give rise to similar landforms, small differences of composition can result in marked changes in behaviour. For instance, Hettner (1972) discusses the importance of cementing material in the case of sandstones. In addition the distribution of rockmass discontinuities and the deposition of different strata with respect to each other are also important. Variation in the topography of this area is generally attributed to the presence of beds of sandstone and shale, in that the

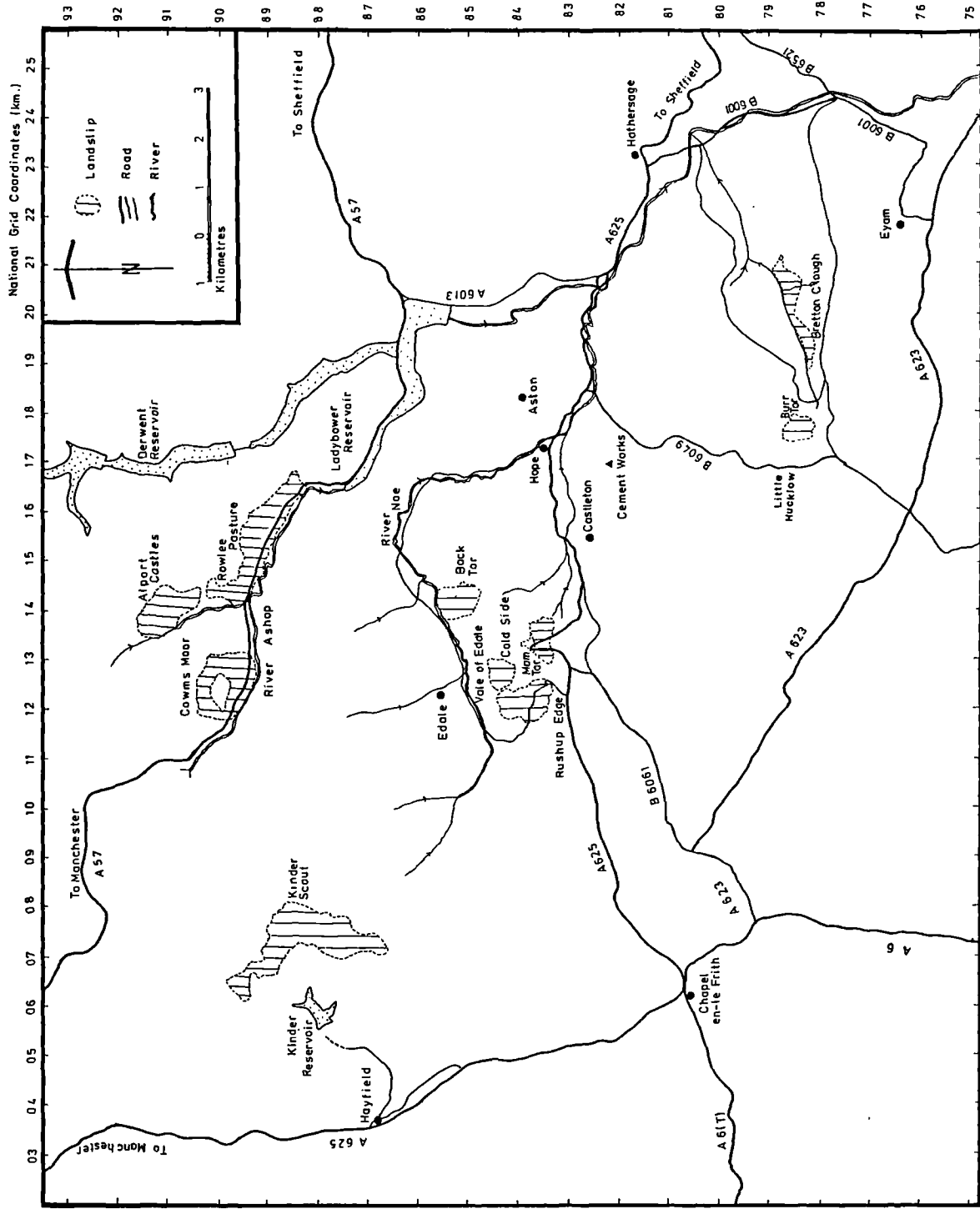


FIG. 2.1 Location map for landslips studied.

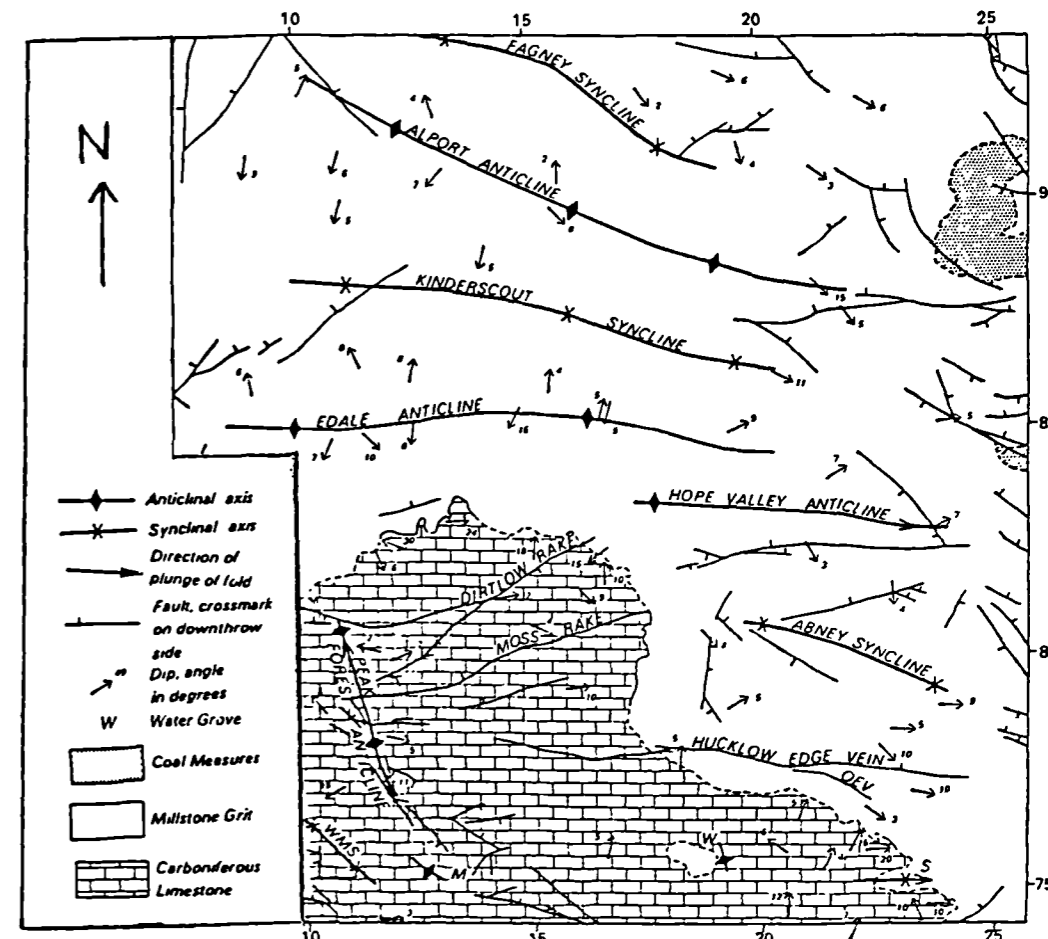
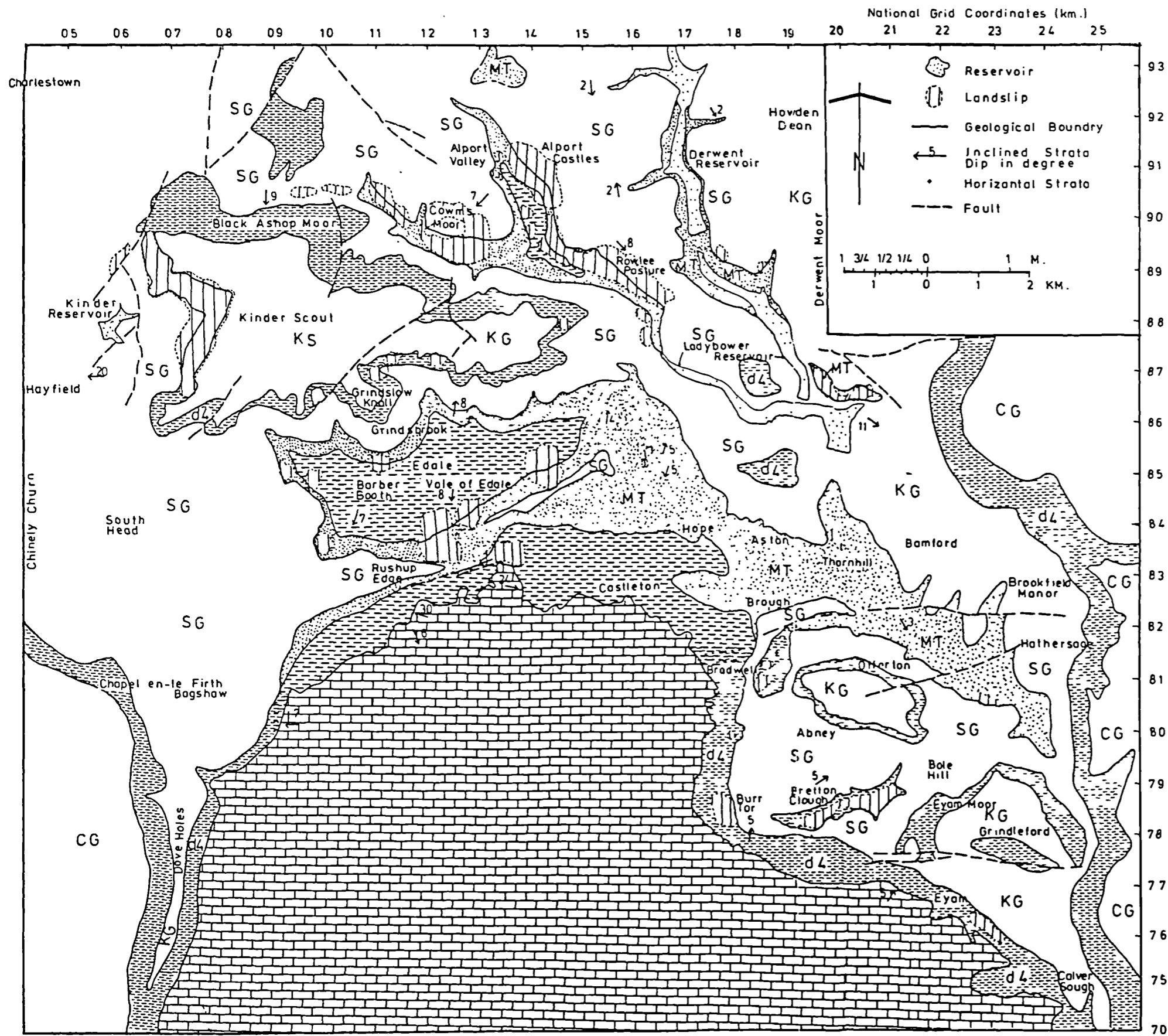
thicker beds of sandstone form steep slopes or cliffs along the upper parts of valley sides. Shallower slopes form where shale is exposed. In a number of cases, shales pass upwards into sandstones via a series of intermediate or mixed beds on which form slopes at angles between those for sandstone and shale.

Some of the river valleys are of narrow 'V' form but wider ones have flattened floors due to the accumulation of Recent alluvial deposits.

2.3 Geological Conditions

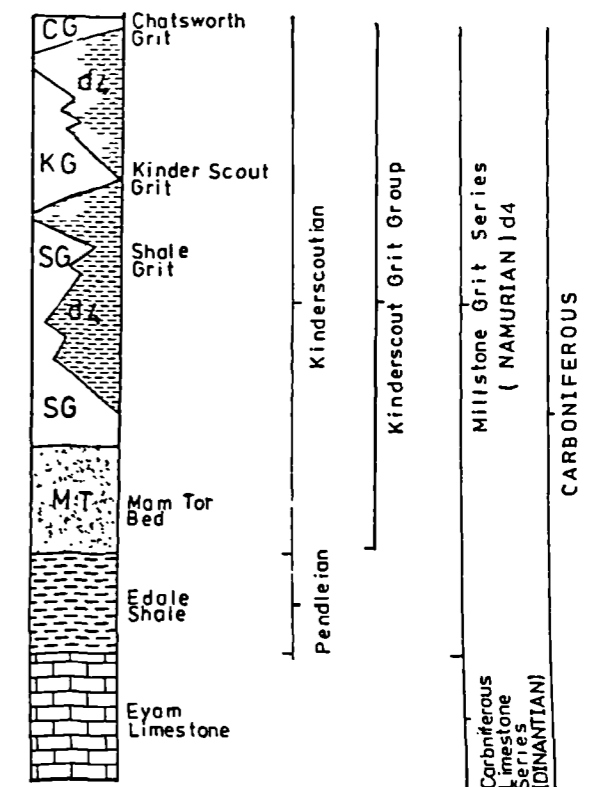
This area of North Derbyshire is familiarly known as the Peak District. In it, rocks of Upper Carboniferous age belonging to Millstone Grit Series are widely exposed. This 823 m (2700 ft.) succession of rocks of Namurian age has been described by a number of researchers, including Jackson (1927), Fearsides et al (1932), Bromhead et al (1933), Hudson and Cotton (1945), Eden et al (1957), Allen (1960) and more recently Stevenson and Gaunt (1971).

The structure of this area has been studied by Stevenson and Gaunt (1971) who summarise their findings in the insert map of Fig. 2.2. Also, included in this diagram is a map taken from part of British Geological Survey (formerly Institute of Geological Sciences, 1967) Sheet 99 (1:63360, 1 inch equals 1 mile). According to Stevenson and Gaunt (1971) Tertiary orogenic movement associated with the main Alpine orogeny account for the uplift and structures observed in this area. The Kinder Scout - Bamford area is characterized by very gentle structures. Faulting is rare in this area and where present the throws are small. The main structural features are two shallow east-west or west-north-west to east-south-east trending anticlines with associated synclines. The Edale anticline is of general east-west trend and extends from west of Barber Booth to near Bamford. The structure is slightly asymmetrical with southern limb



Sketch-map illustrating the structure of the north Derbyshire area. (After Stevenson and Gaunt 1971)

FIG 2.2 Geological map of north Derbyshire. (After Geological Survey Sheet "99")



dips of up to 12° and northern ones of up to 8°. The Alport anticline is a shallower structure and extends a distance of over 11 km in a WNW-ESE direction, from Alport Valley to Derwent Moor. The dip on flanks is up to about 7°. The elevated area of Kinder Scout is formed of the broad and very shallow Kinderscout syncline which occurs between the Edale and Alport anticlines and Fagney Syncline which lies north-northeast of the Alport anticline has a similar trend. The Hope Valley anticline is also a shallow structure trending more or less east-west where it lies parallel to the Edale anticline. The Hope Valley structure extends from Hope in the west to Brookfield Manor in the east where it displays plunge. To the south of this, the Abney syncline trends in an east-southeasterly direction. Various faults are shown on the geological map, the more important of which trends more or less east-west in the south eastern area. Faults in the northern part of the area show north-south, north-westerly or north easterly trends. Many minor faults are not shown on this map.

The Namurian (Upper Carboniferous) sequence begins with Edale Shale of thickness up to 230 m (750 ft.) resting unconformably on Visean (Lower Carboniferous) shales and limestone. The relevant part of the sequence may be divided in the following way.

Top:

- i. Kinderscout Grit, 122 m (400 ft.) Coarse feldspathic sandstone.
- ii. Shale Grit, 137 m (450 ft.) Alternating beds of sandstone and shale.
- iii. Mam Tor Beds, 122 m (440 ft.) Sandstone and shale
- iv. Edale Shale, 230 m (750 ft.) Soft, fissile, black shale.

- v. Eyam limestone 45 m (150 ft.) Limestone, including lavas, igneous intrusions and mineral veins.

Base:

The succession of geology will be discussed in the following sections with reference published work by Stevenson and Gaunt (1971) and Allen (1960) together with Geological Sheet SK18 and part of SK17 published at a scale of 1:25 000 B.G.S. (1969). Fig. 2.3 shows changes in thicknesses, lateral variation and unconformities for this area.

2.3.1 Eyam Limestone

Eyam limestone lies towards the top of the Carboniferous Limestone Series (Dinantian) although Simpson (1982) states that all exposed limestone series rocks are of Upper Visean Age. These beds are some of 45 m (150 ft.) thick and usually consist of thinly bedded dark cherty limestone, resting with a sharp break on the underlying Monsal Dale group. In the southeast of the area they pass laterally in to grey limestones. Near Bradwell an extensive mass of flat - reef limestone is developed. Eyam limestone is a marine deposit and belongs to a limestone massive associated with contemporaneous volcanic activity which has resulted in extrusion of lava and ash as reported by Smith et al (1967)

2.3.2 Edale Shale

Lower Carboniferous rocks are succeeded by a group of marine shales which are best exposed in the Edale Valley, the type area. (See map, Fig. 2.2). These shales are known collectively as Edale Shale which reaches a thickness of about 230 (750 ft.) in the Edale Valley. In the Alport Valley the succession totals 372 m (1220 ft.) Edale Shale is also extensively exposed in the vicinity of the landslip at Mam Tor at which location it has been the subject of research during the course of the present study. In addition, it also occurs in the regions of landslips at Alport Castles and Rowlee Pasture. The chief lithological types within Edale Shales are as follows:

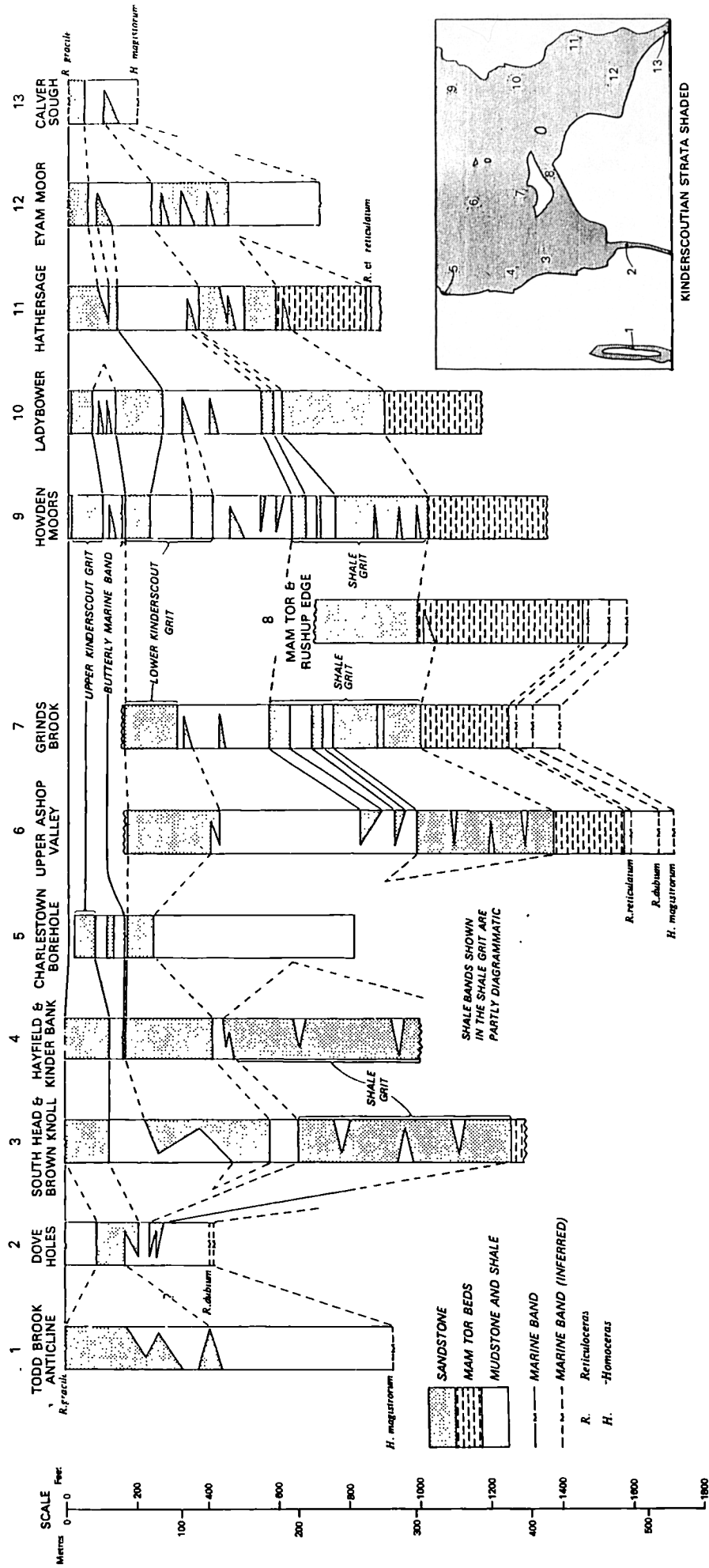


Fig. 2.3 Generalized section of stratigraphy at North Derbyshire (After Stevenson and Gaunt, 1971)

- i. Soft grey poorly fossiliferous or unfossiliferous shale often exhibiting sulphurous weathering activity resulting from the alteration of pyrite. The shale contains ironstone bands and nodules in places, but limestone bands and nodules are rare or absent.
- ii. Dark, usually calcareous shale with an abundant fauna. Thin bands of limestone up to a few inches thick are present in places.
- iii. Silty shales containing interbedded thin siltstone bands.
- iv. Hard quartzite sandstone which is present in the south-west of the area.
- v. Potassium bentonite has been found to occur as a thin bands of yellow, blue or orange - clay, bands of pyritiferous clay are also present in the sequence.

Edale Shale is a deep basinal mudstone and as such contains an abundant marine fauna comprising both thick and thin-shelled goniatites, pectinoid bivalves, brachiopoda and trilobites. Pyrite is known to be a common constituent of many sedimentary rocks particularly mudstone, where it is almost always associated with organic matter. Garrel and Christ (1965) confirms that pyrite is only stable in the absence of oxygen and in the presence of dissolved sulphide. According to Potter et al (1980) such conditions occur in modern sediments, where organic matter first accumulates and subsequently decomposes as a result of anaerobic bacterial action.

2.3.3 Mam Tor Beds

The Mam Tor Beds consist of an alternating sequence of sandstones, siltstones and shales originally described by Jackson (1927) as Mam Tor Sandstone. This name was found inappropriate when these beds were examined over a larger area, as the sandstone is not well developed in all locations so the term Mam Tor Beds has been introduced instead.

The thickness of this formation varies from about 61 m (200 ft.) on the northern side of Edale Valley, in the Ashop and Alport Valleys and near Hathersage to 130 m (450 ft.) at Mam Tor. At the type locality at Mam Tor, the passage from Edale Shale is marked by increase in the silt content of the shale and the development of some thin sandstone bands. The succession of Mam Tor Beds is made up of large number of cyclic units varying from about 0.9 m (3 ft.) to 2.4 m (8 ft.) in thickness in which massive sandstone at the base grades upwards through laminated sandstone and laminated siltstone into shale and mudstone at the top.

Mam Tor Beds are interpreted by Walker (1966) as distal turbidities deposited in a deep basin floor and making the first influx of coarse clastic sediment into the southern part of the central Pennine basin. The beds are characterised by sole structures including trail groove, flute and load casts which are indicative of turbiditic deposition.

The Mam Tor Beds are present in the Edale, Alport, Ashop, Derwent and Hope Valleys as well as at Mam Tor. It is associated with landslip activities at Mam Tor, Rushup Edge, Cold side, Back Tor, Alport Castles, Cowms Moor and Rowlee Pasture (See map, Fig. 2.2).

To the South and East of Brough this formation passes laterally into a sequence of shales, so at Bretton Clough and Burr Tor the Mam Tor Beds are absent. To the north of Mam Tor the thickness of the Mam Tor Beds decreases due to the thickening of sandstones at the expense of shale in the upper part of the sequence. These latter beds are included in the Shale Grit.

2.3.4 Shale Grit

Shale Grit consists of a thick sequence of often massive sandstone with shale bands. The name apparently derives either from the alternation of bands of shale and grit or the common occurrence of shale pellets in the

sandstone or grit beds. As discussed above the lower limit is a gradational transition from the Mam Tor Beds. The beds above the Shale Grit are the Grindslow Shales. Within the district of interest two types of development are apparent.

- i. In the northern part of the area, that is near Kinder Scout and extending eastwards to include the upper Derwent Valley, Hathersage and Offerton, the thickness varies from 213 m (700 ft.) near Hayfield to 182 m (600 ft.) in the Ashop Valley and the western end of the Edale Valley. The thickness decreases to about 91 m (300 ft.) near Hathersage. The lowest part of the Shale Grit shows a lesser development of massive sandstone than the overlying beds, their place being taken by alternating beds similar to the Mam Tor Beds. The middle part shows a marked development of thick massive sandstone, which in places is coarse and pebbly. The highest beds are transitional to the Grindslow Shales with two or more sandstone beds very regularly developed northeast of Kinder Scout.
- ii. In the south-western and south-eastern outcrops the sandstone is irregular in form which contrasts sharply with the beds mentioned above. The individual shale beds coalesce giving rise to a thickness of up to 30m (100 ft.) at Bagshaw and 18 m (60 ft.) at Abney. The Shale Grit thins rapidly to the south and disappears north of Dove Holes. In the south-eastern outcrops the shale partings disappear towards the limestone massive giving a single sandstone at Eyam. The sandstones of the Shale Grit are generally of medium to coarse grain size, usually massive and may contain shale pellets. Large load-casts occur on the under surface of many of the beds. Very coarse sandstone near in lithology to the Kinderscout Grit occurs locally near the top of the middle part of the Shale Grit sequence.

Walker (1966) attributes the deposition of all

arenaceous beds in the Shale Grit to the action of turbidity currents. Beds of Mam Tor type, which are more frequent in the lower part of the sequence can be interpreted as being of distal origin, while the massive sandstone of less obvious turbidite origin which are more frequent in the upper part of the formation are considered to be proximal, the delta front having advanced further into the area. The thicker sandstone beds are regarded as turbidite beds, mainly on account of their sharp sole-marked bases and lack of cross-bedding.

Shale Grit forms part of main scarps of the landslips at Back Tor, Alport Castles, Cowms Moor, Rowlee Pasture, Bretton Clough and Burr Tor.

2.3.5 Grindslow Shales

Shale Grit is separated from the Kinderscout Grit by a series of shales and sandy shales with thin beds of sandstone and siltstone with a few thicker sandstone beds. These beds are about 67 m (220 ft.) thick around Grindslow Knoll and Grinds Brook. The thickness of these beds is quite variable from about 36 m (132 ft.) to 45 m (150 ft.) in the east but they thin towards the south-east to 30 m (100 ft.) at Abney. The maximum development occurs north of the Kinder Scout Plateau where between 106 m (350 ft.) and 122 m (400 ft.) of shale are present. From here rapid thinning towards the south-west occurs giving a thickness of only about 9 m (30 ft.) near Hayfield and beyond Dove Holes this formation cannot be recognized.

In terms of lithology the shales are thinly laminated mudstone with sandy and silty mudstone beds together with horizontally burrowed, unbedded sandy and silty mudstones. The lower part of the Grindslow Shale are interpreted by Collinson and Walker (1967) as slope deposits which formed above the Shale Grit submarine fan. The upper part of this formation is a shallow water deposit. The Shale Grit and Grindslow Shales together makes what is known

as the Alport Group. The landslips in the Kinder Scout area occur in Grindslow Shales.

2.3.6 Kinderscout Grit

Kinderscout Grit is made of one or more leaves of typically coarse and commonly pebbly massive sandstone. The lithology contrasts strongly with that of Shale Grit, but shows features in common with that of higher beds, particularly the Chatsworth Grit.

Except in the Southwest and Southeast of the district the Kinderscout Grit is subdivided into the following groups:

- iii. Upper Kinderscout Grit.
 - ii. Shale with Butterly Marine Band.
 - i. Lower Kinderscout Grit.
- i. Lower Kinderscout Grit

The Lower Kinderscout Grit is a coarse feldspathic massive and frequently pebbly sandstone. The formation reaches a thickness of 91 m (300 ft.) on the west side of Kinder Scout and 76 m (250 ft.) at Hayfield. It thins rapidly northwards from Hayfield to about 22 m (74 ft.) at the Charlestown borehole. To the east of the Derwent Valley the Lower Kinderscout Grit is most fully developed around the head of Howden Dean. Here it consists of a 45 m (150 ft.) lower leaf and an 24 m (80 ft.) thick upper leaf separated by about 36 m (120 ft.) of shale and siltstone. The formation thins appreciably southwards along Bamford Edge and to the north of Hathersage it unites locally with Upper Kinderscout Grit. East and south of Hathersage a number of individual beds again become discernable but they cannot be correlated with any certainty with Upper and Lower Kinderscout formation.

- ii. Shale with Butterly Marine Band.

The sequence of shales containing Butterly Marine Band varies in the western outcrops from thicknesses of 26 m (87 ft.) to 10 m (33 ft.). Some of this

variation may be due to channelling at the base of the Upper Kinderscout Grit. Near South Head, the lateral passage of the upper part of the Lower Kinderscout Grit into shales results in an overall thickening of the overlying formation to about 106 m (350 ft.) A dark Carbonaceous mudstone towards the top of these shales may represent the horizon of the thin coal below the Butterly Marine Band. In the eastern outcrops these shales attain a thickness of approximately 21 m (70 ft.)

iii. Upper Kinderscout Grit.

Upper Kinderscout consists of sandstone, usually of medium grain, with some coarser bands and in places, bands with shale pellets. The thickness varies in the western outcrop between about 18 m (60 ft.) and 45 m (150 ft.) while in the eastern area it lies between 18 m (60 ft.) and 27 m (90 ft.). On the main western outcrop the Kinderscout Grit continues south of Chapel-en-le-Frith to the southern edge of district. In the eastern part of the area, the loss of the intervening shales cause it to join with the Lower Kinderscout Grit at Bole Hill. To the east and south of Hathersage, due to the union of Upper and Lower parts, the Kinderscout Grit Formation is not subdivided. However between Hathersage and Grindleford a shale parting in approximately the position of the Butterly Marine Band shale divides the formation into two nearly equal halves each about 61 m (200 ft.) thick. The Kinderscout Grit is mainly fluviatile or near shore coastal deposits of deltaic character which Amin (1979) classifies as delta front and slope deposits. The Kinderscout Grit forms the main scarps of some landslips on the Kinder Scout plateau.

2.4 Glacial and Periglacial Activity.

The engineering characteristics of the rock and soils have been more profoundly affected by the geological

agencies of the Quaternary period than by those of any other part of geological time. The history of the Quaternary period is chiefly that of the Pleistocene when at least five major glaciations occurred with interglacial periods when warmer conditions prevailed.

According to Higginbottom and Fookes (1971), the term periglacial is defined by Black (1966) to denote conditions under which frost action is the predominant weathering process. Although common, gravitational mass transportation of land surface material and wind action are not definitive features of periglacial conditions unless they are observed in association with other cold climate indicators. Frozen ground or permafrost is also an important characteristic, but these are not essential to the definition of periglacial conditions. Factors such as surface relief, lithology and geological structure have an important influence on the effects caused by periglacial climates, one of the most common features is instability of various forms.

Higginbottom and Fookes (1971) suggest that under periglacial conditions valleys can become over-steepened due to rapid erosion of ground by meltwater in conditions of high rainfall. Thawing of ice inclusions releases water and thus increases the water content of material which has been fractured by ice wedging activity. Under these conditions it is envisaged that shales in particular, will be in a weakened condition. The significance of the removal of overburden due to erosion on the properties of shales is discussed in Section 6.2. Where shales support thick sandstone beds in valley sides, it is envisaged that cambering and valley bulge phenomena result. Such features have been recorded during the construction of the Derwent Valley Dams (See Lapworth, (1911), Sanderman (1920), Hill (1949) and Walters, (1962)). Conditions of high porewater pressure and the weakening of shales due to the combined effects of the removal of overburden, ice wedging and thawing would probably give rise to slippage of the thicker more competent sandstone beds over the shales.

2.5 Concluding Remarks.

The rocks of North Derbyshire are gently folded and consist predominantly of sequences of sandstone and shales. These materials exhibit contrasting engineering properties in that sandstone is permeable, strong and competent whereas shale is impermeable and much weaker. The differences in the resistance to weathering processes of sandstone and shale are reflecting by topography of the area since generally sandstone forms steep slopes and cliffs while shale forms the shallower slopes on valley sides. Extensive plateaux occur where thick sandstone formations have not been incised by valleys. Brown (1977) suggests that most landslipping activity originates from late Devensian time, about 10000-20000 years before present (See Section 7.2), When ice melt would cause an increase in moisture content of rocks particularly shale which would be accompanied by degradation of the material due to ice wedging and the effect of the removal of overburden. Loss of strength due to thawing would lead to failure of shale beneath sandstone beds. These concepts are enlarged upon in Chapter 7. The possibility of this activity would be enhanced by the presence of oversteepened slopes in frozen ground and the absence of vegetation especially of plants with vigorous rooting systems.

CHAPTER 3

PREPARATION OF GEOMORPHOLOGICAL MAPS AND FIELD WORK AT MAM TOR.

The contents of this chapter include details of field work and surveying to determine the geomorphological characteristics of the landslips studied. This work may be considered under three main headings.

- i. Geomorphological mapping.
- ii. Boreholes at Mam Tor.
- iii. Measurement of movements at Mam Tor.

3.1 Geomorphological Mapping

The application of geomorphological mapping techniques to the study of mass movement has been widely advocated. Petley (1984), in particular, emphasises the advantages as follows:

- i. A good understanding of the development and nature of natural slopes and the processes which have contributed to the formation of different features.
- ii. To assist the assessment of the stability of various forms of slopes under given conditions.
- iii. To assess the risk of landslides in the landscape.
- iv. To facilitate the successful redesign of failed slopes as well as the planning and design of preventative and remedial measures.
- v. To analyse slope failures which have already occurred and to define the causes of failure. The mobilised shear strength on the failure surface can be estimated and this can be compared with the results of laboratory tests. Also to determine the sensitivity of the analysis to changes in pore water pressure, geometry of the slope and other factors.
- vi. To deal with the risk of special external factors on the stability of slopes including earthquakes and the presence of fill, lagoons and dams.

To a large extent the methods employed for recording geomorphological data during the course of present work follows those described by the Engineering Group Working Party (1972) and Savigaer (1965). The primary information used for mapping include the following:

- i. Topographic maps.
- ii. Aerial photographs.
- iii. Field observations.

The actual procedures are described in detail in later sections, but briefly at the initial stages topographic maps at a scale of 1:5000 were used, geomorphological information was transferred onto these from aerial photographs and subsequently the data were refined by field observations.

- i. Topographic maps.

Ordnance survey 1:10000 scale contoured maps listed in Table 3.1 were used. These maps were enlarged photographically to a scale of 1:5000 to simplify the representation of the data. For map SK18SW which includes the Mam Tor, Rushup Edge and Cold Side landslips, unpublished 10m. interval contoured 1:10000 map were used. The topographic maps were used for determining the steepness of slopes and the locations of marshes, foot paths, roads and rivers.

- ii. Aerial photographs.

Details of the photographs used during this study are listed in Table 3.2. Some of these photographs were enlarged in order to provide more details of the observable features. The photographs were viewed stereoscopically so that the morphological features including the height of the main scarp, the positions of breaks of slopes, the extent of instability and details of drainage were transferred onto the map.

- iii. Field observations.

The basic aims of the field studies were to record

Table 3.1 Survey maps used in the study.

Ordnance survey map number	Landslip area
SK 18 SW	Mam-Tor, Rushup Edge, Cold Side.
SK 18 NW	Back Tor, Cowms Moor.
SK 18 NE	Rowlee Pasture.
SK 19 SW	Alport Castles, Cowms Moor, Rowlee Pasture.
SK 08 NE	Kinder Scout.
SK 09 SE	Kinder Scout.
SK 17 NE	Burr Tor, Bretton Clough.
SK 27 NE	Bretton Clough.

Table 3.2 Details of aerial photographs used for geomorphological mapping

Landslip area	Contract No.	Photograph number	Average scale	Date	Enlargement
Mam Tor	7145	067 068	1:12000	1972	none
Rushup Edge	"	067 068	"	"	none
Bretton Clough	"	124,295 123,294	"	"	none
Burr Tor	"	124 123	"	"	none
Cold Side	76 015	362 361	1:26000	"	x 1
Back Tor	76 015	362 361	"	"	x 1
Alport Castles	"	365 364	"	"	x 1.5
Rowlee Pasture	"	351,364 350,363	"	"	x 1.5
Cowms Moor	"	365 364	"	"	x 1.5
Kinder Scout	76 016	454,422 453,421	"	"	none

accurately the topography of landslips and adjacent areas, also to look for evidence of recent movement and to determine the lithology of outcrops, geological structure, and other features including slickensided surfaces. In addition, measurements of the steepness and irregularity of slopes, location of seepages, marshes and pools, determination of waterflow and collection of samples for laboratory tests were also carried out.

3.2 Boreholes at Mam Tor.

As mentioned in the introduction, the landslip at Mam Tor received special attention during this study. Two boreholes were drilled into the landslip in order to provide samples of unweathered Edale shale and also in an attempt to determine the depth of the slip surface. The location of these boreholes, one of which was situated in the main unit and the other in the toe area, are shown in Fig. 7.3. In addition, Casagrande type piezometers were installed in the holes so that groundwater levels could be monitored.

3.2.1 Drilling of Boreholes.

It was first proposed to drill three boreholes, the extra one being at the foot of the main unit near the lower road (See map. Fig. 7.3) However, due to problems with the supply of an adequate amount of water this hole was abandoned. In the subsequent discussion the main unit hole will be referred to as Borehole 1 and the toe hole as Borehole 2. Borehole 1, which was started on the 19th of October 1981 and finished on 27th of November 1981, was drilled to a depth of 27.4 m (90 ft.) while Borehole 2, drilled to 20.4 m. (67 ft.), was started on the 20th of April 1982 and finished on the 4th of May 1982.

Details of the drilling machine shown in Plate 3.1 and the bit are as follows:

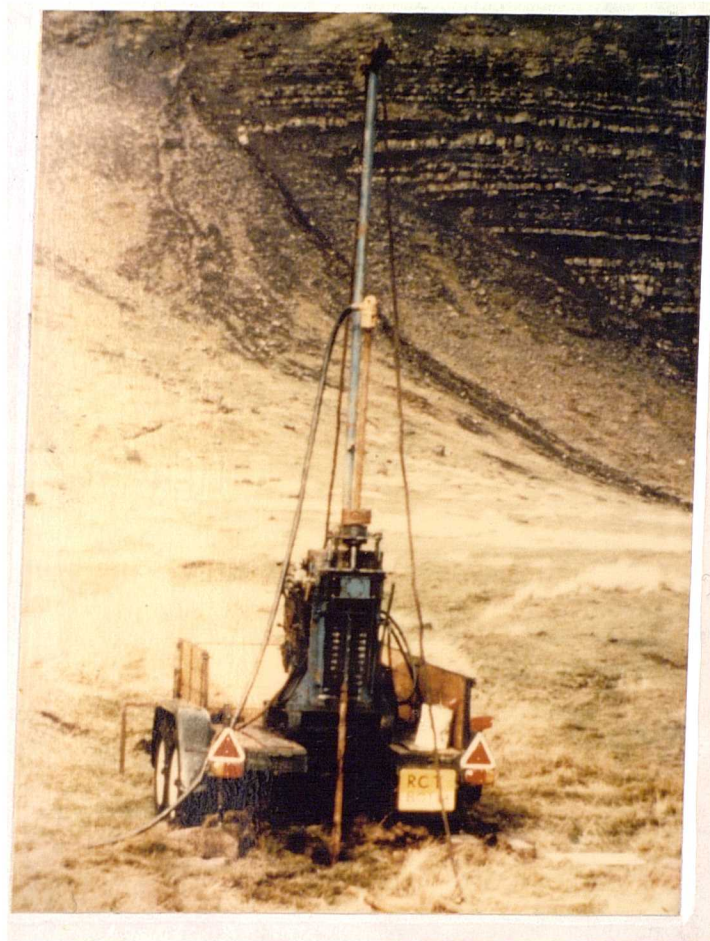


Plate No. 3.1 The drilling machine used for drilling Boreholes at Mam Tor.

Machine	English Drilling Company Mark 8. Diesel powered
Rotation speeds	80 to 300 rpm
Core barrel	Double tube NWX
Bit	Diamond J.K.S.
Orientation	Vertical
Available bits	NX size 2½ inch and BX size 1½ inch.
Slush pump	Capacity up to 1000 gal/hour.

i. Borehole -1-

Drilling commenced with an NX(2.½" diameter) bit which was advanced in 3.05 m (10ft.) runs. The casing was advanced this distance at the end of each run. Continuous waterflush was used during drilling. The hole was extended to a depth of 12.8 m. (42ft.) but since, as shown in the log in Fig. 3.1 A, no material had been recovered it was decided to abandon this hole and begin a new one a few feet away. This time the amount of water flush was greatly reduced. Some material was recovered during this drilling as indicated by the log in Fig. 3.1B. This hole was advanced to a depth of 9.4 m (31 ft.), but due to the casing jamming in the hole, the drilling rig was moved back to the first hole which was continued past 12.8 m (42ft.) down to 27.4 m (90ft.) using BX (1½") sized bit with water flush. The casing was advanced for each run of core as shown in the log, Fig. 3.1 A. Section 3.2.2 includes the description of core.

ii. Borehole -2-

As shown in Fig. 3.2 the NX (2½") bit with water flush was used. Initially drilling continued to a depth of 6.4 m (12ft.) and the casing was driven to this depth. No material was recovered over this section. Drilling increased the depth to 13.7 m (45ft.) and the casing was advanced to a depth of 9.1 m (30ft.) Unfortunately due to ground collapse, it was necessary to re-drill from 9.1 m. (30ft.) and continued to 13.7 m (45ft.) after which the casing was driven to 12.2 m (40ft.). Fragments of silty sandstone and shale were recovered from this

Fig. 3 . 1 A Core Description of Borehole 1 at Mam Tor (main unit)

Site: Mam Tor - main unit					Core Barrel Design and Bit: Double tube NX and BX Bit - Bort Diamond JKS	Borehole No. 1		
Machine: English Drilling						Description of Core	Casing Level	Barrel Level
Drilling and Casing Progress	Solid Core Recovery	Fracture Per metre	Fracture Orientation	Bedding and Lamination Orientation				
casing size N								
5 core size 2 1/2					The shale cutting washed by water	10		
10 water flush								
15								
20 1st. run							20	
25			←	←	CW - HW dark grey with orange staining, soft containing mica flakes. HW, grey medium to coarse grained, strong sandstone.		23	
30							29	
35					Fragment of sandstone and shale. HW, grey, coarse grained with visible quartz, strong and oxidized sandstone. CW, dark grey with orange stained, soft shale.			
40							41	
45			↗	←	Fragment of sandstone and shale with sandstone core. HW, dark grey with orange staining and redish brown along fracture surfaces, coarse grained, strong micaceous sandstone. CW. black with orange staining, soft, fissile shale containing mica flakes.			
50					Fragment of shale, sandstone and siltstone. HW, dark grey with orange staining, soft laminated shale containing mica flakes. HW, grey, coarse and fine with visible quartz grain, strong to moderately strong laminated sandstone and siltstone containing clay lenses.			
55			←	←			60	
60			<	<	HW, light grey with orange staining, medium to fine grained strong micaceous sandstone and siltstone. HW to CW dark, grey soft shale.		60	
65			<	↖	Fragment of shale with a little sandstone and pieces of sandstone core. HW, dark grey with orange to red staining, soft shale with a distinct layering oriented at 25 - 30° to horizontal. HW, grey, medium to coarse grained with visible feldspar grains, strong sandstone containing mica flakes.			
70			↖	<			70	
75					Fragment of shale and siltstone. CW, dark and light grey, soft laminated shale containing mica flakes. CW grey, generally fine grained but with graded bedding, moderately weak siltstone.		75	
80			<	<	Fragment of shale and siltstone and siltstone core. CW - HW, dark grey with orange staining, soft shale. HW, grey with orange staining on bedding plane, fine grained, strong, laminated micaceous siltstone. Fragment of siltstone and shale in clay matrix.		80	
85								
90		10 3	↖	↖	EW, dark grey to nearly black, weak, fissile and laminated shale. Lamina occur at 0.5 mm. interval and the beds nearly horizontal. Some joints appear to dip at 10° to horizontal and others are nearly horizontal, pyrite crystals occur on the joint surfaces.			
							85	
							90	

Borehole depth : 99 ft. (27.4 m.)
Casing depth : 80 ft. (24.0 m.)

↖ 80 - 90°
↙ 60 - 80° w. r. t.
< 30 - 60° vertical depth
< 0 - 30°

Weathering State

F : Fresh
FW : Faintly weathered
MW : Moderately weathered
HW : Highly weathered
CW : Completely weathered
RS : Residual soil





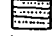
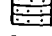
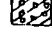
-  Fragments
-  Shale
-  Siltstone
-  Sandstone
-  Laminated Siltstone
-  Laminated Sandstone
-  Fragments in clay matrix

Fig. 3.1 B Core Description of Borehole 1a at Mam Tor (main unit)

Site: Mam Tor		main unit			Core Barrel Design and Bit: Double tube NX Bit - Bort Diamond JKS		Borehole No. 1a	
Machine: English Drilling								
Drilling and Casing Progress	Solid Core Recovery	Fracture Per metre	Fracture Orientation	Bedding and Lamination Orientation	Description of Core	Casing Level	Barrel Level	Symbolic Log
Casing size N					CW, grey, medium to coarse grained micaceous sandstone. CW, dark grey in part orange stained, very soft shale containing mica flake.	6		
Core size 2½ Dry drilling 1 st. run				<			8	
2nd. run			<	<	CW - MW, fragment of sandstone and shale in clay matrix .		10	
3rd. run		1	<	<	HW, fragment, grey with orange staining, medium to coarse grained strong sandstone. Small pieces of CW, grey, very soft shale.		12½	
4th. run			<		HW, fragments of sandstone and shale, light grey, medium to coarse grained sandstone. CW - HW, dark grey, soft shale.		15	
5th. run				<	HW - CW, sandstone fragment mixed with clay slurry. Fracture surfaces show oxidation with orange staining. Also dark grey, soft fissile shale.		19	
6th. run					CW - HW, sandstone fragment oxidized along fracture surface in clay.		20	
Bort Diamond Bit used					Fragment of shale with one piece of sandstone. CW - HW, dark grey with orange staining, soft shale containing mica flakes. HW, grey, medium to coarse grained, strong sandstone. Drilling was stopped due to the jammed of casing in the borehole.			
7th. run							31	

Borehole depth: 31 ft. (9.5 m.)
Casing depth : 6 ft. (1.8 m.)

± 80 - 90°
∠ 60 - 80°
< 30 - 60°
< 0 - 30°
w.r.t.
vertical depth

Weathering State

F : Fresh
FW : Faintly weathered
MW : Moderately weathered
HW : Highly weathered
CW : Completely weathered
RS : Residual Soil



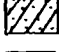

 Sandstone
 Shale
 Sandstone fragments in clay matrix
 Shale fragments in clay matrix

Fig. 3.2 Core Description of the borehole 2 at Mam Tor (Toe).

Site: MAM TOR - Toe		Core Barrel Design and Bit: Double tube NX. Bit - Bort diamond JKS			Borehole No. 2			
Machine: English, drilling		Description of the core			Casing Level	Barrel Level	Symbolic Log	
Drilling and Casing Progress	Solid Core Recovery 20% 40% 60% 80%	Fracture per metre	Fracture Orientation	Bedding and Lamination Orientation				
5 10 1st run Diamond Bit with 3 heads. Casing size N						12	12	
15 2nd run Core size 2 1/8 inch		2	✓	<	Sandstone core with fragments of sandstone, siltstone and shale MW-HW grey medium to coarse grained, strong, micaceous sandstone with oxidized joint and fracture surfaces, containing a lenses of shale. Also highly weathered, black soft shale.		17	
20 3rd run				<	Fragment of sandstone, shale and siltstone. HW grey coarse and fine grained moderately weak to moderately strong sandstone. MW dark grey soft shale. HW fragment of grey, fine grained, moderately weak micaceous siltstone,		22	
25 30 35 4th run		2	✓	<	Fragments of sandstone and shale totalling 190 mm. HW grey with yellowish brown stained joints, coarse grained strong micaceous sandstone. HW grey, very fine grained micaceous siltstone containing mica flakes. HW dark grey, thinly laminated soft fissile shale and HW black with orange staining soft micaceous shale.		30	
40 45 5th run				<	Holed re-drilled from 9.1 m. to 13.7 m. (30ft to 45 ft). MW dark grey with yellowish brown oxidized fracture surfaces, medium to coarse grained, micaceous sandstone, containing a lenses of shales with small clasts of fine grained sandstone. Fragments of alternating micaceous sandstone and shale. The return water was distinctly green in colour with oily smell.		40	
50 6th run					Fragments of FW - MW black with orange staining, weak, fissile shales. Few small fragments of sandstone.		50	
55 60 65 70					Very soft, muddy material with a high specific gravity and a very small fragments of highly weathered black, soft, highly fissile shale forming a plug.		52	

Weathering State

Borehole Depth: 67 ft. (20.4m.)
Casing Depth: 50 ft. (15.0m.)

± 80 - 90
✓ 60 - 80
< 30 - 60
< 0 - 30
w. r. t.
vertical depth

F: Fresh.
FW: Faintly weathered.
MW: Moderately weathered
HW: Highly weathered.
CW: Completely weathered.
RS: Residual Soil.

- Fragments
- Shale
- Siltstone
- Sandstone
- Laminated Siltstone
- Laminated Sandstone
- Plug

section. At depth of 13.7 m (45ft.) the return water was distinctly green in colour and oily smell was noticed.

Drilling was then continued to a depth of 16.7 m. (55ft.) and the casing was advanced to 15.2 m. (50ft.) The last run advanced the hole to a depth of 20.4 m. (67ft.). The description of core is including in Section 3.2.2.

3.2.2 Core Description

The description of core will be carried out with reference to Figs. 3.1A and B and 3.2 which include the abbreviated logs shown here in brackets. Each part of the description is headed by the depth range and thickness of the unit in question.

i. Borehole 1.

0 - 2.4m. 2.4m. (0 - 8ft. 8ft.)
(completely weathered grey, medium to coarse grained Micaceous sandstone. Completely weathered, dark grey in part orange stained, very soft shale containing mica flakes).

The first 2.4m. (8ft.) contain small fragments of sandstone and shale. Including completely weathered grey medium to coarse grained, micaceous sandstone and completely weathered, dark grey and very soft shale with flakes of mica and orange staining along fractures.

2.4m. - 3m. 0.6m. (8ft. - 10ft. 2ft.)
(Completely to moderate weathered fragments of sandstone and shale in clay matrix).

Completely weathered, dark grey and in parts brown stained, very soft shale with flakes of mica, some orange brown ring shaped patches.

Moderately weathered, dark grey, strong sandstone and medium to coarse grained micaceous sandstone containing lenses of dark grey clay. The bedding surfaces dip at about 45° in the vertical core.

Completely weathered dark grey with brown staining and orange patches, very soft shale with flakes of mica.

Moderately weathered, grey with pinky colouration along the fracture surfaces, strong sandstone with flakes of mica. A zone of oxidation up to 10mm. wide is apparent.

Mixed fragments of sandstone and shale with moderately weathered yellowish to grey with bright orange staining covering some faces, strong micaceous sandstone and completely weathered dark grey with bright orange staining, soft shale.

3m. - 3.8m. 0.8m. (10ft. - 12.5ft. ... 2.5ft.)
(Highly weathered, fragmented, grey with orange staining, medium to coarse grained, strong sandstone coated with clay material. Small pieces of completely weathered, grey, very soft shale).

Highly weathered, grey with orange staining, medium to coarse grained, strong sandstone with three small fractures.

Completely weathered, dark grey or orange to almost purple very soft shale fragments.

A mixture of small fragments of highly weathered light grey, coarse grained, non laminated, micaceous sandstone and completely weathered, dark grey, soft, laminated shale.

3.8m. - 4.5m. ... 0.7m. (12.5ft. - 15ft. ... 2.5ft.)
(Highly weathered fragments of sandstone and shale. Light grey, medium to coarse grained sandstone coated with clayey material and completely to highly weathered dark grey soft shale).

Highly weathered, light grey, medium to coarse grained, micaceous sandstone containing clay patches.

Highly weathered, dark grey, in part stratified light grey and dark grey, soft shale with almost horizontal bedding planes about 2mm. apart.

Four pieces of highly weathered grey, medium to coarse grained, strong, micaceous sandstone with clay patches about 5mm. length. Bedding planes dip about 60° to horizontal with a slump structure affecting the bedding plane, and oxidation along the boundary of the slumped material. Another steep bedding plane of approximately 75° to horizontal separates a band of medium grained material from coarser rock above and below it.

Completely to highly weathered, dark grey with orange staining, very soft shale fragments in a clay matrix.

4.5m. - 5.8m. ... 1.3m. (15ft. - 19ft. ... 4ft.)
(Highly to completely weathered sandstone fragment mixed with clay slurry. Fracture surfaces show oxidation with orange staining. Also dark grey, soft, fissile shale).

Completely to highly weathered, grey with purplish staining, medium to coarse grained, strong micaceous sandstone with oxidized surface. This sandstone is underlain by highly weathered, dark grey with some oxidation on partings, soft, fissile shale.

Small fragments of completely weathered, pinky grey with some orange staining, medium to coarse grained with occasional quartz grain, moderately weak sandstone with a light pinky grey clay matrix.

5.8m. - 6.1m. ... 0.3m. (19ft. - 20ft. ... 1ft.)
(Completely to highly weathered sandstone fragment oxidized along fracture surfaces in clay matrix).

Highly weathered, grey, medium to coarse grained, moderately weak sandstone. One piece of sandstone within this part is surrounded by a completely weathered, grey, weak oxidized sandstone in a clay matrix.

Moderately weathered, grey, medium grained very strong, micaceous sandstone with oxidized fracture surfaces.

6.1m. - 9.4m. ... 3.3m. (20ft. - 31ft. ... 11ft.)
(Fragments of shale with one piece of sandstone. Completely to highly weathered, dark grey with orange staining, soft shale containing mica flakes. Highly weathered, grey, medium to coarse grained, strong sandstone).

A piece of core 50mm. long of highly to completely weathered, dark grey with oxidation staining mainly orange, medium to coarse grained, strong sandstone.

Highly weathered dark grey, weak shale.

A piece of highly weathered, grey with purple staining along the bedding plane, medium to coarse grained, strong sandstone. The bedding planes are inclined at about 30° to the horizontal.

Two pieces of highly to completely weathered, dark grey, soft shale containing mica flakes with small patches of oxidation on partings.

9.4m. - 12.8m. ... 3.4m. (30ft. - 42ft. ... 12ft.)
(Fragments of sandstone and shale. Highly weathered, grey, coarse grained with visible quartz. Strong and oxidized sandstone. Completely weathered, dark grey and orange stained soft shale).

Fragments 25 to 70 mm. long highly weathered grey, coarse grained, strong sandstone, extensively oxidized along partings.

Fragments 13-75 mm. long of completely weathered, dark grey with orange staining, soft shale.

A 343 mm. length of highly weathered grey with oxidation staining on some surfaces, medium to coarse grained, strong sandstone. The discontinues dip predominantly at 30° to horizontal.

A 343mm. length of highly weathered grey with oxidation staining on some surfaces, medium to coarse grained, strong sandstone. The discontinuities dip predominantly at 30° to horizontal.

A 127mm. long piece of highly weathered, light grey with orange staining, medium to coarse grained strong sandstone containing mica flakes. Core cut by two horizontal fractures and an inclined one immediately underlain by 2-3mm. of highly weathered, dark grey, weak, thinly bedded shale.

Small pieces of highly weathered, grey with orange staining, medium to coarse grained, moderately strong sandstone containing a mica flakes.

12.8m - 14.6m. ... 1.8m. (42ft. - 48ft. ... 6ft.)
(Fragments of sandstone and shale with sandstone core. Highly weathered, dark grey with orange staining and reddish brown along fracture surfaces, coarse grained, strong, micaceous sandstone. Completely weathered, black with orange staining, soft, fissile shale, containing mica flakes).

Fragments of highly weathered dark grey with orange staining with reddish brown fracture surfaces, coarse grained, strong, micaceous sandstone. The discontinuity surfaces are irregular.

Completely weathered, black with orange staining on surfaces, soft, fissile shale containing mica flakes.

Core 150mm. long of highly weathered, grey, medium grained, strong, laminated sandstone with surfaces irregularities filled with muddy material.

Core 50mm. long of highly weathered, grey, medium grained, strong, laminated sandstone.

Core 75mm. long of highly weathered, grey, medium grained, very strong, micaceous sandstone with unusually high specific gravity.

Aggregation of completely weathered black, soft shale fragments in a clay matrix.

14.6m. - 18.2m. ... 3.6m. (48ft. - 60ft. ... 12ft.)
(Fragments of shale, sandstone and siltstone. Highly weathered, dark grey with orange staining, soft, laminated shale containing mica flakes. Highly weathered, grey, coarse and fine grained with visible quartz grains, strong to moderately strong, laminated sandstone and siltstone containing clay lenses).

Fragments 25 to 38mm. long of highly weathered dark grey with orange to dark red staining along the laminations, soft, laminated, micaceous shale containing mica flakes up to about 1mm. across. The laminations lie at approximately 30° to horizontal.

Small pieces about 6mm long, of completely weathered, grey, soft, laminated shale in a clay matrix. The shale easily breaks along flat smooth laminae about ~~2~~ 2 to 3 mm thick.

Fragments of highly weathered, dark grey, soft, laminated, micaceous shale containing 0.5-1mm. long mica flakes with oxidized lamination surfaces which are inclined at 45° to the horizontal.

Fragments of highly weathered, grey, medium to fine grained, moderately strong, laminated, micaceous sandstone and siltstone with oxidation on exposed lamina surfaces.

Fragments of completely to highly weathered, dark grey with dark orange staining, soft, micaceous shale held in a clay matrix together with fragments of highly weathered, light grey with orange, moderately strong, laminated sandstone with an oxidized bedding plane at 20° to horizontal. The clay matrix includes mica flakes 1mm. across.

Highly weathered, grey, fine to medium grained, moderately strong, laminated, fissile silty sandstone. with high specific gravity containing clay lenses and fractures at 60° to the horizontal and oxidized bedding planes dipping at approximately 30°.

Broken core fragments of completely weathered, light grey, medium to fine grained, moderately strong sandstone and siltstone.

Small fragments of completely weathered dark grey with orange staining, soft, micaceous, laminated shale with mica flakes approximately 1mm. across.

18.2m. - 18.9m. ... 0.7m. (60ft. - 62ft. ... 2ft.)
Highly weathered, light grey with orange staining, medium to fine grained, strong, micaceous sandstone and siltstone containing mica flakes. Highly to completely weathered fragments of dark grey, soft, micaceous and laminated shale).

Fragments 25-38mm. long of highly weathered, grey, fine grained, moderately weak, laminated siltstone containing mica flakes. The lamina are 0.5 to 1mm. thick and dip at about 45° to the horizontal.

Small fragment of highly weathered, light grey with orange staining on fracture surfaces, medium grained, strong sandstone.

Pieces of core 63, 38, 144 and 76mm. long of highly to moderately weathered, grey with very little orange staining on the fracture surfaces, fine to coarse grained with visible feldspar grains and mica flakes, strong sandstone containing some clay lenses. The bedding lies at approximately 45° to the horizontal. Colour variation evidence of graded bedding.

18.9m. - 21m. ... 2.1m. (62ft. - 69ft. ... 7ft.)
(Fragment of shale with a little sandstone and pieces of sandstone core. Highly weathered dark grey with orange to red staining, soft shale with a distinct layering oriented at 25-30° to the horizontal. Highly weathered, medium grey, medium to coarse grained with visible feldspar grains, strong sandstone containing mica flakes).

Highly weathered, dark grey with orange to red staining along some surfaces, other fracture surfaces are light grey, soft to weak laminated shale enhanced by parallel fractures at 25-30° to horizontal.

Pieces 25 to 50mm. long of highly weathered, grey, medium to coarse grained with visible feldspar and mica flakes, strong sandstone.

Pieces of core 100, 140, 89, 82mm. long forming a total length of 411mm. comprising highly weathered light and medium to dark grey or occasionally very dark grey to grey-black with orange and red staining on a steeply dipping joints, coarse and in parts fine grained, strong sandstone containing micaflakes about 1mm. across and feldspar. The bedding is oriented at 45° to the horizontal. The fractures are heavily oxidized and the larger one is apparently filled with shale pieces of approximately 0.5mm. in size embedded in a clay matrix.

Highly weathered, dark grey with oxidized surfaces of yellowish orange and red to purple, soft, laminated shale with abundant small mica flakes. The laminae are oriented at approximately 5-10° to the horizontal and are about 1mm. thick. Breakage along plane parallel to the layering exposes smooth flat heavily oxidized surfaces. There are also joint surfaces perpendicular to the laminae.

Fragments of highly weathered, light grey and dark grey, medium to coarse grained, strong sandstone containing mica flakes and feldspar.

Small pieces of shale and clay material adhere to the surfaces which are probably joints surfaces inclined at 70°-90° to horizontal.

21.0m. - 23.1m. ... 2.1m. (69ft. - 76ft. ... 7ft.)
(Fragments of shale and siltstone. Completely weathered, dark and light grey, soft laminated shale containing mica flakes. Completely weathered, grey, generally fine grained but with graded bedding, moderately weak siltstone).

Completely weathered dark and light grey (probably depending on the amount of organic material,) soft, laminated shale, containing mica flakes. The laminae are 0.5-1mm. thick oriented at about 5° to the horizontal and have oxidized surfaces.

Fragments 13mm. to 25mm. long of completely weathered grey, fine grained and graded bedded, moderately weak siltstone in which the bedding dips approximately 30° to horizontal. Also containing oxidized surfaces .

23.1m. - 25.9m. ... 2.8m. (76ft. - 85ft. ... 9ft.)
(Fragments of shale, siltstone, and siltstone core. Completely to heavily weathered, dark grey with orange staining, soft shale. Highly weathered, grey with orange staining on bedding planes, fine grained, strong laminated micaceous siltstone. Fragments of siltstone and shale in a clay matrix).

A 700mm. long fragment of completely to highly weathered, dark grey with orange staining on flat surfaces, soft shale.

A piece of 900mm. long of highly weathered, grey with orange staining along the bedding planes, fine grained, graded bedded, laminated, micaceous siltstone in which mica flakes are visible. The laminae are inclined at approximately 45° to the horizontal. Also steeply dipping fractures with oxidation evident in the upper half.

Broken pieces approximately 13mm. long of highly weathered, grey, fine grained, moderately strong, laminated, micaceous non-oxidized siltstone in a clay matrix.

25.9m. - 27.4m. ... 1.5m. (85ft. - 90 ft. ... 5ft.)
(Faintly weathered, dark grey to nearly black, weak fissile and laminated shale. Laminae occur at 0.5mm. intervals and the beds are nearly horizontal. Some joints appear to dip at 10° to horizontal and others are nearly horizontal. Pyrite crystals occur on the joint surfaces).

A 970mm. long pieces of core, illustrated in Plate 3.2 comprising faintly weathered, dark grey to nearly black weak, highly fissile and laminated shale. The laminae are 0.5mm. thick and the bedding is nearly



Plate No. 3.2 Unweathered Edale Shale from between 25.9m. and 27.4m. (85-90ft.) in Borehole 1, at Mam Tor.

horizontal. The rock is highly jointed and the joint appear to dip at 10° to the horizontal. Some joints are nearly horizontal and as indicated in Plate 3.3 crystals of pyrite occur on some surfaces. In addition a network feature of a very fine bands of gypsum can be observed in Plate 3.4.

The foregoing description relates to the longest piece of unbroken core obtained during the drilling of this borehole. It is believed that the difference in the appearance of the core below a depth of 25.9m. (85ft.) is due to the presence of the slip surface. Unfortunately more conclusive evidence of the presence of the slip surface including slickensides and other effects were not observed but the dramatic change in the dip of the beds would suggest that undisturbed ground has been penetrated.

The poor recovery of core from the zone of material above the slip surface is attributable to its highly weathered state and the presence of sandstone blocks in a matrix of degraded shale or clay. Generally the barrel became blocked with compacted clay that prevented core from entering. The lower surface of this clay plug was generally polished by rotation. Generally above this solid sandstone core was recovered. This material was smeared with clayey material and in some cases, fragments in clay slurry were also recovered. It seems likely that at the beginning of the run the material was cored and harder fragments retained in the barrel, but on encountering very soft material it was driven into a barrel until it jammed.

ii. Borehole 2.

0 - 3.6m. ... 3.6m. (0 - 12ft. ... 12ft.)

A roller bit was used, so no samples of rock were obtained. The return water carried black shale cuttings.

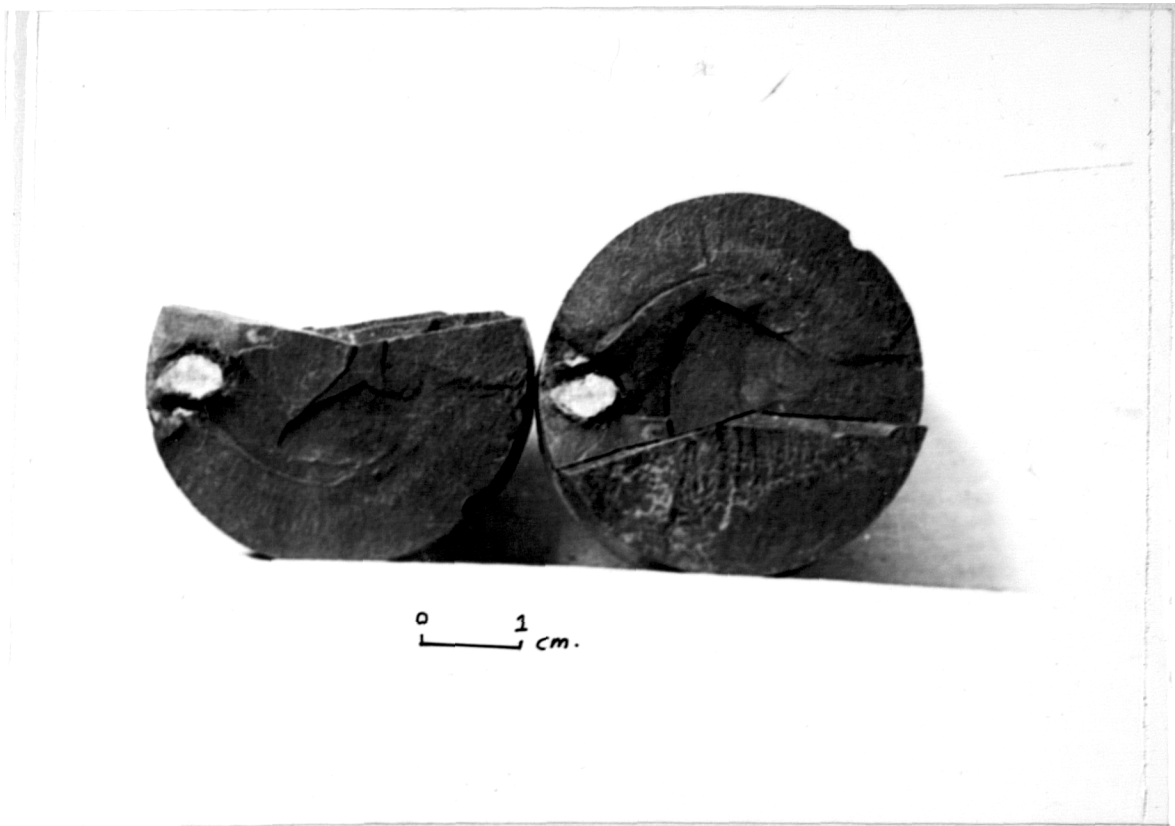


Plate No. 3.3 Unweathered Edale Shale from borehole 1, 25.9 to 27.4 m. (85-90ft.), note the pyrite crystal and jointing.

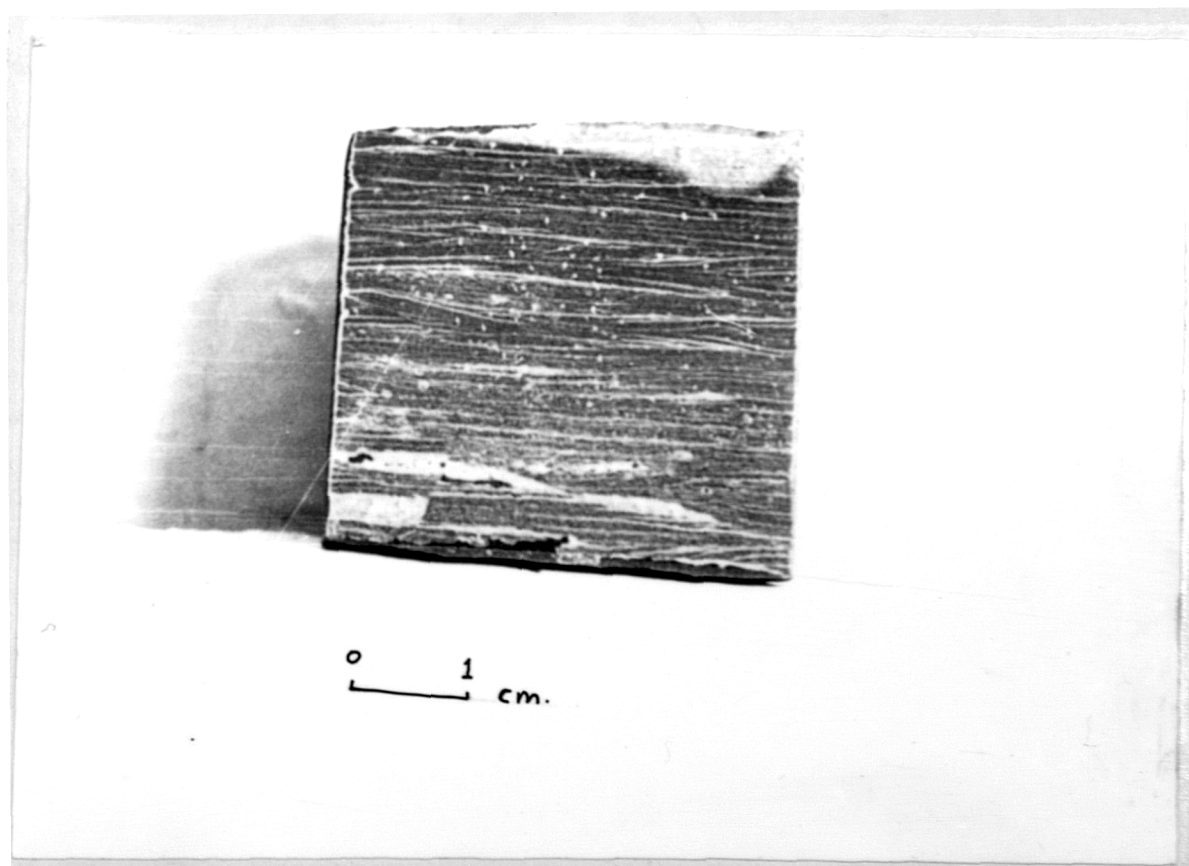


Plate No. 3.4 Gypsum in fractures in Edale Shale from depth of 25.9 m. (85ft.) in Borehole 1.

3.6m. - 5.2m. ... 1.6m. (12ft. - 17ft. ... 5ft.)
(Sandstone core with fragments of sandstone siltstone and shale. Moderately to highly weathered, grey, medium to coarse grained, strong, micaceous sandstone with oxidized joint and fracture surfaces containing lenses of shale. Also highly weathered, black, soft shale).

Moderately to highly weathered, grey, medium to coarse grained, strong, micaceous sandstone with mica flakes and quartz grains clearly visible. Intersecting and open fractures some with dark green surfaces surrounded by yellowish brown material. Otherwise the joint surfaces are oxidized and one dips at 80° to the horizontal.

A fragment 140mm. long of moderately to highly weathered, grey with yellowish brown fracture surfaces, medium to coarse grained, strong, micaceous sandstone containing mica flakes and quartz. An open fracture dips at about 45° to the horizontal.

A 230mm. length of moderately weathered, dark grey with yellowish brown parts and in the lower 150mm. reddish brown fracture surfaces, medium to coarse grained, micaceous sandstone containing mica flakes, quartz, and some lenses of shale ranging in thickness from 2mm to 13mm. The rock is affected by an open joint at the top which becomes closed towards the base.

A length of 210 mm. comprising a mixture of fragments of sandstone and shale in a brownish yellow clay matrix. Highly weathered, black, soft shale fragments and moderately to highly weathered, grey, medium to coarse grained, strong micaceous sandstone containing coarse grained mica flakes.

Moderately weathered, greenish with yellowish brown oxidized bedding planes, very fine grained, laminated, moderately strong siltstone. A 1mm. thickness of moderately to highly weathered, dark grey to black, soft, micaceous shale at the base of the siltstone fragments.

A fragment 228mm. long of highly weathered, dark grey with brown yellowish oxidized surfaces along the joint surfaces, fine grained, strong, micaceous sandstone containing obvious mica flakes. The joint surfaces dip at 15° to the horizontal.

A 133 mm. length of highly weathered dark grey with yellowish oxidized joint surfaces, very fine grained, moderately weak, micaceous siltstone.

5.2m. - 6.7m. ... 1.5m. (17ft. - 22ft. ... 5ft.)
(Fragments of sandstone, shale and siltstone. Highly weathered, grey, coarse and fine grained, moderately weak to moderately strong sandstone. Moderately weathered, dark grey, soft shale. Highly weathered fragment of grey, very fine grained, moderately weak micaceous siltstone).

A 790mm. length of highly weathered, grey, coarse grained, moderately weak sandstone.

Highly weathered, grey, with yellowish brown oxidized fracture surfaces, fine grained, moderately strong sandstone.

Fragments of moderately weathered, dark grey, soft shale with numerous sub-horizontal joints.

One fragment of highly to moderately weathered, grey, very fine grained, moderately weak very micaceous siltstone.

Fragments amounting to 109mm. of highly weathered, grey, fine grained, moderately strong sandstone and highly weathered dark grey, soft shale in a muddy matrix.

6.7m. - 11.5m. ... 4.8m. (22ft. - 38ft. ... 16ft.)
(Fragments of sandstone siltstone and shale totalling 190mm. Moderately weathered, grey with yellowish brown stained joints, coarse grained, strong, micaceous sandstone. Highly weathered, grey, very fine grained, micaceous siltstone containing mica flakes. Highly weathered, dark grey, thinly laminated, soft, fissile shale and highly weathered black

with orange staining, soft, fissile, micaceous shale).

Moderately weathered, grey with yellowish brown joint surfaces, coarse grained with a white mineral which may be feldspar, strong, micaceous sandstone containing mica flakes. There are numerous small voids. At the top of these fragments there is 1-2mm. thickness of highly weathered, black, fissile, micaceous shale.

Highly weathered, grey with brownish yellow, very fine grained, moderately strong micaceous siltstone containing a mica flakes. The upper and lower ends of the fragments contain a 2mm. thickness of highly weathered, black, fissile, very soft, and very micaceous shale.

Highly weathered black, with orange staining along joint surfaces, soft, highly fissile, micaceous shale.

Highly weathered, grey with orange staining on fracture surfaces, coarse grained micaceous sandstone containing mica flakes and voids or small cavities.

Moderately weathered, grey with reddish brown fracture surfaces, very fine grained, laminated, moderately strong, micaceous, siltstone containing mica flakes and intersecting 45° dipping bedding planes and vertical joints.

11.5m. - 13.7m. ... 2.2m. (38ft. - 45ft. ... 7ft.)
(Hole re-drilled from 9.1m. to 13.7m.(30ft. - 45ft.).
Moderately weathered, dark grey with yellowish brown oxidized fracture surfaces, medium to coarse grained, micaceous sandstone containing lenses of shale with small clasts of fine grained sandstone. Fragments of alternating micaceous sandstone and shale. The return water was distinctly green in colour with an oily smell).

A 30mm. long piece of moderately weathered, dark grey, with yellowish brown joint surfaces, medium to coarse grained, micaceous sandstone containing mica flakes together with lenses of shale 48mm. long by 10mm. wide and 34mm. long by 1mm. wide. One of the lenses contains

a small cavity filled with fine grained white laminated sandstone. The core is terminated by a 5mm. thickness of high weathered, black, soft, highly fissile shale.

A 63mm. length of alternating sandstone and shale fragments. Highly weathered, light and dark grey, medium to coarse grained, strong laminated sandstone. The beds dip at approximately 45° to the horizontal. A small fragment of highly weathered, black with orange brown staining, soft highly fissile shale.

A piece 50mm. long of moderately to highly weathered, grey with yellowish brown surfaces, medium to coarse grained, strong micaceous sandstone in which the oxidized area is moderately weak with a white spots and voids. Also 63mm. of moderately weathered, grey, coarse grained, strong sandstone.

Moderately weathered, grey, fine to medium grained, strong, micaceous sandstone containing mica flakes with white spots and voids underlain by about 4mm. highly weathered black, soft, micaceous shale and moderately weathered grey and light grey banded fine grained, micaceous sandstone containing mica flakes. These beds dip at about 30° to the horizontal.

Fragments of sandstone and shale consisting of moderately weathered, dark grey and orange stained, coarse grained, strong, micaceous sandstone with mica flakes and small voids together with highly weathered black, soft, fissile shale.

Fragments of moderately weathered, dark grey, medium to coarse grained, strong, laminated, micaceous sandstone becoming completely weathered, soft grey with orange staining and yellowish brown surfaces, soft, fissile shale at the base.

13.7m. - 15.8m. ... 2.1m. (45ft. - 52ft. ... 7ft.)
(Fragments of faintly to moderately weathered, black with orange staining, weak, fissile shales with a few small fragments of sandstone).

Faintly to moderately weathered, black with orange staining and yellowish brown oxidized fractures surfaces, weak, fissile shale.

A few small highly weathered, grey medium to coarse grained, strong sandstone fragments.

15.8m. - 20.4m. ... 4.6 (32ft. - 67ft. ... 15ft.)
(Very soft, muddy material with a high specific gravity and a very small fragments of highly weathered black, soft, highly fissile shale forming a plug).

About 1.21m. plug of completely weathered, very soft, relatively high specific gravity muddy material shown in Plate 3.5. At the base of the core there are a few very small fragments of moderately weathered black, weak, highly fissile shale.

3.2.3 Installation of Piezometers

After the completion of the boreholes, Casagrande type standpipe piezometers were installed so that the elevation of the water table could be monitored. This type of piezometer was chosen in preference to pneumatic and hydraulic equipment due to its inherent simplicity and also its simplicity of installation and since measurements do not necessitate the use of air pressure or de-airing systems in the remote situation of this instrumentation.

The installation procedure adopted in the case of borehole 1 was as follows:-

- i. Before pulling out the casing, sufficient sand to make a plug 1.5m. long was tipped into the hole and allowed to settle. Sharp builders sand was used for purpose.
- ii. The depth of the top of the sand was measured by pumping the hole.
- iii. The piezometer was attached to sufficient tubing to reach sand at a depth of 24.3m. (80ft.). Thick walled plastic tube was used and all joints were

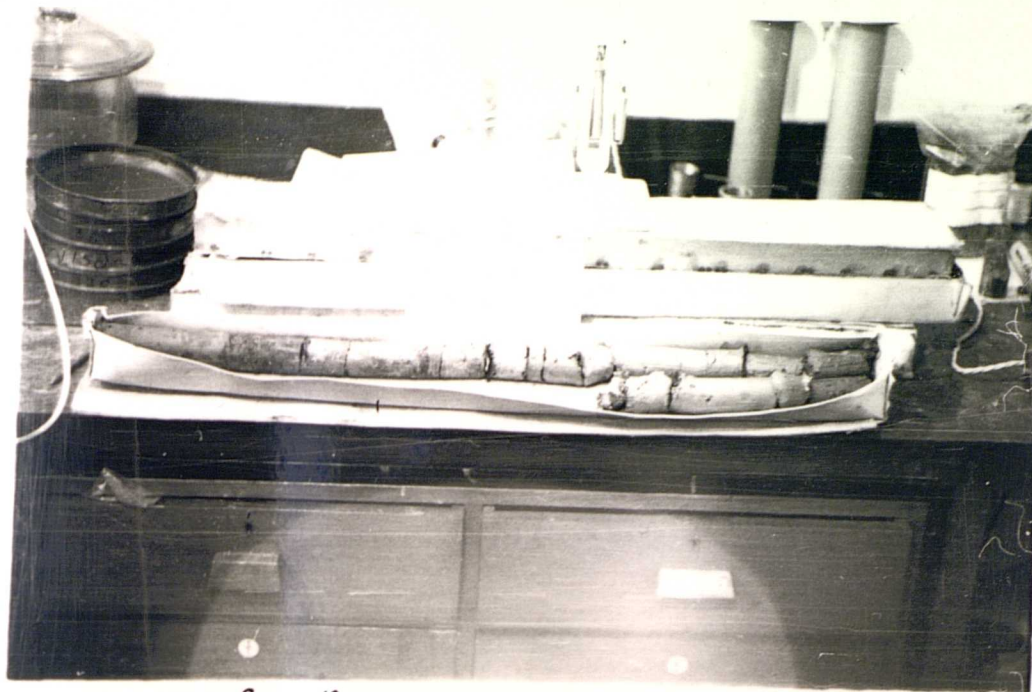


Plate No. 3.5 Borehole 2 material from a depth of 15.8 to 20.4 m. (52-67ft.).



Plate No. 3.6 Measuring the elevation of the water table at Mam Tor.

sealed with suitable adhesive. The piezometer and tube were lowered down the hole. More sand was dropped into the hole to form a 2m. filter around and above the piezometer tip.

- iv. Sufficient bentonite pellets to form a seal of about 1-2m. long above the sand were then introduced.
- v. The casing was withdrawn in stages.

Unfortunately, this procedure was not completely successful since the piezometer tube jammed in the casing. Attempts to prevent this from happening by holding the tubing down while pulling up the casing were only partially successful. Initially the piezometer was pulled up by one casing length of 3.05m. (10ft.) before it was realized that this was happening. Subsequently, problems arose with actually getting a purchase on the tube and as a result of this problem the piezometer was pulled up to a depth of 17.3m. (56.7ft.). Once the casing had been completely withdrawn it was clear that bentonite had blocked the casing and the projecting tube joint unions were not able to slide through this material.

- vi. A sand and cement slurry was added to the hole until it reached the top (See Fig. 3.3).
- vii. A cap was placed on the top of the tube to prevent surface water from flowing down the tube. At the ground surface a locking plate was installed to protect the top of the access tube.

In view of the problems which had been experienced during the installation of the piezometer in Borehole 1 the procedure was modified for Borehole 2. The hinged wing devised shown in Fig. 3.4 was made to fit just above the piezometer tip. The wings fold against the tube when it is being pushed down the hole but dig into the sides if it is pulled up. The sand below the piezometer tip was added until it reached a depth of 2-1.5m. and the casing was withdrawn to this level after which piezometer

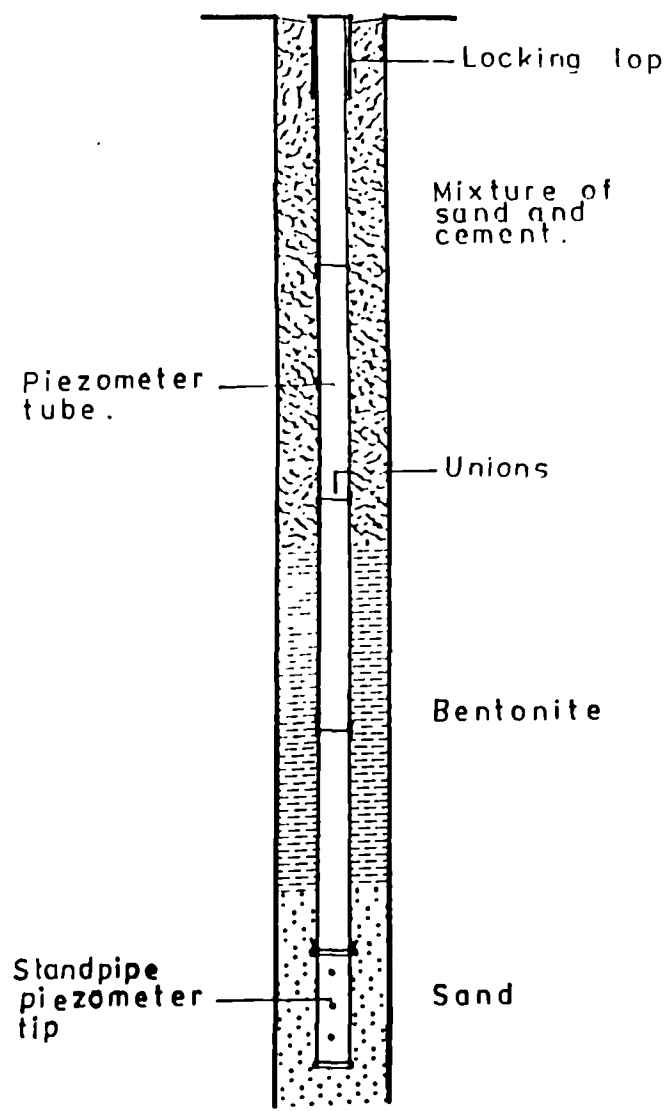


Fig. 3.3 Installation of piezometer.

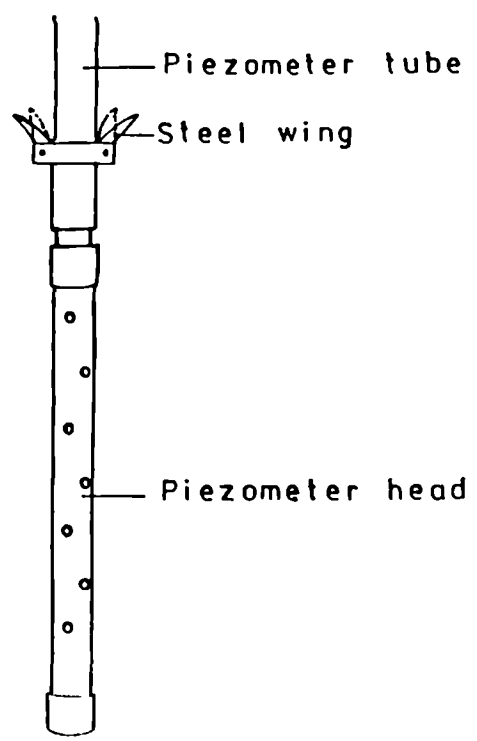


Fig. 3.4 Modification to piezometer.

tube assembly and hinged wing device were lowered to this depth. About 1m. of sand was added and the casing was withdrawn 3.05m. (10ft.). Following this bentonite was mixed with water and this slurry was tremied to the base of the hole using the drill flush pump. Withdrawal of the rest of the casing resulted in an upward movement of the piezometer of only 75mm. As previously the hole was filled with a sand cement slurry and a locking plate set in place.

The depth of water table was measured using an electric dipmeter (Geotechnical Instruments Ltd.) which emits a tone when a probe lowered on a calibrated cable touches the water. (See Plate 3.6).

3.3 Measurements of Movements at Mam Tor.

Since Mam Tor landslip is still active, movements were measured in order to determine the rate and the style of instability. Metal pins 19mm. diameter of a different lengths were used. The main reason for using these pins was that they are not liable to be noticed and disturbed by vandals. Also National Park Authority was anxious to minimize disturbance of the environment. The pins were hammered into the ground at the locations shown in Fig. 3.5 which were chosen since they cover nearly the whole landslip area and could be seen from the stable station point. 17 pins of length 750mm., 600mm. and 300mm. were used depending on the depth of the soil. Where it became impossible to install a long pin, a shorter one was used. Nails were used along the road. A centre punch was used to punch a hole in the top of each survey point. An Electronic Distance Measurement (E.D.M.) apparatus was employed during the survey due to the resulting high accuracy and rapid survey compared with the theodolite and chaining method. The quoted accuracy is $\pm 5\text{mm}$ and 2×10^{-6} over distance. The basic method was measure the distance with the E.D.M. fixed on tripod with a theodolite at a stable station outside the influence of the slip

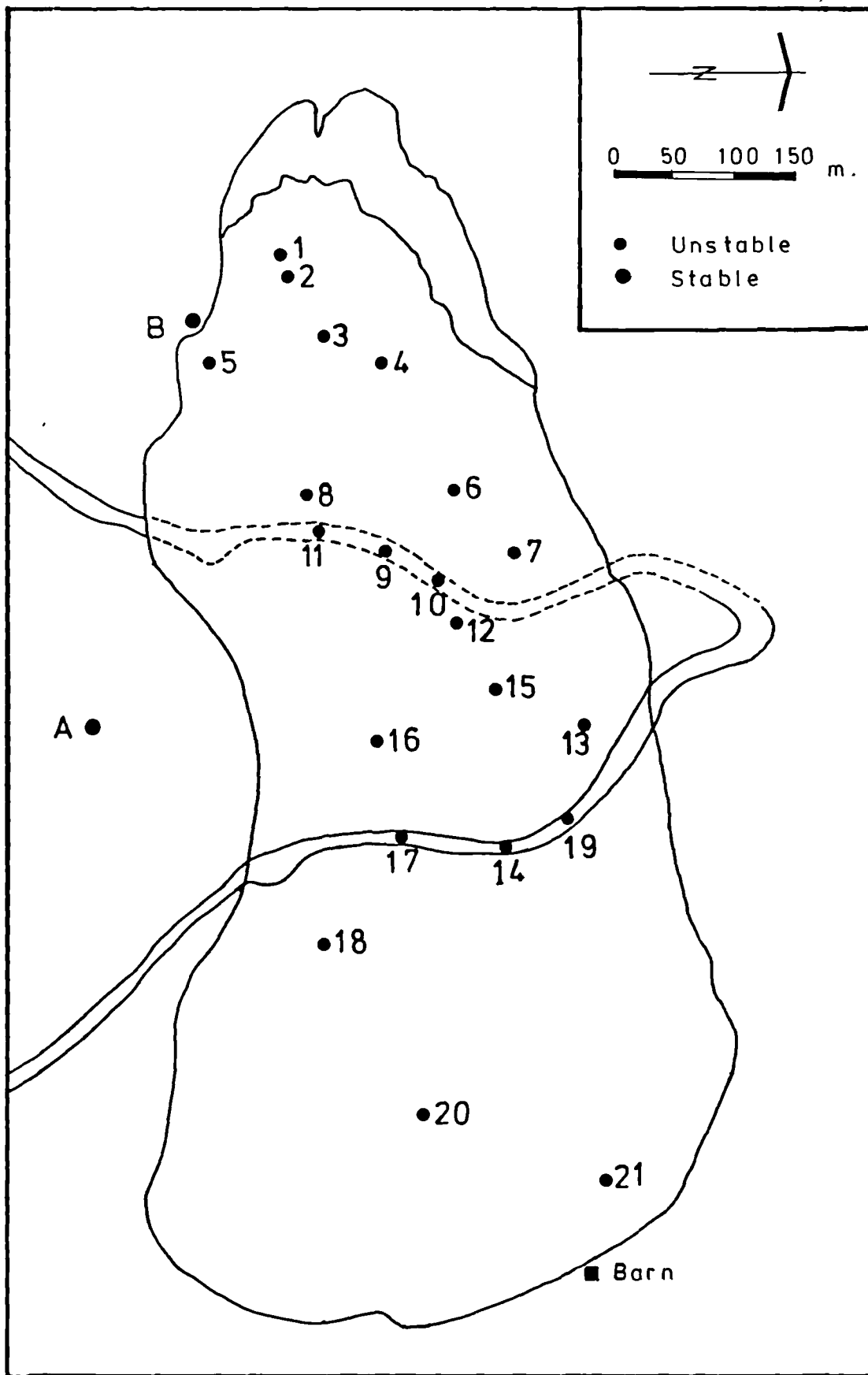


Fig. 3.5 Location of survey points at Mam Tor

area to the other pins in the slip area. A prism was set up on an adjustable plumbing rod in the centre punch hole on top of each of the pins.

Plate 3.7 shows the equipment and details of the Eldi 3 E.D.M. and TH2 theodolite used are given in Table 3.3. The measurements for each station consisted of the following observations:

- i. The horizontal angle measured with reference to the base line between station A and B (measured twice and averaged).
- ii. The vertical angle (Measured twice and averaged).
- iii. The slope distance (Measured twice and averaged).

In addition the height of the target above the pin was also recorded. The method entailed changing from an optical target for the angular measurement to a retro reflective prismatic one for the distances. To ensure the smooth running of the surveying, walkie talkies were employed to aid communications over the area of the landslide. The period of the survey was between October 1981 to May 1983, the survey was carried out regularly every month except when this was prevented by adverse winter weather.

3.3.1 Surveying

The general procedure for the survey was as follows:-

- i. The theodolite and Eldi 3 were assembled centred and levelled at fixed station A.
- ii. A survey target was centred and levelled on a tripod at the second fixed station B, and the horizontal and vertical angle were measured. The retro-reflective prism was mounted on this tripod and the slope distance measured. After this the survey target was put back on the tripod so that the survey could be closed back on to this station at the end of the survey or so that the reference base line could be checked during the remainder of the survey.
- iii. The work was done systematically over the stations being surveyed on slip area measuring the slope distance

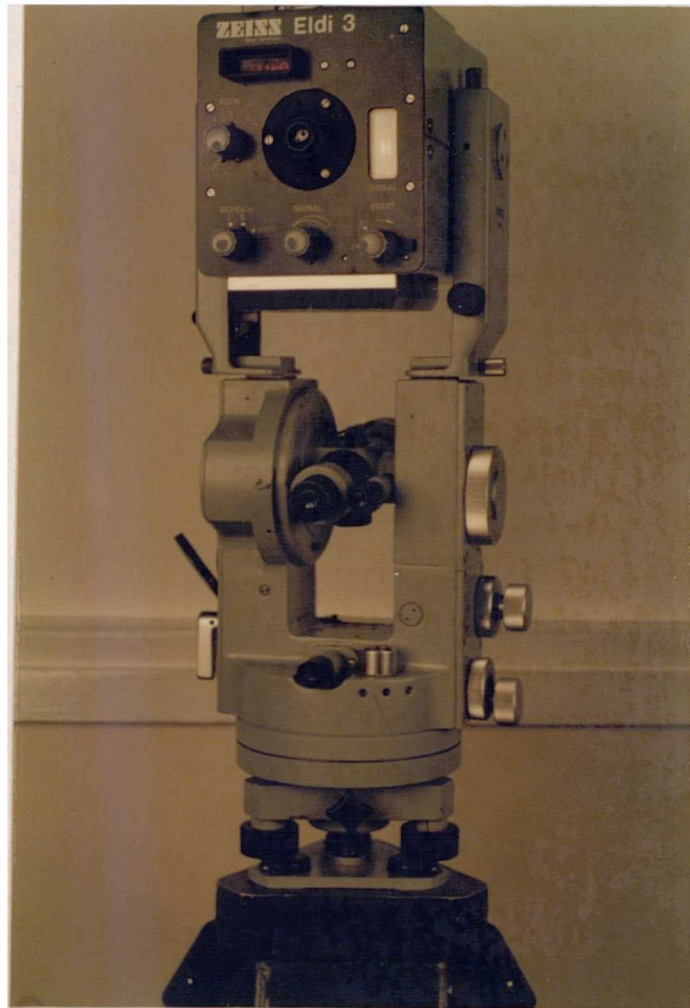


Plate 3.7 Eidi 3 EDM and TH 2 theodolite equipment used in the survey at Mam Tor.

Table 3.3 Details of the Eldi 3 and TH2 theodolite used in the survey of Mam Tor

ELDI 3 EDM

Manufacturer	Carl Zeiss Oberkochen
Range	With single prism 400m on range 1. With single prism 700m on range 2.
Measuring time	5 secs.
Accuracy	Range 1 $\pm 5\text{mm}$ } mean error of distance Range 2 $\pm 1\text{-}2\text{cm}$ } measured once.
Carrier name	Light (infra red) wavelength 910nm.
Frequency	150 KHz and 15 mHz
Display	6 digit.

TH2 Theodolite

Manufacture	Carl Zeiss Oberkochen
Least count	1 sec.
Type	Double circle microptic

by Eldi 3 and horizontal and vertical angle from theodolite at each station from fixed station A.

3.3.2 Calculation of Data.

The horizontal and vertical angles and the slope distance were calculated as follows:

i. The horizontal angle "θ" between the fixed station A and B and the other stations along the landslip area were calculated according to equation 3.1.

$$\theta = \theta_x - \theta_0 \dots\dots\dots 3.1$$

where: θ is the true horizontal angle between the base line A - B and any station along the landslip area.

θ₀ is the horizontal angle between A and B fixed station.

θ_x is the horizontal angle obtained from the theodolite on its station.

ii. The vertical angle α between the fixed station A and any station along the landslip area were calculated according to equation 3.2.

$$\alpha = 90 - \alpha_x \dots\dots\dots 3.2$$

where: α is the true vertical angle between the fixed station A and any station in the landslip area.

α_x is the vertical angle obtained from the theodolite.

iii. The horizontal distance between the fixed station A and any station in the slip area were calculated using equation 3.3.

$$H = S \times \cos\alpha \dots\dots\dots 3.3$$

where:

H, is the horizontal distance

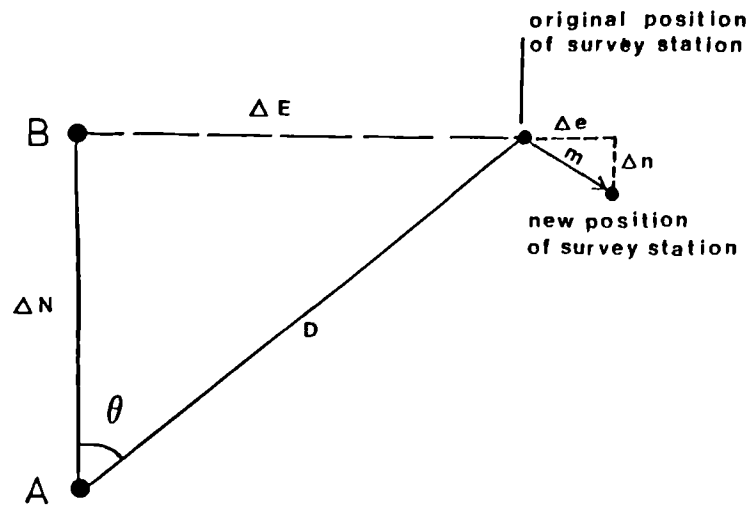
S, is the slope distance

α, is the true vertical angle.



3.3.3 Presentation of Data.

The distribution of the surveyed points over the area of the landslide is indicated in Fig. 3.5. The locations of these stations were fixed by positioning the fixed points on aerial photographs and then locating the other stations on the map of the landslide using coordinates determined from the true horizontal angle (θ) and the horizontal distance to the station (D) as shown in Fig. 3.6. The positions of the survey stations were checked on the topographic map by shooting bearings onto distance objects. A plan of the original positions of the survey station relative to the base line was plotted at a scale of 1:1000. Then the movements of individual survey stations were coordinated as a change from the original position expressed in terms of the horizontal angle and horizontal distance and plotted as a change in coordination (Δe , Δn) of the individual survey stations at a scale of 10:1 on the plan. The actual movement (m) of a particular survey station was then measured off this plan and is presented on the 1:5000 scale map shown Fig. 7.5. The coordinates were calculated for two periods of October 1981 to October 1982 and October 1982 to May 1983 as shown on Map Fig. 7.5 and Table 7.3 which give the total movement of stations over this period.



$$\Delta E = D \sin \theta$$

$$\Delta N = D \cos \theta$$

Where D is the horizontal distance between fixed station A and any station on the landslide area.

θ is the horizontal angle between the fixed station A and any station on the landslide area.

Fig. 3.6 The coordination of the horizontal angle for the location of stations and measurement of the amount of movement.

CHAPTER 4

SHEAR STRENGTH PARAMETERS FOR SOILS

4.1 Introduction

The strength of the soil may be defined as the resistance to continuous shear displacement developed either between soil particles or the material en masse. It occurs upon application of a tangential shear stress to a soil mass and is the maximum resistance mobilised to shear displacement work on the soil. Studies of shear strength by numerous investigators have been summarised by Jumikis (1965) who indicates that shear strength is composed of three main components.

- i. The structural resistance to displacement of soil because of interlocking of soil particles.
- ii. The frictional resistance to translocation between the individual soil particles at their points of contact.
- iii. Cohesive forces which occur between the surface of soil particles.

The usual forms of shear stress - shear deformation curves for soils are shown in Fig. 4.2a. According to Capper and Cassie (1969) and Scott (1969), Coulomb first suggested in 1733 that the shear strength of soil might be expressed in the form shown in Fig. 4.2b that is:-

$$\tau = c + \sigma_n \tan\phi \dots\dots\dots(4.1)$$

where:

- τ = Shear strength
- c = Cohesion of soil
- σ_n = Normal stress on shear plane
- ϕ = Angle of internal friction of soil

Since, typically soils can display a combination of types of strength or resistance to strain, it is convenient to consider three basic types of soil.

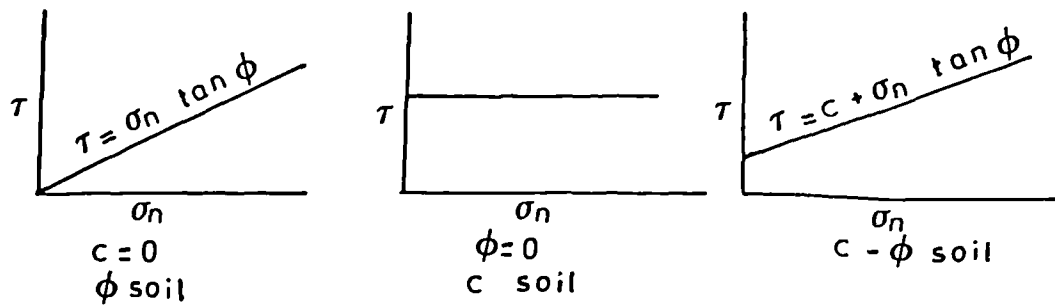


Fig. 4.1 Types of soil.

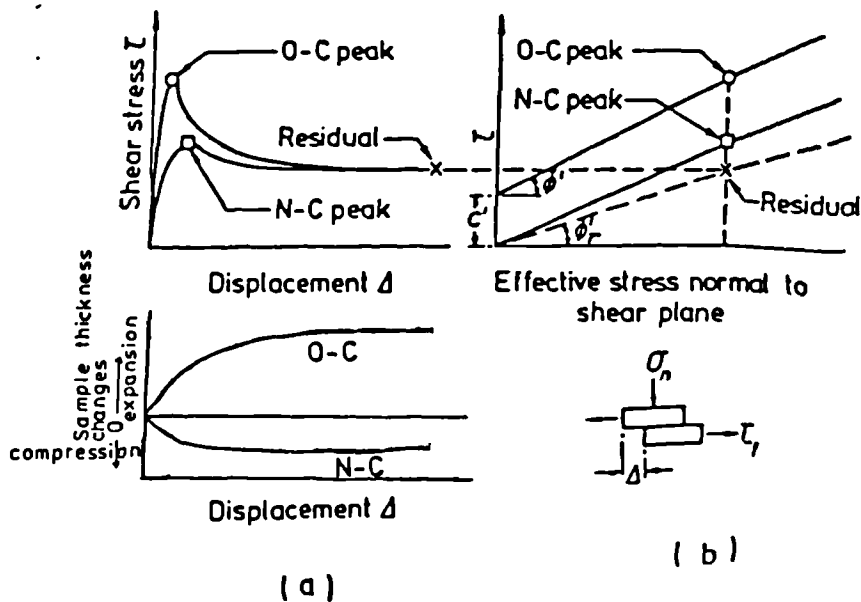


Fig. 4.2 Shear stress deformation and normal stress relationship for typical soil.

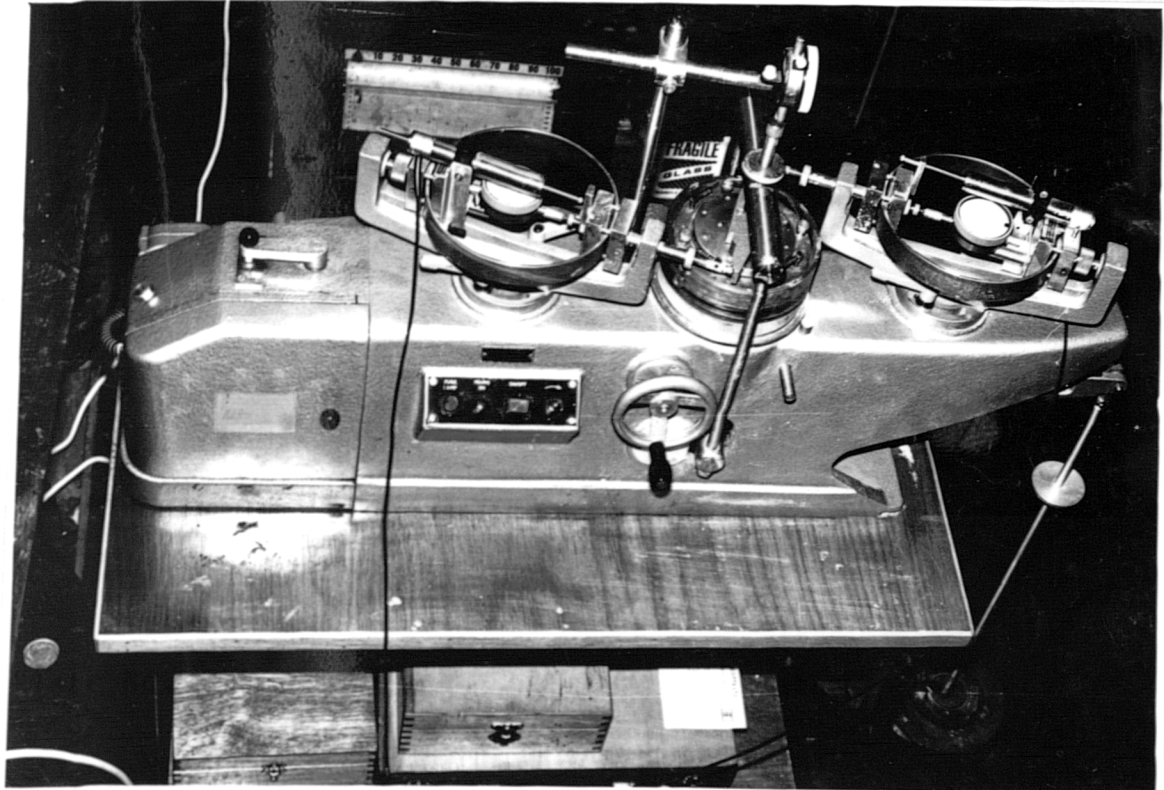


Plate No. 5.1 Bromhead ring shear apparatus.

- i. Frictional soils in which the strength is accounted for mainly by interparticle friction. Coarse grained soils in which most particles are greater in size than 0.06mm display frictional types of behaviour with little or no cohesive resistance (ϕ soil).
- ii. Cohesive soils in which the strength is accounted for mainly in terms of interparticle bonding forces. These soils are generally fine grained with particles less than 0.06mm across (c soil).
- iii. Soil which display combined cohesive and frictional strength (c - ϕ soil). These styles of behaviour will be considered with reference to Fig. 4.1.

In practical situations it is necessary to distinguish between total and effective stresses (See Scott, 1974). The voids between solid particles and soil are filled with fluid, either water or air or both, which can offer no resistance to static shear forces. Fluid can support normal pressures which constitute part of the stress (σ_n) in soil mass. During shearing volume changes give rise to changes of pore water pressure which effect the stress acting in the sample. For practical purpose it may be assumed that:

$$\sigma_n' = \sigma_n - u \dots\dots\dots(4.2)$$

- σ_n' = Normal effective stress.
- σ_n = Total stress.
- u = Pore fluid pressure.

The shear strength characteristic of soil may be expressed in terms of effective stress thus:

$$\tau = c' + (\sigma_n - u) \tan \phi' \dots\dots\dots(4.3)$$

$$\tau = c' + \sigma_n' \tan \phi' \dots\dots\dots(4.4)$$

where:

- c' = Cohesion of soil in terms of effective stress
- ϕ' = Angle of internal friction in terms of effective stress.

τ = Shear strength of soil.

Although equation 4.4 may be expressed graphically in Fig. 4.2b in fact shear strength defined in this way has no physical meaning in that the angle ϕ' or ϕ is not a true angle of friction. It is termed the coefficient of internal friction of the soil and represents increases in shear strength commensurate with increased normal stress on the failure surface (angle of shearing resistance). The parameter c' or c in Fig. 4.2b represents that part of shear strength which is independent of the normal stress value and is termed the apparent cohesion by Jumikis (1965) and Scott (1974). In Fig. 4.2b any point above the stress line represents a fail condition. While points below the line represent non-fail conditions.

4.1.1 Mohr-Coulomb Failure Criterion

Analysis of an arbitrary system of shear and normal stress acting on soil mass indicates that it may be resolved in to orthogonal system of stresses known as 'principal stresses' shown in Fig. 4.3a where:

- | | |
|--|--------------------|
| σ_1 = Major principal stress | Greatest Magnitude |
| σ_2 = Intermediate principal stress | |
| σ_3 = Minor principal stress | Smallest Magnitude |

The analysis also shows that no shear stresses act in the direction of the principal stresses. It is simple matter to calculate the resulting shear - and normal - stresses acting within the soil mass. In practical terms it is generally acceptable to ignore σ_2 and express the stresses in terms of σ_1 and σ_3 . Thus for a surface inclined at an angle θ to the σ_3 direction in Fig. 4.3b the normal stress, σ_n and shear stress, τ are:-

$$\sigma_n = \frac{\sigma_1 + \sigma_3}{2} + \frac{\sigma_1 - \sigma_3}{2} \cdot \cos 2\theta \dots\dots\dots 4.5$$

$$\tau = \frac{\sigma_1 - \sigma_3}{2} \cdot \sin 2\theta \dots\dots\dots 4.6$$

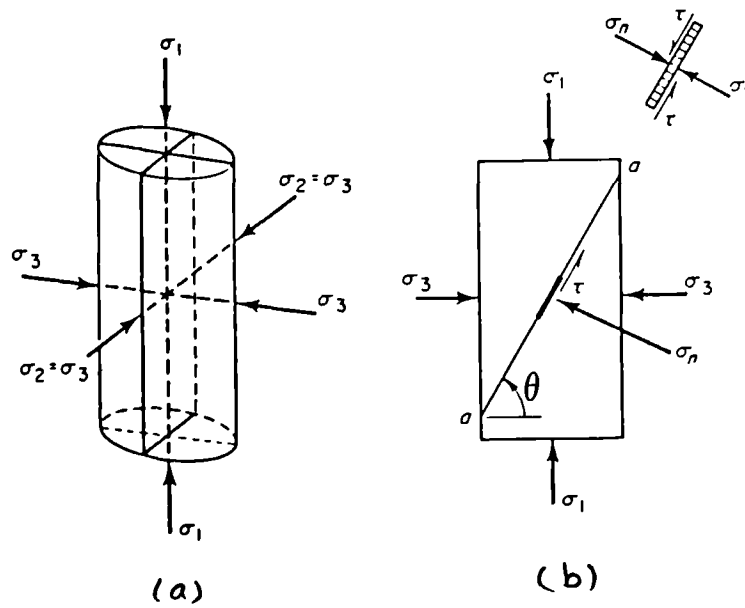


Fig. 4.3 Stress acting on soil sample in triaxial compression test (After Jumikis, 1965).

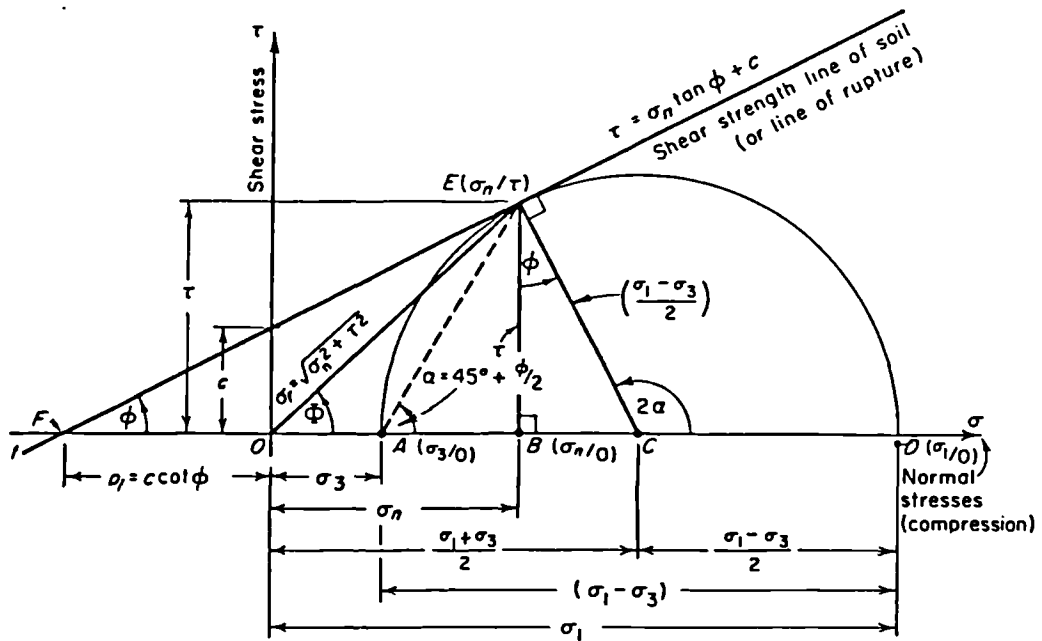


Fig. 4.4 Mohr's stress circle.

Equation 4.5 and 4.6 maybe combined and expressed graphically in terms of τ and σ_n in which case Fig. 4.4 results. Thus, the shear stress and the normal stress acting on any plane of known orientation can be expressed in terms of principal stresses and represented by what is known as a Mohr's stress circle. To a fairly close approximation Coulomb's equation may be taken to be identical with the Mohr envelope for the failure condition in a combined form are known as the Mohr - Coulomb theory. For Mohr's circle representing the failure condition σ_3 is constant, while σ_1 is increased until failure occurs. The tangent to these failure circles at different σ_3 represents the stress envelope as shown in Fig. 4.8.

4.1.2 Peak and Residual Shear Strength

Figure 4.2 shows a typical response in terms of mobilized shear resistance, (τ) to shear deformation. In the case of an intact over-consolidated clay in its undisturbed state, displacement causes an increase in mobilized resistance to shear with increasing deformation. However, under a particular effective normal pressure there is a practical limit to the amount of resistance the soil can offer. For a clay soil in its natural and undisturbed state the effect of shear displacement on a small element of soil can be considered in terms of Fig. 4.5. If the element is subjected to a constant and uniform normal stress (σ_n) and an increasing shear stress (τ), then for a very small values of shear stress the strain increases more or less linearly so that the system behaves in an elastic manner. At higher values of shear stress the sample is said to "yield" and significant plastic shear strains develop. At low values of shear stress the plastic strains are strictly limited in magnitude because they result in an increased resistance to further deformation, a process known as 'work or strain hardening' during which yield is said to be stable. Strain hardening can only increase the resistance to shear stress to strictly

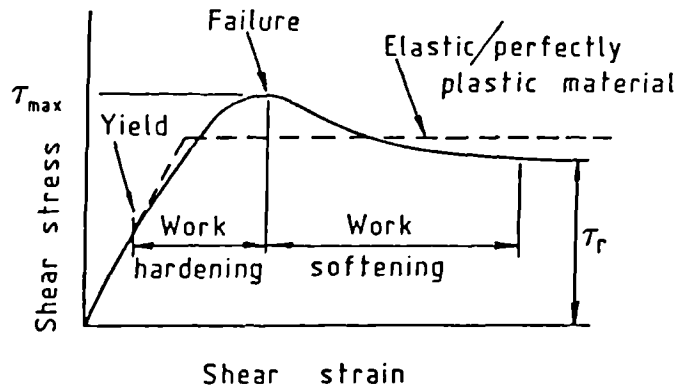


Fig. 4.5 Stress strain relationship for typical soil and for an elastic perfectly plastic model soil (After Scott, 1980).

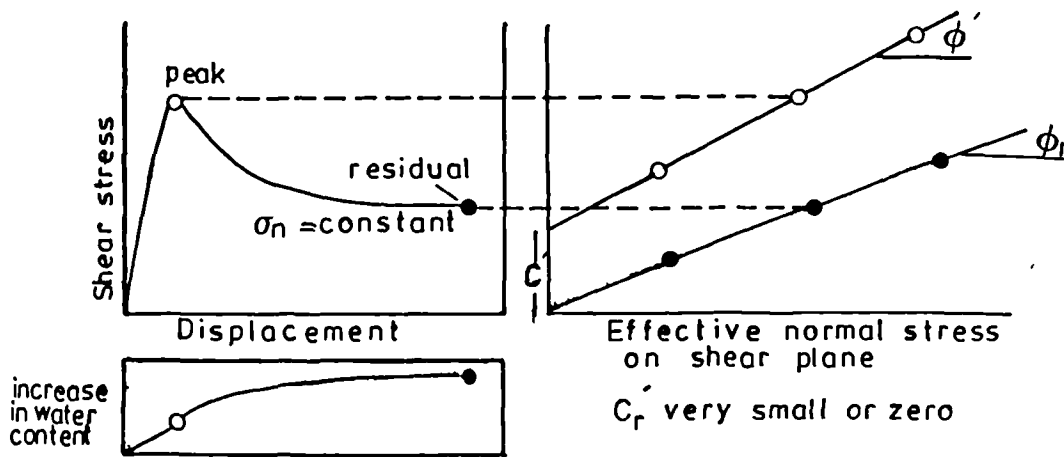


Fig. 4.6 Typical shear stress - shear strain and shear stress - effective normal stress relationships.

limited extent. Once the applied stress exceeds a limiting value (τ maximum, peak shearing resistance) the shear strain increases continuously for as long as the shear stress is maintained because the external work done exceeds the internal dissipation of energy in overcoming the resistance of the soil to deformation. At this point yield become unstable and the soil is said to fail. The shearing resistance decreases after failure by the process of 'strain or work softening'. After a relatively large strain has occurred residual strength (τ_r) is developed which is nearly independent of further strain.

The Coulomb-Mohr theory predicts that, if several similar test are conducted under different effective pressure conditions the peak and residual strength when plotted against the effective normal pressure will show the straight line relationship in Fig. 4.6. In practice this occurs within a limited range of normal effective stress values. However, peak strength and residual shear strength can be expressed according to Coulomb-Mohr law, thus:-

$$\text{peak } \tau_f = c' + \sigma_n' \tan \phi' \dots\dots\dots 4.7$$

$$\text{residual } \tau_r = c_r' + \sigma_n' \tan \phi_r' \dots\dots\dots 4.8$$

In practice the value of c_r' is generally small or zero, but even so it may exert a significant influence on soil behaviour.

Following to Wilun and Starzewski (1975) and Lagatta (1970) the shearing of soil is generally accompanied by volume changes illustrated in Fig. 4.2a in that dense soil increases in volume or dilates, whereas very loose soils decrease in volume or compress. After considerable deformation both the shearing resistance and the voids ratio become constant, a condition which is called the 'critical' or constant volume condition. The corresponding angle of internal friction and voids ratio are usually respectively referred to as the critical angle of friction

and the critical voids ratio. For any given soil both these parameters are independent of its original density, but are a function of the normal effective stress at which the shearing occurs. In the case of clays, both normally consolidated and over-consolidated types show a further loss of internal shearing resistance due to a gradual re-orientation of clay particles and the formation of slickensides (See Lagatta, 1970 and Hvorslev, 1960). This seems to take place after the clay has reached an essentially constant volume, that is at the critical voids ratio.

Shearing may cause increases or decreases in the pore water pressure 'u' depending whether it is consolidated or swelled during shearing. This has implications in terms of the stress conditions which are introduced in Section 4.1. Hence the conditions under which shearing may be performed can be classified into the following type:-

i. Immediate or undrained test.

The sample is subjected to an applied pressure under conditions in which changes of pore water pressure are prevented. The sample is then sheared also under conditions of no drainage. The shear strength parameters (c_u , ϕ_u) obtained by undrained testing are in terms of total stresses. They are used for problems relating to saturated clays where changes in stress produces no immediate changes in moisture content and therefore no change in volume. These parameters are often used for investigating short term stability.

ii. Consolidated - undrained test.

The sample is allowed to consolidate with drainage under the required confining pressure and then sheared under conditions of no drainage. In this case the pore fluid pressures generated during the test are measured so that effective stresses for the failure condition can be calculated. Consolidated-undrained test are used where changes in moisture content are expected to take place during the test.

iii. Drained test.

The sample is consolidated as in the previous test

but the shearing is carried out slowly under conditions in which excess pore water pressure is allowed to dissipate. Drained test are always used in problems relating to sandy soils since in these permeable materials drainage is rapid. In clay soils drained tests are used for the analysis of long-term stability problems. In these impermeable material rates of strain sufficiently slow for excess pore water to equalise are used.

4.1.3 Determination of Shear Strength

A number of tests are available. The most reliable and generally accepted are:-

- i. Triaxial
- ii. Shear box
- iii. Vane shear
- iv. Ring shear

i. Triaxial

As the name implies in this test the soil specimen is subjected to three compressive stresses mutually at right angles to each other. These represent σ_1 , σ_2 , σ_3 in Fig. 4.3. In practice the sample is subjected to a constant confining pressure in which $\sigma_2 = \sigma_3$ and σ_1 , the vertical stress applied to the end of a cylindrical specimen is increased until the sample fails in shear. An important distinction between the triaxial and shear box test is that in the former the orientation of the failure surface is not predetermined as in later test, since the deviator shear stress and the normal stress acting on the shear surface are computed from the principal stresses, triaxial test are known as an 'indirect' test.

The apparatus which is illustrated in Fig. 4.7 consists of a triaxial cell, a means of providing a constant confining pressure, a loading devise for producing an increasing axial load on the specimen and means for measuring the axial deformation of the specimen, the applied axial load and the confining pressure. In some tests in addition to these measurements the pore water pressure

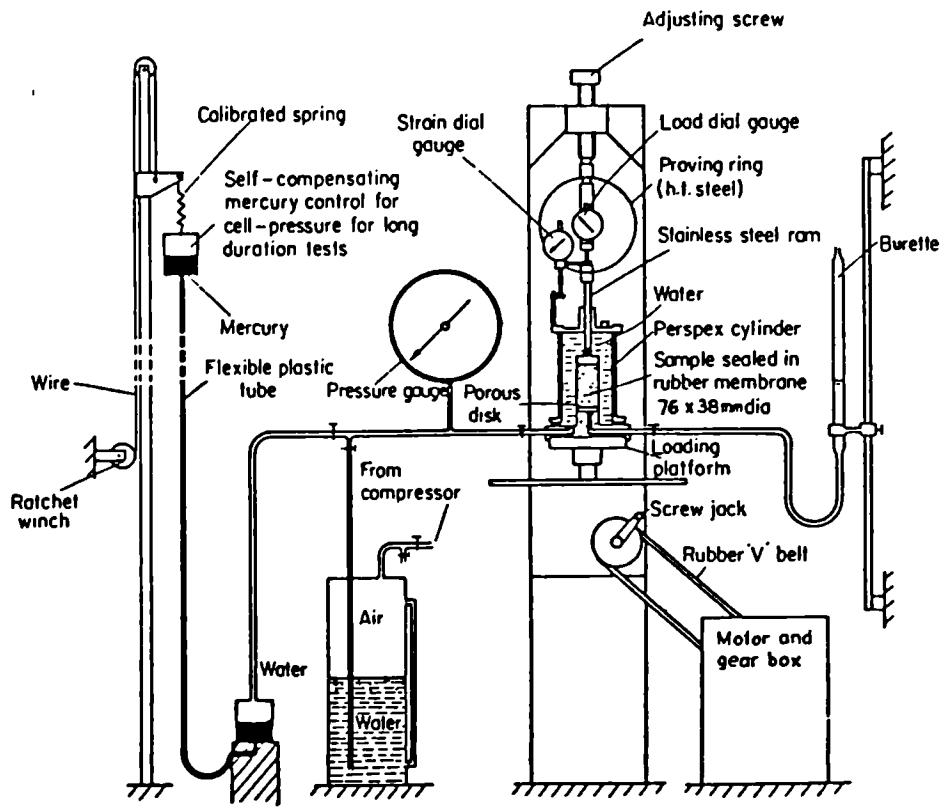


Fig. 4.7 Triaxial apparatus.

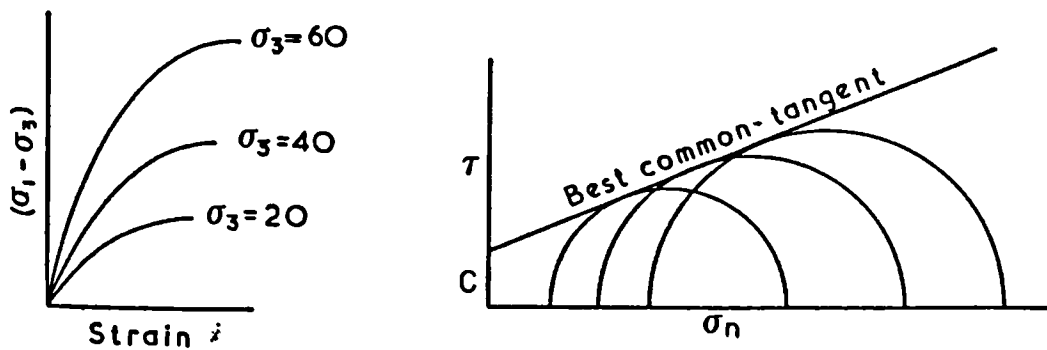


Fig. 4.8 typical triaxial test results.

and the lateral deformation are also monitored. A typical arrangement comprising a triaxial cell, proving deformation gauge, confining pressure gauge and volume change burette is shown in Fig. 4.7. The confining pressure is generally applied to the specimen by loading the triaxial cell with water held at the required pressure. In order to prevent this confining fluid from percolating into the specimen, the latter is incased in a thin rubber membrane which is attached to the end caps above and below the specimen by means of rubber 'O' rings.

During the test the confining pressure (σ_3) is maintained at a constant value while the axial load is gradually increased, generally by pushing the cell upwards against the proving ring held stationary by reaction against a loading frame. In fact the top of the specimen is not held absolutely stationary due to the deflection of proving ring, but although this displacement is equal to the proving ring dial gauge reading due to its small magnitude compared with the deformation of the specimen, it is usually ignored.

In the standard test a cylindrical sample is used in which the height equals twice the diameter. In the British Standard test (B.S. 1377 (1975)) the usual size of sample is 38mm. diameter by 76 mm. high or 220 mm. high by 110 mm. diameter. Fig. 4.8 shows typical triaxial test results from which c and ϕ are obtained. Failure is defined in terms of a maximum σ_1 value corresponding with the chosen σ_3 value. By carrying out tests at other σ_3 values it is possible to draw a series of Mohr's circles from which as shown in Fig. 4.4 the c and ϕ parameters are determined. Alternatively the shear stress and normal stress acting on the shear surface may be computed from equation 4.5 and 4.6.

ii. Shear box

The sample is contained within two halves of box split horizontally as shown in Fig. 4.9. A horizontal shearing force (τ) is applied to one part of the box while the other is held stationary. A constant normal load

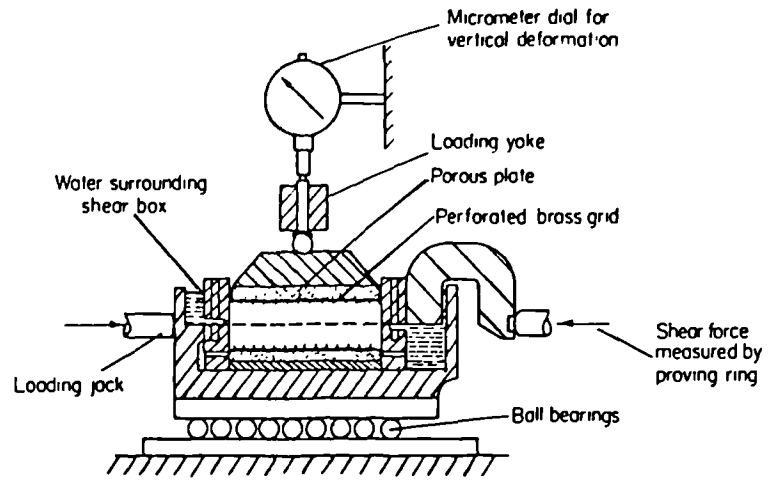


Fig. 4.9 Schematic diagram of shear box apparatus.

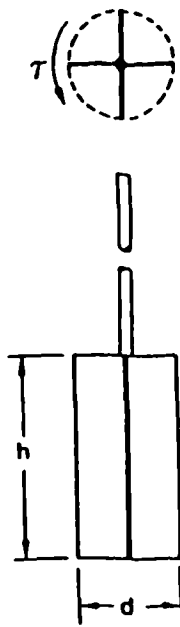


Fig. 4.10 Vaneshear test apparatus.

(σ_n) is applied to the top of the sample. During the test the shear force is increased and the vertical deformation, relative horizontal shear displacement and shear force are all measured as a shear surface is induced to form along the joint between the boxes. Further details of apparatus are given in Chapter 5.

iii. Vane shear test

This test is used for both in situ and laboratory determination of undrained strength of intact fully saturated clays. The test is not suitable for other types of soil but is particularly useful in the case of soft clays having undrained shear strength of less than about 100 kN/m^2 . Craig (1983) points out that the test may not give reliable results if the clay contains sand or silt laminations.

Details of the test are given in B.S. 1377 (1975). The equipment shown in Fig. 4.10, consists of a stainless steel vane comprising four thin rectangular blades, mounted at the end of a high tensile steel rod., the rod is enclosed by a sleeve packed with grease. The length of the blades is equal to twice their overall width, typical dimensions being 150 mm. by 75 mm. or 100 mm. by 50 mm.

The vane and rod are pushed into the clay below the bottom of a borehole to a depth of at least three times the borehole diameter. Steady bearings are used to keep the rod and sleeve central in the borehole casing. The test can also be carried out in soft clays without a borehole or in laboratory samples, by direct penetration of vane. Torque is applied gradually to the upper end of the rod by means of suitable equipment until the clay fails in shear due to rotation of the vane. Shear failure takes place over the surface and end of a cylinder having a diameter equal to the overall width of the vanes. The shear strength is calculated from the expression:

$$T = \pi \tau \left(\frac{d^2 h}{2} + \frac{d^3}{6} \right) \dots\dots\dots 4.9$$

where:

T = Torque at failure
 d = Width of blade
 h = Length of blade
 τ = Shear strength

Jumikis (1965) states that vane shear tests usually give values of the shear strength about 15% greater than uniaxial compressive strength measurements.

iv. Ring shear test

The principle of the ring shear test is to produce a shear surface by torsional displacement so that very large shear displacements can be achieved by continuing rotations. The arrangement of the type of the test used during this research in which a thin annular sample was subject to a tangential stress applied by means of an external torsional moment is shown in Fig. 4.11. This was achieved by clamping it between two metal discs which are then rotated in opposite directions. The tangential force increases until failure. The vertical displacement is measured and the horizontal or rotational displacement is computed from the angular movement. Further details of the test conditions are given in Chapter 5.

In the shear box and ring shear tests, shown respectively in Fig. 4.9 and 4.11 a particular normal stress is applied perpendicular to the plane of shear displacement. Shear stress is applied across the plane of shear displacement and during the test it is measured. Thus at the point of failure of the soil mass the normal stress and shear stress are known and hence the test is referred to as a 'direct' shear test. Carrying out the test at a different normal pressure so that the corresponding shear stress is obtained gives another point on the graph in Fig. 4.6 which defines the failure criterion and hence the values of c and ϕ for the soil. Although in theory it would be possible to define criterion in terms of just two points on the shear stress - normal stress diagram of Fig. 4.6 due to variation between different soil

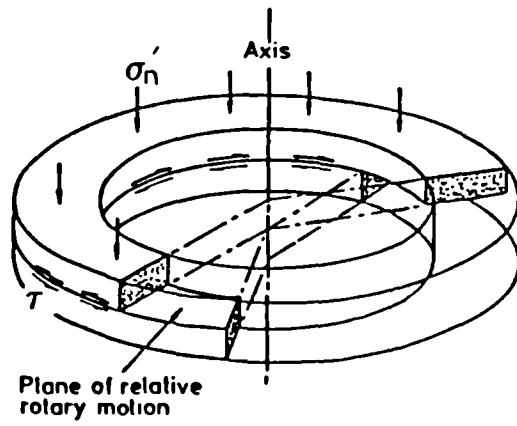


Fig. 4.11 Ring shear test sample.

samples and also because of curvature of the failure criterion, in practice it is necessary to use three or more shear stress-normal stress values.

Measurement of the peak value of shear strength requires the use of at least three intact specimens. On the other hand, the value of residual shear strength can be determined from tests in which the shear stress value is measured for a series of effective normal stress values applied to the same sample.

4.1.4 Determination of Residual Shear Strength.

Studies of concept of residual strength have contributed much to a better understanding of the properties of soils. In fact the residual shear resistance is usually quite low in comparison with the peak strength determined by conventional laboratory procedures and equipment. The achievement of the residual condition is dependent on producing large displacement on the shear surface.

The historical background of the use of residual shear strength concepts has been researched by Lagatta (1970) who traces the use of either this term or the term 'permanent strength' to Collin (1846). Apparently, the first determination of residual strength of an undisturbed clay was in early 1930's by Tiedemann using a rotational shear machine. Shortly afterwards, Hvorslev in 1936 and Haefeli in 1938 also used rotational shear machines to investigate the strength of clays. Lupini et al (1981) attributes the term 'residual' to Haefeli. In 1937, Tiedemann recognized the existence of a constant strength at a large shear displacement and he called it the 'puresliding strength'. Probably the first use of the word 'residual' in connection with the shear strength of the soil was by Cassagrande in 1949, when he realized that heavily overconsolidated slickensided soil has a shear strength approximately equal to the residual shear strength.

According to Lagatta (1970), Hvorslev (1960) pointed out that the large displacement attained in rotational shear machines causes orientation of clay particles which

results in the formation of a slickensided and polished shear surface. In fact this was probably the first time that the reduction in strength after the development of peak strength and the formation of slickensides were linked to reorientation of clay particles in the failure zone.

The significance of residual strength in the field was appreciated in the early 1960's in which of particular relevance is the work of Skempton (1964) who in the 4th Rankine Lecture shed more light on the concept of residual shear strength and its application to the analysis of stability of slopes in soil.

Residual shear strength has been considered to be a fundamental property of a soil as well as being of practical importance and in relation to the analysis of stability of field slopes. Hence it is important to measure this quantity as accurately as possible. Various laboratory tests have been used, including the triaxial test, reversing shear box test, and ring shear test. In each case a large shear displacement on a shear surface must be generated and in addition the test must be carried out under conditions of controlled drainage rate, stress measurement and volume. In fact, large displacement can not be obtained in the triaxial test although some results are quoted by authors including Chandler (1966) who measured used specimens with polished surfaces cut at an angle corresponding with the anticipated failure surface. Both the reversing shear box and ring shear test were used in the course of this study.

The main difference between the three basic methods lies in the amount of displacement that can be obtained, in view of the fact that the residual condition represents good preferred orientation of platy grains. In the triaxial test the amount of movement is strictly limited. Ideally, the movement of 20% along the whole length of sample gives about 20 mm. displacement along the shear surface, but this displacement may be not represented the true displacement which can be obtained by experiment due to the change in surface area, but this is overcome

to some extent if the sample is precut and polished by a knife or glass plate to orientate the grains in the direction of shear. In the shear box test the amount of displacement achieved in a single travel is about 6-7 mm., the limitation of insufficient shear displacement also occurs but can be overcome by successively reversing the direction of shearing to accumulate enough shear displacement. In fact reversing the direction of shear on the shear surface may disturb the orientation of the grains. In ring shear test unlimited displacement can be obtained, the shearing continues in one direction so that good preferred orientation of the grains can be obtained.

The advantages of determining the residual shear strength by a ring test method may be summarised as follows:-

- i. The cross-sectional area of the sample remains constant during the test.
- ii. The sample can be subjected to any uninterrupted unidirectional displacement in a direct shear configuration. Simons and Menzies (1978) suggest that the disturbance of particle orientation due to changes in direction of principal stresses with each reversal of the reversing shear box method may significantly change the value of ϕ_r measured.
- iii. The shear surface stays in the same plane. In the reversing shear box any consolidation or dilation of the sample results in the shear surface not coinciding with the joint between the boxes.
- iv. In the case of multiple reversal direct shear tests difficulties arise due to variations of shear stress during a particular travel. Generally, an initial peak is followed by a trough and then the value steadily increases until end of the travel. Some investigators take the trough values as the (τ) corresponding to the residual condition, while others use the terminal value. For ring shear tests there is no such ambiguity.
- v. The so-called flip-over effect which produced a small

peak during the reversing of the shear box (See Section 4.2.3) such effects are not present in the ring shear test.

Unfortunately, ring shear test are not without their problems. In particular there is a tendency for soil to be extruded from the boundaries of the specimen. This may cause the normal stress to be lower at the periphery than at the centre of the specimen. The effect or redistribution of effective normal stress increases as a ratio of the inner radius to the outer radius of an annular specimen decreases. Probably this error increase as the rate of soil extrusion increases.

4.2 Variation in Residual Shear Strength

Past research has indicated that residual shear strength depends on a number of factors, a brief review of which will be undertaken. This includes consideration of lithological effects, type of specimen, type of test and test conditions.

4.2.1 Lithological Effects

These effects can be put under the headings of:

- i. Size and shape of grains.
- ii. Mineralogy.
- iii. System chemistry.

- i. Size and shape of grains.

The size of the individual particles comprising the material and the percentage of clay sized particles play an important role in determining the magnitude of the residual shear strength. From a study of case records Skempton (1964) shows that the value of $\phi'_{r.}$ decreases with increasing clay percentage. These data together with other data have been summarized by a number of workers including Cripps and Taylor (1981) and Lupini et al (1981) in Figs. 4.12 and 4.13 respectively.

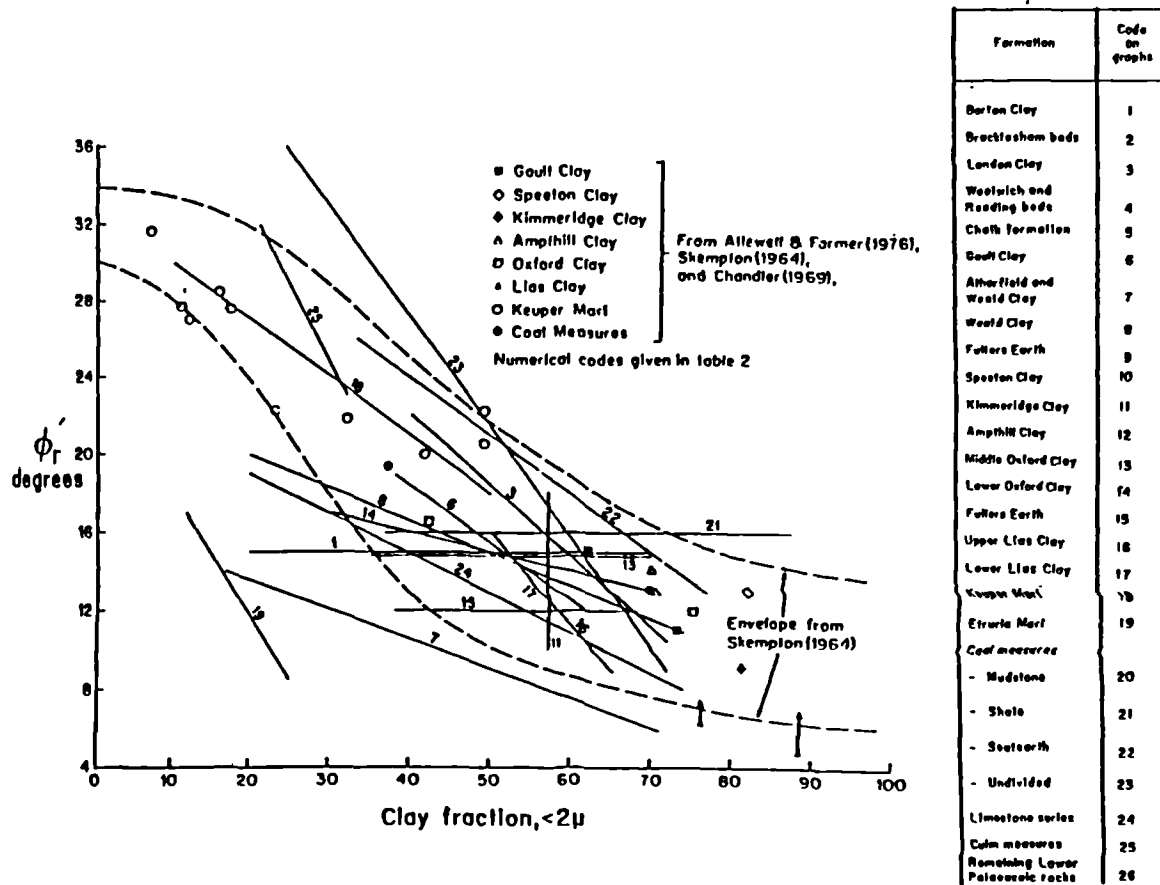


Fig. 4.12 Residual shear strength and clay size fraction of U.K. mudrocks (After Cripps and Taylor, 1981).

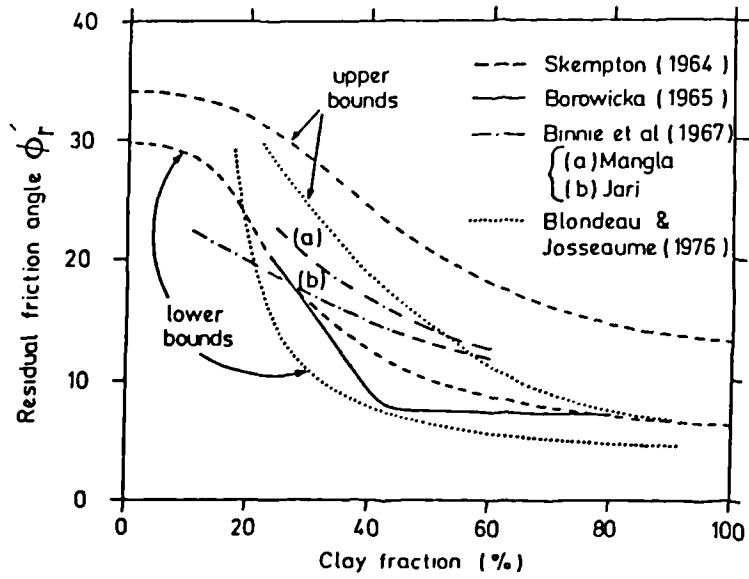


Fig. 4.13 Residual strength: correlations with clay fraction (After Lupini et al, 1981).

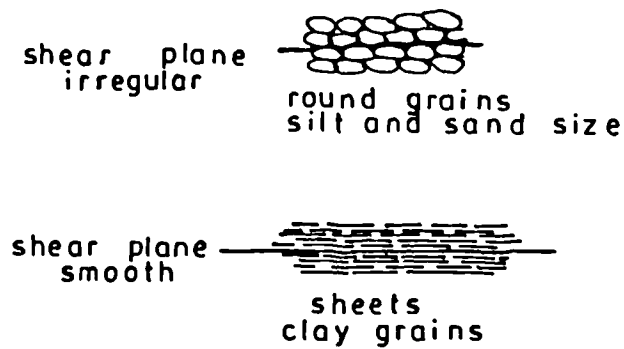


Fig. 4.14 Type of grains and the characteristic of shear plane.

Owing to their molecular structure, clays form plate like particles which are capable of orientation in the direction of shear. Silt and sand particles which consist predominantly of quartz and feldspar are roughly spherical in shape and will not become orientated by shear displacement. As demonstrated in Fig. 4.14 since sliding friction between the flat-surfaces of clay particles is lower than that for an irregular surface composed of sand or silt particles the residual shear strength becomes greater as the percentage of rounded particles increases.

Following work carried out by Lupini et al (1981) it is possible to recognise three main modes of residual shear behaviour. These relate the residual angle of friction ϕ_r' to the ratio of platy particles plus voids to the volume of rotund particles. This latter ratio is also known as the granular void ratio, e_g .

a. Turbulent mode

The turbulent mode occurs when the material is dominated by rotund particles or by platy particles which have a high coefficient of interparticle friction. The residual strength is relatively high and no preferred particle orientation occurs. The residual friction angle depends primarily on the shape and packing of the rotund particles rather than the coefficient of interparticle friction. The shear zone can be distinguished by its relatively high porosity and it is subject to considerable re-arrangement if subsequently loaded.

b. Sliding mode

The sliding mode occurs when behaviour is dominated by platy particles with low interfacial friction and a high degree of preferential particle orientation, the material has low shear strength in a direction parallel to the plane of the particles and residual friction angle depends primarily on the the mineral composition, pore water chemistry and the coefficient of interparticle friction. The shear surface is not significantly affected by subsequent loading. The formation of a shear surface is due primarily to the re-arrangement of platy particles into a preferred orientation.

c. Translational mode

The translational mode occurs when neither platy nor rotund particles dominate the behaviour. It consists of a mixture of turbulent and sliding behaviour with different parts of the shear zone displaying a range of characteristics typical of both types of shear. The residual friction angle is sensitive to the small changes in the grading of soil.

Lupini et al (1981) show that the change from one mode of behaviour to another depends not only on relative proportion of platy rotund particles but also on their relative sizes.

The plasticity characteristics of fine grained sediments has been found to correlate with many other physical properties as well as providing a convenient method classifying fine grained sediments. Quantitative measurement of plasticity defined in terms of liquid and plastic limits as respectively the upper and lower limits of the range of water contents over which a soil exhibits plastic behaviour (See Akroyd, 1964) was first proposed by Atterberg (1911). These limits and also plasticity index which is the difference between the liquid and plastic limits are mass properties of remoulded soil that depend upon the mineral composition, grain size distribution, grain shape, percentage of organic material and pore water chemistry. The relationship between the plasticity and ϕ_r' had been investigated by many authors including Lupini et al (1981) and Mitchell (1976) who provide the data given in Figs.4.15 and 4.16. These graphs and also similar one given by Cripps and Taylor (1981) indicate that in general ϕ_r' decreases with increasing of plasticity index, although the relationship is not linear.

In fact Voight (1973) has demonstrated that there is a definite statistical relationship of decreasing ϕ_r' with increasing plasticity index. Results lying outside the general trend are explained in terms of material consisting of coarse fragments composed of clay aggregations which are not broken down during the plasticity

index test, although they would be if on a shear plane. A similar process would appear to be operating in tests performed by De et al (1973), Mitchell (1976), Lupini et al (1981).

ii. Mineralogy

The influence of mineralogy on residual shear strength has been investigated by Kenney (1967) who concluded that the type of clay minerals is a governing factor. In tests on monomineralic clays, the residual friction angle reported are about 4° for sodium montmorillonite 10° for calcium montmorillonite, about 15° for kaolinite and 14°-16° for hydrous mica and illite. Massive or rotund minerals such as quartz and feldspar exhibit high values of ϕ_r' in excess of 30°. Kenney (1967) concluded that for massive minerals the residual shear strength depends on particle shape rather than particle size or stress magnitude within the range of testing experience. Horn and Deer (1962) showed that each mineral group might have characteristic shear strength properties, so that the residual strength properties of natural soil might be controlled the relative properties of the different component minerals.

Fig. 4.17 shows the relationship between ϕ_r' and quartz: clay ratio obtained by Spears and Taylor (1972) using reversing shear box test on number of intact mudstones. The results clearly show that ϕ_r' decreases with increasing clay: quartz ratio. Furthermore, Cripps and Taylor (1981) demonstrated in Fig. 4.18 the influence of the clay fraction on residual shear strength using the ratio of clay minerals to massive minerals (detrital plus diagenetic minerals) determined by XRD methods. The importance of ratio of platy (clay) to massive (quartz) minerals present is amplified by work of Kenney (1977) who define the term relative residual strength of a mineral mixture ($R \phi'$) as:

$$R \phi' = \tan \phi_r' - (\tan \phi_r')_c / (\tan \phi_r')_m - (\tan \phi_r')_c$$

where:

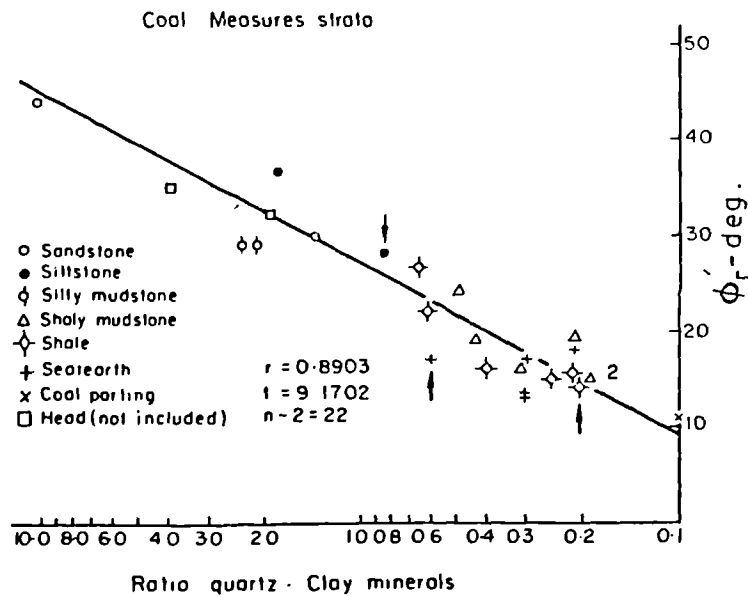


Fig. 4.17 Quartz: Clay minerals ratio (logarithmic) plotted against residual ϕ_r' (c' assumed zero) (After Spears and Taylor, 1972).

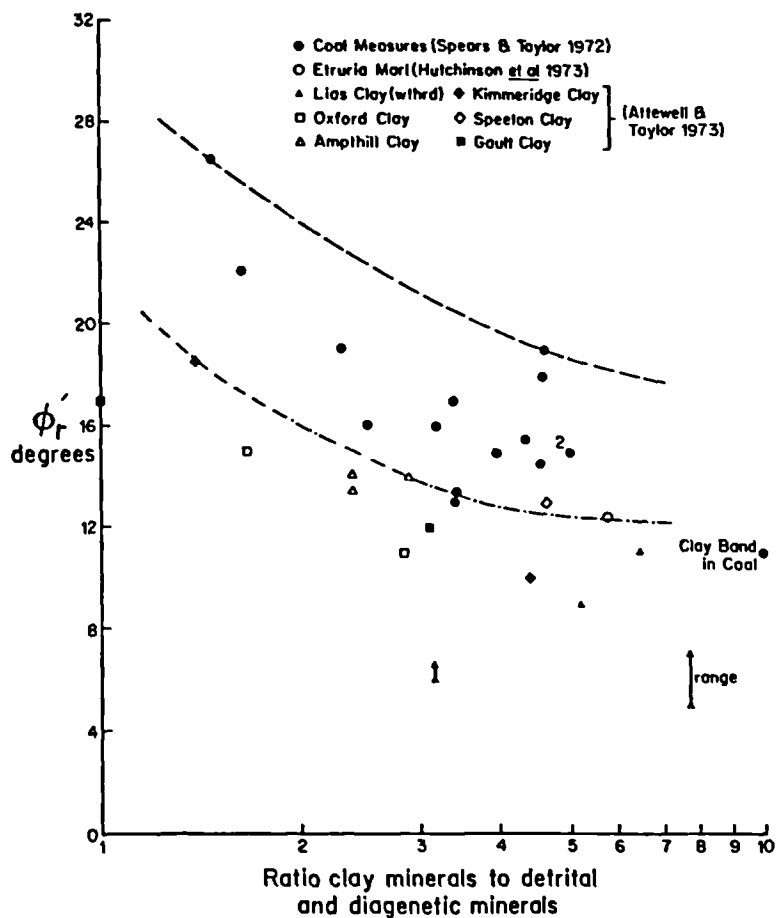


Fig. 4.18 Influence of clay minerals on residual shear strength all mineralogical data from the same XRD machine and ϕ_r' values from the same reversing. (After Cripps and Taylor, 1981).

- ϕ_r' = residual friction angle of mixture
 $(\phi_r')_c$ = residual friction angle of clay minerals
 $(\phi_r')_m$ = residual friction angle of massive minerals

He concluded that the relative residual strength of all mixtures by weight of montmorillonite and massive minerals are similarly influenced by the relative volumes of the component clay minerals (clay mineral + water and massive minerals).

Chattopadhyay (1972) has studied the effect of mode of cleavage and type of bonding along the cleavage planes of various minerals. Thus he demonstrated that most the minerals that have good 001 basal cleavage display relatively low residual angle of friction. Common clay minerals including montmorillonite, kaolinite and hydrous mica all have 001 basal cleavage but they exhibit different residual friction angles due to the thickness of absorbed water layers. These results confirm Kenney's (1967) findings.

iii. System chemistry

Many investigators have studied the effects of system chemistry on residual shear strength. In the course of his investigation on the shear strength properties of clay minerals including hydrous mica and montmorillonite, Kenney (1967) found that strength was increased by increased ion concentration of the pore fluid, this increase was larger for higher valency and greater polarizability. Ramiah et al (1970) reported the results of reversing shear box on silty clay in which the pore water chemistry was altered from flocculating to dispersive condition with a corresponding reduction in the residual friction angle from 33° to 28°.

The chemical weathering of pyritic shale at Mam Tor landslide has been reported by Steward and Cripps (1983). The results show that the residual shear strength of Edale Shale appears to be modified during weathering because of sensitivity of pore water chemistry and mineralogical composition. In ring shear experiments in which pore

fluid composition was changed during shearing it was found that K^+ ions increased and Na^+ ions decreased ϕ_r'

4.2.1.1 Conclusion

The above review regarding causes variation in the residual angle of shearing resistance indicates that care must be taken when interpreting the results of experimental determinations. Clearly sample pre-treatment is very important since although crushing of sample to pass a 425 μm (35 mesh) sieve as suggested by British Standard B.S. 1377 (1975) may separate most soil particles it would leave many clay aggregation complete. This may well be important in the case of residual shear strength testing since although it would be expected that disaggregation would occur on a shear plane it may not and would be expected to modify significantly the results of plasticity and particle size determinations. In fact, different methods of sample pre-treatment including crushing and tumbling in water were used during the course of the present research in order to investigate these effects.

4.2.2 Type of Specimen

The residual shear strength of soil may be determined using either intact or remoulded specimens. In the case of intact specimens, samples of material taken in an undisturbed state must be carved to fit the sample holder. Remoulded specimens are disaggregated and reconstituted at a particular water content and reformed in the sample holder.

i. Intact

Intact specimens at their natural water content may be tested in which case a peak shear strength is measured before continued shear displacement produces the residual condition. In many cases it is convenient to test a sample containing an existing shear surface, hence an intact

piece of material at its natural water content is subjected to a shear test so that the residual shear strength mobilized on the shear surface is determined. Generally, tests on intact material are performed by shear box shear methods since it is difficult to prepare annular specimens. If the peak strength of an intact sample is not required, then the test duration can be considerably shortened by pre-cutting the sample. Two pieces of intact material at natural water content are prepared so that they have plane surfaces which are then put into contact coinciding with the join between the boxes. The two pieces may either be trimmed separately before being placed in the shear apparatus or a single piece may be cut using thin wire.

In his study of the properties of heavily overconsolidated clay, Parry (1972) carried out direct shear test on orientated pre-cut unweathered samples of overconsolidated Oxford Clay in which the bedding was orientated vertically, horizontally and inclined at 30° to the horizontal to simulate the field discontinuity system. The results of these test are presented in Table 4.1 from which it will be seen that although the shear strength is lower in the horizontal and inclined samples, no significant difference exists in the ϕ_r' results. Parry makes the following observation.

- a. In the case of the horizontal and inclined test the peak shear strength tended to occur at a shear displacement of 2.7 - 4 mm., whereas for the vertical tests it was reached at 4-6 mm. displacement.
- b. The shear strength tended to drop more rapidly after peak for horizontal tests than vertical test with inclined samples between these values.

In reversing shear box test on Oxford Clay by Jackson and Fookes (1974) samples sheared perpendicular to the bedding required greater displacement compared with parallel samples. In these tests both ϕ_p' and ϕ_r' were higher in the perpendicular specimens amounting to a difference in ϕ_r' of between 10° and 2° which the authors attributed

Table 4.1 Shear strength parameter for drained shear box test on Oxford Clay, after Parry (1972).

Orientation of shear plane with respect to shear surface	Peak		Residual	
	c_p KN/m ²	ϕ_p degree	c_r KN/m ²	ϕ_r degree
H	10	21½	0	13
V	20	32½	0	13
30° to H	20	21½	0	13

to the effect of a high degree of preferred orientation in the clay. The small differences in value of cohesion intercepts suggested the existence of relatively strong cementation bonding. Since if the residual condition was probably achieved, it would be anticipated that complete reorientation of the clay particles on the shear surface would destroy any prior particle orientation, the difference in ϕ_r value may be due to the presence of silt lamina cut through by shearing which would release relatively coarse particles on to the shear plane in the perpendicular test but not the horizontal ones.

ii. Remoulded

For tests of this type the material is thoroughly disaggregated, slurried and reconsolidated to either a normally or an overconsolidated state. Usually consolidation is carried out in the shear apparatus sample container. The resulting material may then be tested either as an intact or a pre-cut specimen.

Although overconsolidated in their natural state, since many clays, clay shales and other mudstones are tested in a remoulded condition it is of interest to consider the effects of remoulding on the residual shear strength. Since Section 4.1.2 suggests for any given soil the residual shear strength is independent of the initial density but a function of normal effective stress and orientation of soil particles, it is expected both the undisturbed and remoulded sample give the same results.

Early work using the reversing shear box, carried out by Petley (See Skempton, 1964) on remoulded clay derived from the underlying Carboniferous Mudstone at Waltons Wood Staffordshire. The clay was normally consolidated from a slurry with a water content equal to the liquid limit and gave residual shear strength of $\phi_r = 13^\circ$. Skempton (1964) argues that this value is compatible with the value obtained for large strain tests on samples of undisturbed clay. Small disparities in ϕ_r between undisturbed and remoulded samples have been noted by some

authors, while many results indicate little difference. In ring shear tests on London Clay, Lagatta (1970) determined a value of 9.3° for undisturbed samples compared with 8.3° for remoulded ones. The reason for this change is not known but it may be associated with a reduced ion concentration in pore fluid since the remoulding was carried out with distilled water. Garga (1970) also reports similar results on tests on air dried brown London Clay from Edmonton. In these tests the value of ϕ_r' for the slurried samples was 0.5° lower than that for the undisturbed material, although again the effect of changing the pore water composition by drying and remoulding is not known. Bishop et al (1971) and Kenney (1967) suggests that remoulding causes little difference in that the former author quotes an increase from 9.4° for undisturbed clay to 9.5° for slurried material but unfortunately only one test was carried out.

On the basis of this work on London Clay it would appear that remoulding specimens may cause a reduction in ϕ_r' of up to 1° , the exact cause of this change is uncertain since the chemistries of the pore waters are not known and insufficient information with regard to the method of disaggregation for re-moulding is unavailable.

In fact the method of disaggregation may have an effect on the results since Townsend and Gilbert (1976) have shown in Table 4.2 that severe methods such as processing by blender produces somewhat lower residual strength values than those measured for undried or air-dried material. Clearly preparation can cause a greater disaggregation of soil particles than is achieved during shearing. Of course greater disaggregation of the soil reduces the amount of shearing required to attain the residual condition but care must be taken to ensure that the disaggregation achieved is realistic in terms of the shearing process.

For certain indurated rocks including shales preparation of the specimen for shear strength testing requires crushing. The effect of this process on the residual shear

Table 4.2 The effect of method of processing on the residual shear strength of Strawn Shale and Dawson Shale, after Townsend and Gilbert (1976).

material	processing method	Normal stress kN/m^2	rate of displacement cm/day	residual shear strength ϕ_r deg.	displacement required to achieve residual (cm) (non cumulative)
Strawn Shale	Undried	588	69	9.6	91.2
	air dried	588	69	9.1	6.0
	blender	588	69	7.2	1.4
Dawson Shale	undried	588	69	7.3	73.1
	air dried	588	69	7.0	31.9
	blender	588	69	6.8	19.5

strength has been studied by various investigators. Lagatta (1970) shows that at least ten times more displacement was necessary to reach the residual state tests using uncrushed Cucaracha Shale compared with crushed material. Although crushing of Cucaracha Shale is reported by Bishop et al (1971) to enhance the clay fraction and thus reduce considerably the displacement required to reach the residual shear strength value. It would appear that the large displacement required to define the residual strength is associated with progressive break down of aggregations of clay particles and that crushing only short cuts this process.

There is only limited published information concerning moisture contents at the residual state. However, Chowdhury et al (1977), Nagaraj and Navasimha (1974) found that the residual shear strength is independent of the initial moisture content. In their tests, these authors found that the moisture content in the shear zone at the residual state correlates well with residual shear strength, but there is no collaborative investigation to support this idea. They also confirmed that the final water content for the residual state is not related to the initial value.

4.2.3 Type of Test

The irregular character of failure surfaces observed for both undisturbed and remoulded clay specimens has been noted by many investigators. Heley and MacIver (1971) remark that during the first shear displacement of a specimen from its initial position an undulating separation of two halves may form. The formation of this undulating surface is confirmed by Morgenstern and Tchalenko (1967a and b), Hvorslev (1960) and Skempton (1964), who point out that the failure surface in any material is initially non-planer due to the development of families of discontinuous shear surfaces. These are probably formed due to extension of flaws, pore spaces and mineral or rock particle interfaces which do not necessarily all lie in the same plane.

Although with subsequent displacement the presence of undulations gives rise to a geometrical component of shear strength, from Fig. 4.19 it is clear that shear straining must be accompanied by either en masse lifting of material along the shear surface or a grinding away of the irregularities. Heley and MacIver (1971) explain that as the surface irregularities are displaced further from their initial mating position the geometrical component increases due either to irregularities, sliding upwards on matching irregularities or for larger displacement, the increased contact of dissimilar irregularities. If the irregularities are not orientated in the direction of shear movement a binding or a rotational effect may also be introduced. Reversal of the direction of shear is accompanied by the return of the two surfaces to their initial mating positions. Thus the geometrical component will reduce the measured shear stress, as the irregularities slide downwards on matching irregularities and unless surface modifications have occurred it vanishes as the surfaces pass through their initial position.

In nature, shear straining may grind away irregularities, and the amount of grinding depends on the amount of movement. But it may still have an effect on the true residual shear strength in the field. According to Heley and MacIver (1971) Fig. 4.20a represents an idealized relationship between the shear stress and displacement. This is modified in Fig. 4.20b due to the geometric component, where the difference between c and c' or f and f' represent the resulting increase in strength. During stroke DF , the increase in geometrical component $d'f'$ obscures the continuously decreasing shear stress df . The effect of the so called flip-over effect which produces small peak on the curve is also demonstrated in Fig. 4.20c. In fact, the nature of the flip-over is not fully understood, but it probably relates to the movement and rearrangement of platy particles on the shear surface. The rise in shear stress that occurs on the resumption of a test which has been stopped may be due to a slight reversal caused by relaxation of the proving

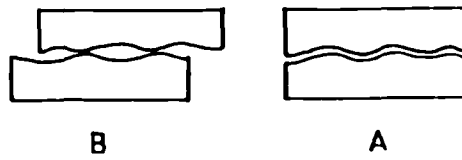


Fig. 4.19 Geometrical component due to the undulating shear surface.

- A: Upper and lower half match each other.
Lower shear strength.
- B: Upper and lower half not match each other.
Higher shear strength.

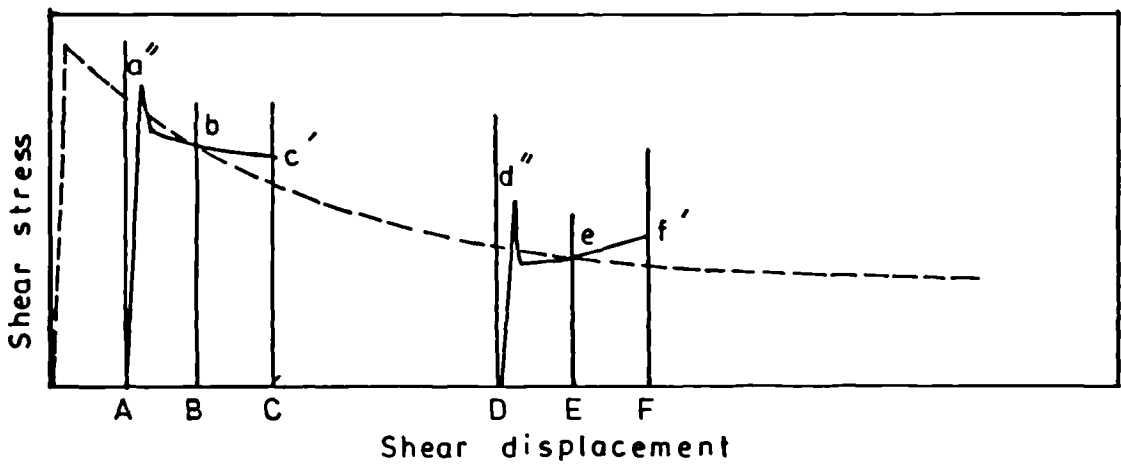
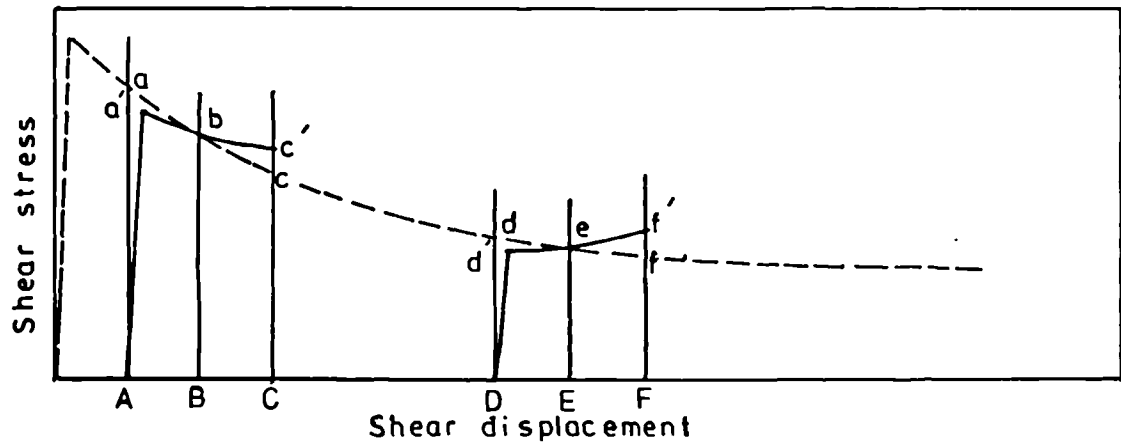
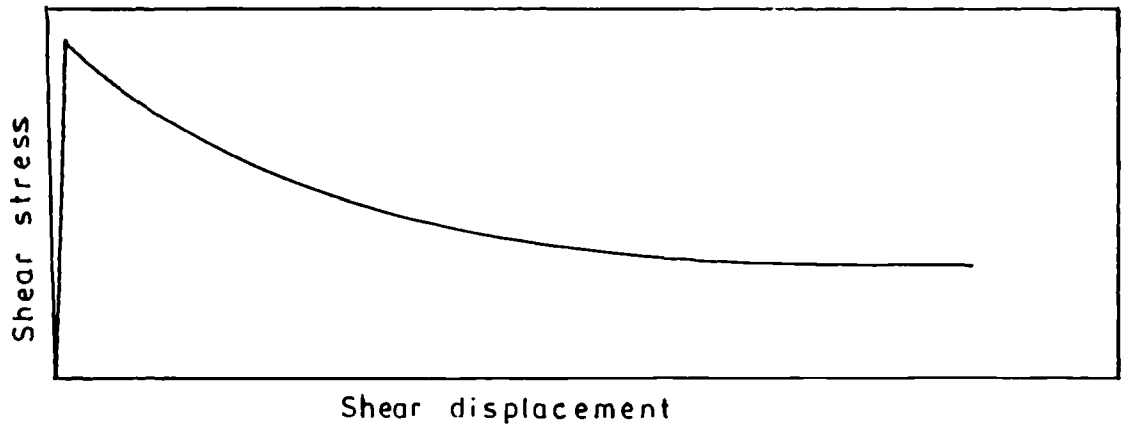


Fig. 4.20 Idealized expression of the three components of shear stress measured in the repeated direct shear test. (After Heley and MacIver, 1971)

ring. This small peak disappears after only very small shear displacement (less than 0.5 mm.) and the shear stress displacement relationship appears unaffected. Heley and MacIver (1971) argue that, although this may be a manifestation of slight re-organization of material on the shear surface, reversing the direction of the shear movement does not appear to drastically disrupt the tendency towards parallel orientation of clay particles on the shear surface. However, residual shear strength determined by the ring shear suggests that re-orientation of particles may well have a significant effect.

Heley and MacIver (1971) also point out that rubbing together of two geometrical matched surfaces should readily reorient the clay particles at the interface to produce minimal friction. In an annular shear test the geometrical component is present during the entire shear displacement except when rotation of 360° is attained. Thus the dissimilar irregularities on the two surfaces must be completely worn away before a valid residual condition is produced. Hence it is believed that the annular shear test is a more realistic representation of field conditions.

In Table 4.3 are presented the results of many residual shear strength tests including ring shear, reversing shear box and triaxial tests. These data show that the residual shear strength given by the ring shear test is generally lower than that obtained by the reversing shear box and triaxial tests. Bishop et al (1971) shows that the difference can not be explained by differences in index properties or clay fraction. Also even artificial polishing of the slip surface using a spatula or glass plate (often employed in triaxial determination) does not necessarily establish the maximum particle orientation. Lagatta (1970) compares the results of the residual shear strength of remoulded London Clay obtained by rotational shear to that obtained by Skempton et al (1969) by triaxial tests. Both samples were from the same site and had the same Attenberg Limits and grain size

Table 4.3 Effect of equipment type on the residual shear strength of London Clay

Location	Test Type	Average ϕ_r degree c=0	Reference	Remarks
Wraysbury	Drained, multiple, direct shear test undisturbed. LL=70 PL=29 CF=58	13.5	Agarwal (1967)	Blue London Clay
"	Drained triaxial test. undisturbed, presheared sample to large displacement LL=72 PL=29 CF=57	10.5	Garaga (1970)	"
"	Ring shear test undisturbed LL=72 PL=79 CF=57	9.4	Bishop et al (1971)	"
"	Ring shear test undisturbed LL=72 PL=72	9.3	La Gatta (1970)	"
"	Ring shear test remoulded	9.5*	Bishop et al (1971)	"
"	Ring shear test remoulded	8.3	La Gatta (1970)	"
Walthanstow	Drained direct shear box test Slip surface.	14.0	Petley (1969)	Brown London Clay
"	Cut plane drained direct shear test undisturbed LL=70 PL=26 CF=50	14.2	Petley (1969)	"
"	Drained triaxial Slip surface. LL=71 PL=26 CF=63	13.7	Petley (1969)	"
"	Ring shear test undisturbed LL=66 PL=24	10.0	Bishop et al (1971)	"
"	Ring shear test slurried	9.7	Bishop et al (1971)	"

continued overleaf

Continued

Location	Test type	Average ϕ_r degree c=0	Reference	Remarks
Herne Bay	Drained multiple direct shear test undisturbed LL=81 PL=33 CF=61	13.5	Petley (1966)	Blue London Clay
"	Cut plane drained triaxial test undisturbed LL=81 PL=33 CF=61	14.7	Petley (1966)	"
"	Ring shear test LL=95 PI=61	9.4	Maugeri (1976) ⊕	"

* = one test only

⊕ = According to Lupini et al (1981)

- Shear box sample size 6x6x2 cm
- Triaxial test size 38mm diameter x 76mm long
- Ring shear test by Bishop et al, ring shear described by Bishop et al (1971)
- " " " by La Gatta, at Harvard ring shear

LL = Liquid Limit

PL = Plastic Limit

IP = Plasticity Index

CF = Clay Fraction

distributions. Again the triaxial shear gives higher value of $\phi_r' = 16^\circ$ while the rotational shear value is $\phi_r' = 9.3^\circ$. The reason for this difference is attributed by Lagatta (1970) to limitation of shear strain possible in the triaxial shear test.

The main conclusion is that reversing shear box tests generally give values of ϕ_r' higher than those determined by ring shear tests. It is argued (See Section 4.1.4) that this is maybe due to the disturbance of particle orientation caused by the change in direction of principal stresses with each reversal. Also the effect of geometrical component may also be significant so that a true residual state is not attained. Polishing cut-plane triaxial tests also give higher values of residual shear strength which may be due to a lack of shear displacement to achieve sufficient preferred orientation of clay particles. The ring shear test which gives unlimited unidirectional displacement and enables preferred particle orientation to be obtained that produces a lower residual shear strength and is probably more representative of field conditions.

4.2.4 Test Conditions

The residual shear strength determined in the laboratory may be sensitive of a number of factors including normal effective stress value, loading sequence, rate of displacement and amount of displacement. These aspects will be considered in the following pages:

i. Normal effective stress σ_n'

Much data exist in the literature which indicates that ϕ_r' decreases with increase in σ_n' value. Work by many authors including Chandler (1966), Skempton and Pelely (1967) Hermann and Wolfskill (1966), Lagatta (1970), Garga (1970) Bishop et al (1971), Mitchell (1976), Townsend and Gilbert (1976), and Lupini et al (1981) confirm this trend. However, some for example, Townsend and Gilbert (1976) have shown that residual envelopes for

micaceous silty sand of Paraitinga material exhibits a slight curvature at lower values of normal effective stress. This curvature is in agreement with the findings of Bishop et al (1971), Lagatta (1970) and Kenney (1967) who record that up to a stress level of about 196 kN/m², ϕ_r' decrease as the normal effective stress increases. This decrease in ϕ_r' is possibly due to the higher normal effective stress forcing the clay platelets into a more orientated structure. For brown London Clay, tested by Bishop et al (1971), ϕ_r' varied from 14° at $\sigma_n' = 7$ kN/m² down to 8° at $\sigma_n' = 250$ kN/m² (See Fig. 4.21), the decrease in ϕ_r' was very marked for stresses up to 70 kN/m². Heley and MacIver (1971) suggest that both normal and shear stresses contribute to the disgregation of the material and the increase in parallel orientation of particles in the direction of the shear displacement. Also at higher normal stress values, irregularities on the shear surface would be more rapidly and completely worn away. They recommend that both low and high normal stresses be avoided and suggests that the most satisfactory results would probably be obtained using normal stress between 392 kN/m² and 782 kN/m². However, it appears sensible to use stress values which simulate field conditions being considered.

ii. Loading sequence

Research by various authors including Townsend and Gilbert (1976), Simons and Menzies (1978), Bishop et al (1971) and others indicates that the order in which the various normal effective pressures are sequenced has an insignificant effect on the value of ϕ_r' eventually computed. Fig. 4.21 is from a multistage test carried out by the latter authors. Apart from the first shear, when the residual condition was being established, a unique curve exists.

iii. Rate of displacement

Many researchers have investigated the effect of shearing rate on the measured value of ϕ_r' . Although some authors, notably Bishop et al (1971), Vaughan et al

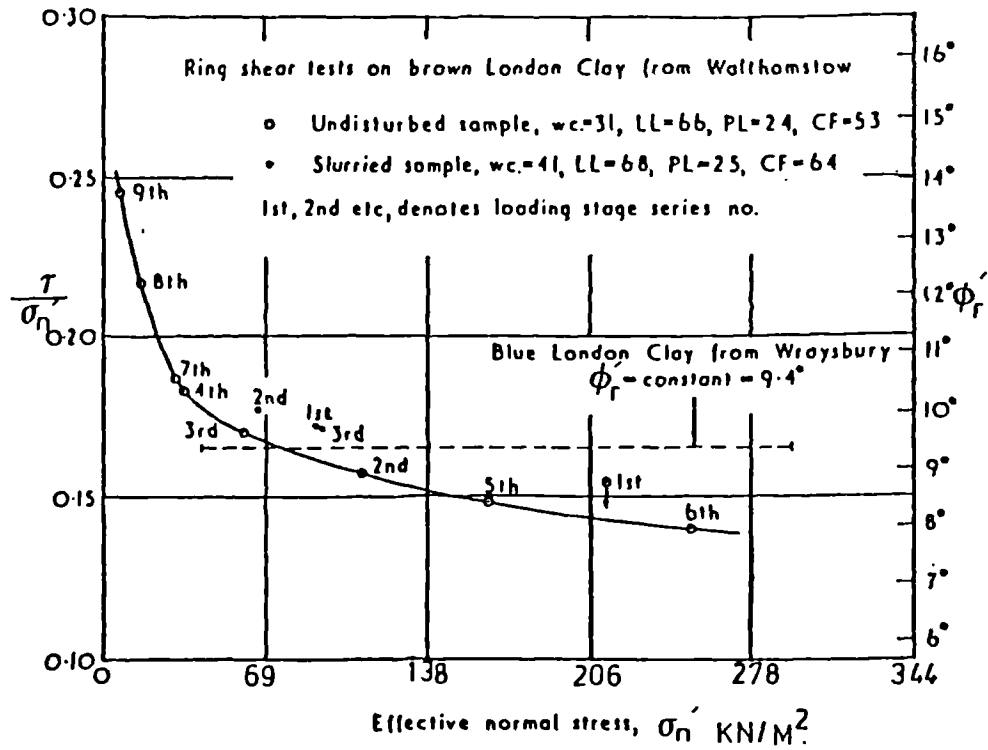


Fig. 4.21 Effects of loading sequence and value of effective normal stress on residual shear strength value. (After Bishop et al, 1971).

(1978) Skempton and Hutchinson (1964) and De Beer (1967) noticed an increase, many including Kenny (1967), Skempton (1965), Garga (1970) and Ramiah et al (1970) have not. Of particular interest are the data of Vaughan et al (1978) who recorded an increase in the value of ϕ_r' of 24% caused by an increase in the rate from 1.5×10^{-2} mm/min. to 15 mm/min. On the other hand, Lagatta (1970) recorded no change in ϕ_r' value due to a hundred fold change in rate in his tests. It would appear that for practical purpose ϕ_r' can be considered to be independent of shearing rate but there must be the proviso that full drainage of pore water occurs. Also very rapid rates produce turbulence on the shear surface and the rate of soil extrusion from the shear surface appears to increase as the rate of shearing is raised.

iv. Amount of displacement

Lagatta (1970) found that for Pepper Shale, the displacement required to reach the residual condition was reduced with increasing σ_n' . Confirmatory results were obtained by Herrmann and Wolfskill (1966), Garga (1970) and Bishop et al (1971).

The results of the shear strength test are generally displayed in the form of a graph of shear stress versus displacement or strain. Generally, τ_r is taken as minimum constant value of τ . However, Lagatta (1970) has cast doubt on some previous determinations of ϕ_r' obtained by reversing shear box test. By plotting the stress ratio τ/σ_n' against the logarithm of displacement, it is clear that in many of the cases he reviews a constant residual strength was not reached. Thus further displacement was necessary to establish the true residual condition.

To advocate plotting (τ/σ_n') against Log (displacement) implies that a true residual shear strength can not be assumed immediately after two or three constant values of τ , whether or not this causes any significant difference to ϕ_r' depends on the circumstances and, in particular, the slope of τ - strain curve.

4.3 Conclusion

From the above review of published literature on the residual shear strength of soils, some general conclusions can be derived.

- i. The main causes of reduction of the shear strength of soil from its peak to residual state are due to the orientation of clay particles in the direction of shear and formation of slickensides.
- ii. Clearly the percentage of clay sized particles plays an important determinative role in the residual shear strength of clays. The residual shear strength value decreases with increase percentage of platy clay particles.
- iii. Residual shear strength increases with increasing ion concentration of pore fluids.
- iv. There is an inverse relationship between the plasticity index and residual shear strength.
- v. Investigations of the effect on residual shear strength of increasing the normal effective stress indicate that it reduced and the amount of displacement necessary to achieve the residual strength is also lower.
- vi. The loading sequence would appear to have no effect on the residual shear strength.
- vii. The measured value ϕ_r does not appear to be sensitive to the rate of displacement provided that conditions for full drainage of pore water are maintained.
- viii. Remoulding overconsolidated clay may have a slight effect on the residual shear strength although in the case of severe preparation methods lower residual shear strength values can be obtained.
- ix. The orientation of intact samples has been found to have a significant effect on the peak shear strength of anisotropic soils, it has either no, or only a slight effect on residual shear strength.
- x. In respect to testing method the ring shear apparatus gives the lower value of residual shear strength compared with the triaxial and shear box tests. This is due to the lack of particle orientation or disturbance during shearing.

CHAPTER 5

RESIDUAL SHEAR STRENGTH TESTS

In this chapter the methods of determination, sample preparation and results for various engineering tests carried out on samples of Namurian shale from North Derbyshire are considered. The engineering properties chosen to characterise the shales and to provide data for stability analyses are those of residual shear strength of remoulded material (ϕ_{rr}' , c_{rr}'), liquid limit, plastic limit, and water content before and after shear strength testing.

5.1 Introduction

During the course of the present study, material from three sources was used:

- i. Hope Valley Cement Works (See map Fig. 2.1)
- ii. Various samples outcrops of shale at the sites of landslides (See map Fig. 2.1) for locations).
- iii. Borehole at Mam Tor (See map Fig. 7.3)

Details of the samples are presented in Table 5.1

TABLE 5.1 Source and Description of Samples Used in Analyses.

Identifier	Source	Description
CW1	Hope Valley Cement Works (See Fig. 2.1).	Coarse aggregate of wide dark grey, hard, slightly weathered fissile (fissility surface weak) shale fragments with some mica and possibly pyrite. (Particles approximately 4 - 8 cm. in size).

Table 5.1 cont'd.

Identifier	Source	Description
CW2	Hope Valley Cement Works (See Fig. 2.1).	Medium aggregate of wide similar to CW1 except for presence of thin bands of siltstone. (Particles approximately 2 - 3 cm. in size)
CW3	Hope Valley Cement Works (See Fig. 2.1).	Fine aggregate of grey to dark green forming a residual soil of a very fine shale fragments mixed with silt and sand grains. (Particles up to approximately 0.5 cm. in size).
MTBH	Mam Tor landslip core from a depth of 26 mm. Borehole 1 at Mam Tor Fig. 7.3.	Core approximately 54 mm. diameter, fresh dark grey, hard, well-jointed, very thinly laminated silty micaceous shale.
MT5	Mam Tor landslip Retrogressive unit (See Fig. 7.3)	Aggregate of fragments up to 0.5 cm. in size of dark grey, weathered, very soft, fissile shale, with bedding and lamination surfaces at 1 to 2 mm. intervals. The surfaces are covered by a reddish brown material which is probably an iron oxide. The joints and fractures are filled with brownish gypsum crystals.
MT6	Mam Tor landslip Retrogressive unit (See Fig. 7.3)	Similar to MT5 but comprising aggregate of average size 3 - 5 cm. with joint surfaces infilled with yellow sulphur compounds, probably Jarosite.
RP	Outcrop sample from Rowlee Pasture landslip (See Fig. 7.13)	Dark grey, weathered, soft, highly fissile, micaceous shale with thin siltstone lamina. Fissility and joint surfaces are covered with brownish red material indicative of Iron oxide.

Table 5.1 cont'd.

Identifier	Source	Description
AC	Outcrop sample from Alport Castles landslip (See map Fig. 7.12)	Dark grey, soft, fissile, weathered, micaceous shale. Fissility and joint surfaces have a brownish coloration. Joints surfaces undulate.
BUT	Outcrop sample from Burr Tor landslip (See Fig. 7.10)	Dark grey, soft to medium hardness, fissile, weathered shale with brownish joints and fissility surfaces.
CM	Outcrop sample from Cowms Moor landslip (See Fig. 7.14).	Dark grey, fissile, soft, weathered, micaceous shale with thin bands of siltstone. Joints surfaces are crystalline with infilling orange yellowish crusty gypsum.
CS	Outcrop sample from Cold Side landslip (See Fig. 7.8).	Grey, weathered, hard, fissile shale with thin bands of siltstone. Irregular joints surfaces.
BCL	Outcrop sample from Bretton Clough landslip (See Fig. 7.11).	Dark grey, hard, weathered shale with bands of light grey siltstone .
KS	Outcrop sample from Kinder Scout landslip (See Fig. 7.15)	Dark grey, weathered, fissile, hard shale with bands of siltstone.

The review in Chapter 4 distinguishes between the residual shear strength of intact, remoulded, crushed and disaggregated samples. Clearly the method of disaggregation may influence the shear strength properties. Incomplete breakdown during preparation may result in the release of clay particles during shearing. In order to obtain a high degree of disaggregation of the shale and also to provide a standardized method of preparation, samples were tumbled and the results compared with those for crushed material.

As shown in Section 4.2.3, the residual shear strength obtained in the laboratory may differ from that

obtained in the field and may not represent the true residual shear strength. In this study the parameters of shear obtained in laboratory by ring shear and shear box tests will be defined as remoulded residual ϕ_{rr}' , c_{rr}' and ϕ_{rp}' , c_{rp}' for remoulded peak parameters for the aggregates tested.

5.2 Sample Preparation

The shale used in this series of tests was cemented shale which was subjected to disaggregation pretreatment. Some samples were subjected to crushing by mortar and pestle while other material was disaggregated by tumbling in water.

Most geotechnical tests were carried out on material which was pre-treated by tumbling. About 600 gm. of pea sized shale fragments was put in water. The associated dusty material was discarded to avoid the inclusion of non-clay contaminants. This mixture was tumbled by end over end rotation in a 1000 ml. polythene bottle at a rate of about 50 cycles per minute for a period of 5-7 days. The disaggregated material was sieved through 36 mesh (425 μ m sieve) mixed with water and left to settle overnight. After this the clear water above the sediment was syphoned off and the suspension was centrifuged at 3000 rpm for five minutes. The excess water was removed, following which the resulting paste was thoroughly mixed on a glass plate with palette knives. This material was stored in glass beakers with a tight polythene covers to exclude air.

For crushing, air dried shale fragments free from dust were gently broken in a crock mortar using a ceramic pestle. Material passing a 36 mesh (425 μ m sieve) sieve by wet sieving, was then prepared by settling and centrifuging as for the tumbled samples. It was found by microscopic examination that much of the material retained on the sieve was composed of sand and silt sized aggregations of clay sized particles. It is also likely that crushing causes fracturing of individual mineral grains

which is likely to effect the results of the tests due to the increased proportion of rotund particles.

One sample was crushed by mortar and pestle and separated into the following size fraction by dry sieving.

- i. Passing 36 mesh retained 72 mesh.
- ii. Passing 72 mesh retained 200 mesh.
- iii. Passing 200 mesh.

Dry sieving was employed in order to *minimize* dis-aggregation by the action of water.

5.3 Experimental Procedure

In this section the laboratory experimental procedures adopted to determine the grading, plasticity and composition are described. In most cases references are made to standard description of procedures but attention is drawn to deviations from these in particular cases. The experimental procedure used in the determination of the shear strength parameters are the subject of Section 5.4.

5.3.1 Index properties

The liquid limit was determined by the cone penetrometer test described by Vickers (1978) and the plastic limit test was found by the rolling thread method described by Akroyd (1964). The plasticity index is the difference between the liquid and plastic limits.

5.3.2 Grading

Wet sieving and sedimentation were used for the determination of grain size. Samples were sieved through 72, 100, 200 B.S. mesh sieves and the material passing 200 B.S. mesh was determined by the pipette sedimentation method (Akroyd, 1964). The resulting grain size distribution was expressed as a cumulative curve and the percentages of clay silt and sand were obtained from this plot. The specific gravity of the shale was determined

by the density bottle method.

5.3.3 Composition

Extensive studies of the composition of the samples subjected to engineering tests were made. In particular the mineralogy was determined by X-ray diffraction analysis and the amount of organic carbon present was obtained by using the chromium trioxide technique.

i. Mineralogy

The procedure adopted for the determination of mineralogy by X-ray diffraction are fully described in Appendix C. The determination was carried out of ground whole rock using smear mounts. In addition, the clay mineralogy was subjected to more detailed study by analysing the $< 2 \mu\text{m}$ size fraction and carrying out tests on glycolated material. For quartz determination a powder mount was employed using the method described by Till and Spears (1969).

ii. Organic - carbon determination

The method used is described by Jeffrey (1970) in which the amount of organic carbon was determined by first removing soluble carbonate with phosphoric acid treatment and then oxidizing the remaining carbon using chromium trioxide. The carbon dioxide liberated during these processes is also measured.

5.4 Residual Shear Strength

Values of residual shear strength (ϕ_{rr}' , c_{rr}') were determined using both the ring shear and reversing shear box methods. In addition remoulded peak values (ϕ_{rp}' , c_{rp}') were measured for certain samples using the ring shear apparatus.

5.4.1 Ring Shear

The description of the ring shear test is dealt with under the headings of apparatus, sample preparation and test procedure.

i. Apparatus

As shown in Fig. 5.1 and Plate 5.1, the apparatus is a Bromhead ring shear machine manufactured by Wykham Farrance Ltd. (WF25850). An annular soil sample 4 mm. thick with inner and outer diameters of 70 and 100 mm. respectively is confined radially between concentric rings. Vertical compression is applied between two porous bronze loading platens by means of a counter balance 10:1 lever loading system. Rotation imparted to the base plate, lower platen and the lower part of the sample by means of a variable speed motor and gear box driving through a worm drive. A horizontal shear surface is caused to form close to the upper platen which is held stationary by reaction of a torque arm against load measuring matched proving rings. Both the upper and lower porous bronze platen are artificially roughened to prevent slip at the soil interface. The settlement of the upper platen during consolidation and shear can be monitored by means of a dial gauge bearing on the top of the loading hanger. The deflection of the proving rings is monitored by dial gauges and the load determined by reference to calibration charts.

ii. Sample preparation

Test were conducted only on remoulded specimens which were prepared by the methods described in Section 5.2. The sample container was saturated with water before about 40 gm. of sample was added. The material was carefully tamped into the sample recess, care being taken to avoid trapping air. The upper surface of the sample was trimmed flush with the top of the recess and some of the surplus material was set aside for water content determination. After the sample container had been clamped into position the torque arm assembly and top platen were replaced. The centreing pin was smeared with light oil to minimize friction.

The torque arm was adjusted so that the proving ring bearing rods were just touching at right angles.

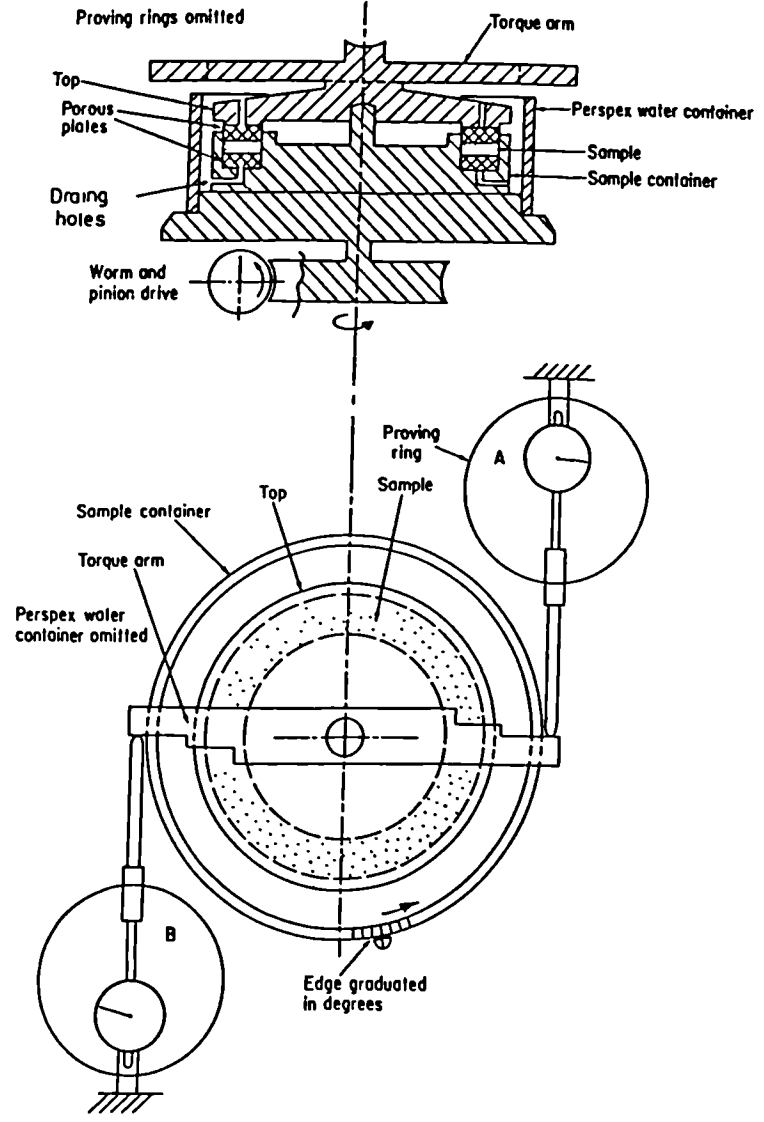
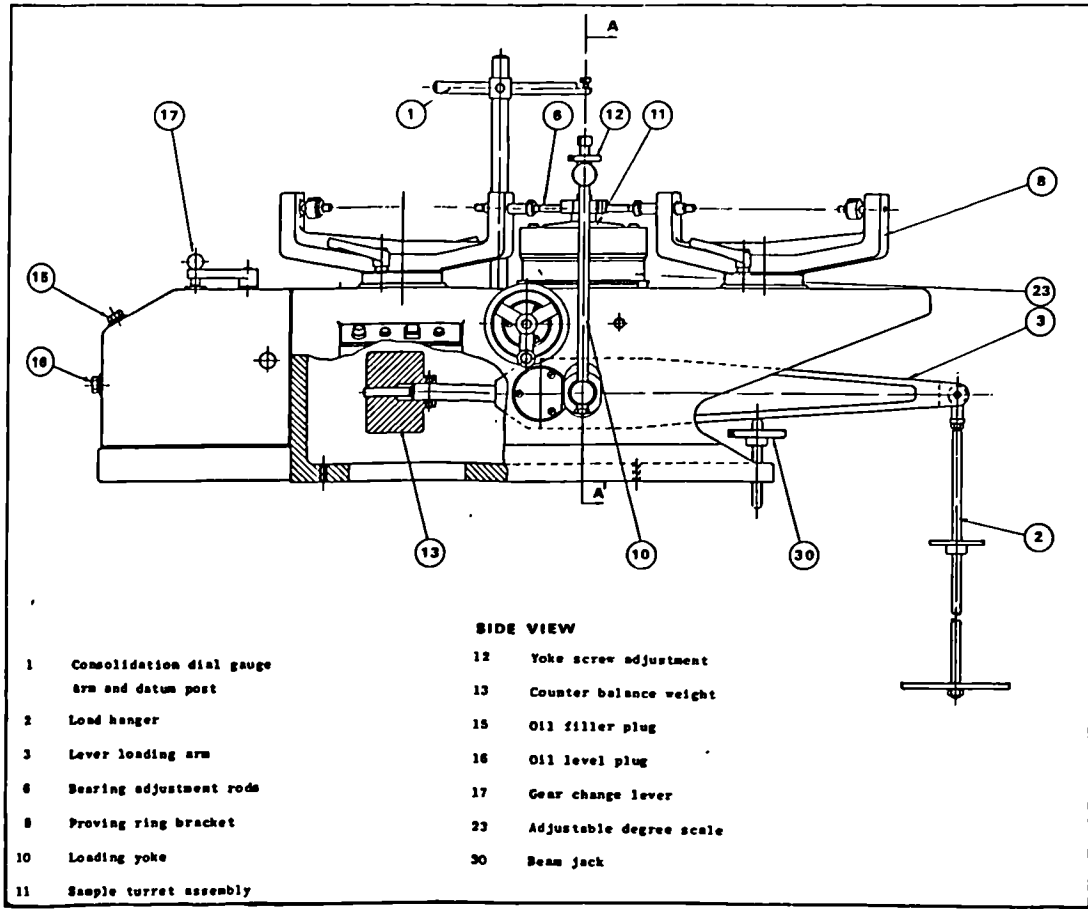


Fig. 5.1 Ring shear apparatus.

The loading yoke was then swung into position and the lever arm was levelled by adjustment to the beam jack and the yoke adjustment nut. Finally, the dial gauge was brought into contact with top of the yoke and the required weights placed on the hanger. Once the sample container had been flooded with distilled water the sample was ready for consolidation to begin.

iii. Testing procedure

Before being sheared, samples were allowed to consolidate or swell under a constant load. Detailed consolidation records were made in the case of some samples in order to calculate an appropriate strain rate to ensure fully drained test conditions. The initial consolidation of specimens was carried out under very low loads in order to minimize the squeezing of soil from the clearance between the upper platen and the sample container. Subsequently the load was increased to the required value and consolidation was completed at new pressure before shearing was begun. Checks and appropriate adjustments were made to ensure that the proving rings were bearing at right angles to the torque arm (See Fig. 5.1) and also that the lever arm remained horizontal. Once an appropriate strain rate had been selected the machine was switched on to start the shearing during which the following readings were taken

- a. Distorsion of proving rings.
- b. Angular displacement at the sample holder.
- c. Change of thickness (vertical dial).

When a test was finished, the water from the sample container was removed using a thin sponge and the apparatus was then dismantled. The top platen was removed carefully and the sample excavated in order to reveal any shear surface. A portion of the specimen was retained for water content determination and any shear surfaces were photographed.

The data were processed in the manner explained in Appendix A so that graphs of shear stress-

displacement and shear displacement - vertical displacement curves for the various normal effective stresses could be plotted. These results are included in section 5.5 in which the shear strength parameters are also derived from the data.

The remoulded shear strength of some samples was measured in the ring shear apparatus. Three different normal effective stresses were used for each sample and the procedure for preparation of the sample was the same as already described except that a different sample of soil was used for each load.

5.4.2 Shear box

The procedure for the shear box tests is described with reference to the following headings: apparatus, sample preparation and test procedure.

i. Apparatus

The apparatus is shown in Plate 5.2. It is a Wykham Farrance (WF25300) direct shear apparatus which has a facility for reversing the direction of travel on the shear plane. Some samples tested in the ring shear apparatus were also tested in the shear box apparatus to investigate the effect of testing method on the residual shear strength value. The equipment is capable of accepting both 100 mm. square and 60 mm. square sample. Attempts were made to use the 100 mm. x 100 mm. shear box since with greater displacement per travel possible this would decrease the number of reversals necessary. However difficulties were experienced since soil squeezed through the gap between the two halves of the box. Unfortunately, the top half of the shear box was forced upwards during the first reversal stroke of shear which caused increases in shear strength. Soil was lost from the gap and thus a smooth slickensided surface could not be produced. To overcome this difficulty, a bridge shown in Fig. 5.2 was fitted on the lower half of the shear box with an adjustable

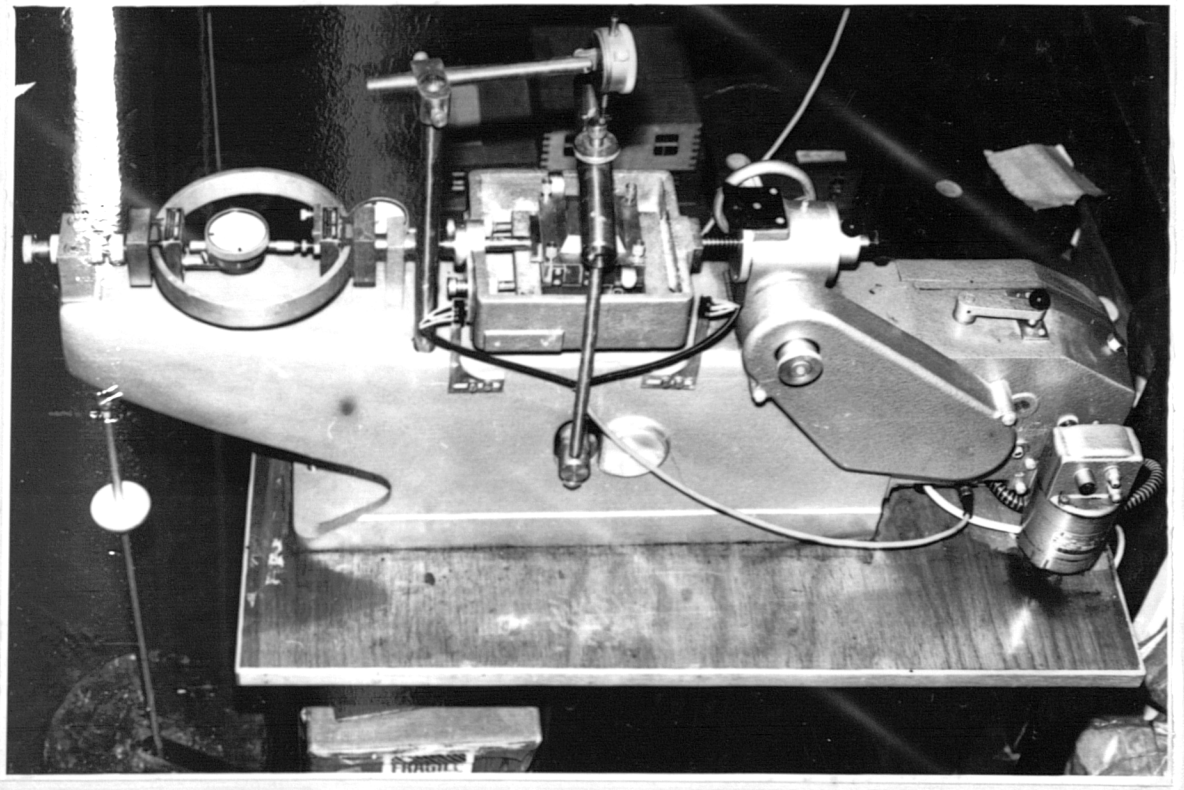


Plate No. 5.2 Shear box apparatus.

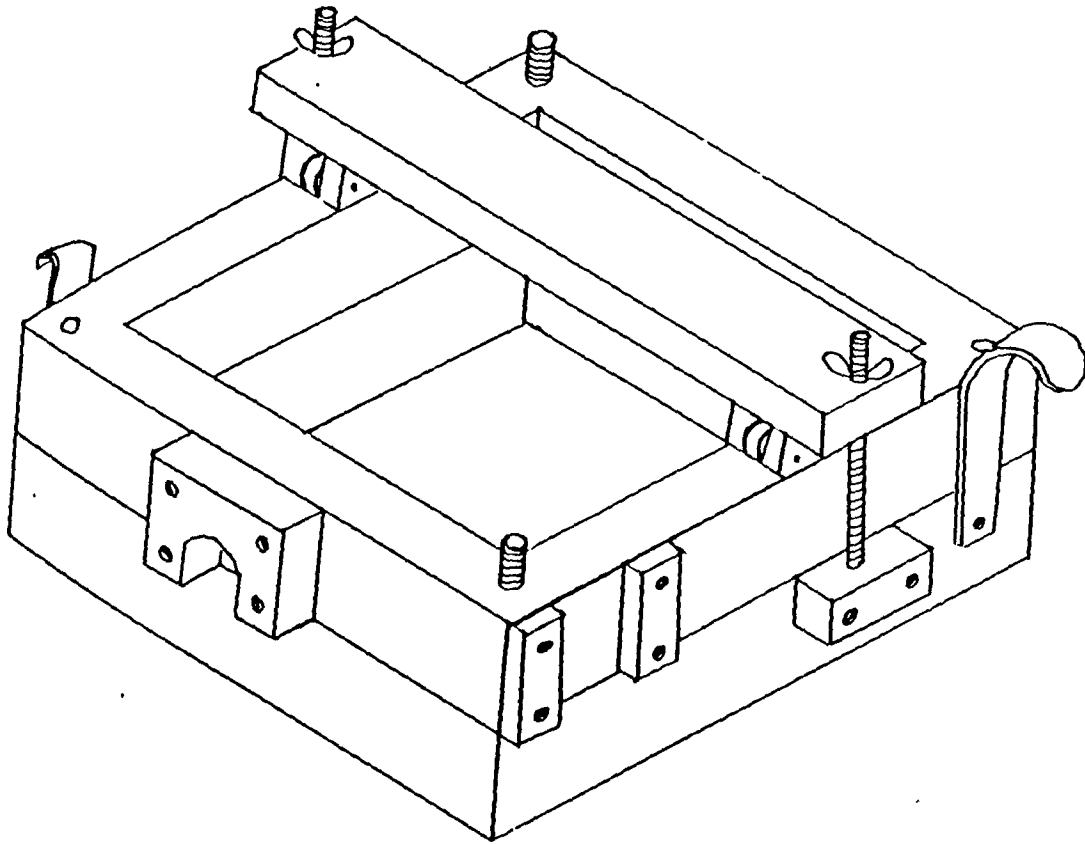


Fig. 5.2 Bridge arrangement filled to 100mm square shear box.

roller bearing on the upper half to keep the gap closed. It was found that when the shearing was reversed into compression increases in shear stress indicated that the bridge caused increased force to be generated. Also soil was still extruded and although very slow rates of strains were also tried, sample squeezing still occurred. The reasons for these difficulties are not known but they probably stem from the fact that the large surface area allows a large number disturbed grains to move towards the edge of the shear box and hence to force the gap open during reversals. Also any small non-uniformities of shear stress on the surface are liable to cause disturbance to the remoulded sample.

The small 60 x 60 mm. shear box operated with a displacement of 5 - 6 mm. per travel was found to be quite satisfactory in terms of soil extrusion. In order to reduce machine attendance electrical reversing switches were fitted. Unfortunately these were not fully reliable since the switches required displacement to operate so that although they would switch off they would not always activate the reverse shear.

ii. Sample preparation

To prepare for shear box test, the equipment was first washed in distilled water to leave the upper and lower porous stone saturated with water. The box was then assembled with the base plate porous stone and lower ridged plate. A small portion of remoulded sample (See Section 5.2) was retained for water content determination and the remainder was packed into the box in three layers. Care being taken to ensure that air was not trapped. The top of the sample was smoothed level at 8-10 mm. below the top of the sample container and the upper ridged plate, porous stone and pressure pad were then put in place. The shear box assembly was then placed in the carriage and engage with the drive and proving ring attachments. The loading yoke was then adjusted so

that the lever arm was horizontal and very light pressure rested on the top pad. With the lever arm supported on the screw jack the weights necessary to give the required normal pressure (See Appendix A) were added to the hanger and the vertical displacement dial gauge was positioned and read, after which the carriage was filled with distilled water. The arrangements were completed by setting up the shear and displacement dial gauge and zeroing both this and the proving ring dial gauge.

iii. Test procedure

Samples were consolidated by multiple stage loading, in which complete consolidation was indicated by the vertical dial gauge before further loading. The results of some consolidation stages were used to determine a suitable rate of strain which ensured full dissipation of pore water pressure during the test (See Appendix A). During the initial stage of shearing, readings of the proving ring, shear displacement and vertical displacement dial gauges were made at 0.002 - 0.004 mm displacement intervals. Where a sample were tested at more than one normal pressure it was allowed to consolidate or swell at the new normal pressure before shearing was commenced.

On completion of the tests, the sample container was drained using a sponge and the shear box was dismantled carefully to reveal and photograph any well developed shear surface. A small sample of soil was set aside for water content determination.

5.4.3 Presentation of the results

The observations made during the tests were process using the methods described in Appendix A. As directed in Section 5.4.1 graphs of shear displacement versus shear stress and vertical displacement were plotted and hence the shear strength parameters were obtained by least

squares regression of shear stress - effective normal stress diagrams. For the ring shear results the calculation of the shear stress and plotting was programmed on the 1906 computer (See Appendix B), while for the shear box tests a desk calculator was used and the results plotted manually.

5.5 Test Results and Discussion

Table 5.2 summarizes the sample numbering and preparation techniques discussed in the previous sections of this chapter. In Section 5.5.1 the classification and composition results are presented and discussed. The remainder of Section 5.5 is devoted to the consideration of the shear strength tests.

5.5.1 Classification and composition

Under this heading the results of tests to determine the Atterberge limits, grading, mineralogy, organic-carbon and other engineering properties are considered.

i. Atterberg limits

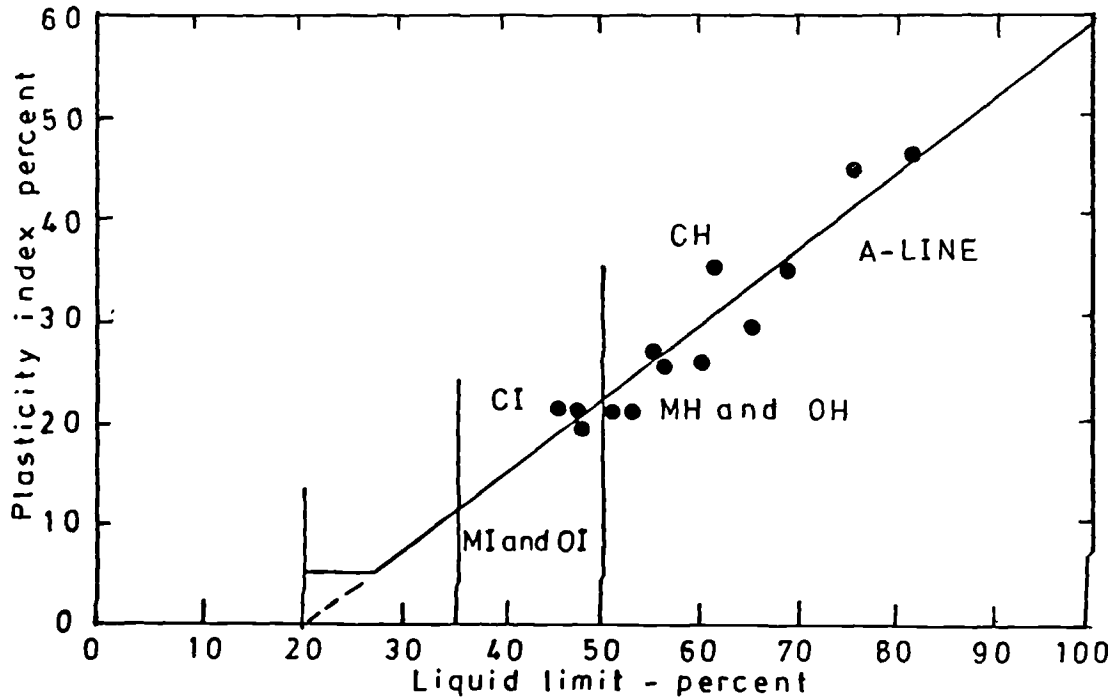
The engineering properties of the samples tested are summarized in Table 5.3. Fig. 5.3 indicates a fairly narrow grouping of plasticity values parallel to the 'A' line with the majority of samples having high plasticity, while a few have medium plasticity. The relation between the liquid limit and clay fraction in Table 5.3 is shown in Fig. 5.4. These data are somewhat scattered, but the approximately linear relationship agrees with findings of Davidson and Sheeler (1952). A linear relation is also seen between clay fraction and plasticity index in Fig. 5.4, since the activity of soil (Skempton, 1953 C), is the ratio of plasticity index to the abundance of the clay fraction defined as the percent dry weight of less than 2μ fraction. Table 5.3 shows the activity of the samples used. Thus the average activity is about 0.85, indicative normal activity. A

Table 5.2 Sample numbering and preparation techniques

Sample	Preparation technique
MTBH ,CW1,CW2,CW3,MT5, MT6,CM,BUT,AC,RP,CS, BCL,and KS (tumbled)	Prepared by tumbling sieved through 36 mesh B.S.
CW1C,CW2C,CW3C, (undifferentiated crushed)	Same sample of CW1,CW2 and CW3 but sample prepared by crushing. Sieved through 36 mesh B.S.
CW1CP200 CW1CR200 CW1CR72 (differentiated crushed)	Same sample as CW1. crushed sample grains passing 200 mesh. Crushed sample, Grain retained 200 mesh. Crushed sample. Grain retained 72 mesh.

Table 5.3 Results of Alterberg limits, grading, mineralogy, organic carbon, soluble carbonate, clay / quartz ratio determinations and activity

Sample	Liquid limit LL %	Plastic limit PL %	Plasticity Index IP %	% by weight			Quartz % by XRD	Clay/ Quartz ratio	organic carbon %	Co ₂ Or soluble carbonate %	activity IP%/ = clay%
				clay %	silt size grain %	sand size grain %					
MTBH	76.5	31.0	45.5	61.5	37.5	1.0	21.0	2.9	2.9	0.1	0.74
CW1	58.0	31.5	26.5	39.0	61.0	0.0	15.5	2.5	1.4	0.1	0.68
CW2	48.5	27.5	21.0	30.0	63.0	7.0	20.5	1.4	1.4	1.1	0.70
CW3	46.5	24.0	22.5	30.0	60.0	10	22.0	1.3	1.8	0.9	0.75
MT5	83.0	37.0	46.0	50.0	50.0	0.0	18.0	2.7	3.0	0.05	0.92
MT6	61.5	25.5	36.0	30.0	68.5	1.5	24.5	1.2	2.8	0.05	1.20
CM	65.0	36.0	29.0	45.0	54.5	0.5	15.5	2.9	1.4	0.04	0.64
BUT	60.5	34.0	26.5	37.0	62.5	0.5	20.5	1.8	1.4	0.05	0.71
AC	58.0	30.5	27.5	32.0	67.0	1.0	24.5	1.3	1.4	0.07	0.86
RP	69.5	34.5	35.0	34.0	65.5	0.5	22.5	1.5	2.7	0.02	1.02
CS	51.5	29.5	22.0	33.0	66.0	1.0	18.0	1.8	1.8	0.04	0.66
BCL	52.5	31.5	21.0	27.0	71.0	2.0	34	0.8	2.9	0.08	0.77
KS	48.0	29.0	19.0	23.0	76.5	0.5	27.5	0.8	1.8	0.05	0.82



- CH inorganic clay of highly plasticity fat clay.
- CI clay inorganic of medium plasticity.
- OI organic clay of medium plasticity.
- MI silty clay inorganic with medium plasticity.
- OH organic clay of high plasticity.
- MH highly compressible micaceous soil of high plasticity.

Fig. 5.3 Plasticity chart for samples used in shear strength tests.

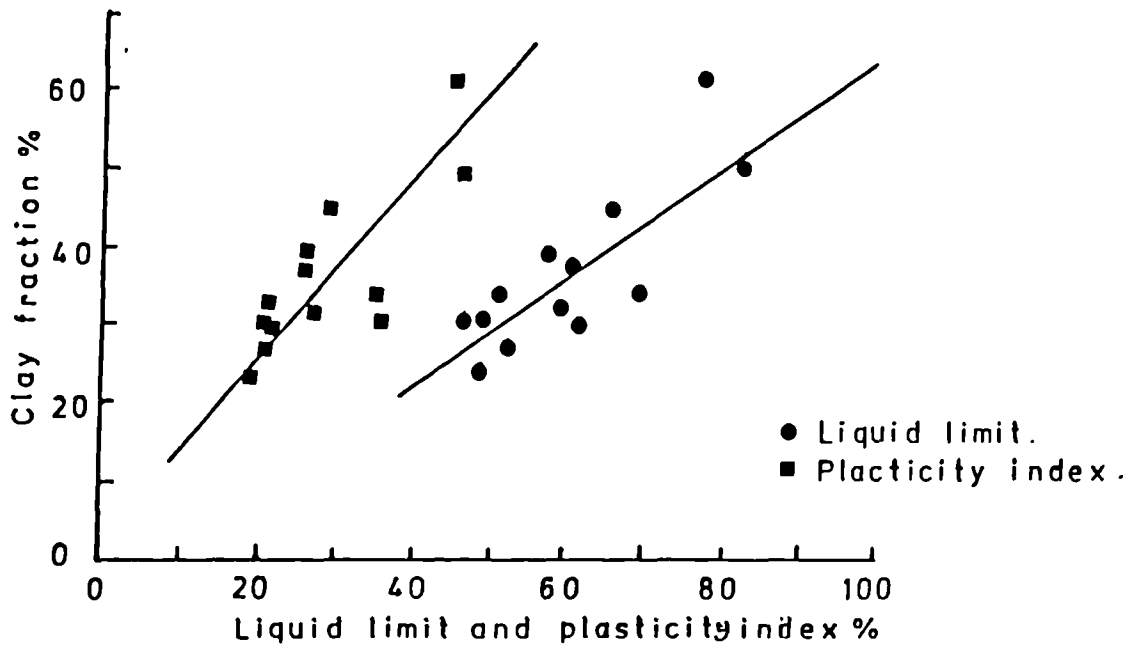


Fig. 5.4 Effect of clay fraction on liquid limit and plasticity index.

ratio of less than 0.75 would be inactive clay and values greater than 1.25 refer to active clay.

ii. Grading

The practical size distribution of all the tumbled samples are presented in Fig. 5.5A and B. The samples can be considered in terms of their clay contents ($< 2 \mu\text{m}$ fraction) and further distinguished with reference to silt content ($< 0.06 \text{ mm.}$ fraction). The percentages of clay, silt and sand sizes shown in Table 5.3 are taken from Fig. 5.5A and B. Grading will be discussed with respect to residual shear strength in Section 5.6.

iii. Mineralogy

The quartz percentages shown in Table 5.3 are determined as shown in Section 5.3.3. The ratio of clay grain $< 2 \mu\text{m}$ to quartz are also shown in Table 5.3.

The mineralogy of the whole sample was determined by the XRD technique shown in Appendix C. The most important minerals obtained from the 13 tumbled samples are in order of abundance: quartz, kaolinite and illite, pyrite was found in trace amounts in the Hope Valley Cement Works. Gypsum was also detected in samples from the Hope Valley Cement Works and trace amount of feldspar also occurred in all tumbled samples.

The percentages of the clay minerals estimated by the semi-quantitative method described in Appendix C are shown in Table 5.4 together with ratios of each clay mineral to quartz. The relation of ϕ_{rr} to the mineralogy will be discussed in Section 5.6.

iv. Organic - carbon

The result of the organic-carbon determination mentioned in Section 5.3.3 are shown in Table 5.3. As indicated in this table the amounts range between 1.4% and 2.9% for the 13 tumbled samples tested in the ring shear apparatus while soluble carbonate forms a very low percentage of 0.02 - 0.1% in all except samples from Hope Valley Cement works where it is 0.9 to 1.1%. The relationship of organic-

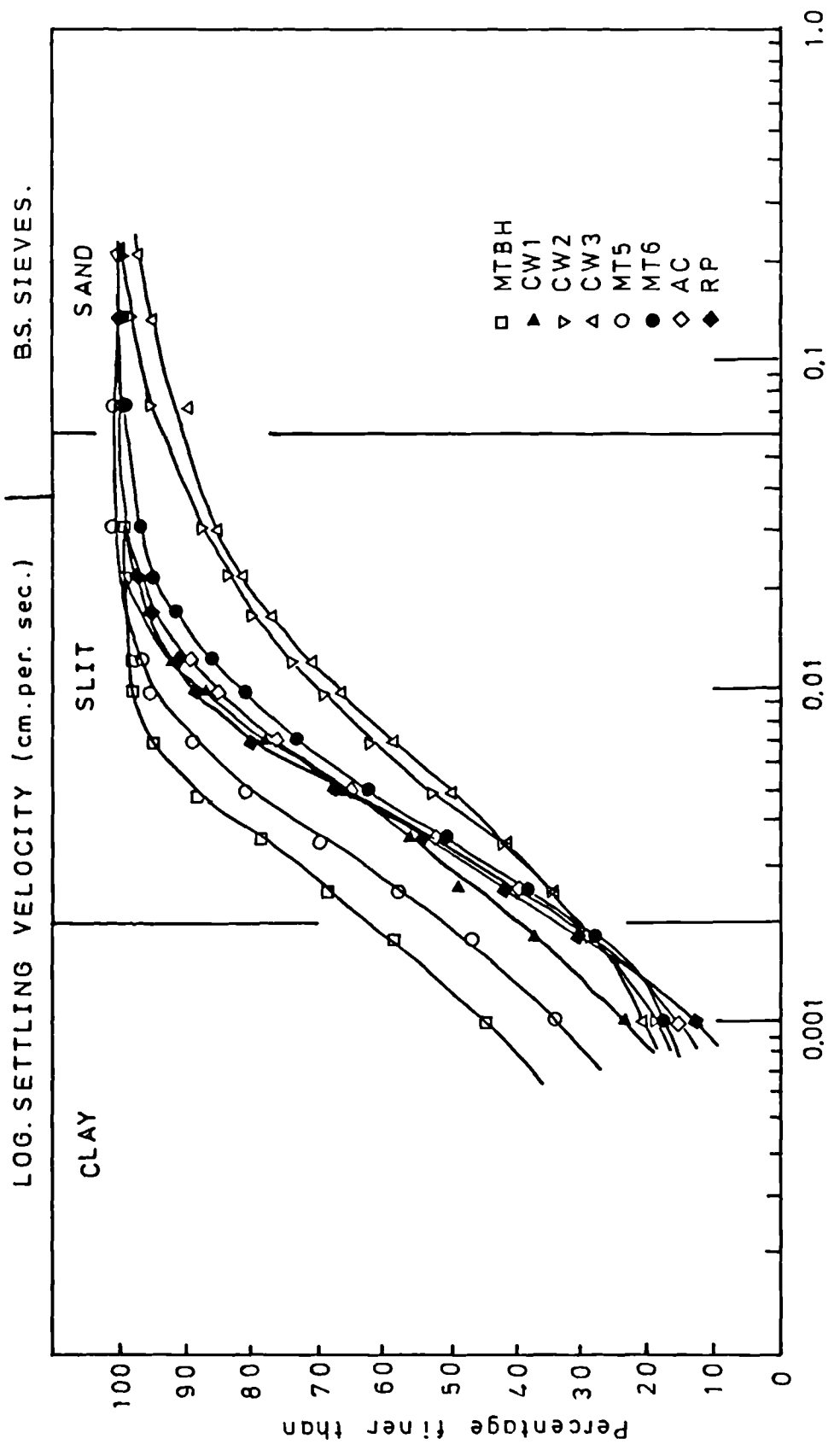


Fig. 5.5 A Grain size analysis for tumbled samples.

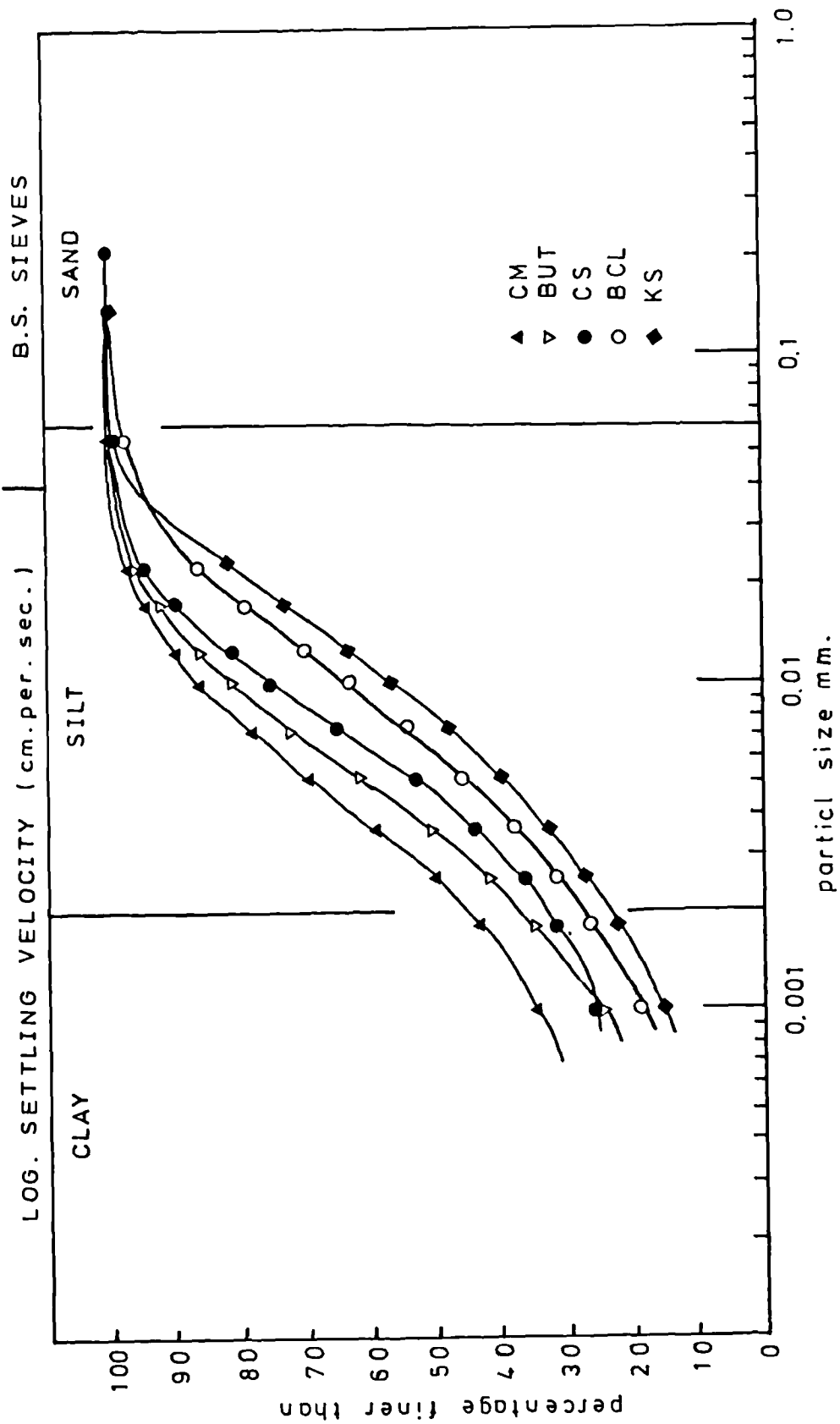


Fig. 5.5 B Grain size analysis for tumbled samples.

Table 5.4 Clay mineral abundances expressed as percentages (<2 micron clay fraction). and the ratio of clay mineral abundances expressed as a percentage of the clay size fraction.

sample	clay mineral (weight)			Clay mineral (weight) (% clay fraction)			kaolinite% quartz%	Illite% quartz%	chlorite quartz%	mix-layer% quartz%		
	kaolinite		mixed layer	kaolinite		Illite						
	%	chlorite		%	chlorite							
MTBH	40.9	4.8	8.0	46.2	25.2	2.9	4.9	28.4	12	0.23	0.13	1.35
CW1	54.4	4.6	22.3	18.5	21.2	1.8	8.7	7.2	1.35	0.56	0.11	0.46
CW2	45.5	8.6	24.1	21.6	13.6	2.6	7.2	6.4	0.66	0.35	0.12	0.31
CW3	34.8	9.1	29.8	26.6	10.4	2.7	8.9	7.9	0.47	0.40	0.12	0.36
MT5	36.8	-	20.7	42.0	18.4	-	10.3	21.0	1.00	0.56	-	1.15
MT6	16.8	-	17.7	65.4	5.0	-	5.3	19.6	0.20	0.20	-	0.80
CM	30.7	8.4	43.0	17.7	13.8	3.7	19.4	7.9	0.88	1.23	0.23	0.50
BUT	45.3	17.0	13.9	23.6	16.8	6.3	5.1	8.8	0.82	0.24	0.30	0.43
AC	45.0	9.0	27.6	18.2	14.4	2.9	8.8	5.8	0.58	0.35	0.11	0.23
RP	37.3	20.4	19.2	22.9	12.7	6.9	6.5	7.7	0.55	0.28	0.30	0.34
CS	25.0	14.3	35.6	25.0	8.2	4.7	11.7	8.2	0.45	0.65	0.26	0.46
BCL	17.0	27.8	21.1	33.9	4.6	7.5	5.7	9.1	0.13	0.16	0.22	0.76
KS	38.2	7.6	38.5	15.5	8.8	1.7	8.8	3.5	0.31	0.31	0.06	0.12

carbon content to ϕ_{rr}' for ring shear tests on tumbled samples is discussed in Section 5.6.

5.5.2 Ring shear

The shear stress-shear displacement relationship are shown in Fig. 5.6 for tumbling samples and Fig. 5.7 for crushed samples. It is noticeable that a much smoother stress-displacement curve is obtained for the tumbled samples except for samples MTHB in Fig. 5.6a. The cause of this fluctuation may be the extrusion of soil while for CW2 and CW3 (in Fig. 5.6c and d), the reason may be the presence of rotund particles of silt and sand. Table 5.3 indicates that both have a relatively high percentage of sand grains.

In most tests (See Figs. 5.6 and 5.7) a gradual increase in shear stress after the minimum value has been reached is observed. Sometimes this followed by gentle decrease. The increase may be due to either overnight drying of samples or the effect of the loss of material through the gap.

All samples were carefully examined for the presence of slip surfaces. Plates 5.3 and 5.4 show the slip surfaces in samples MTBH and CS in which slickensides are well developed.

5.5.3 Shear box

Fig. 5.8 presents the shear stress-displacement curves for the shear box tests. In fact some difficulty arises with the interpretation of these data due to the variation of the shear stress for the tensional and compressional conditions. During tensional shear a steady increase in shear stress is attributed to irregularities on the slip surface. The surface formed after the few mm. displacement for peak strength will not be flat (See Section 4.2.3) so that continued shearing causes the mating points of the upper and the lower halves to move away from each other. The work done in forcing the two

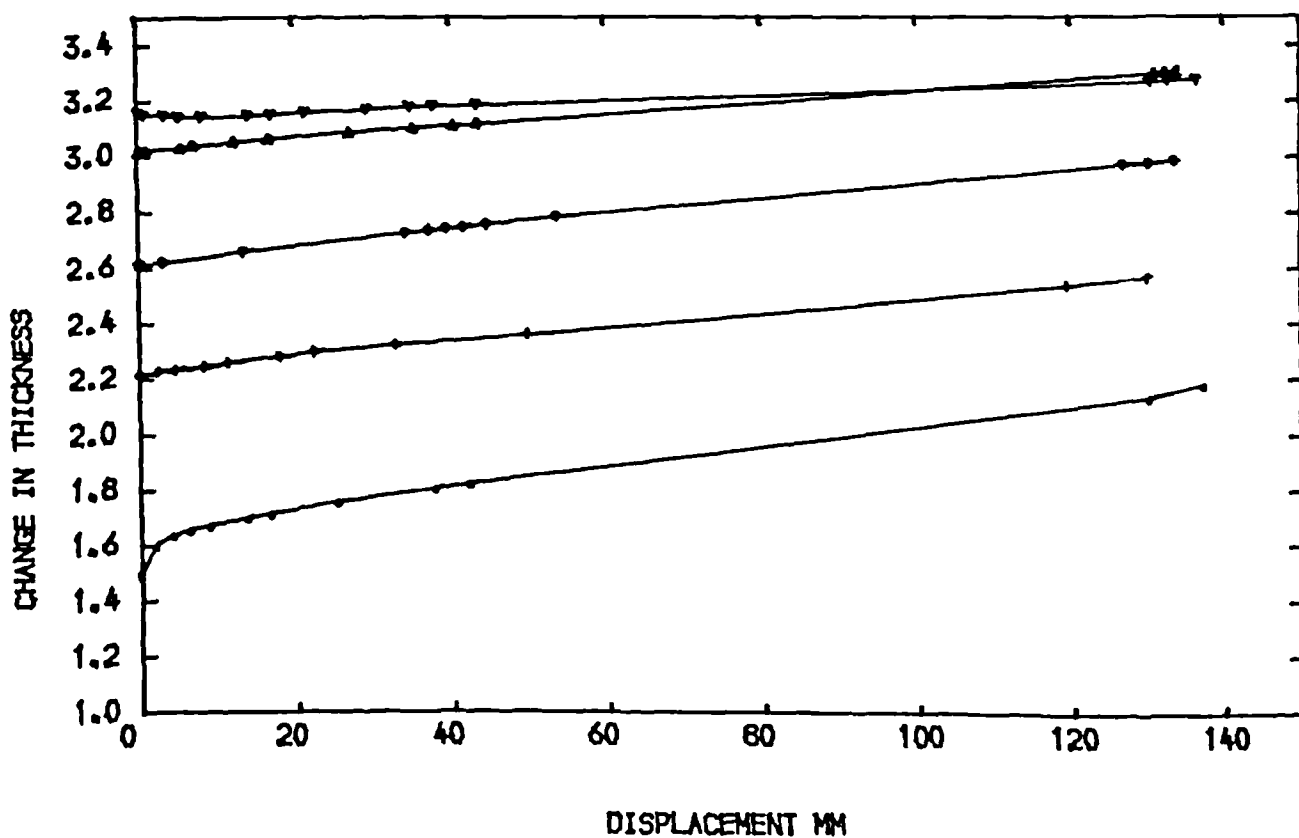
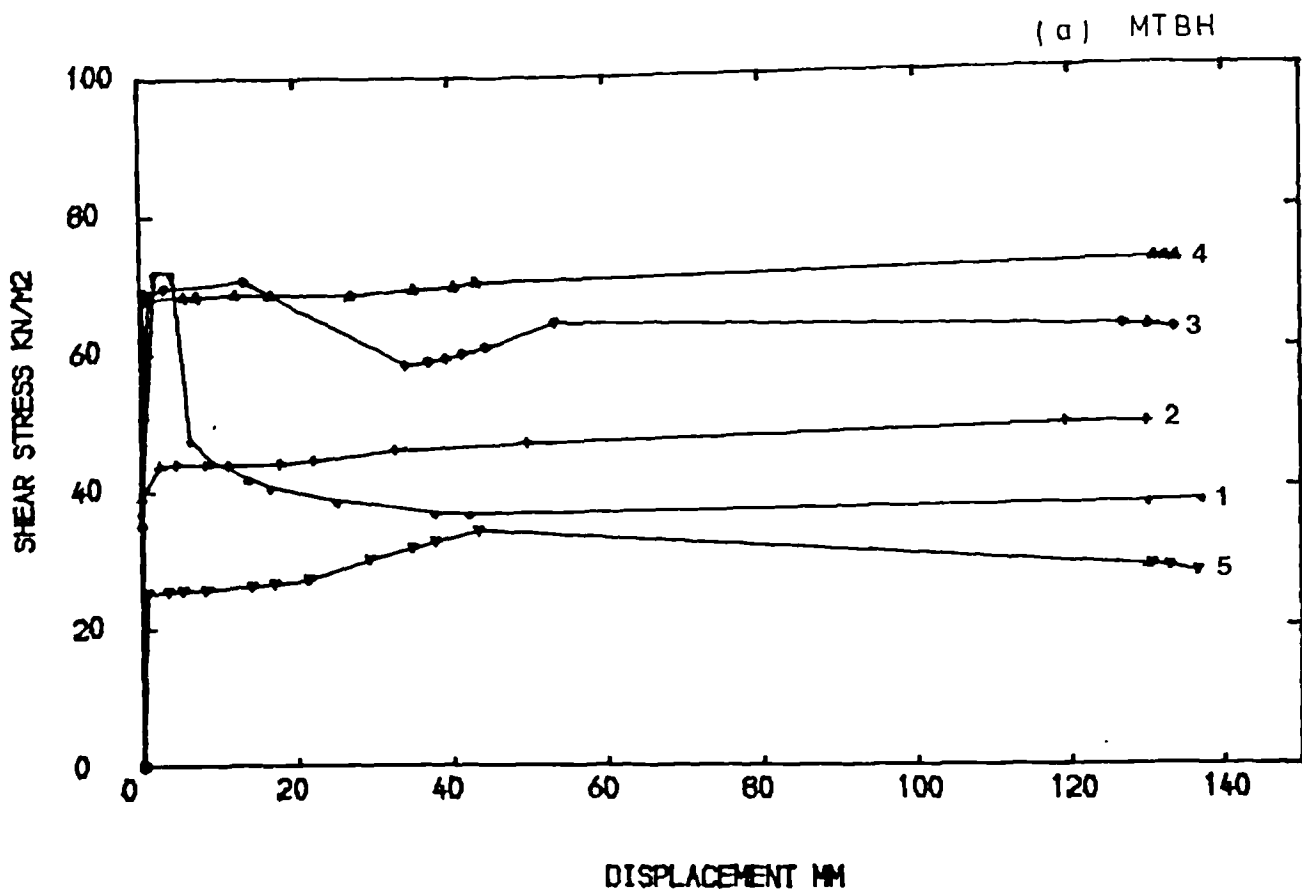


Fig. 5.6_a Shear stress-displacement and displacement vertical thickness relationship for ring shear tests on tumbled remoulded samples.

(b) CW1

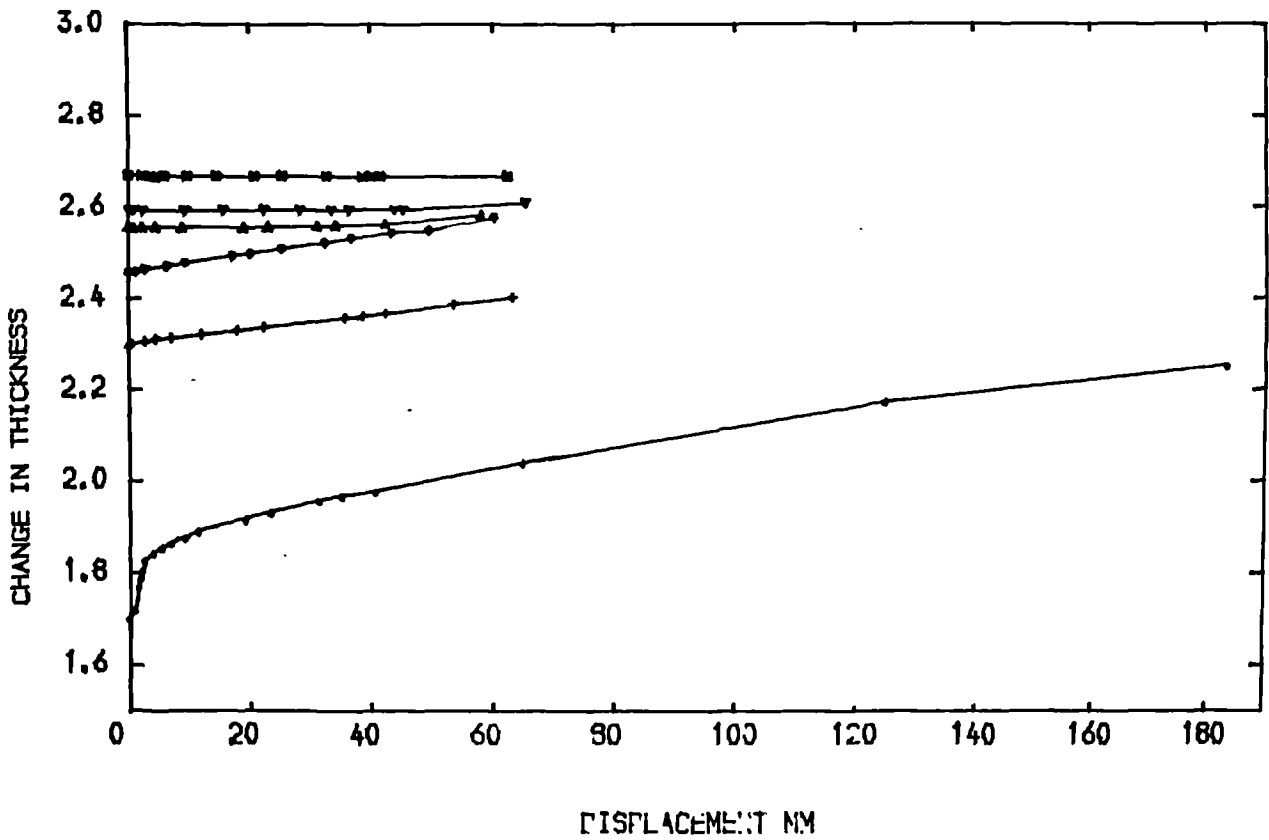
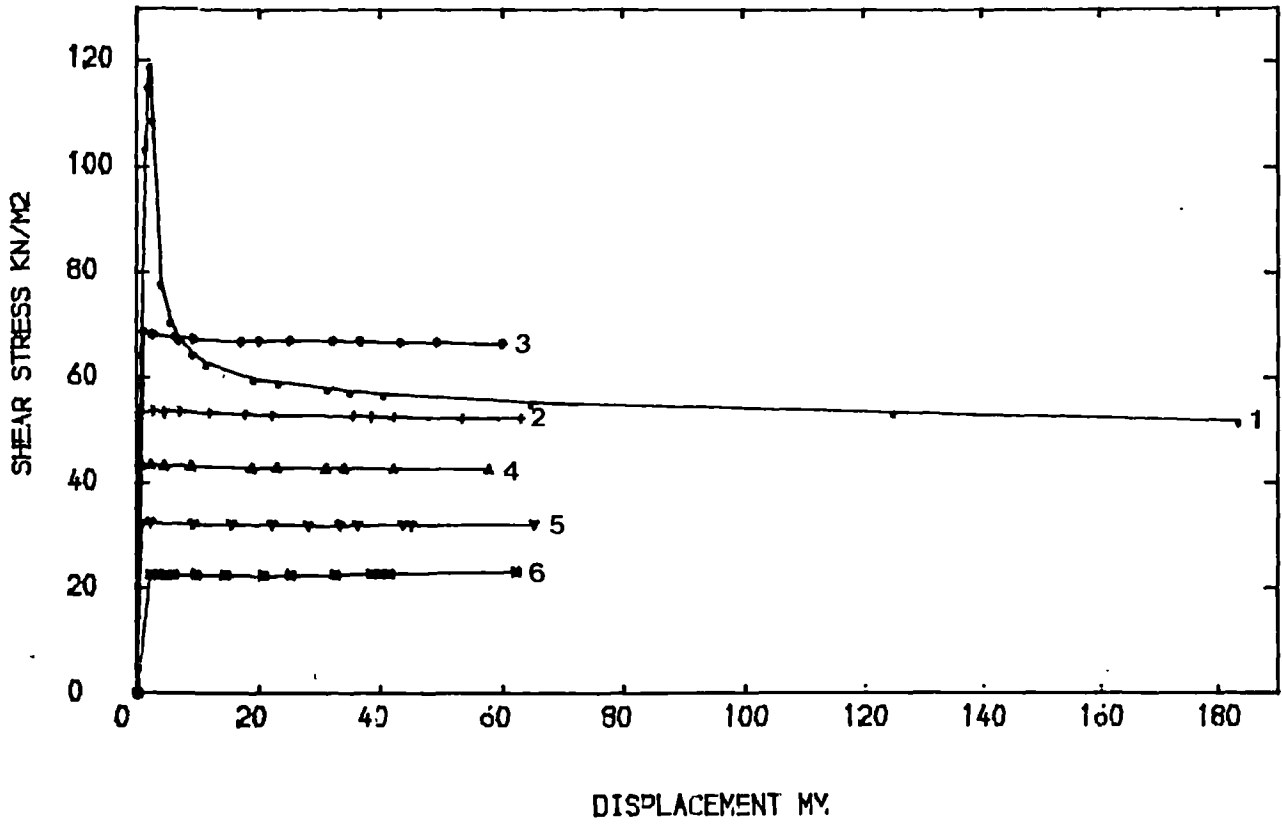


Fig. 5.6b Shear stress-displacement and displacement vertical thickness relationship for ring shear tests on tumbled remoulded samples.

(c) CW2

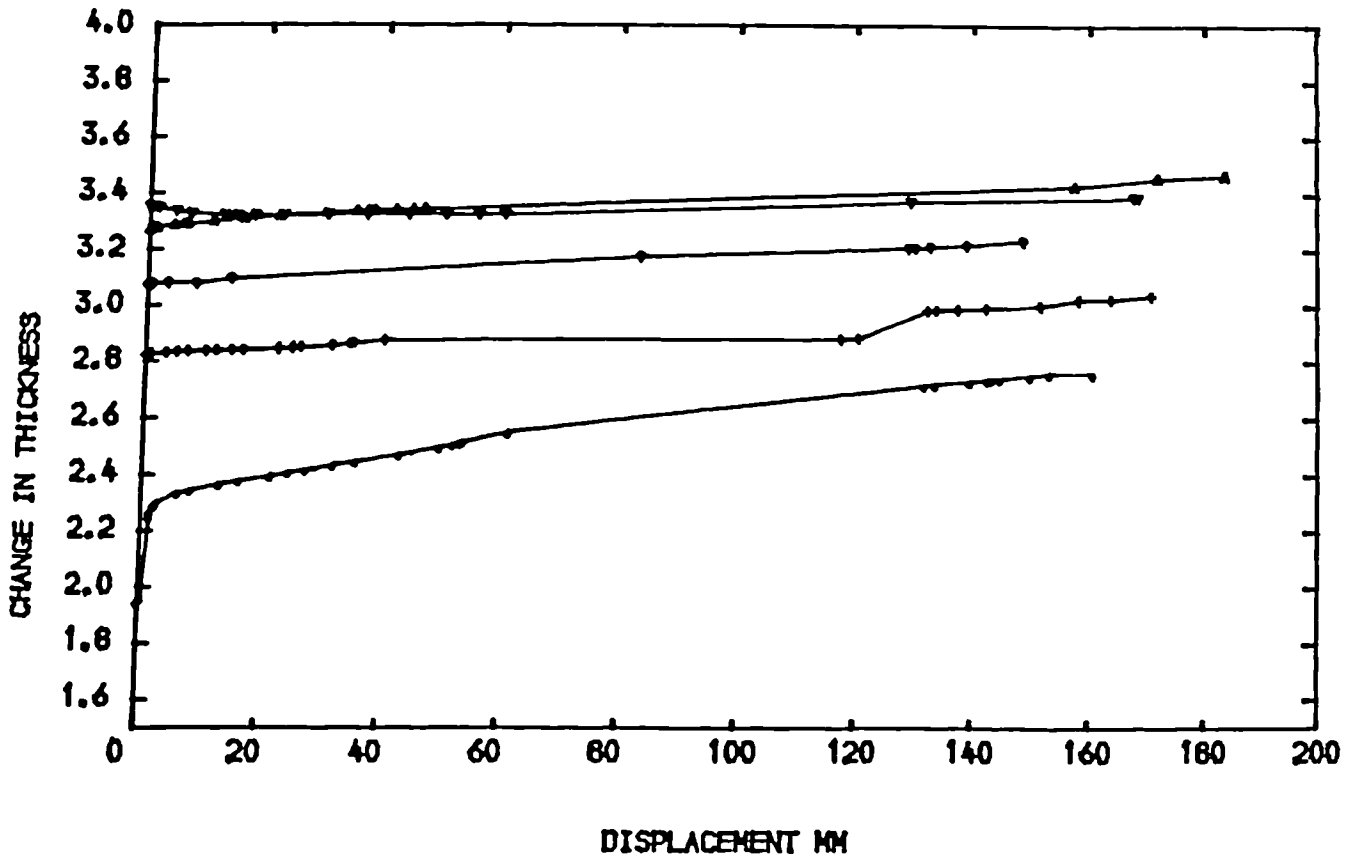
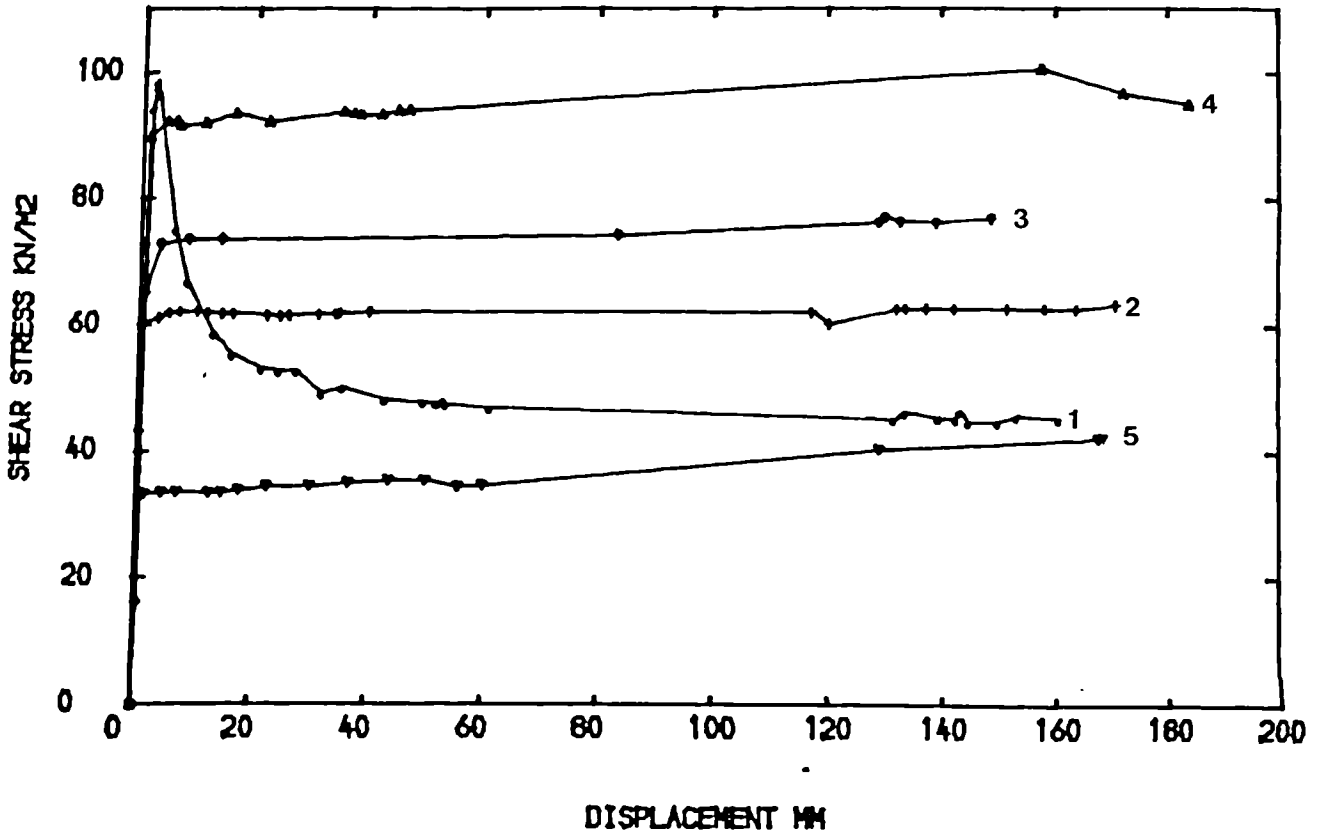


Fig. 5.6c Shear stress-displacement and displacement vertical thickness relationship for ring shear tests on tumbled remoulded samples.

(d) CW3

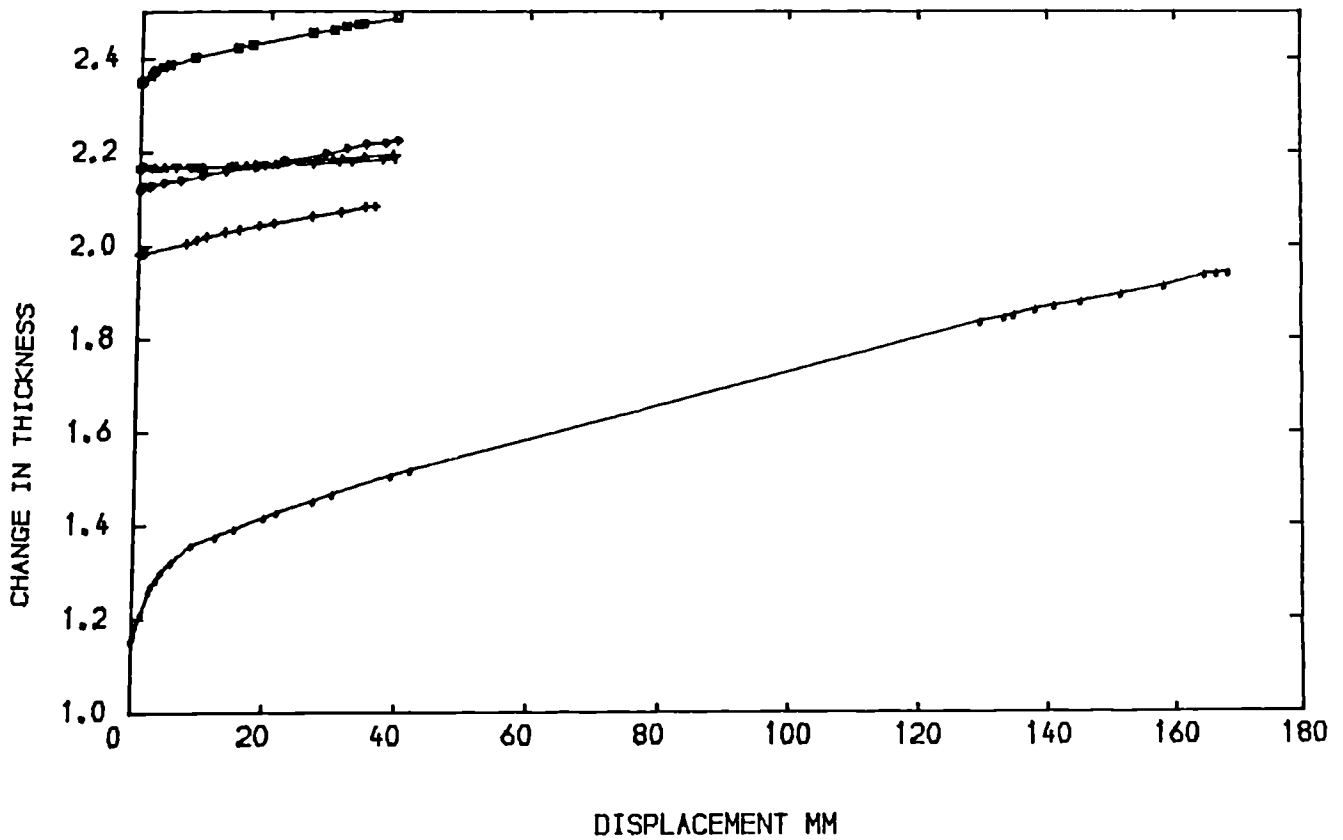
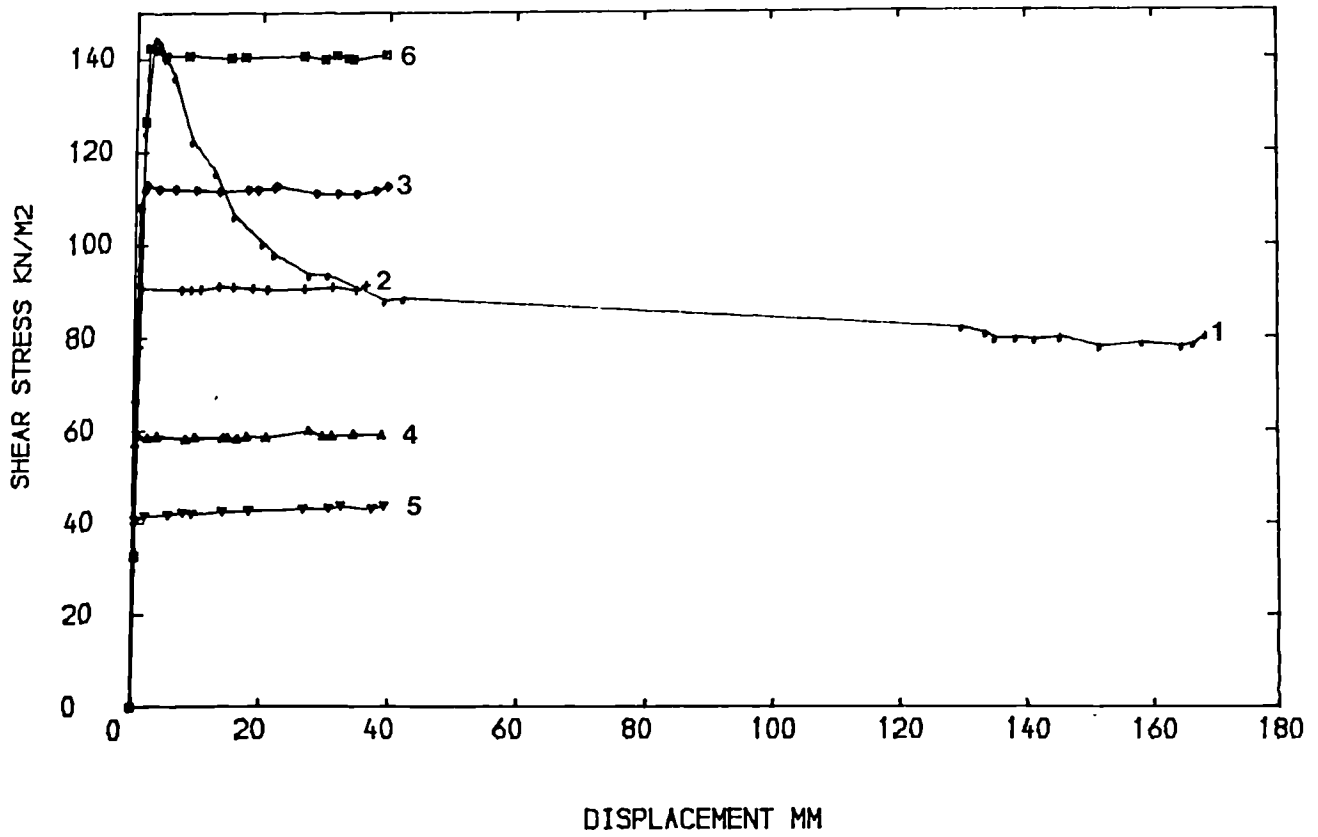


Fig. 5.6a Shear stress-displacement and displacement vertical thickness relationship for ring shear tests on tumbled remoulded samples.

(e) MT5

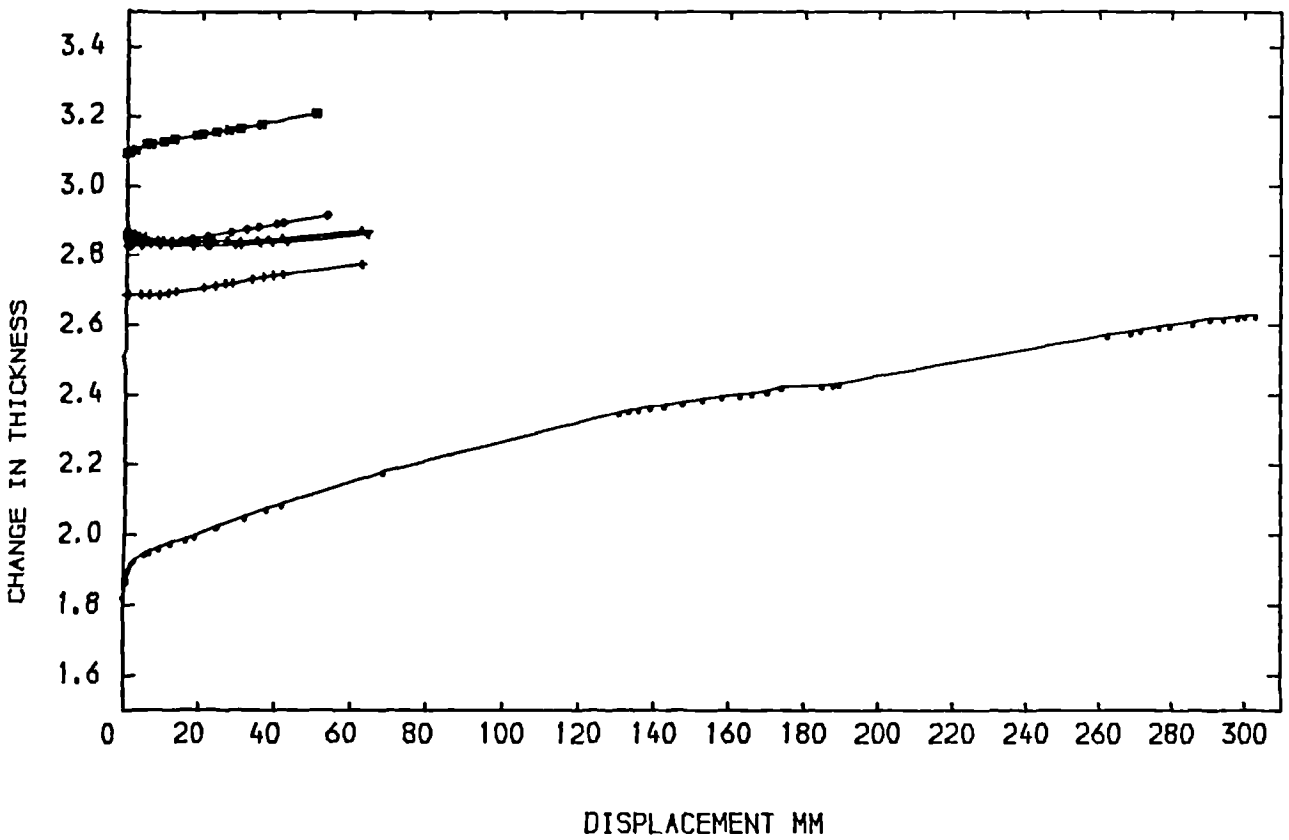
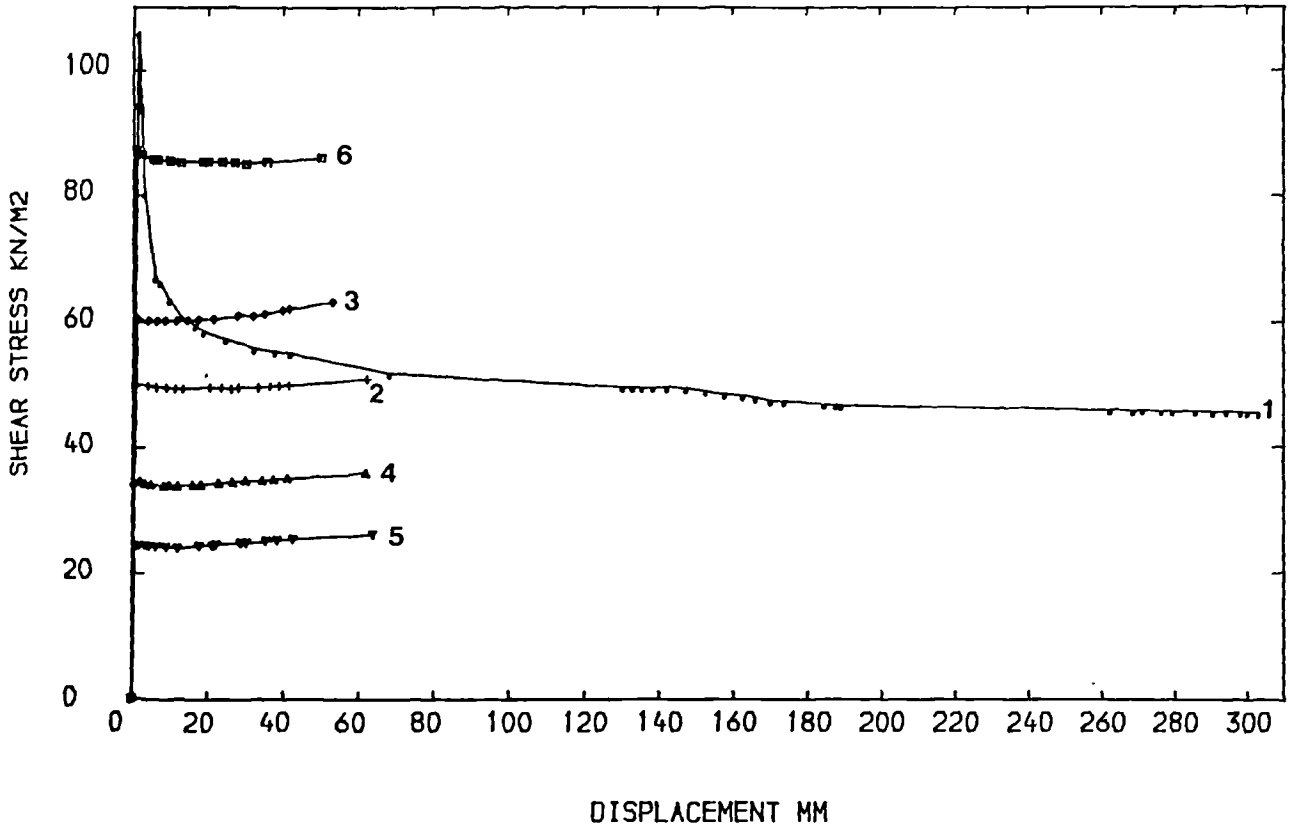


Fig. 5.6e Shear stress-displacement and displacement vertical thickness relationship for ring shear tests on tumbled remoulded samples.

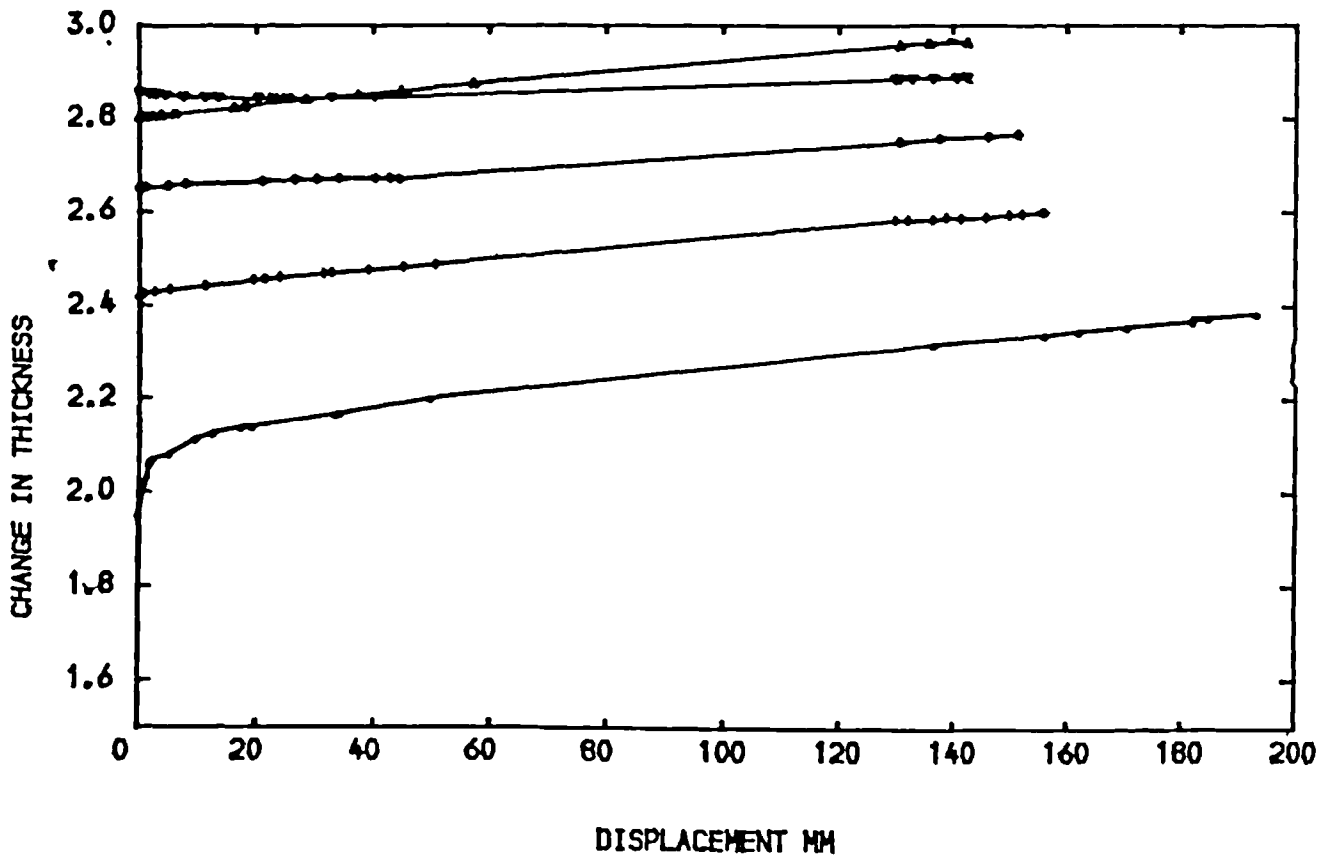
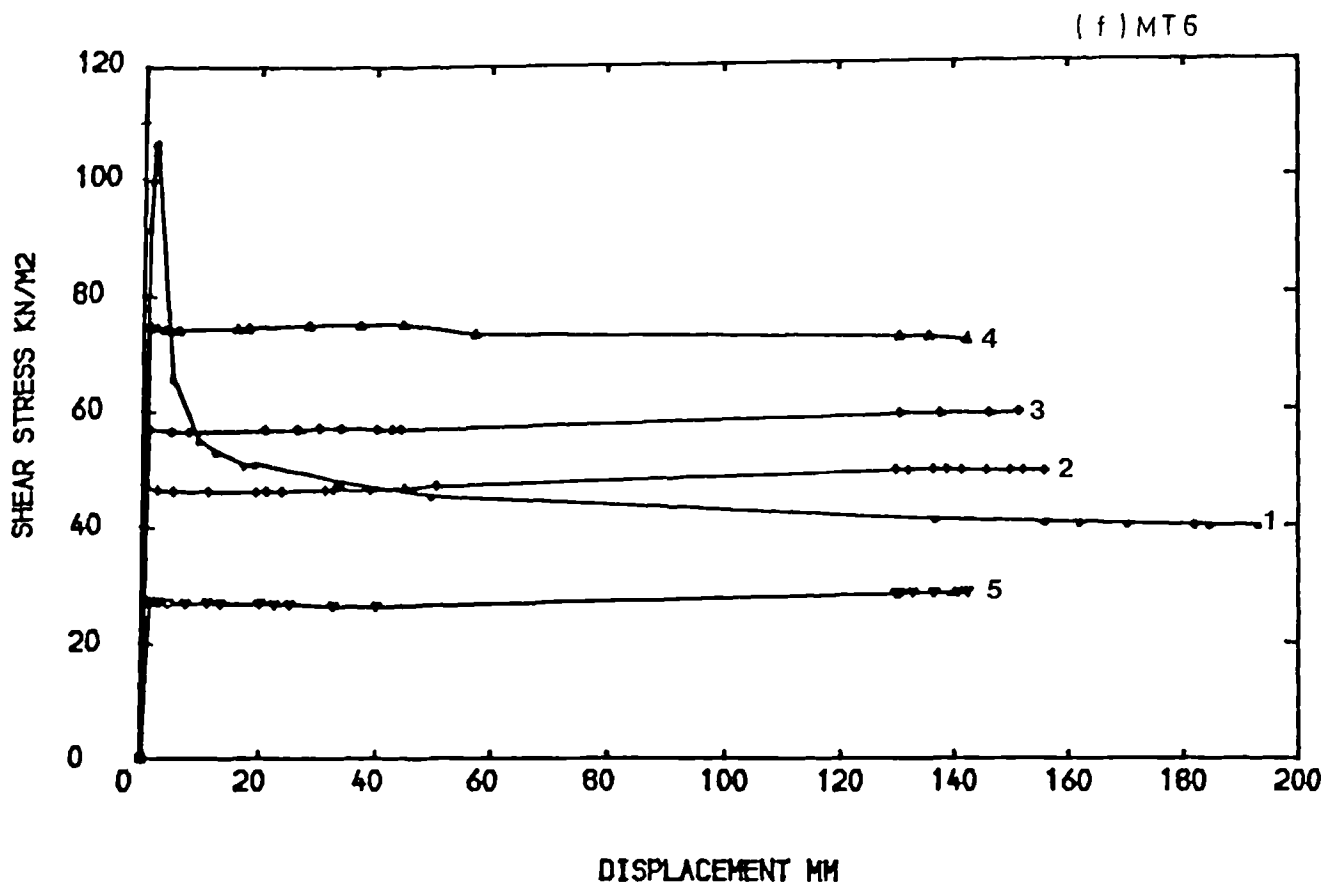


Fig. 5.6f Shear stress-displacement and displacement vertical thickness relationship for ring shear tests on tumbled remoulded samples.

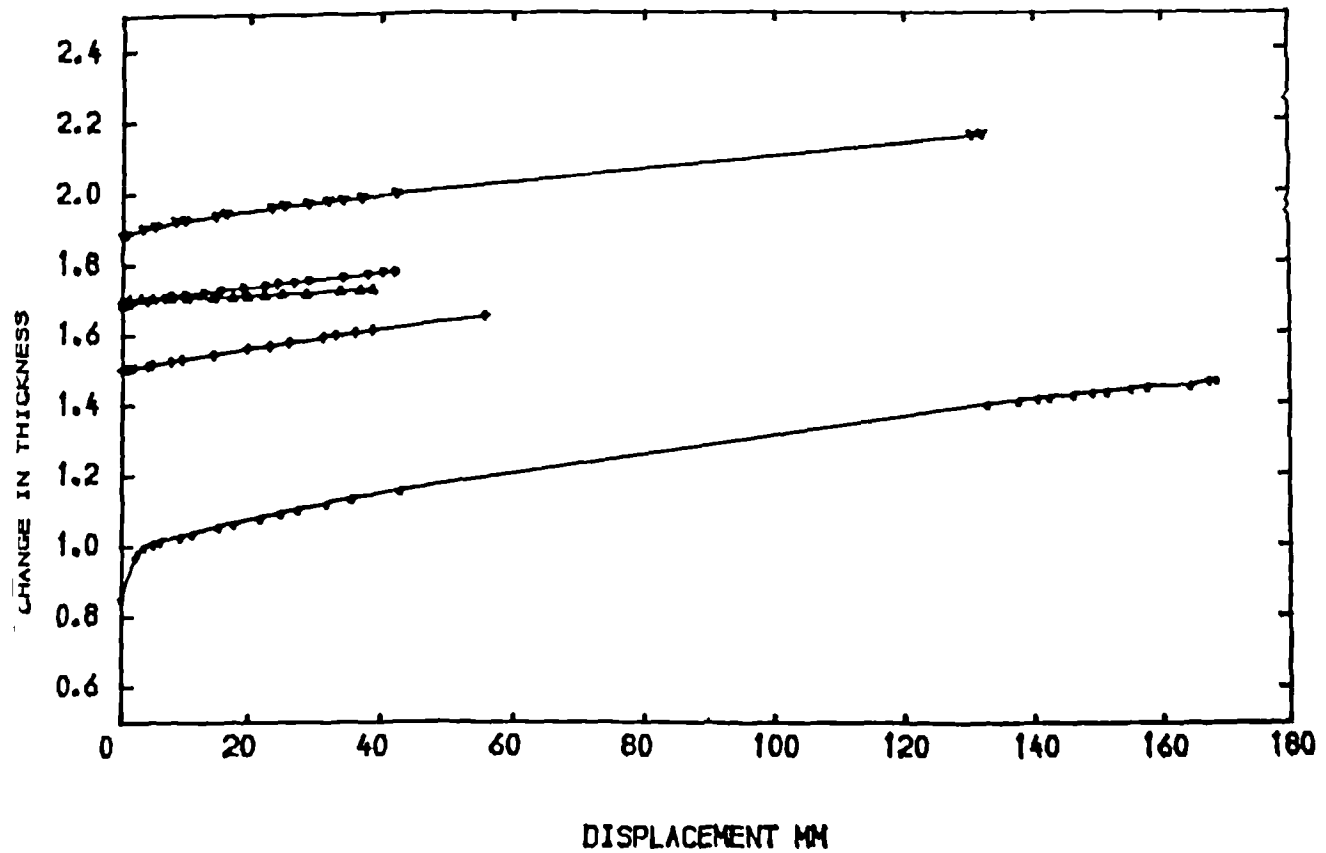
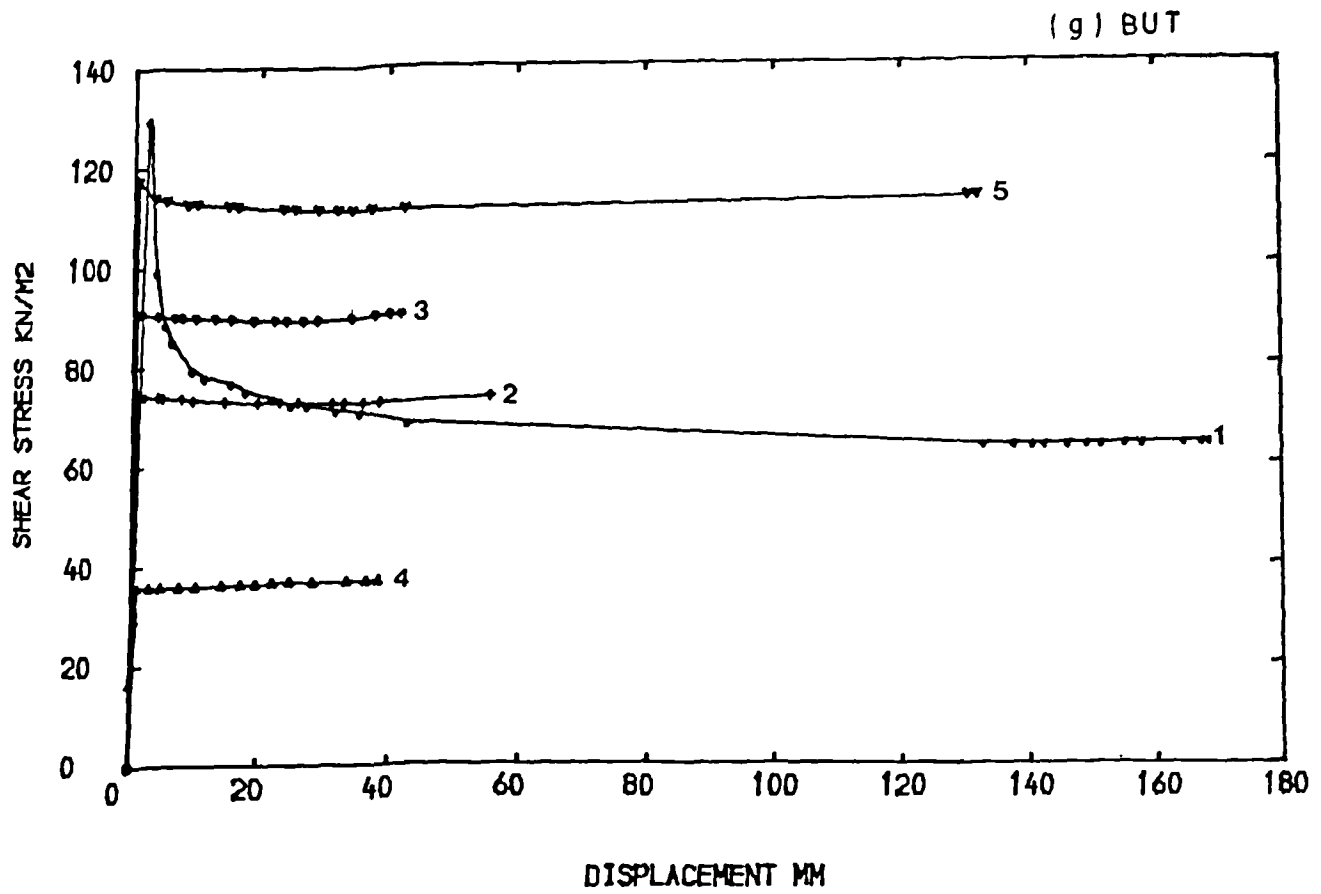


Fig. 5.6g Shear stress-displacement and displacement vertical thickness relationship for ring shear tests on tumbled remoulded samples.

(h) CM

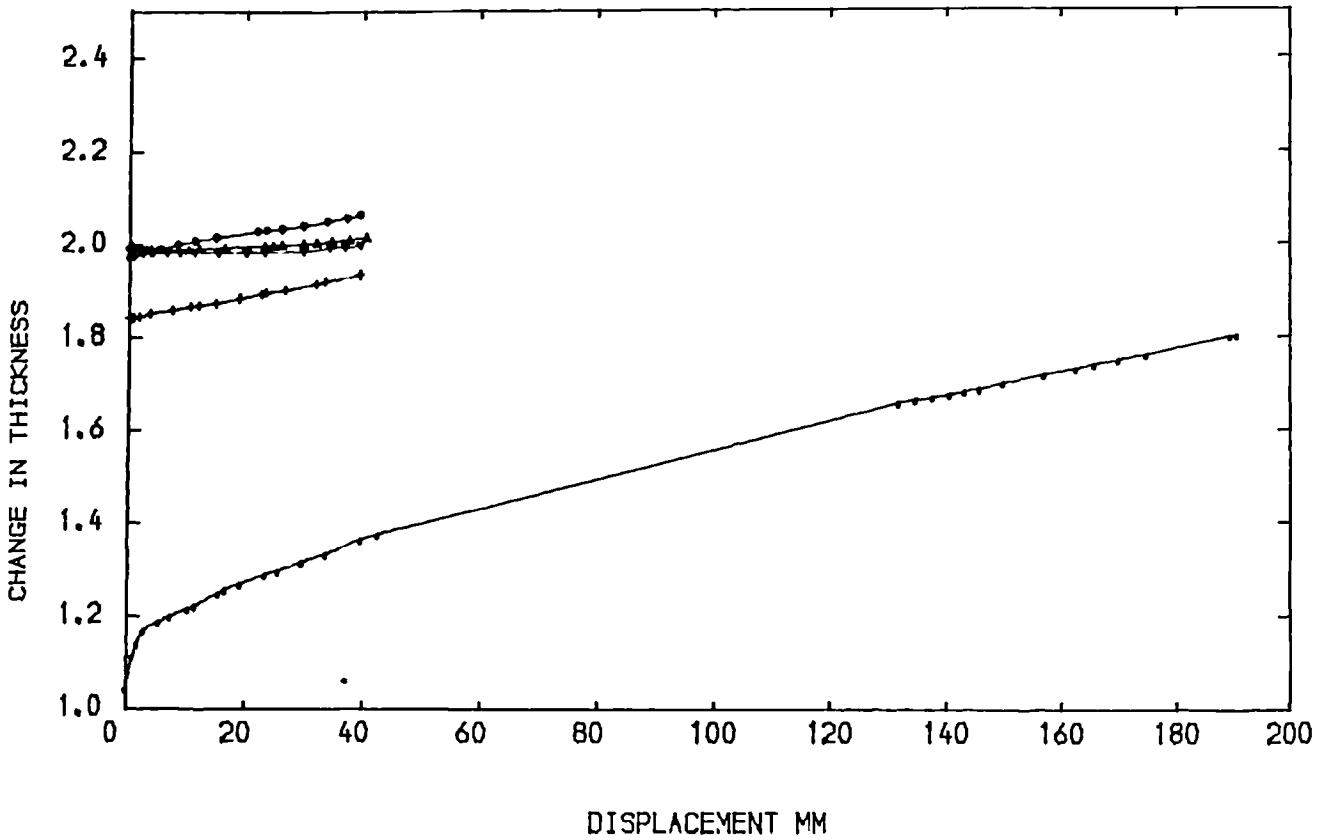
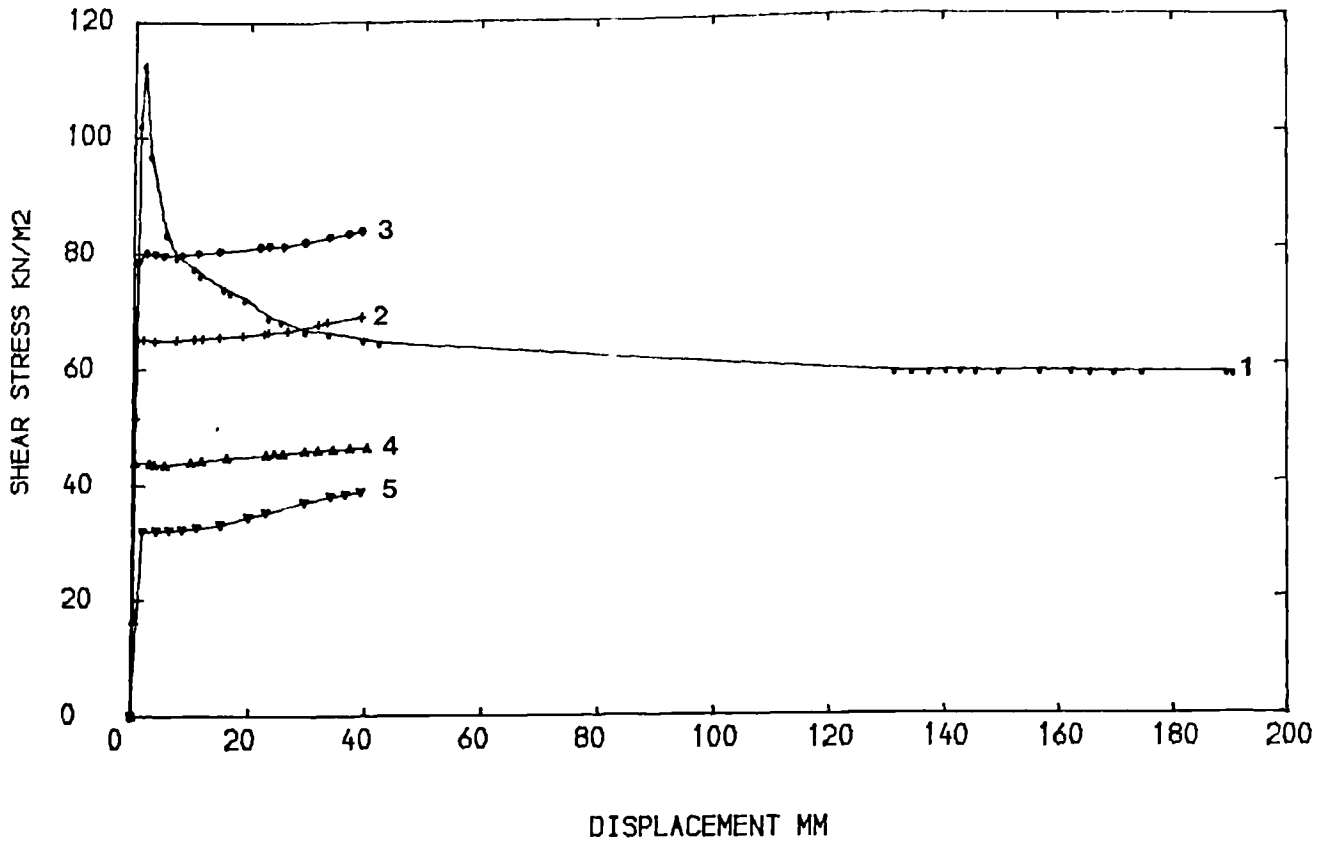


Fig. 5.6h Shear stress-displacement and displacement vertical thickness relationship for ring shear tests on tumbled remoulded samples.

(i) RP

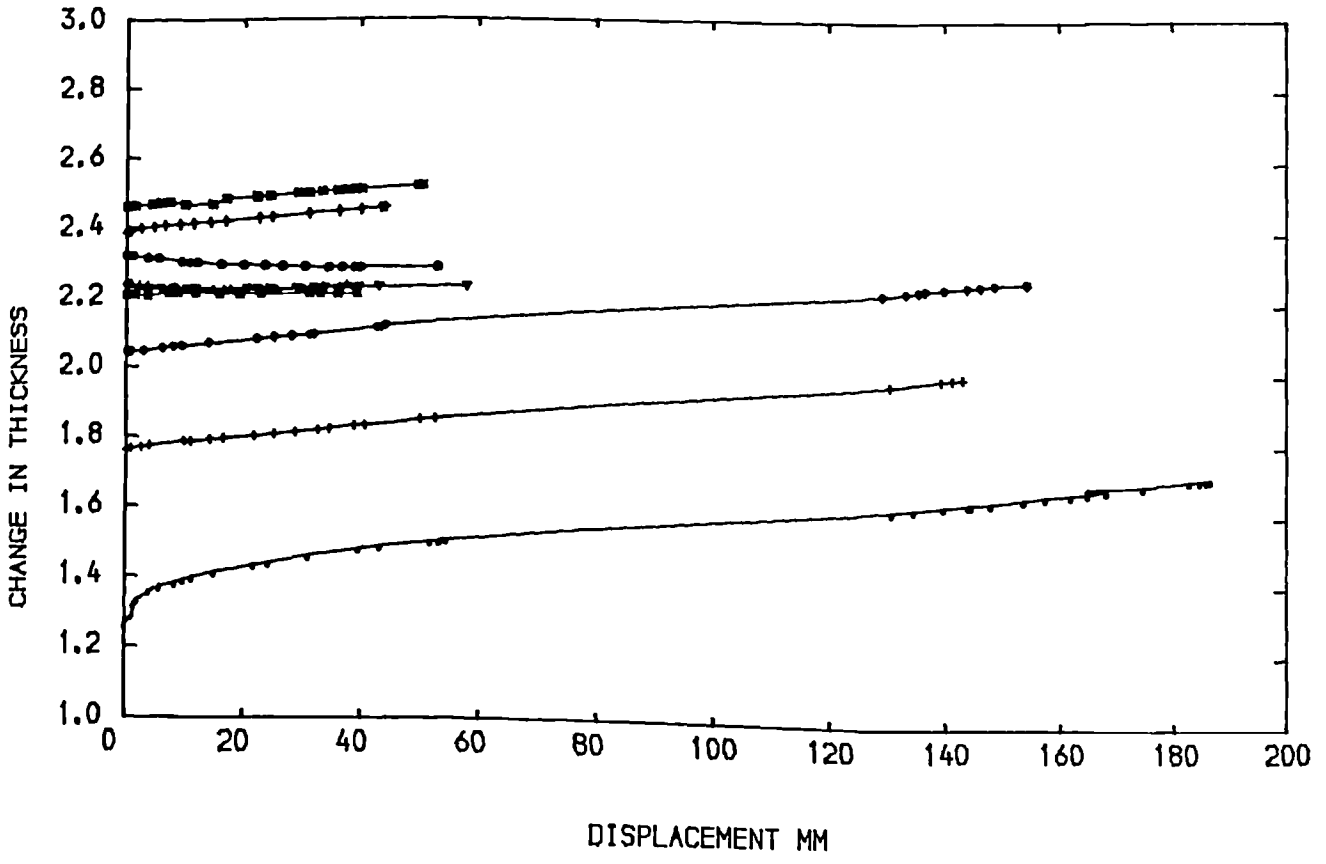
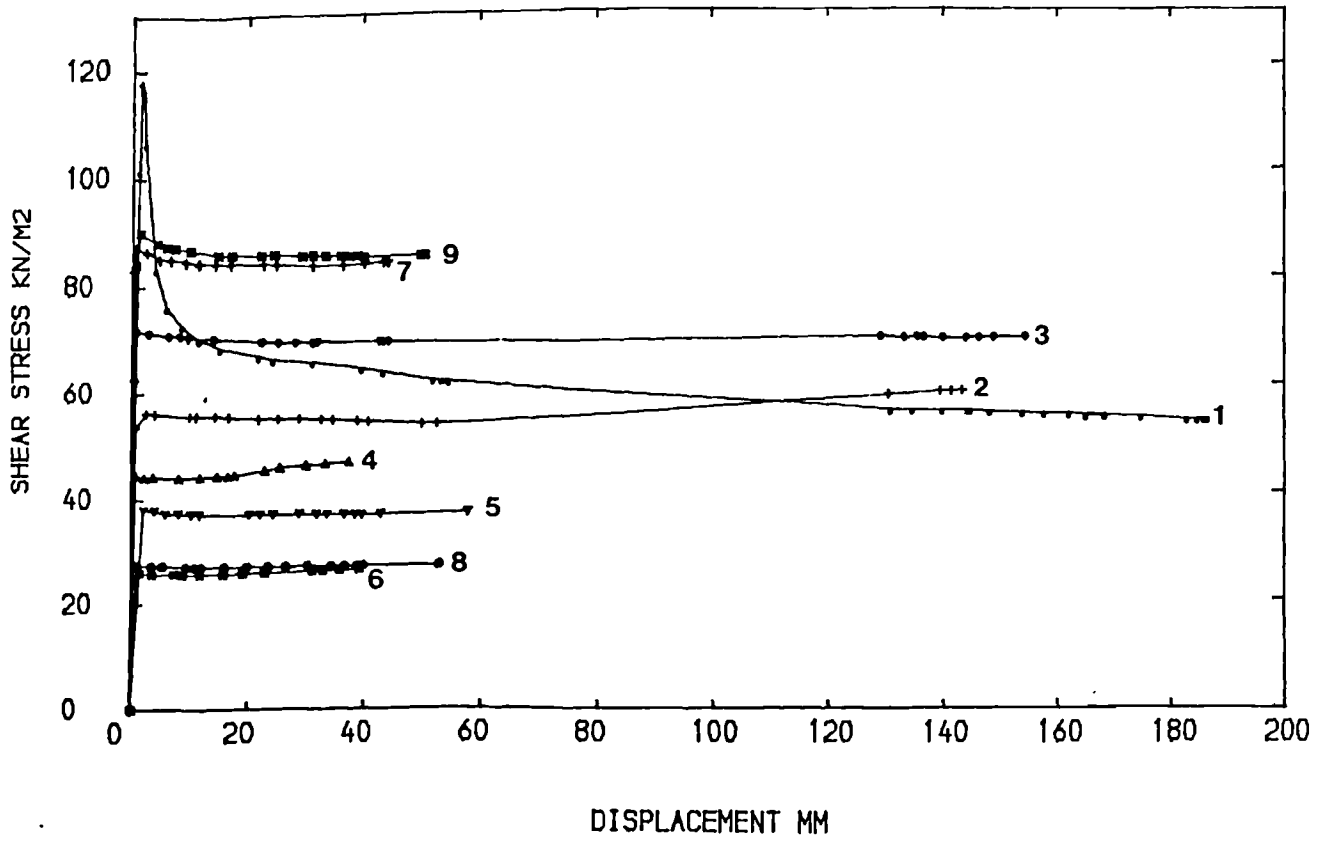


Fig. 5.6i Shear stress-displacement and displacement vertical thickness relationship for ring shear tests on tumbled remoulded samples.

(j) AC

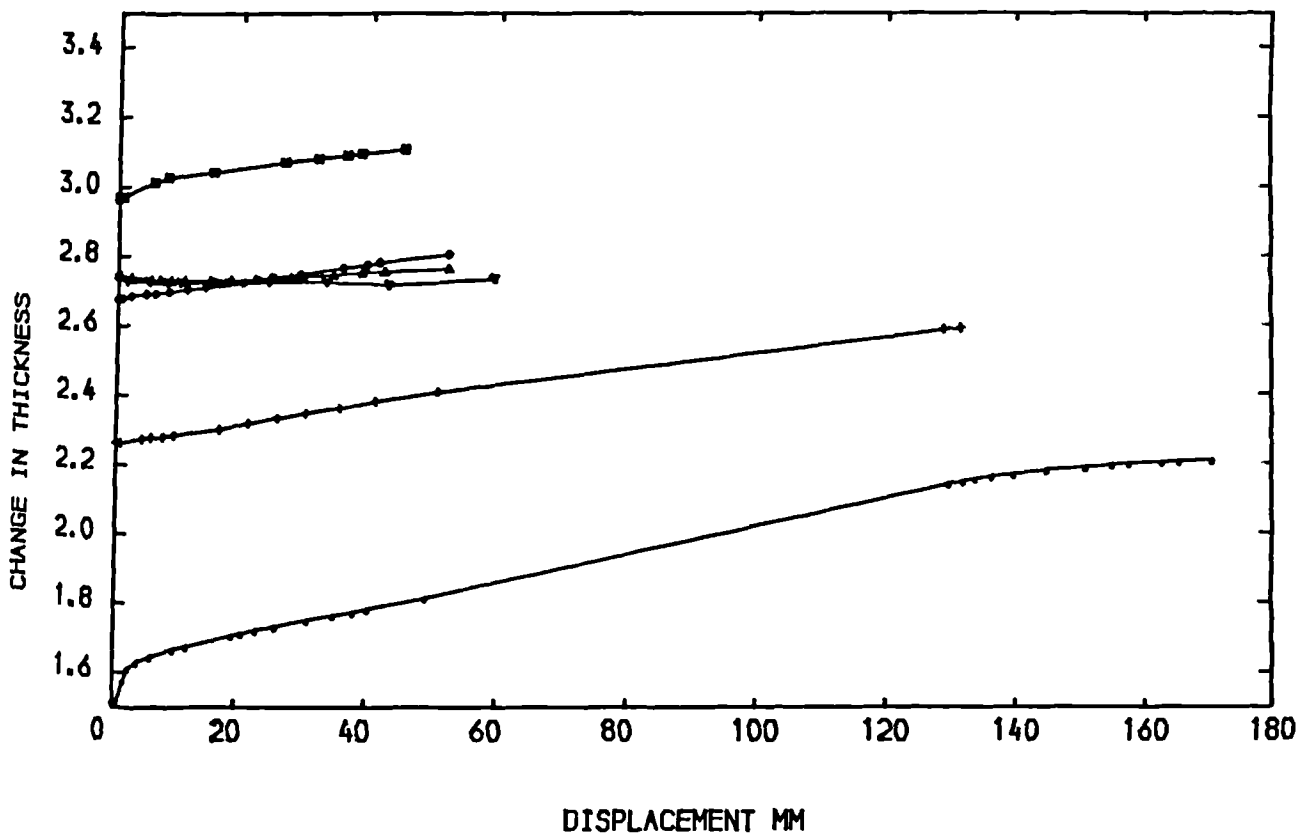
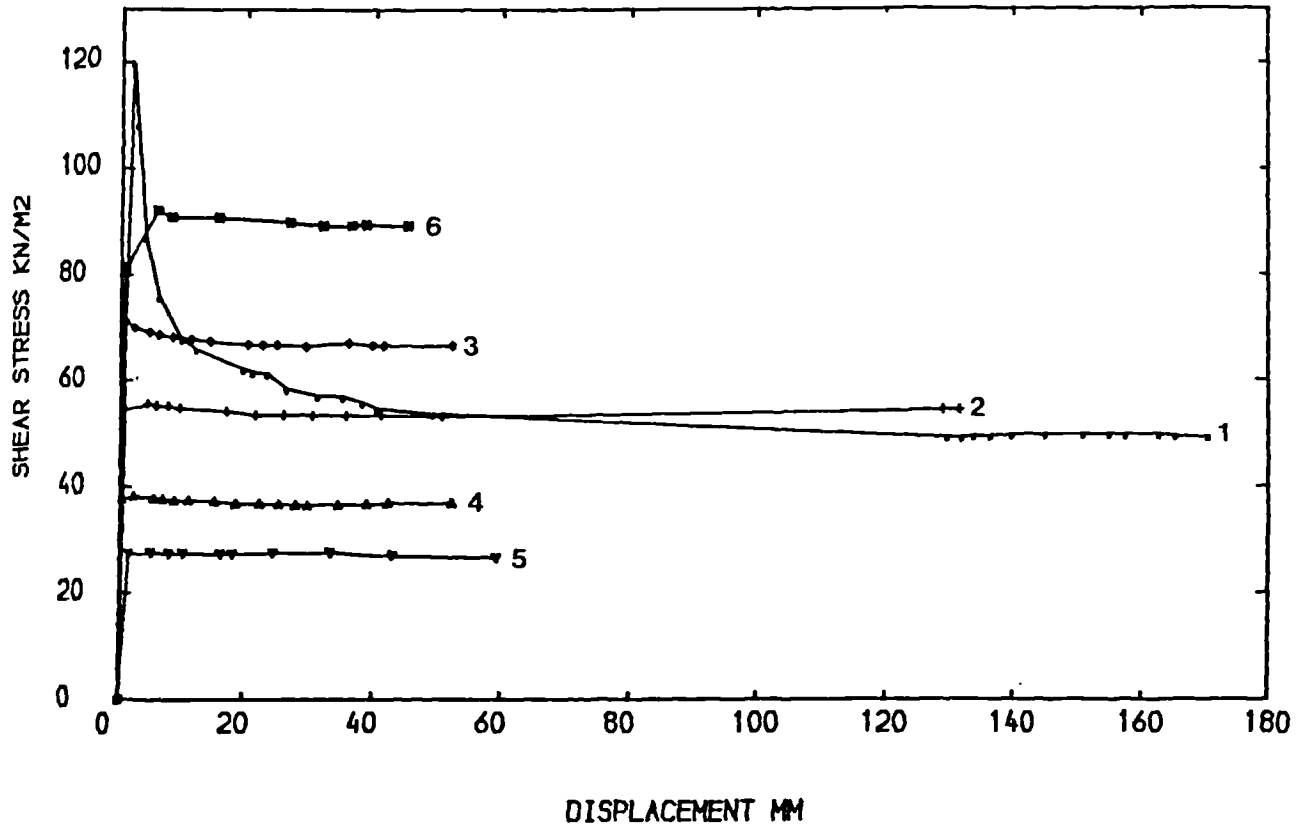


Fig. 5.6_j Shear stress-displacement and displacement vertical thickness relationship for ring shear tests on tumbled remoulded samples.

(k) BCL

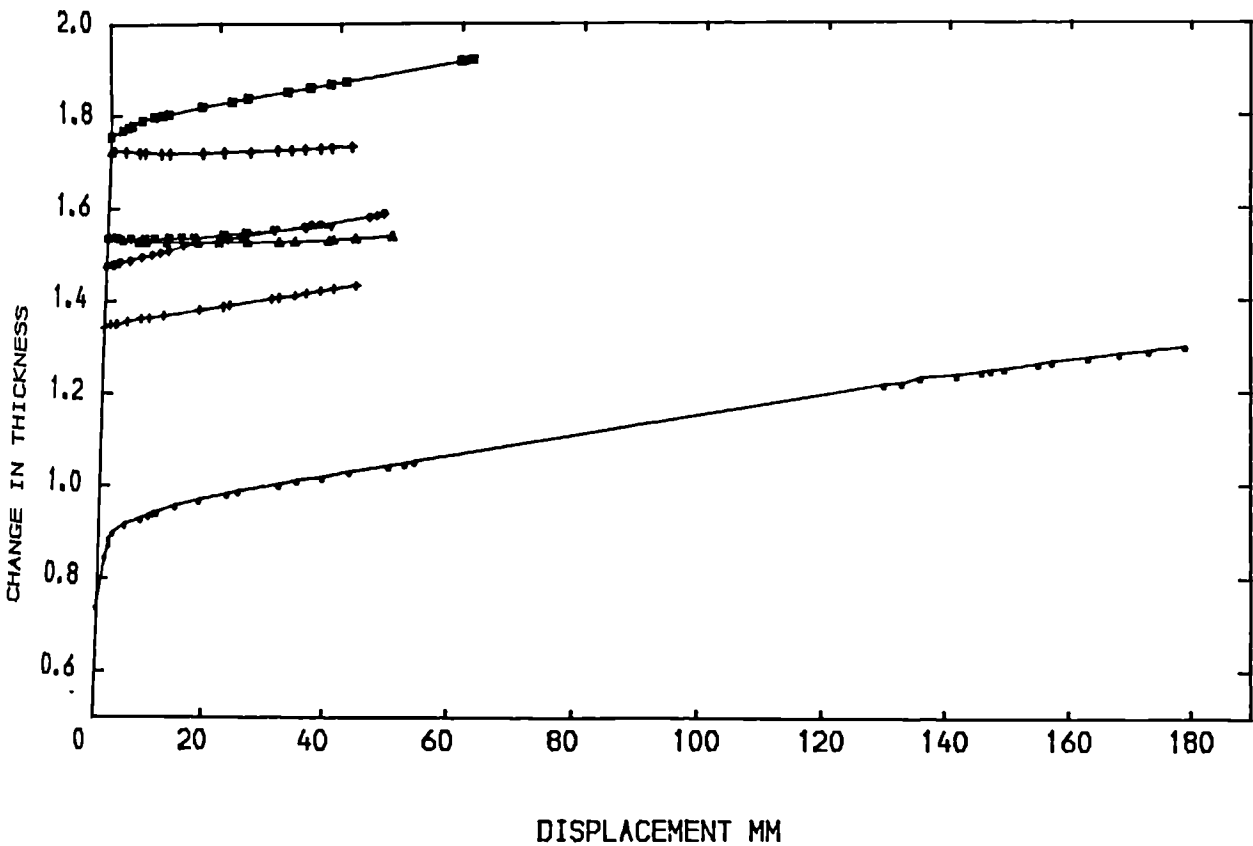
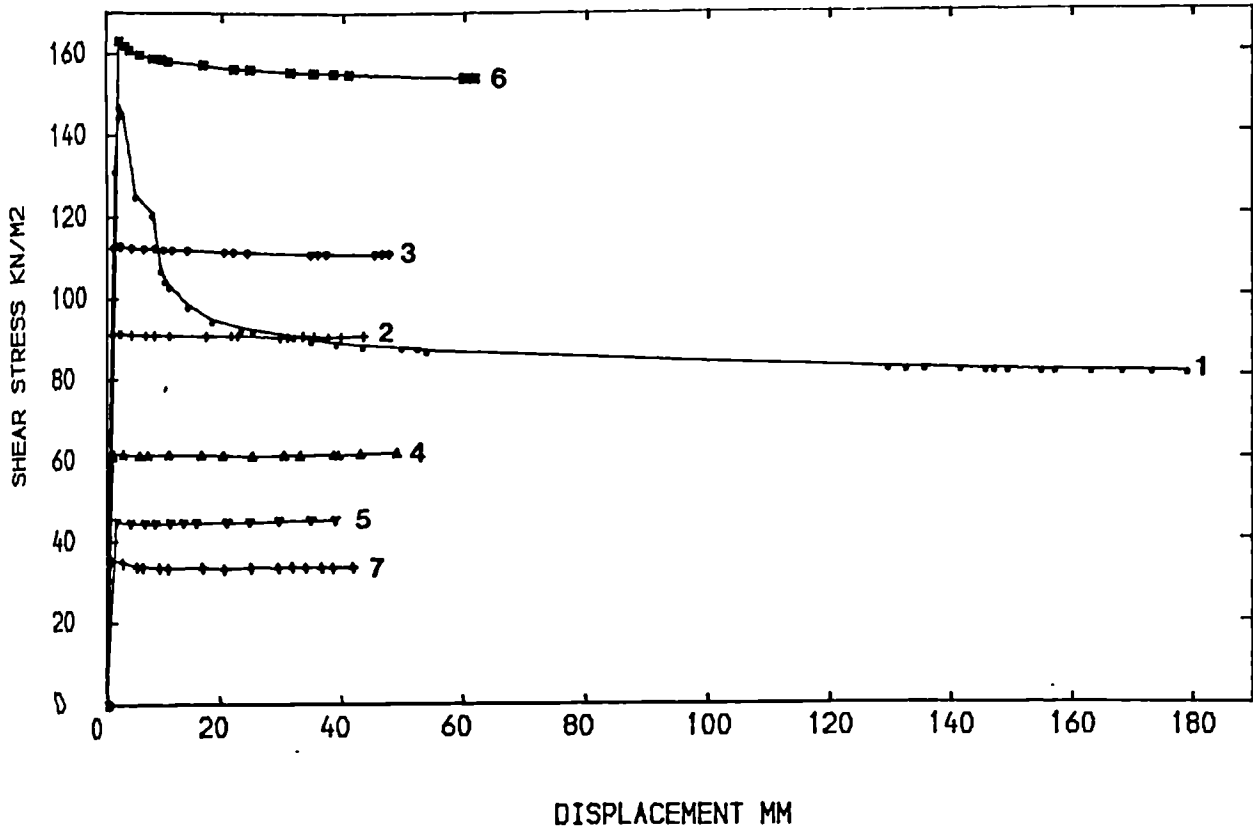


Fig. 5.6k Shear stress-displacement and displacement vertical thickness relationship for ring shear tests on tumbled remoulded samples.

(1) CS

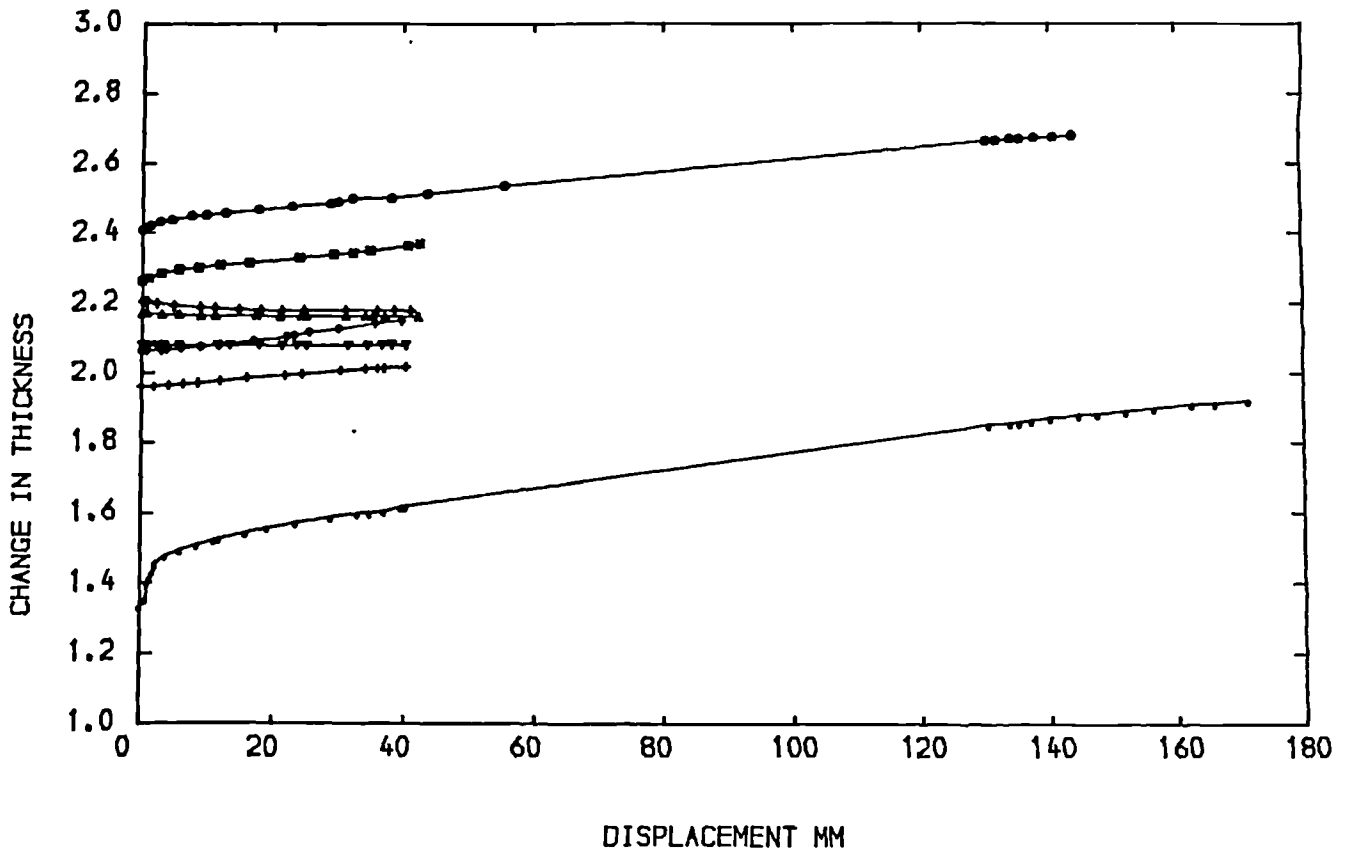
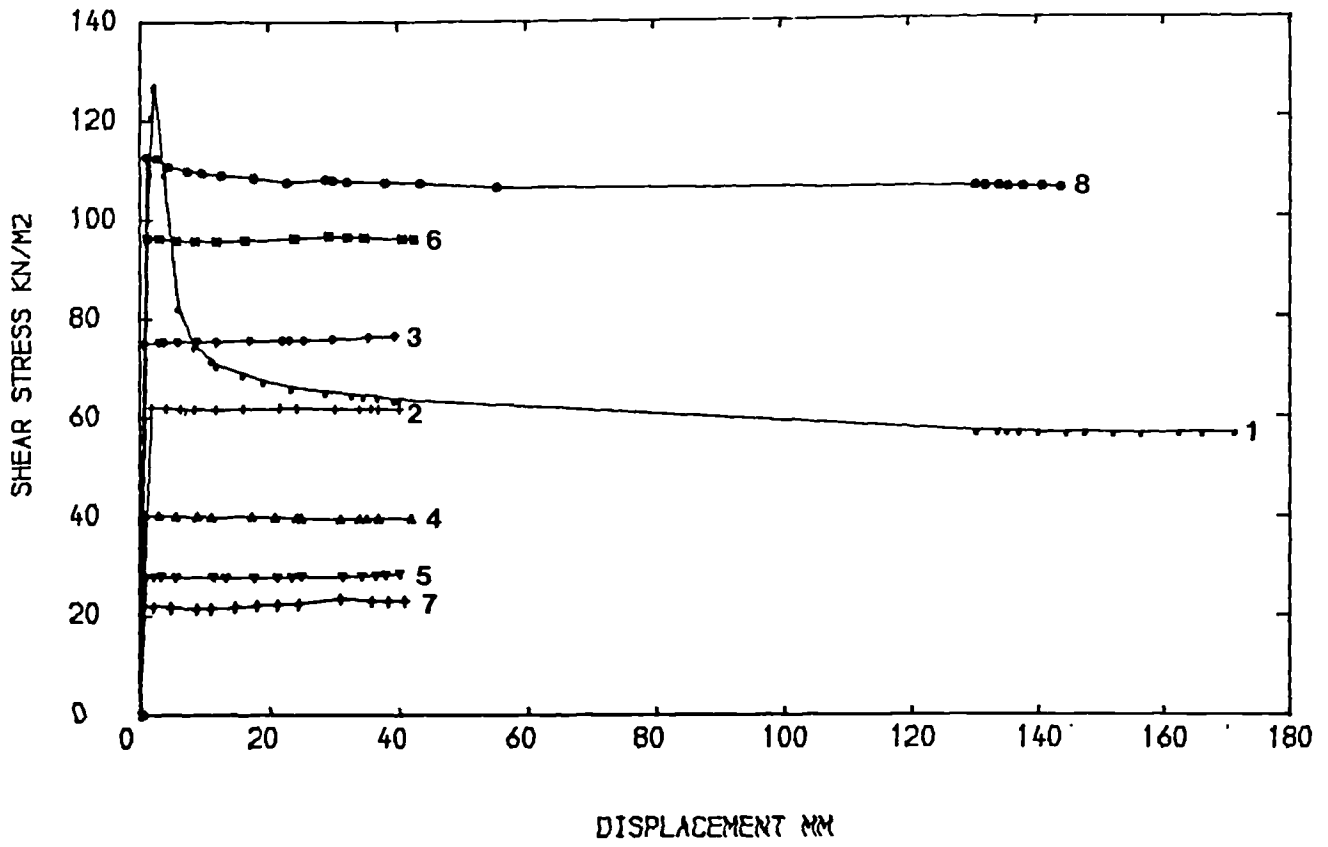


Fig. 5.6L Shear stress-displacement and displacement vertical thickness relationship for ring shear tests on tumbled remoulded samples.

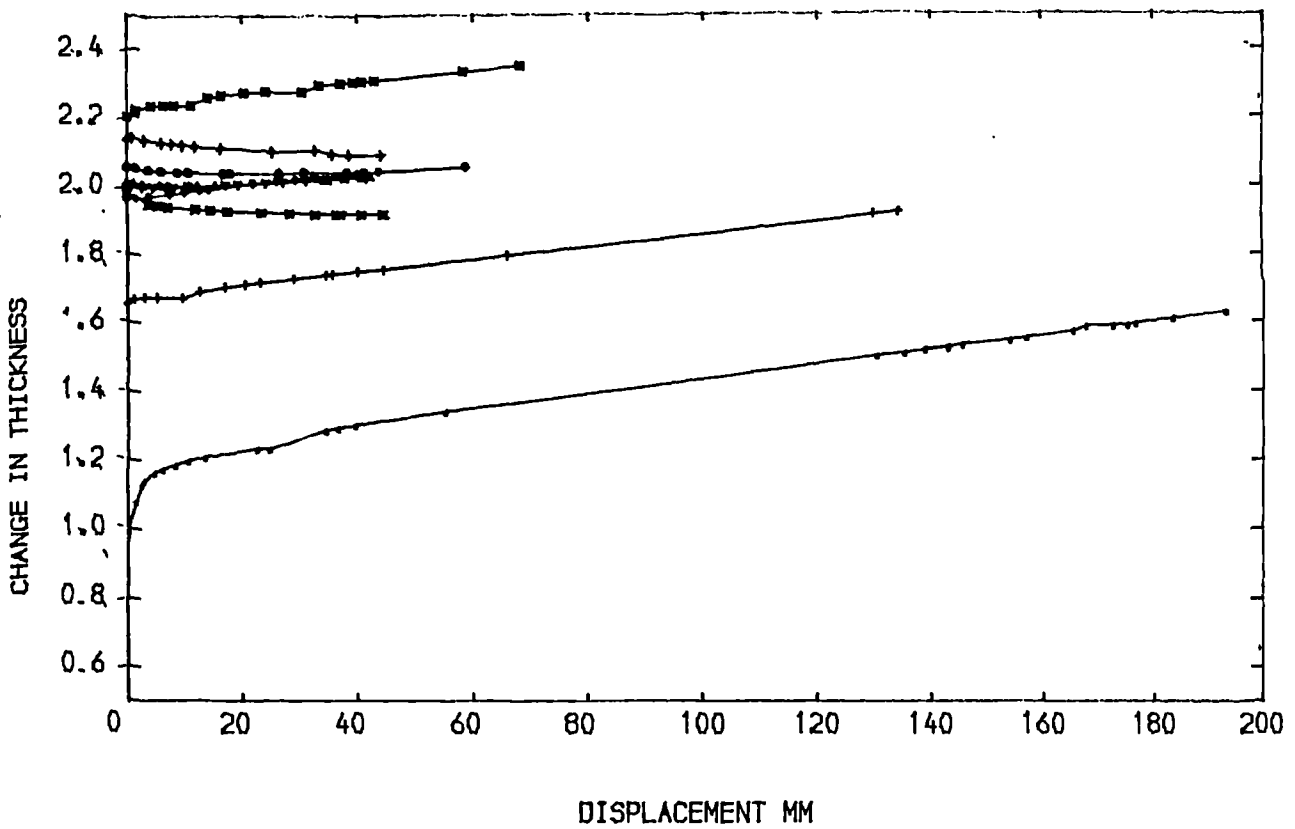
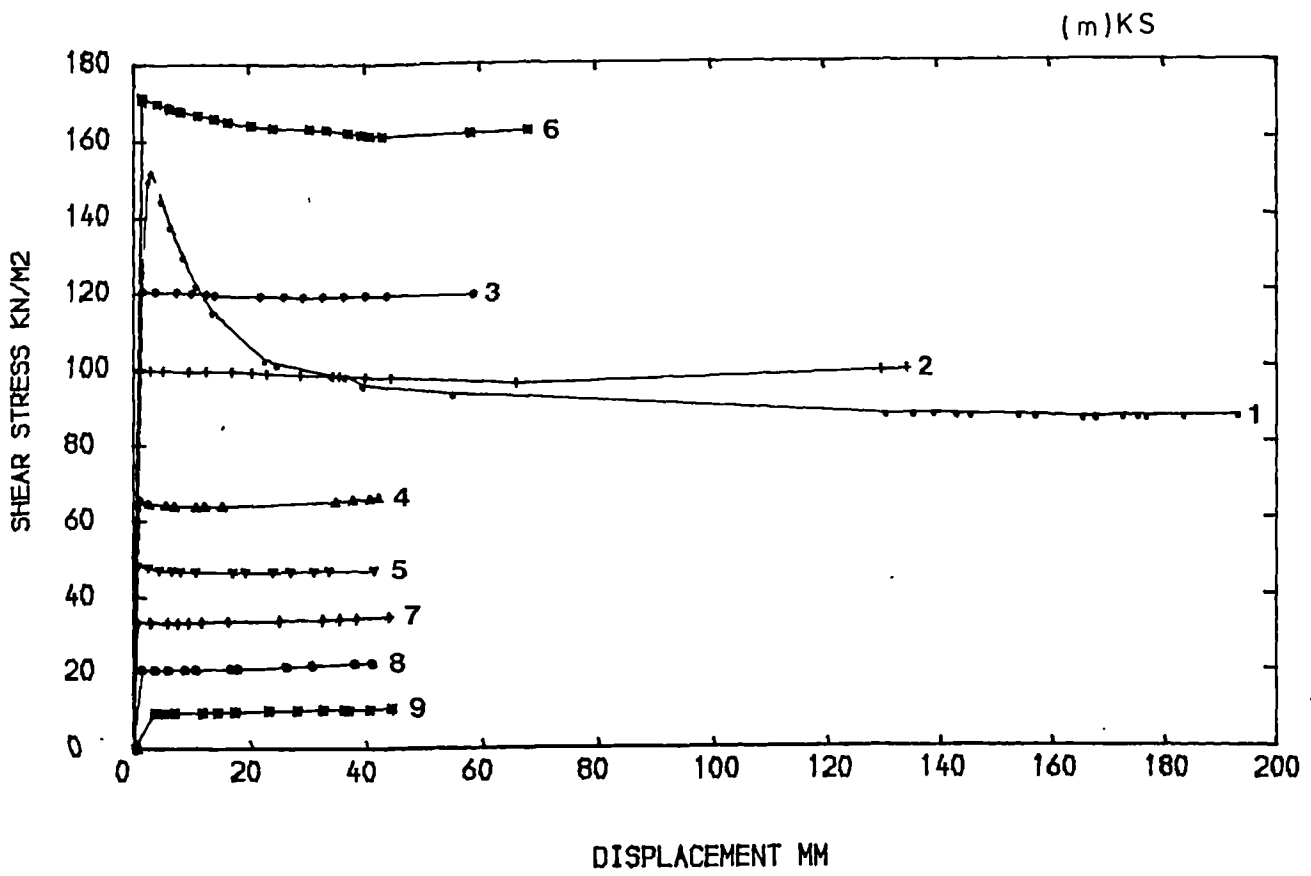


Fig. 5.6_m Shear stress-displacement and displacement vertical thickness relationship for ring shear tests on tumbled remoulded samples.

(a) CW1C

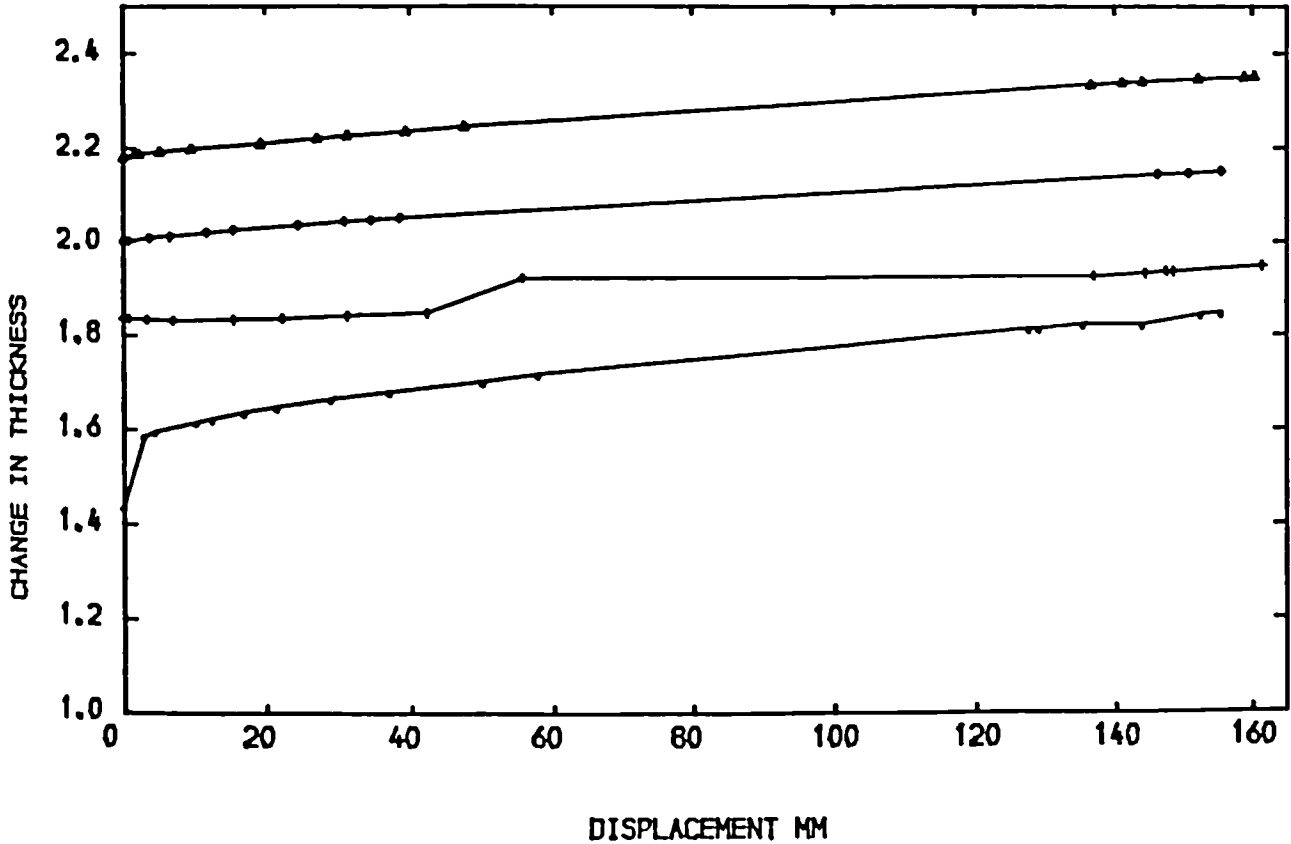
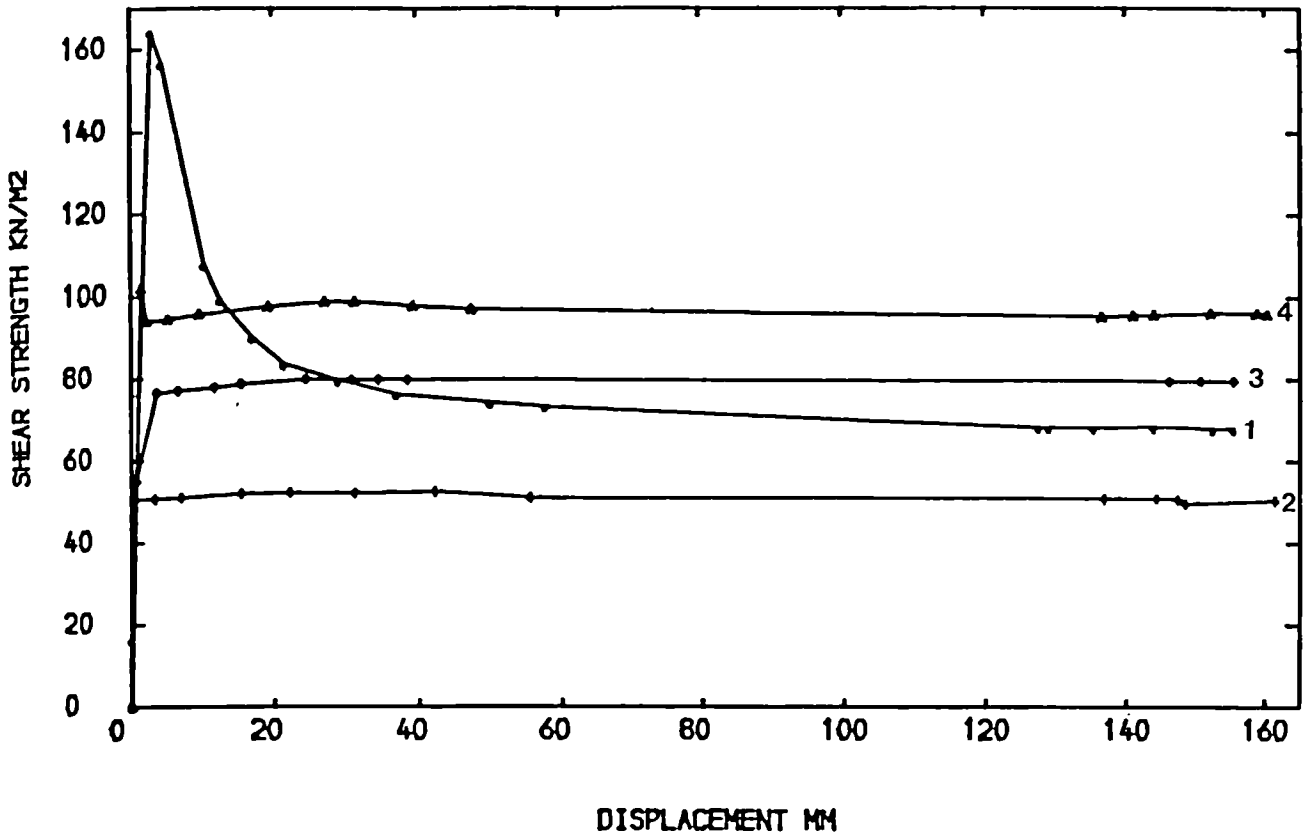


Fig. 5.7 Shear stress - displacement and vertical thickness relationship for ring shear test on remoulded crushed and crushed sieved samples.

(b) CW2C

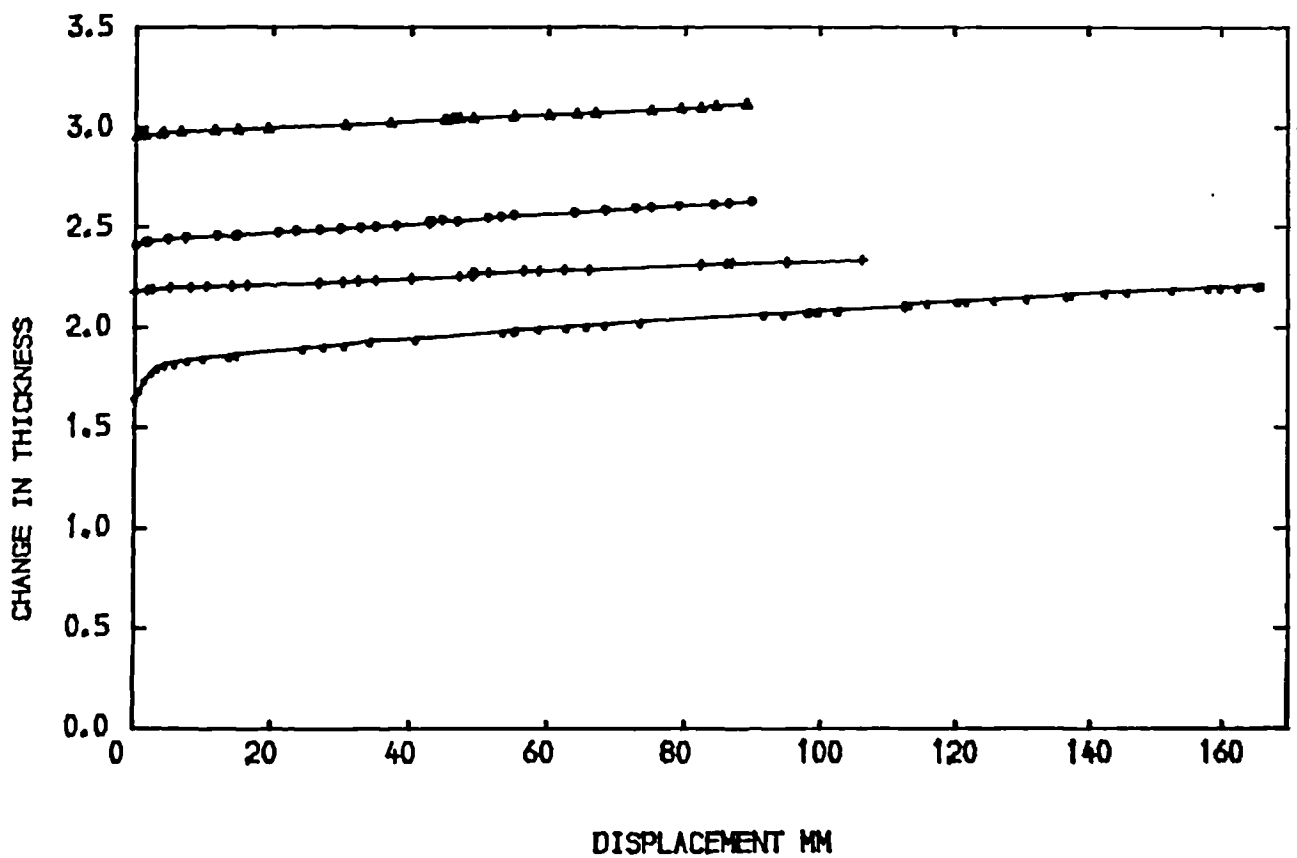
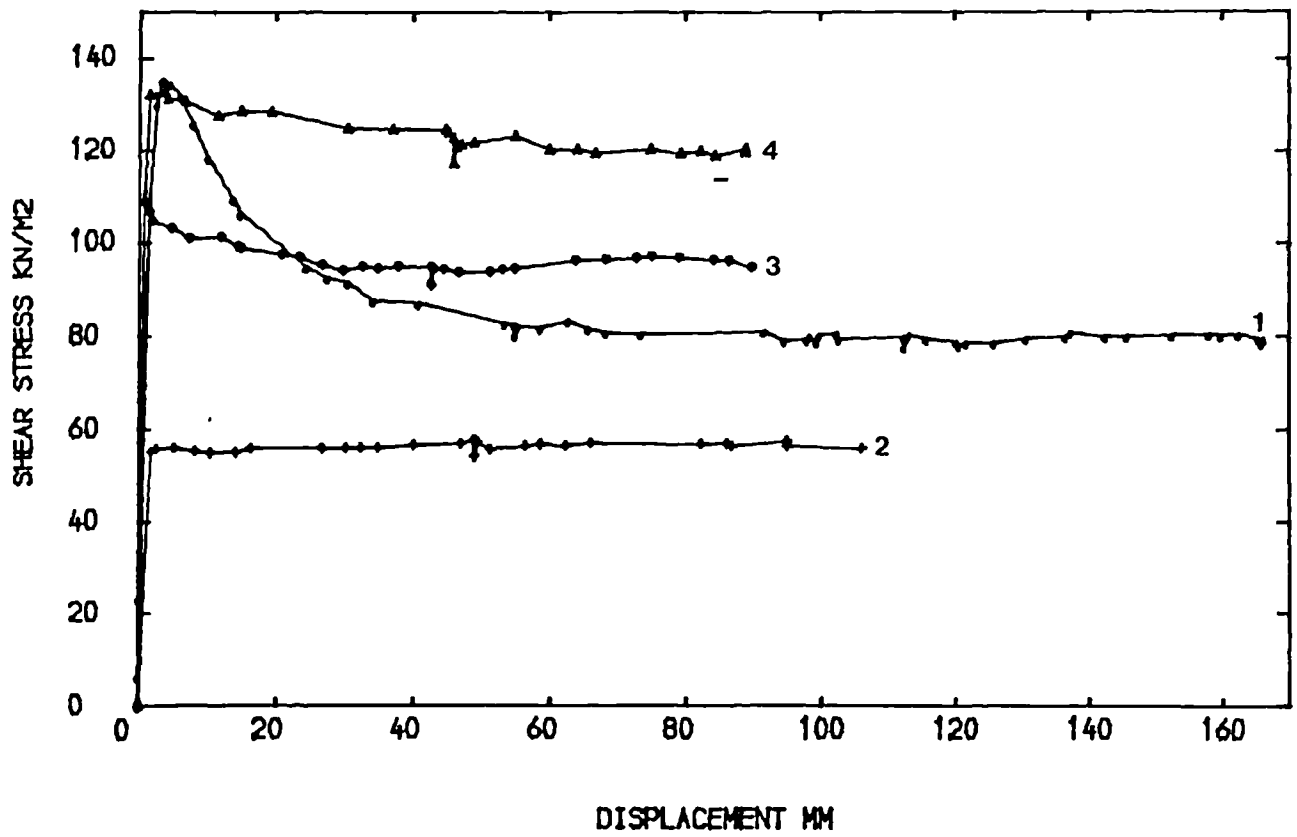


Fig. 5.7 Shear stress - displacement and vertical thickness relationship for ring shear test on remoulded crushed and crushed sieved samples.

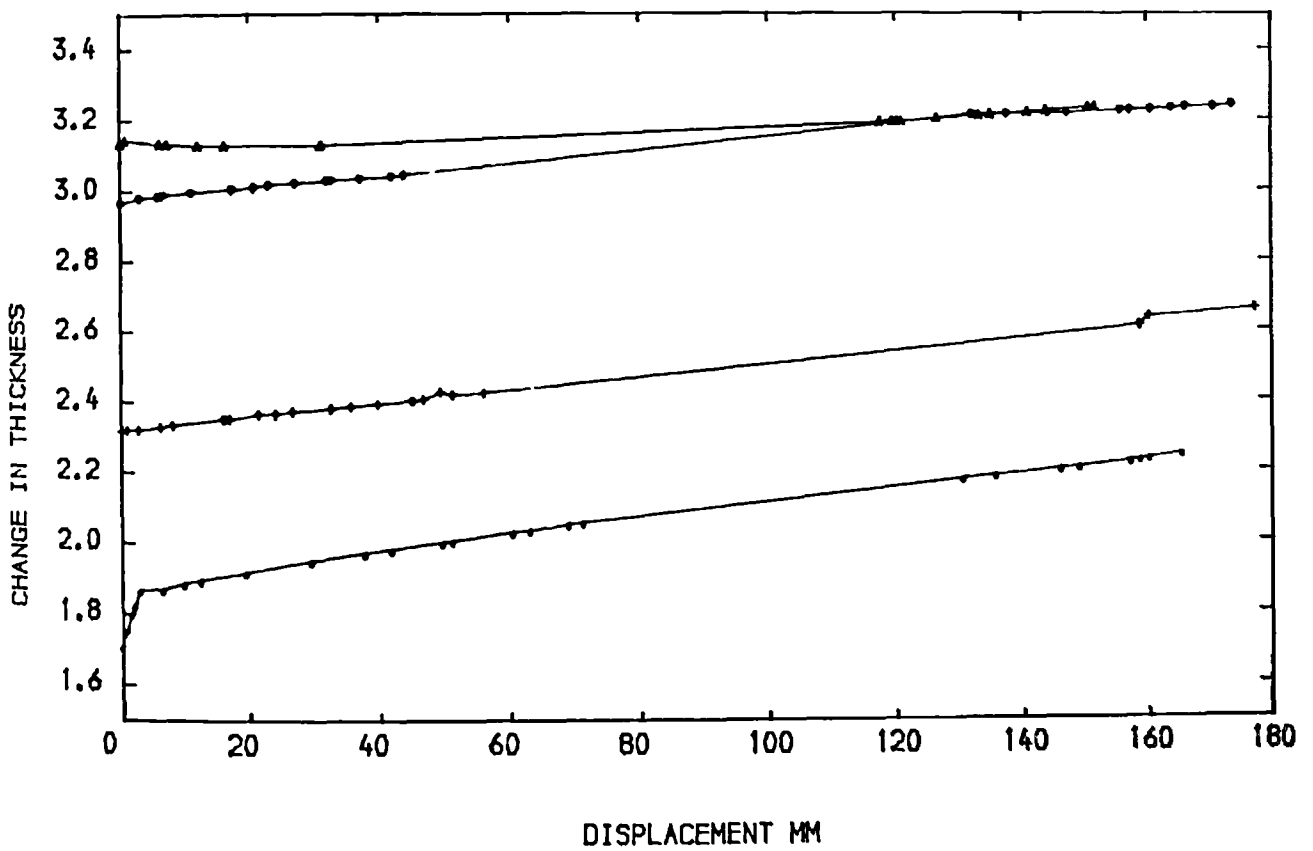
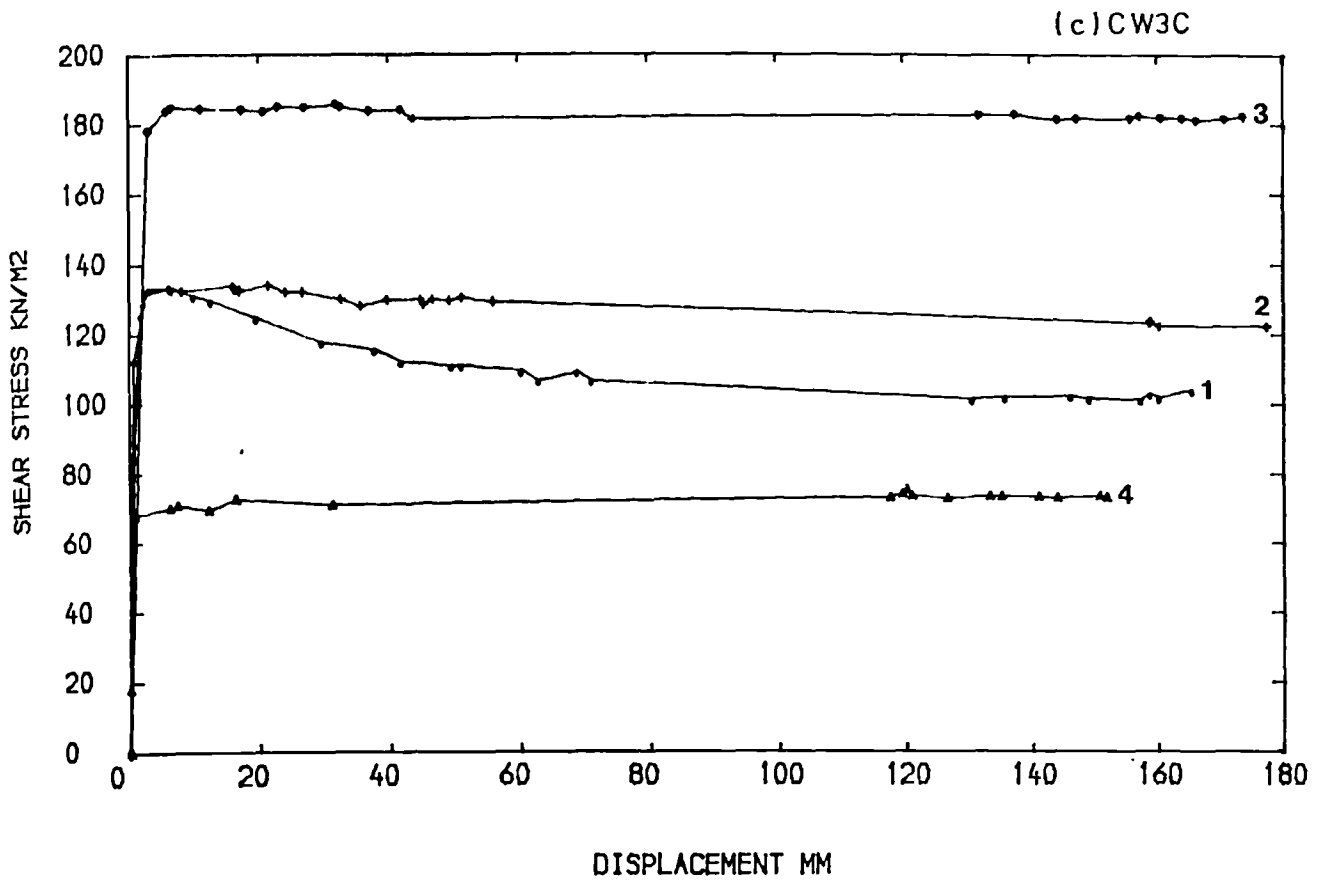


Fig. 5.7 Shear stress - displacement and vertical thickness relationship for ring shear test on remoulded crushed and crushed sieved samples.

(d)CW1CP200

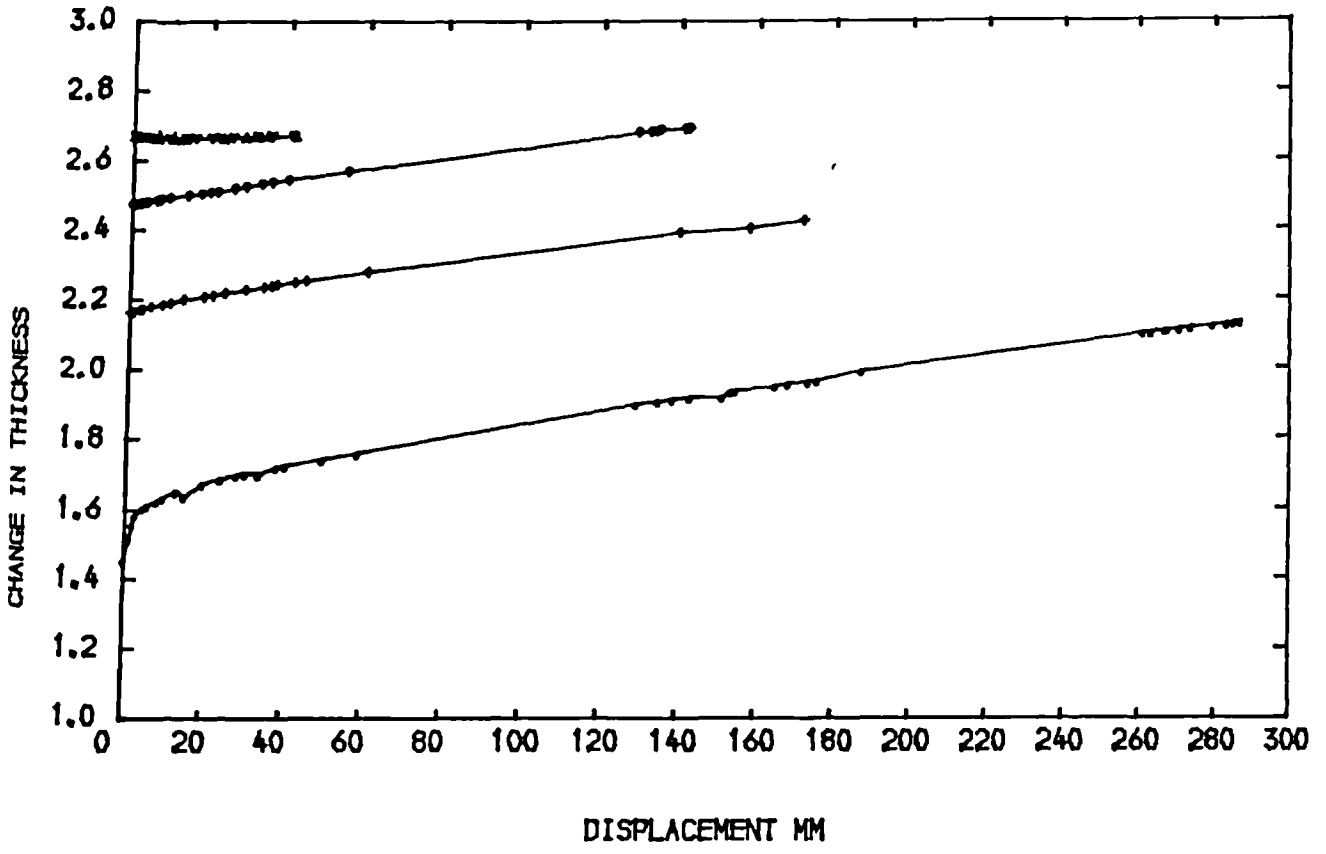
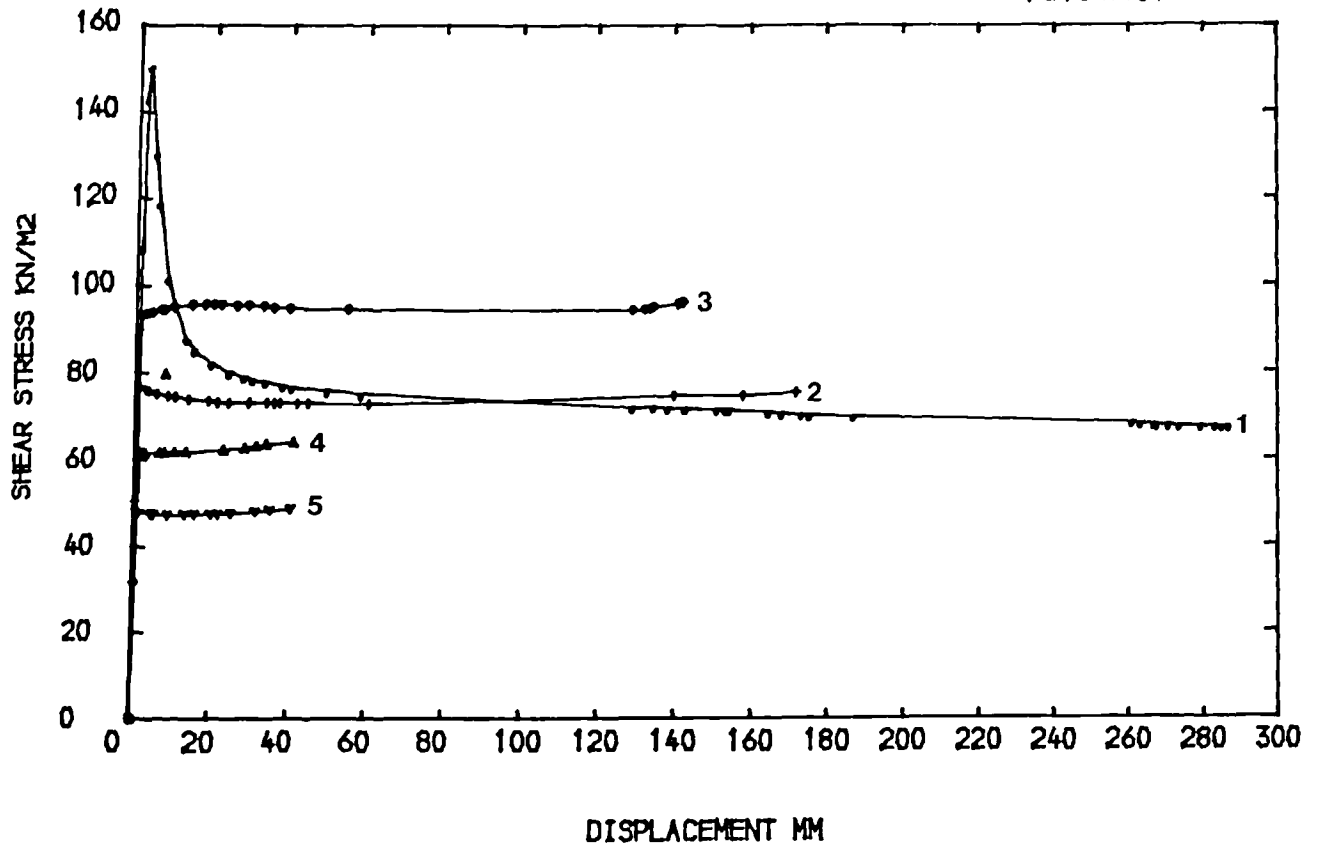


Fig. 5.7 Shear stress - displacement and vertical thickness relationship for ring shear test on remoulded crushed and crushed sieved samples.

(e) CW1CR200

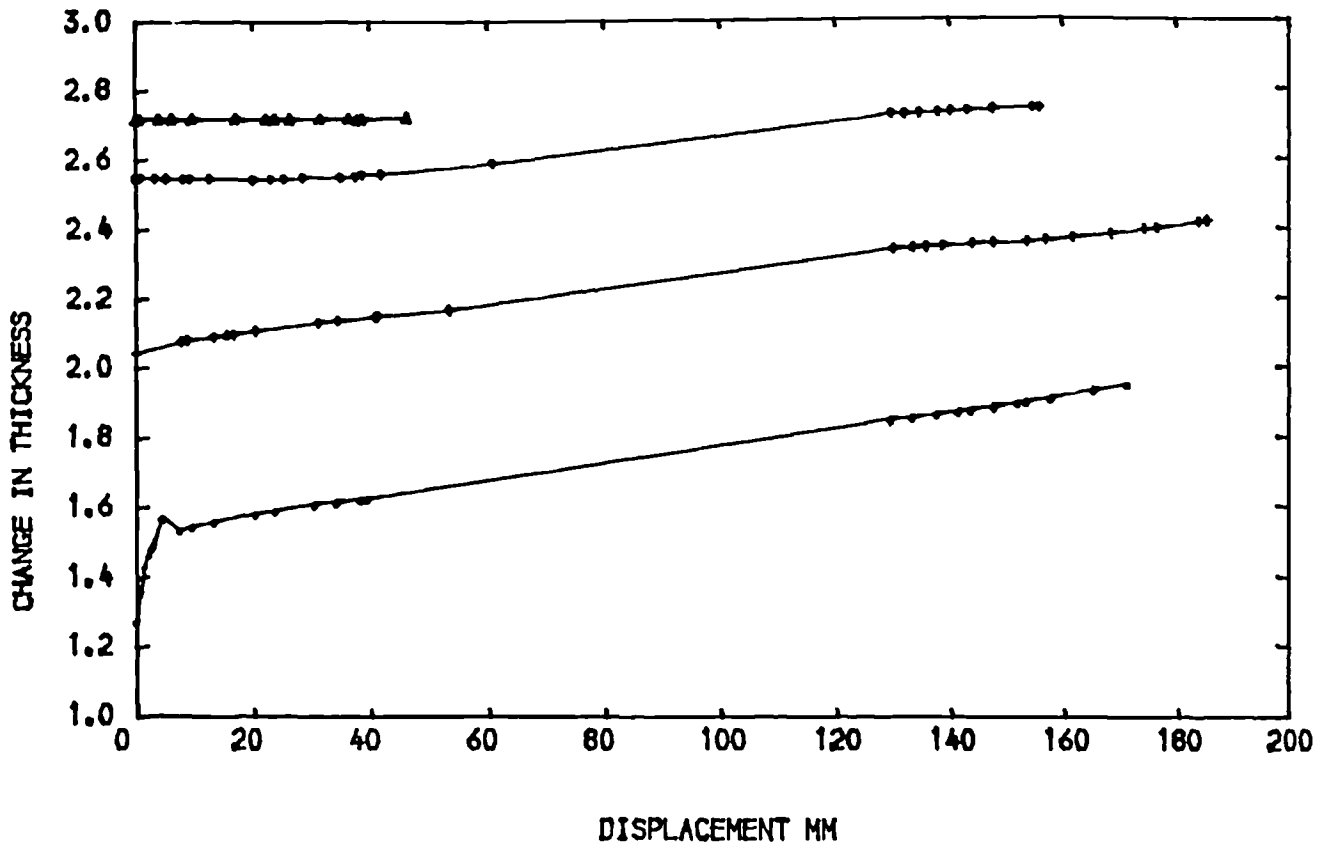
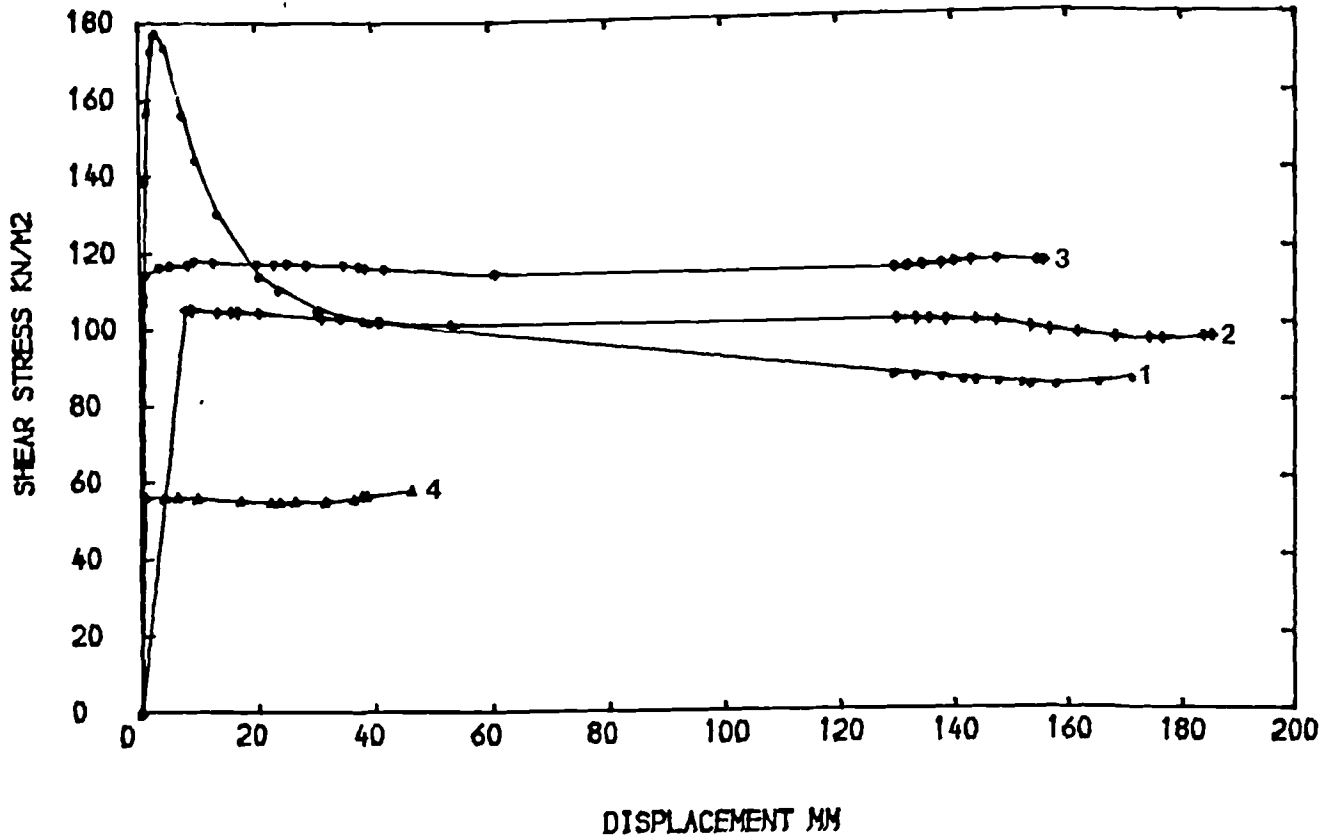


Fig. 5.7 Shear stress - displacement and vertical thickness relationship for ring shear test on remoulded crushed and crushed sieved samples.

(f) CW1CR72

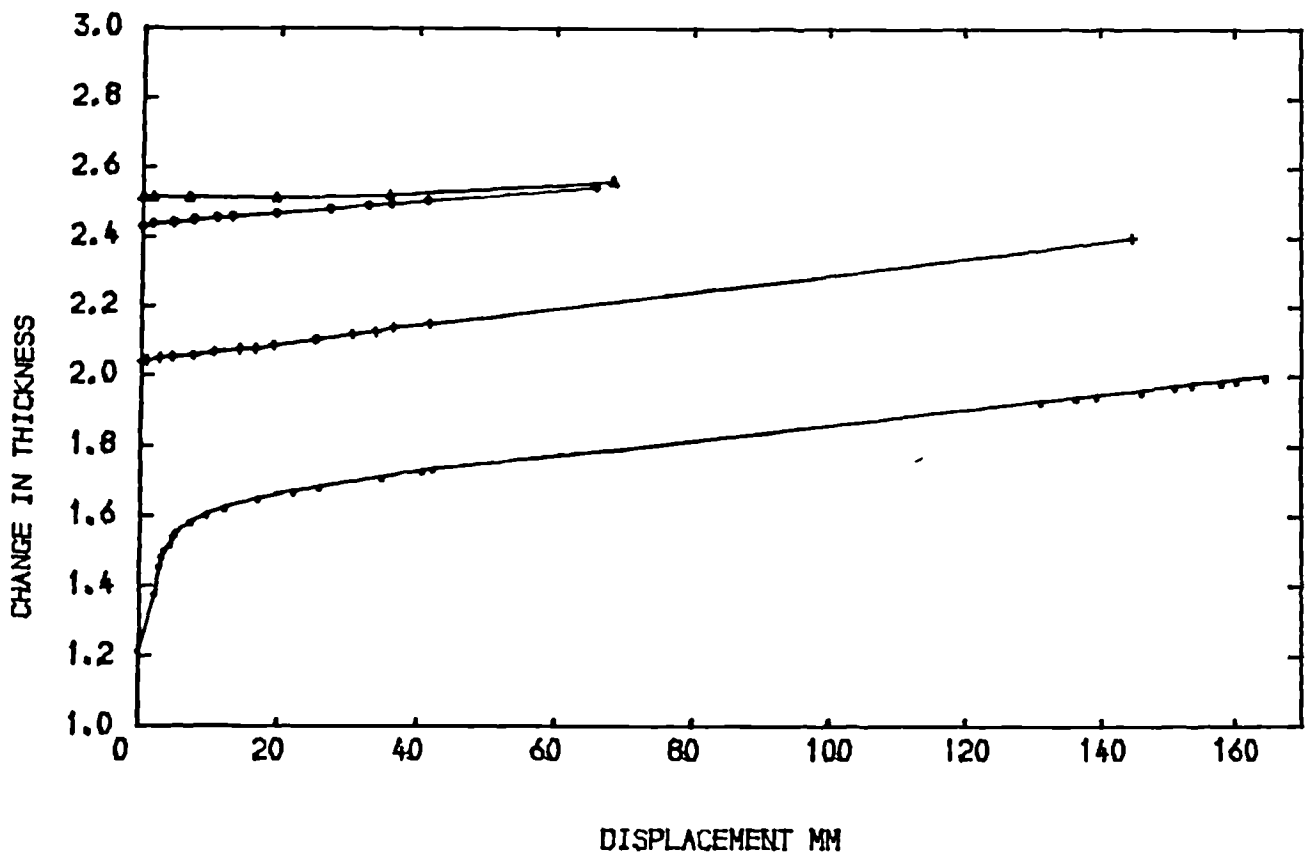
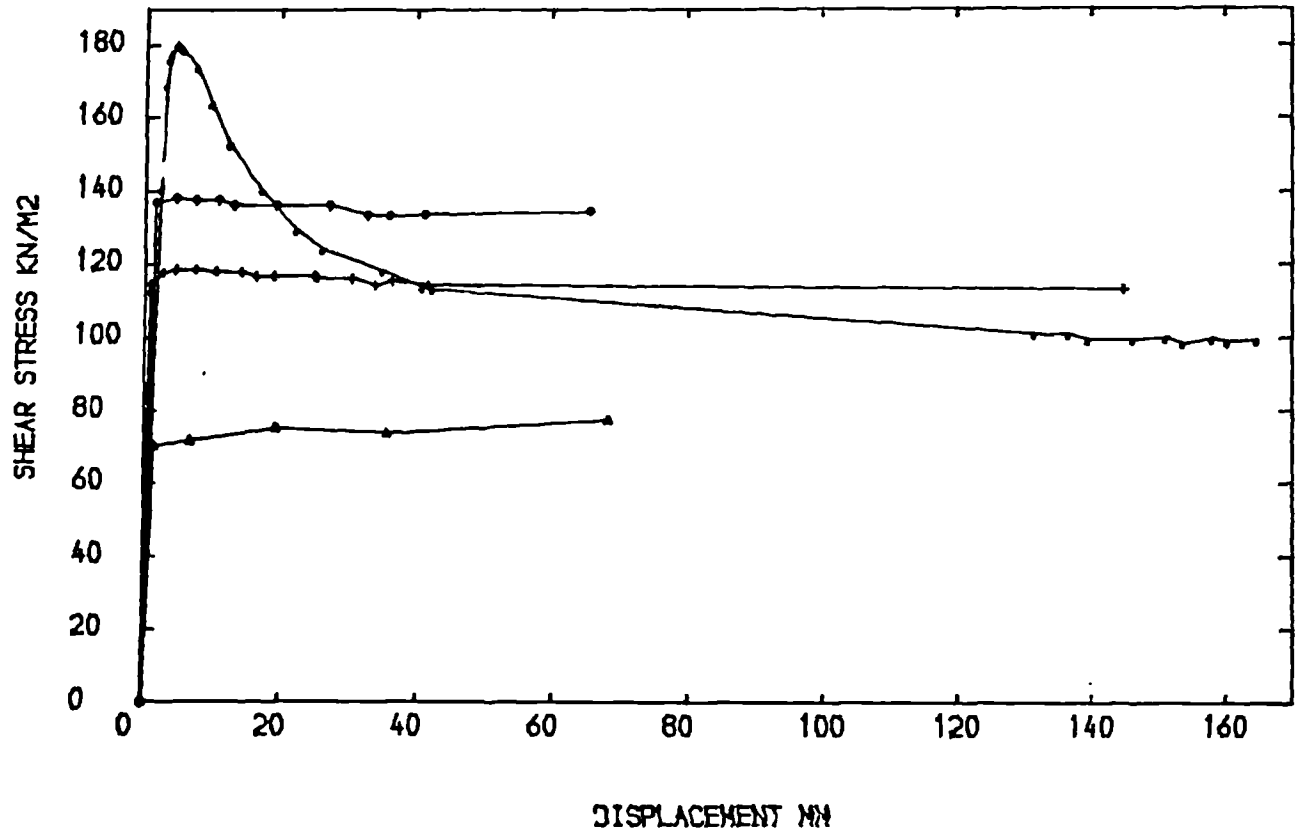


Fig. 5.7 Shear stress - displacement and vertical thickness relationship for ring shear test on remoulded crushed and crushed sieved samples.

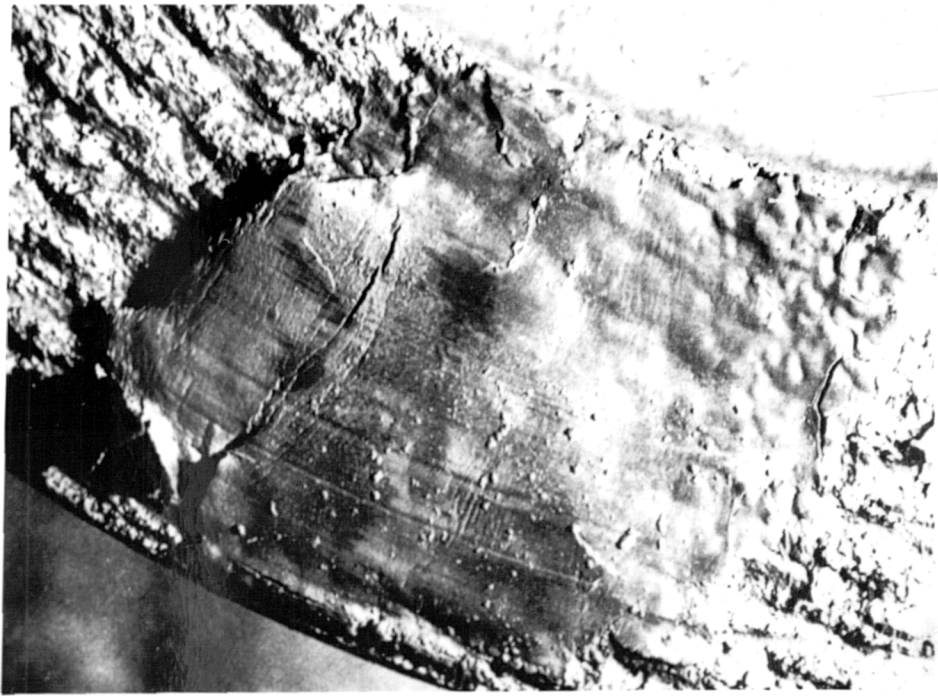


Plate No. 5.3 Slickensided shear surface - ring shear test on sample MTBH.

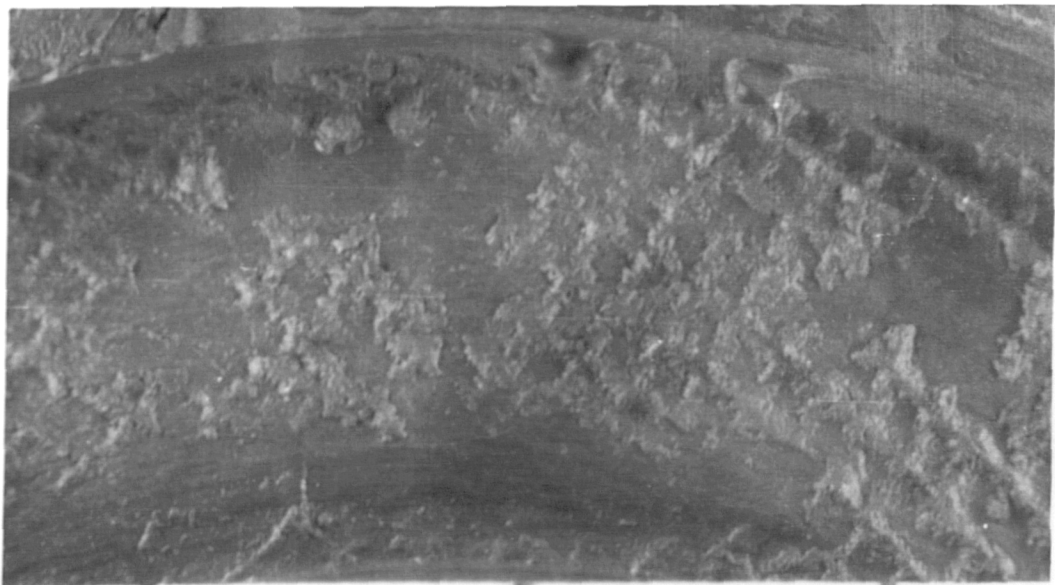


Plate No. 5.4 Slickensided shear surface - ring shear test on sample CS.

(a) MT.BH sample

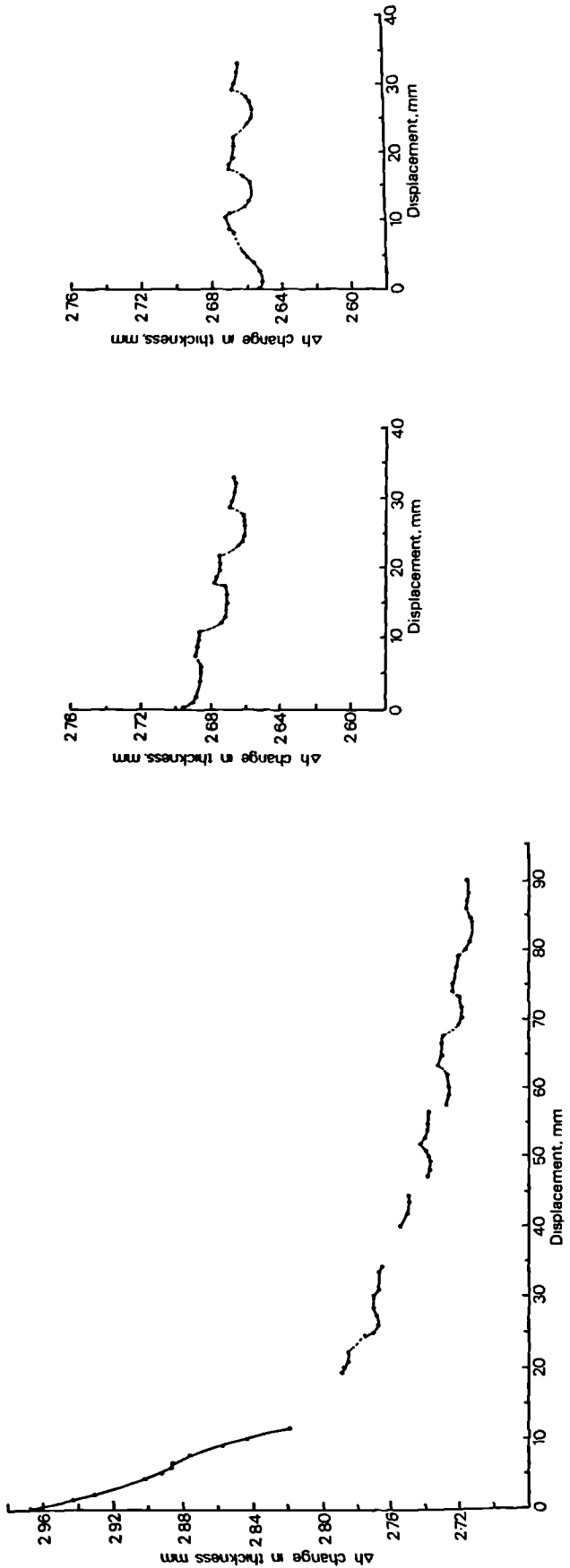
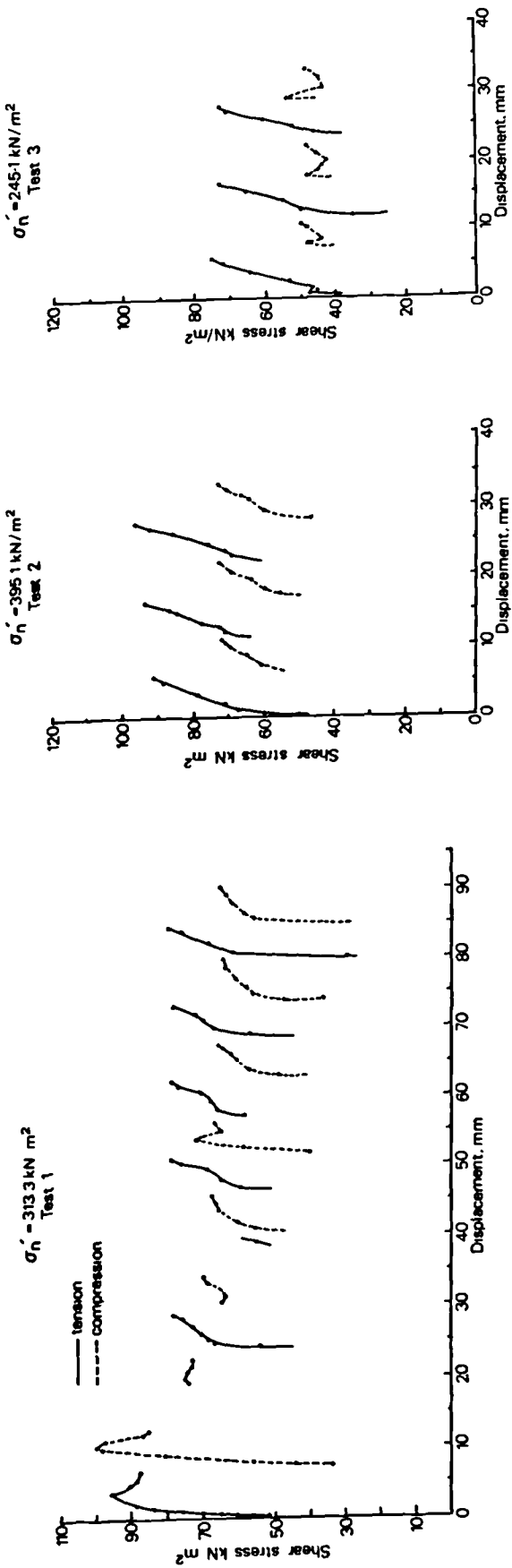


Fig. 5.8 Shear stress - displacement and displacement-vertical thickness relationships for shear box tests on remoulded tumbled and crushed sieved samples.

(a) MT.BH sample

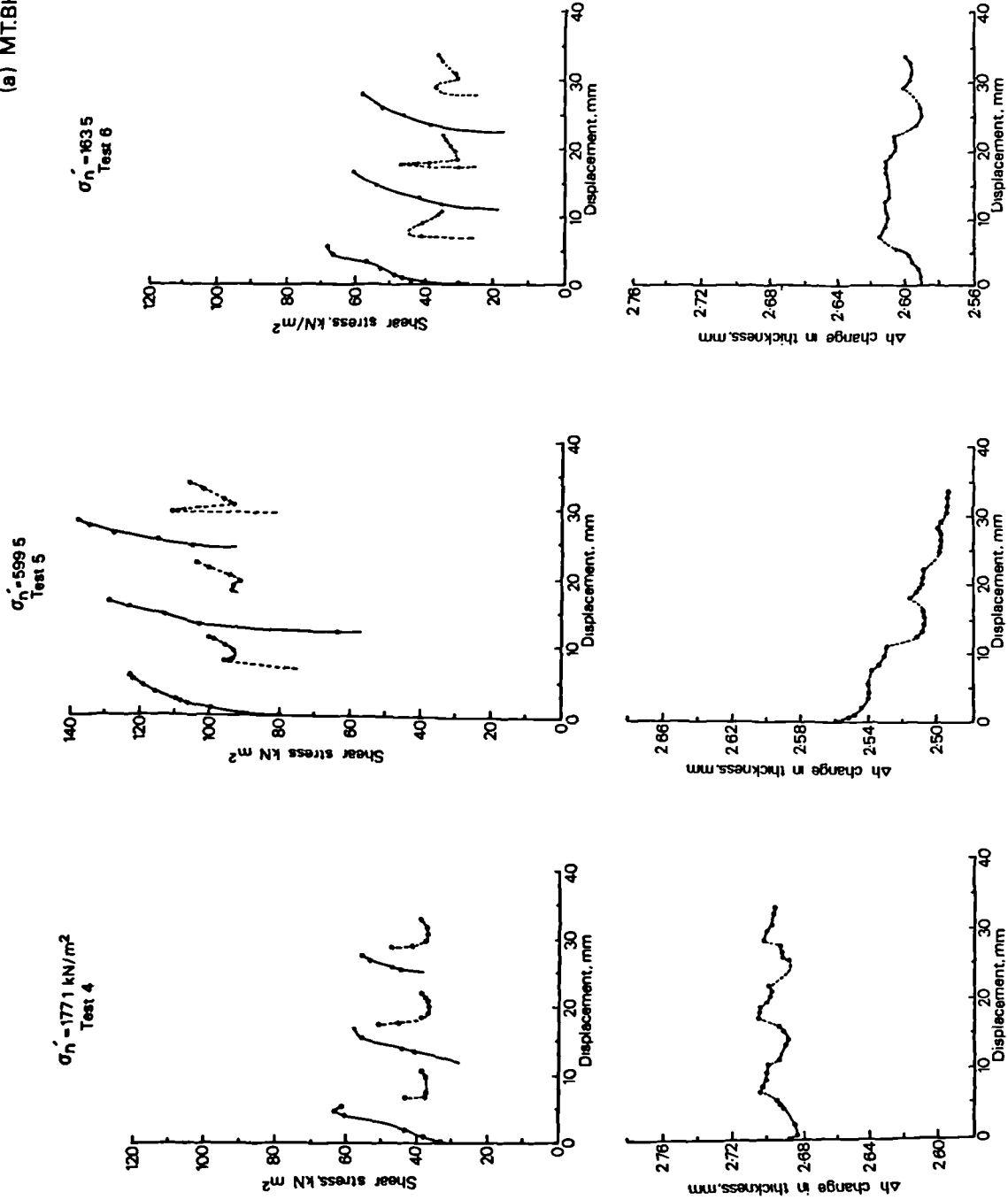


Fig. 5.8 Shear stress - displacement and displacement-vertical thickness relationships for shear box tests on remoulded tumbled and crushed sieved samples.

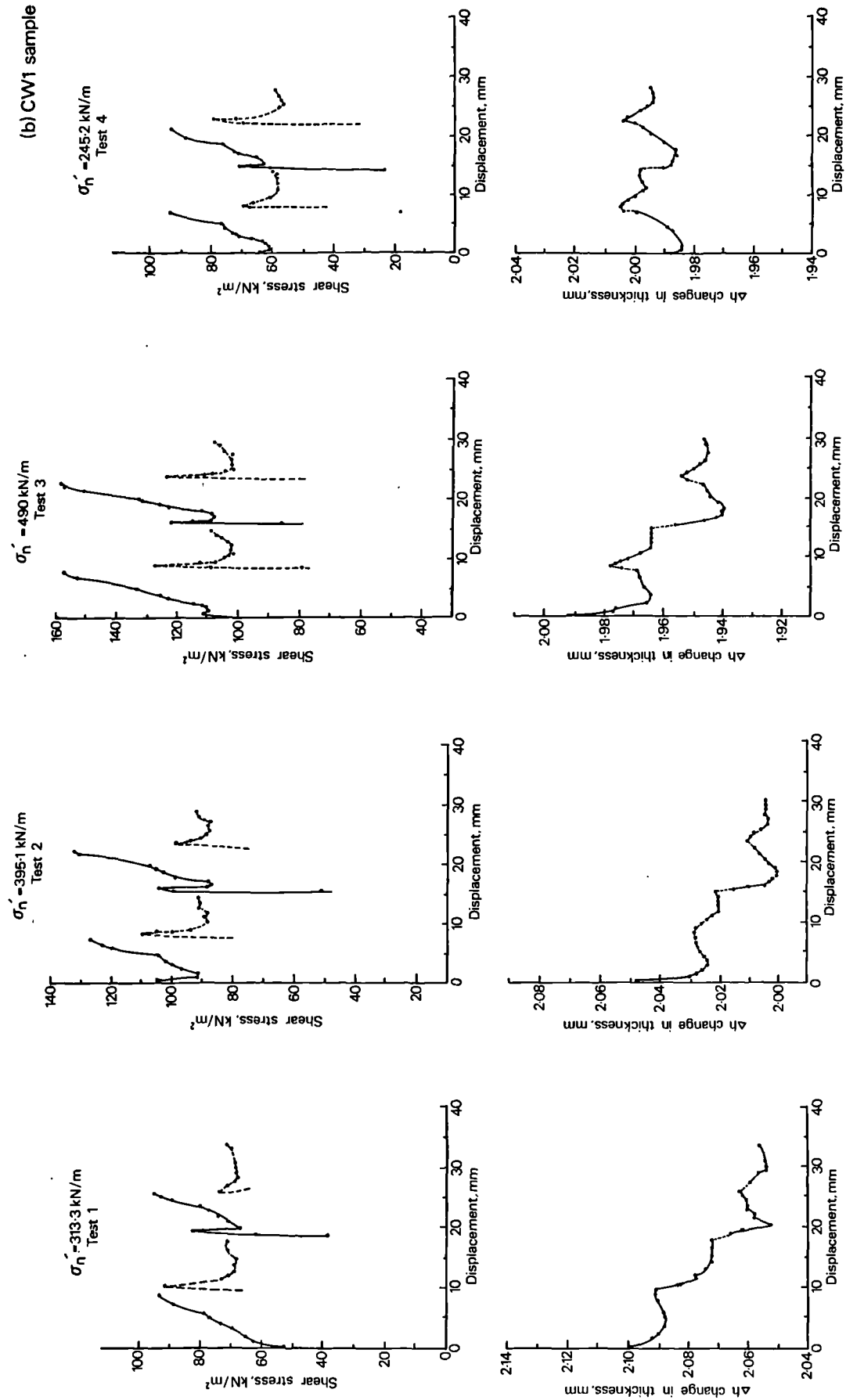
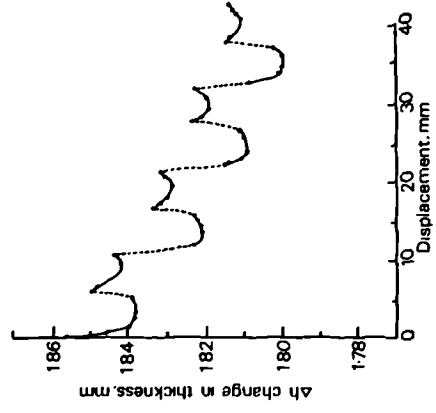
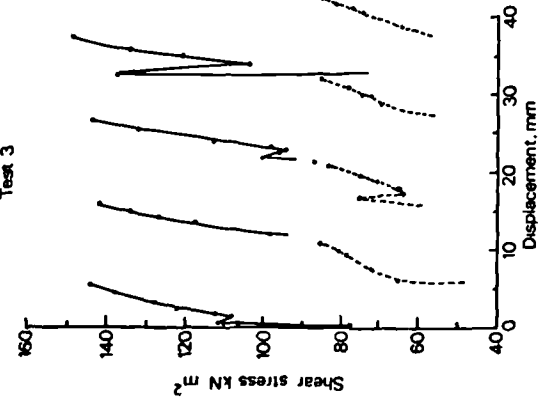


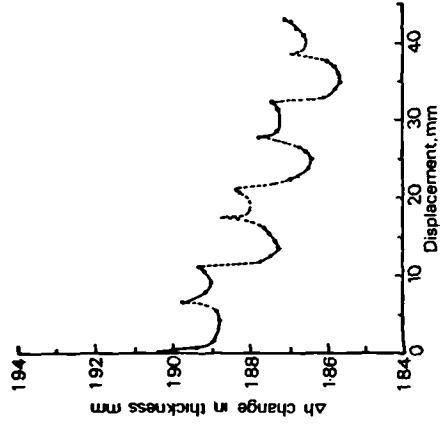
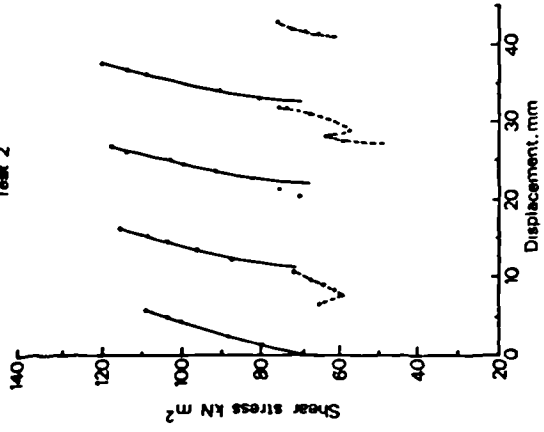
Fig. 5.8 Shear stress - displacement and displacement-vertical thickness relationships for shear box tests on remoulded tumbled and crushed sieved samples.

(c) MT.5 sample

$\sigma'_h = 490.0 \text{ kN/m}^2$
Test 3



$\sigma'_h = 395.1 \text{ kN/m}^2$
Test 2



$\sigma'_h = 313.3 \text{ kN/m}^2$
Test 1

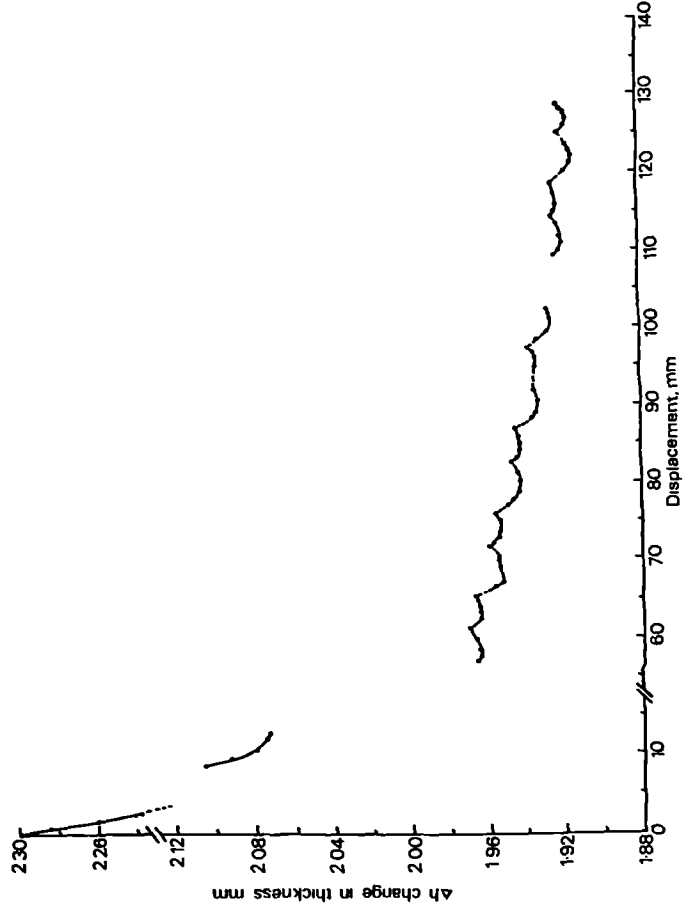
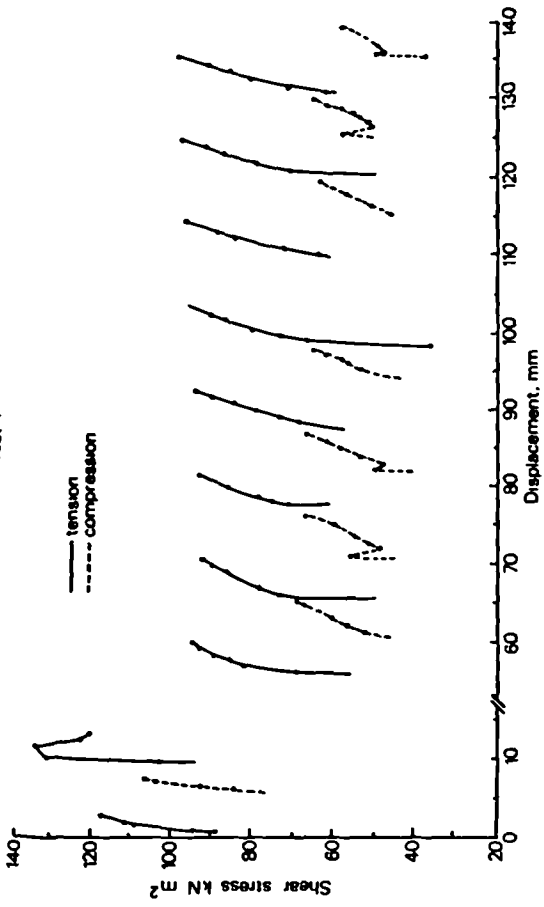


Fig. 5.8 Shear stress - displacement and displacement-vertical thickness relationships for shear box tests on remoulded tumbled and crushed sieved samples.

(c) MT5 sample

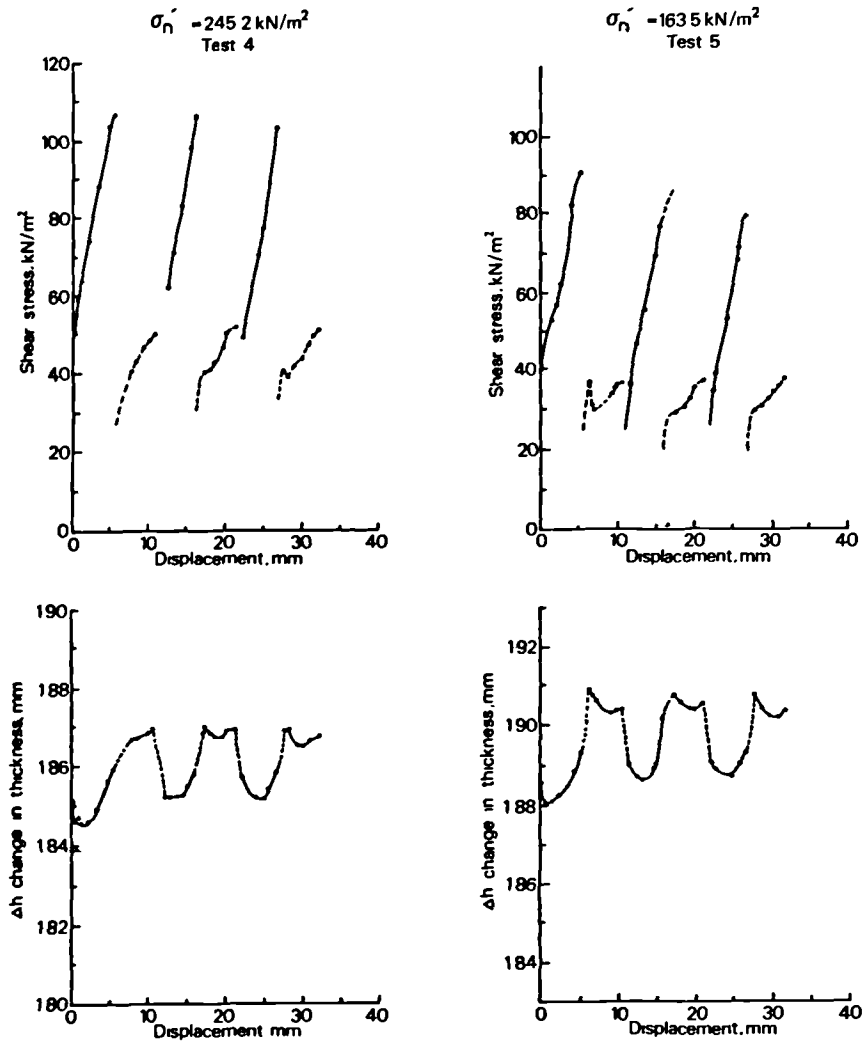


Fig. 5.8 Shear stress - displacement and displacement-vertical thickness relationships for shear box tests on remoulded tumbled and crushed sieved samples.

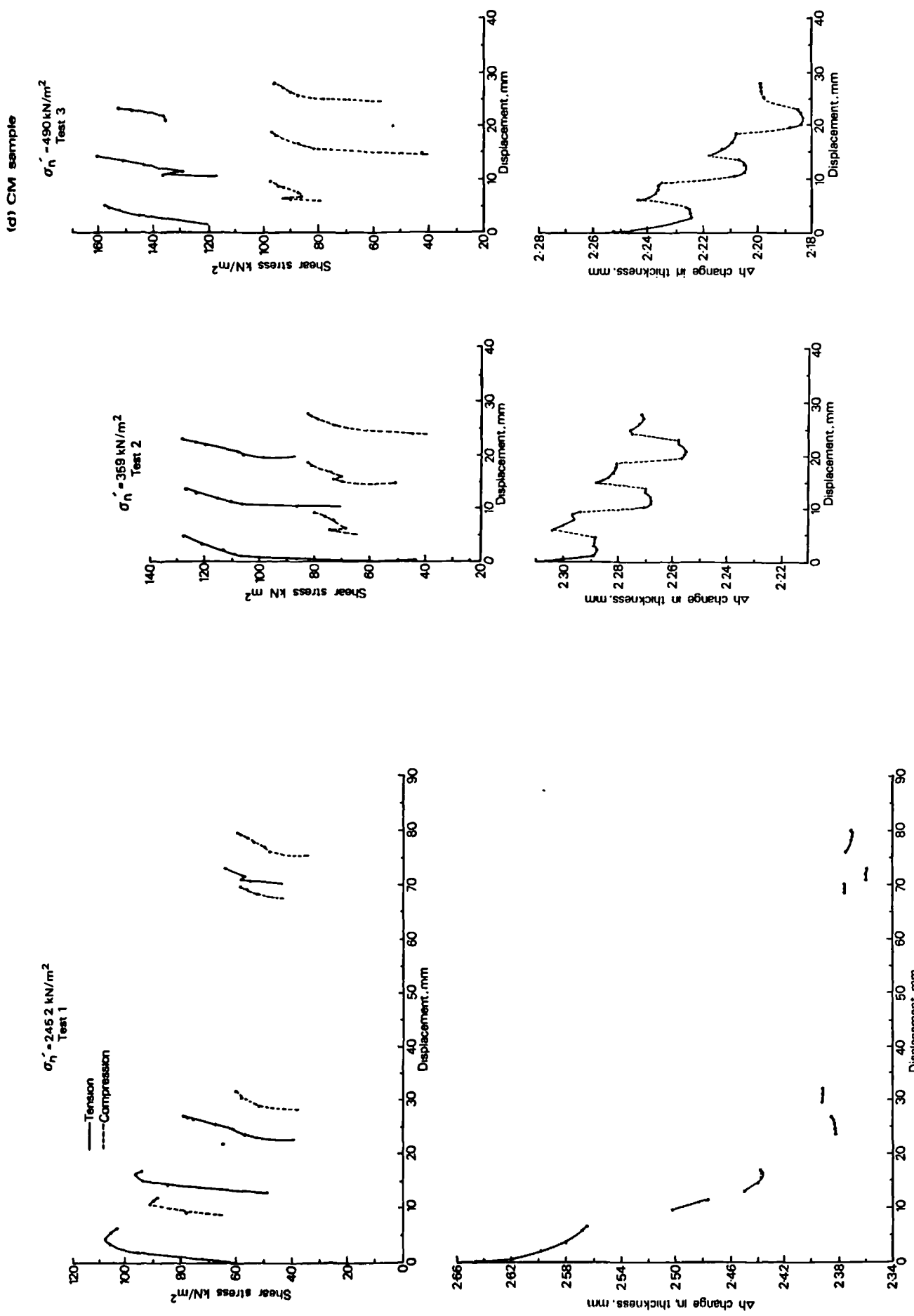


Fig. 5.8 Shear stress - displacement and displacement-vertical thickness relationships for shear box tests on remoulded tumbled and crushed sieved samples.

(d) CM sample

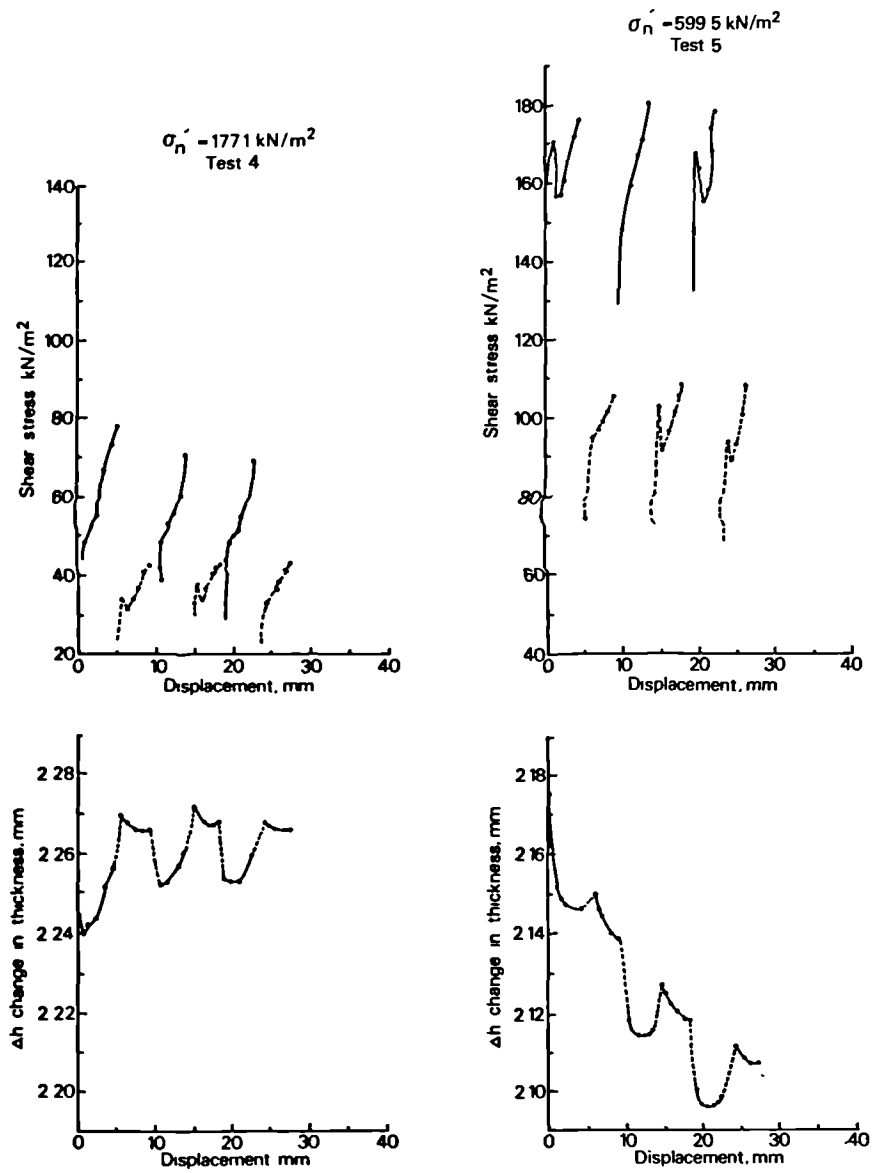


Fig. 5.8 Shear stress - displacement and displacement-vertical thickness relationships for shear box tests on remoulded tumbled and crushed sieved samples.

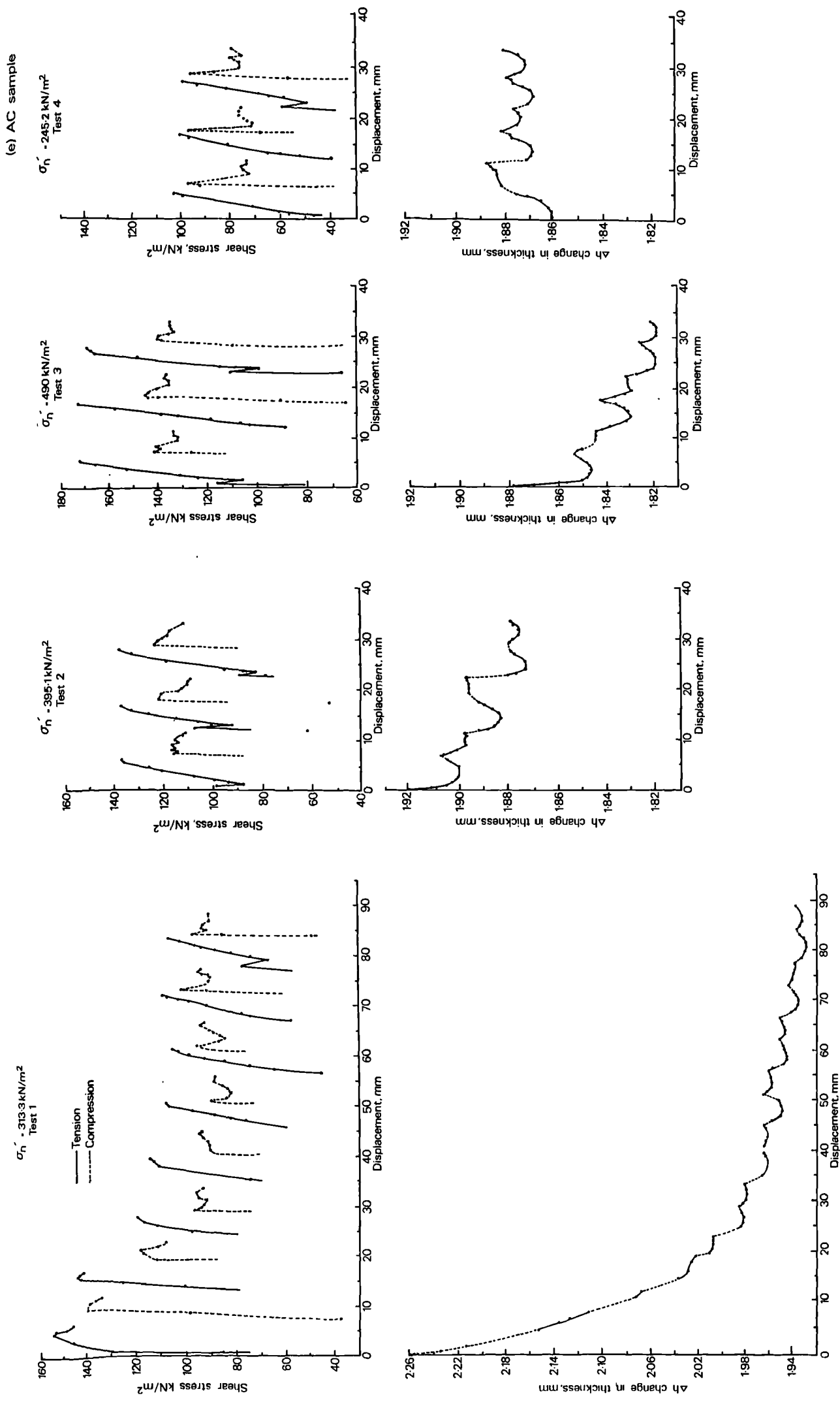
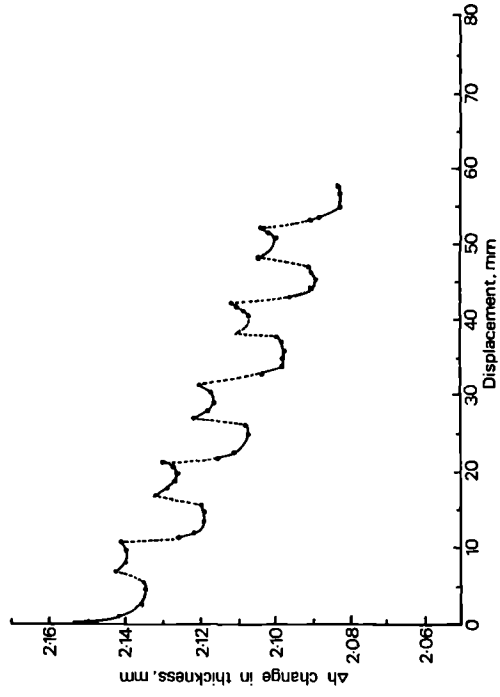
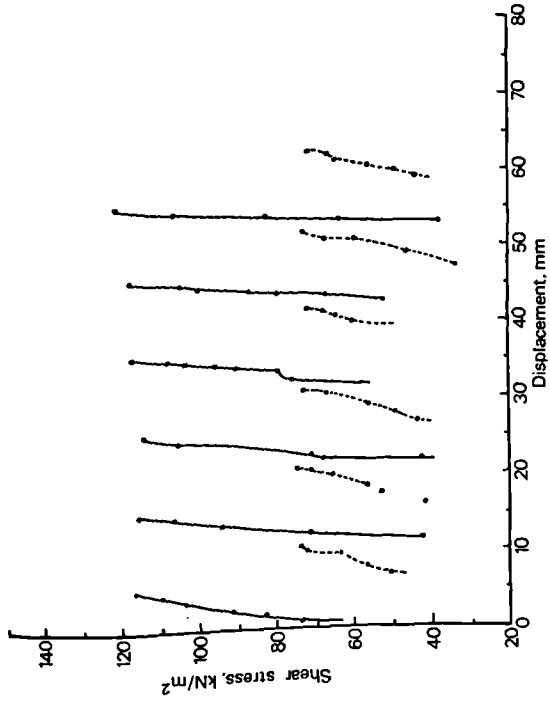


Fig. 5.8 Shear stress - displacement and displacement-thickness relationships for shear box tests on remoulded tumbled and crushed sieved samples.

(f) RP sample

$\sigma'_h = 359.1 \text{ kN/m}^2$
Test 2



$\sigma'_h = 313.3 \text{ kN/m}^2$
Test 1

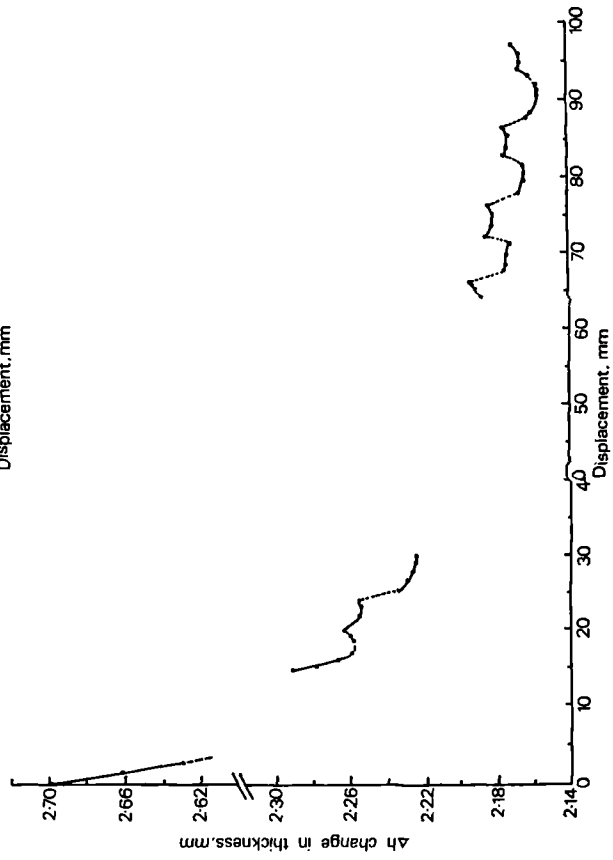
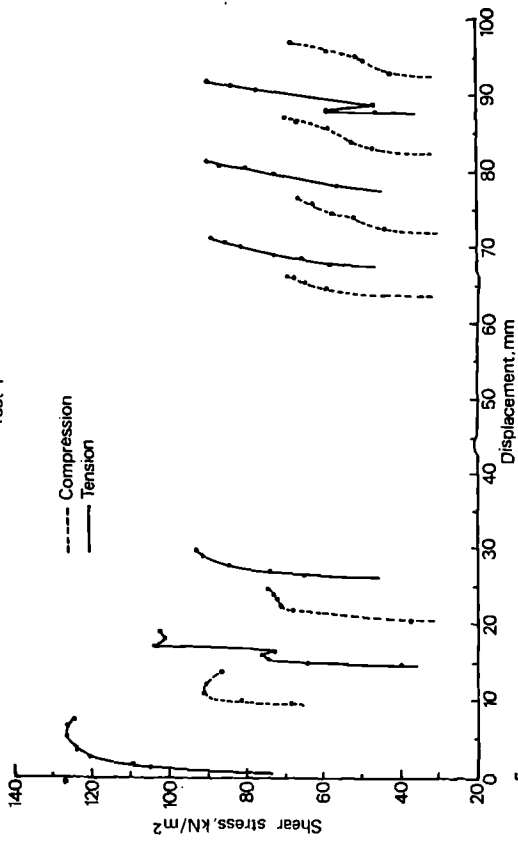
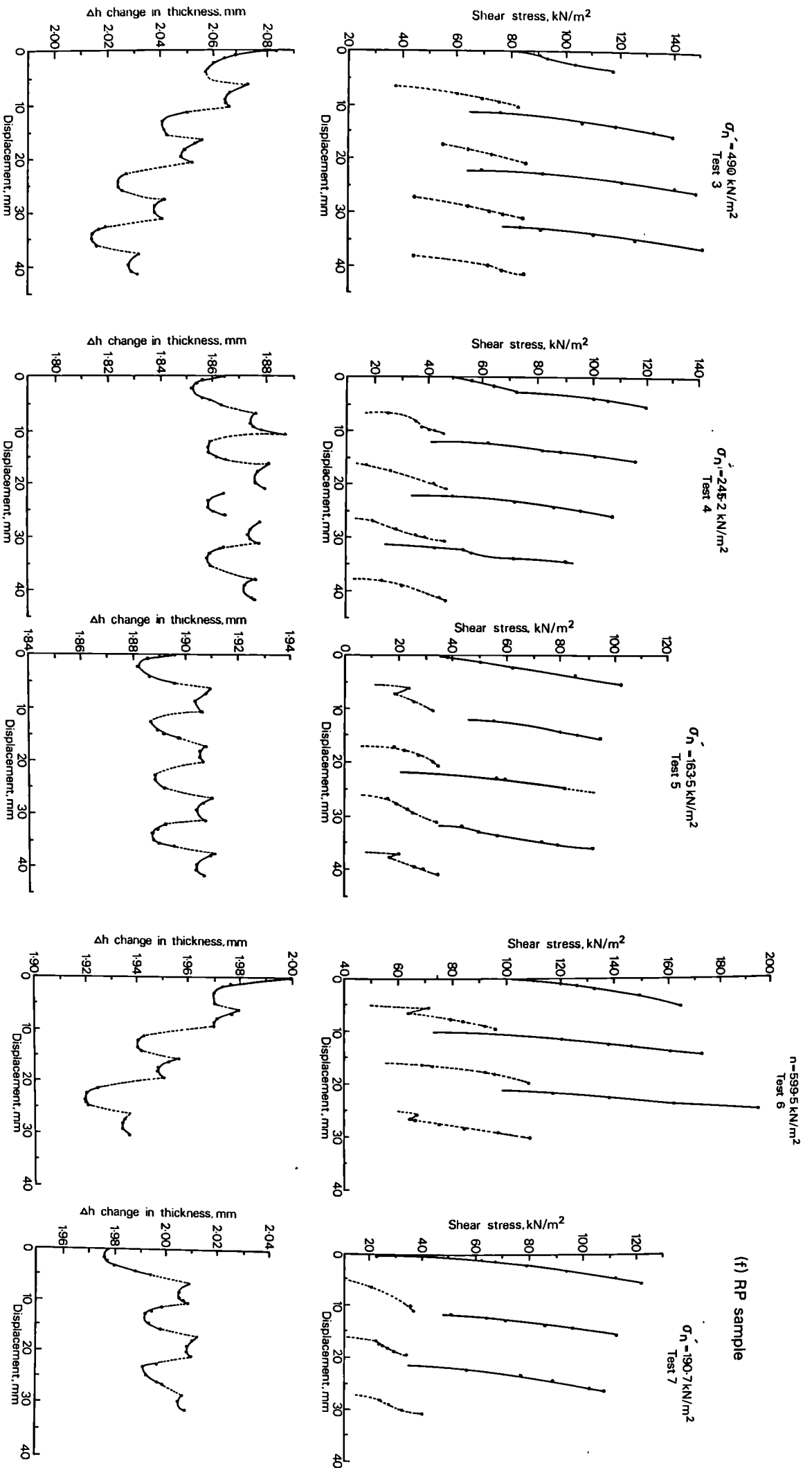


Fig. 5.8 Shear stress - displacement and displacement-vertical thickness relationships for shear box tests on remoulded tumbled and crushed sieved samples.



(f) RP sample

Fig. 5.8 Shear stress - displacement and displacement-
vertical thickness relationships for shear
box tests on remoulded tumbled and crushed
sieved samples.

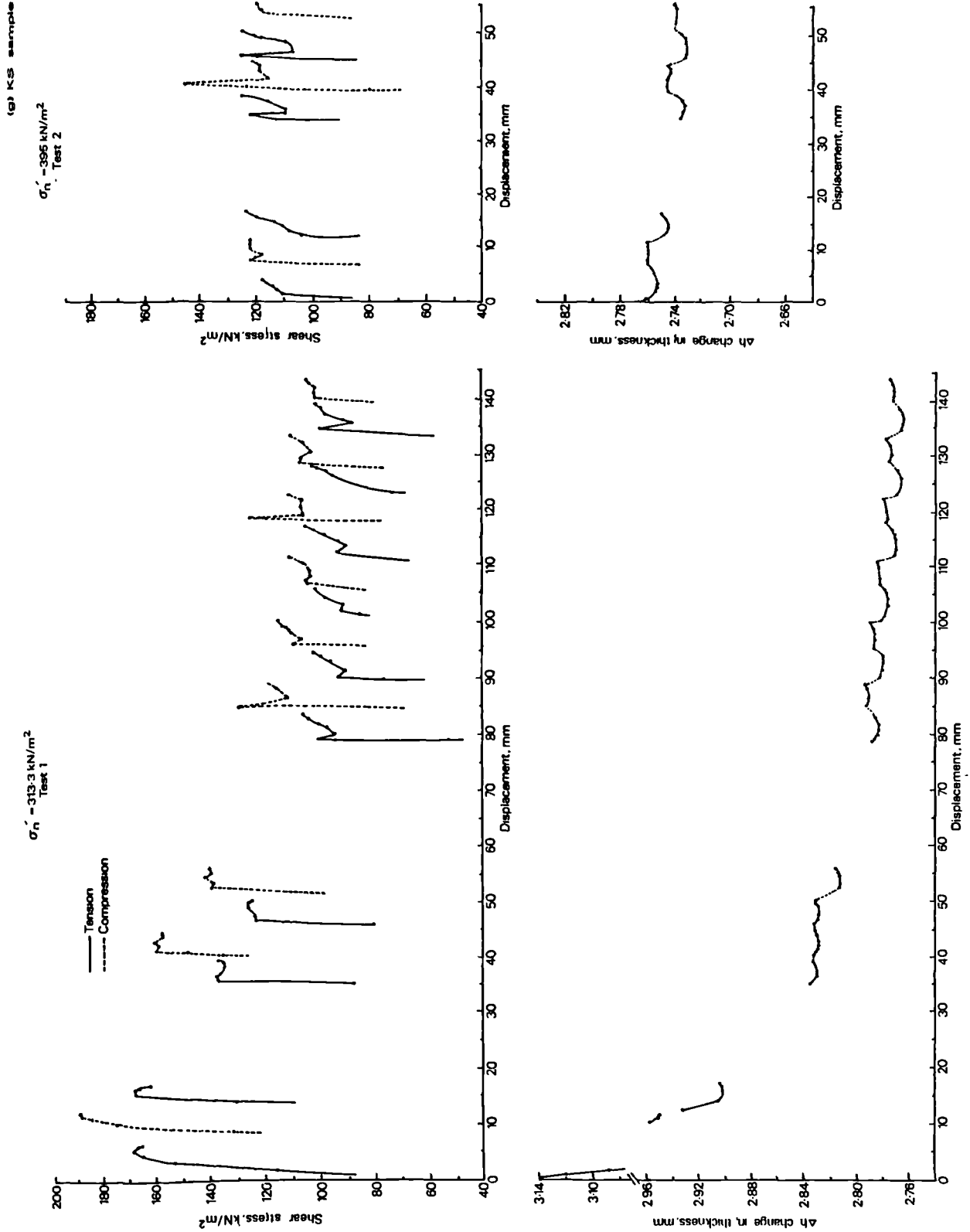


Fig. 5.8 Shear stress - displacement and displacement-vertical thickness relationships for shear box tests on remoulded tumbled and crushed sieved samples.

(g) KS sample

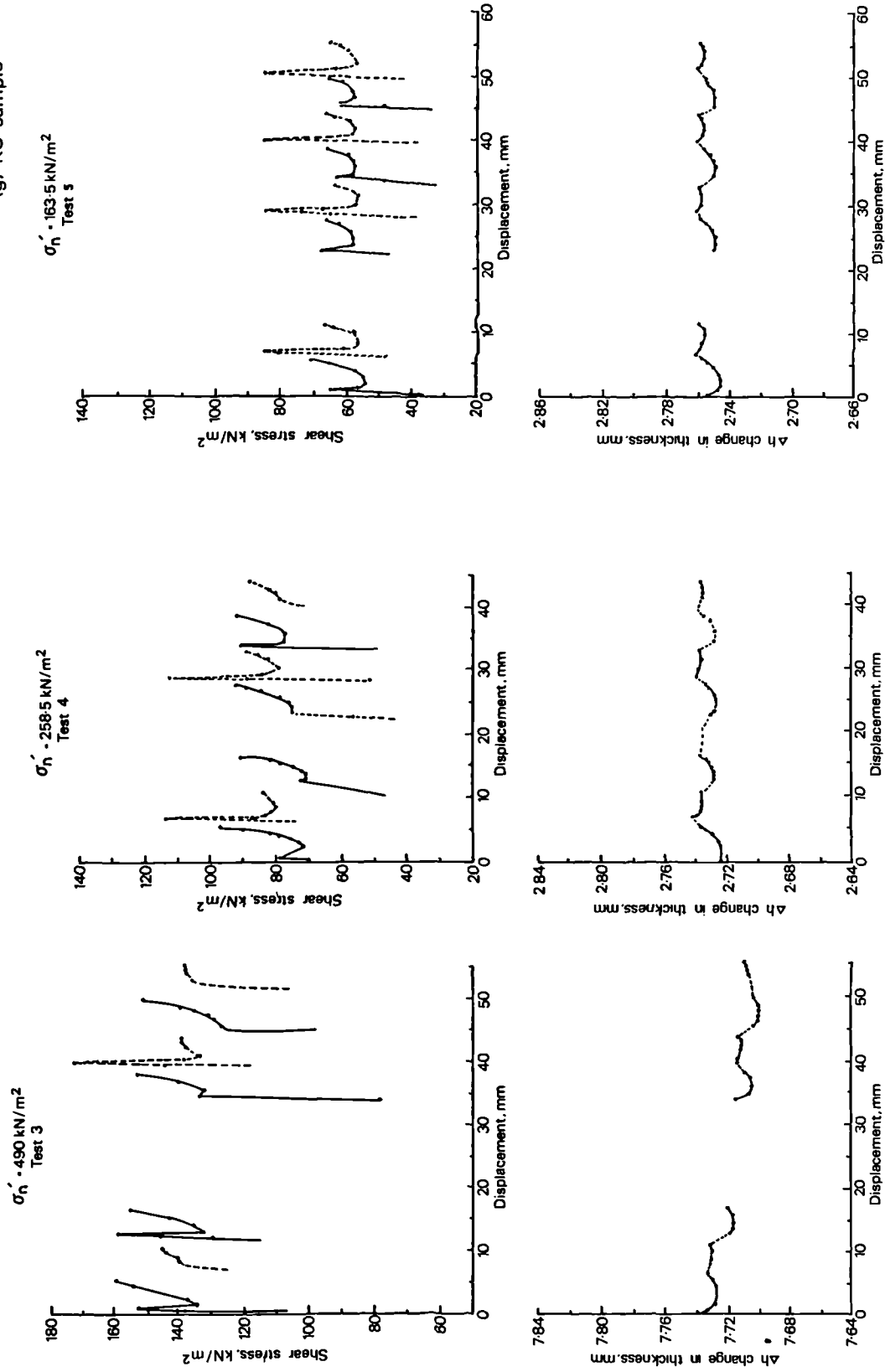
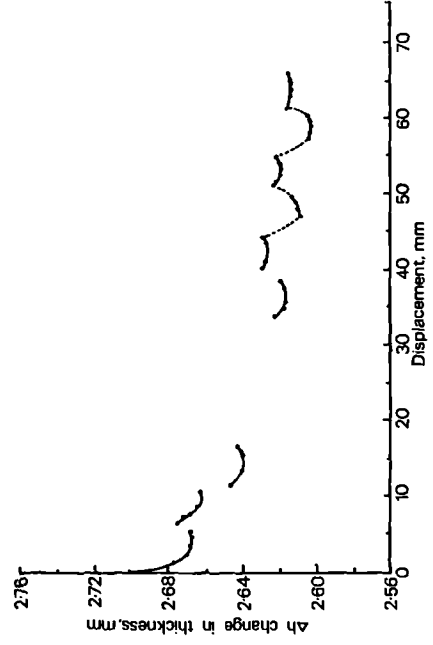
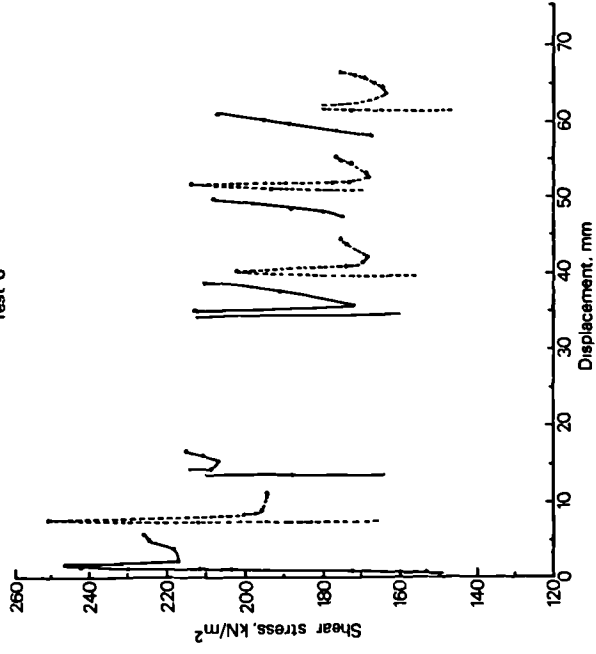


Fig. 5.8 Shear stress - displacement and displacement-vertical thickness relationships for shear box tests on remoulded tumbled and crushed sieved samples.

$\sigma'_n = 2812 \text{ kN/m}^2$
Test 6



(g) KS sample

$\sigma'_n = 1096 \text{ kN/m}^2$
Test 7

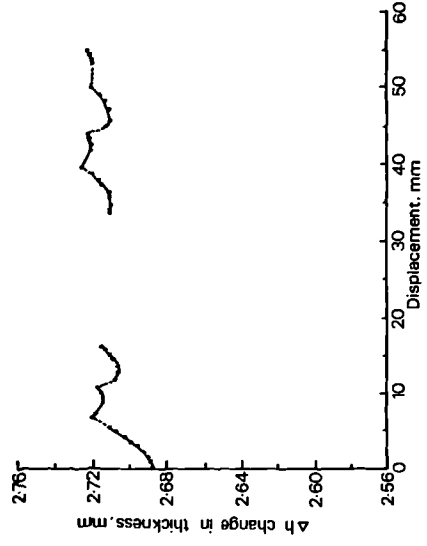
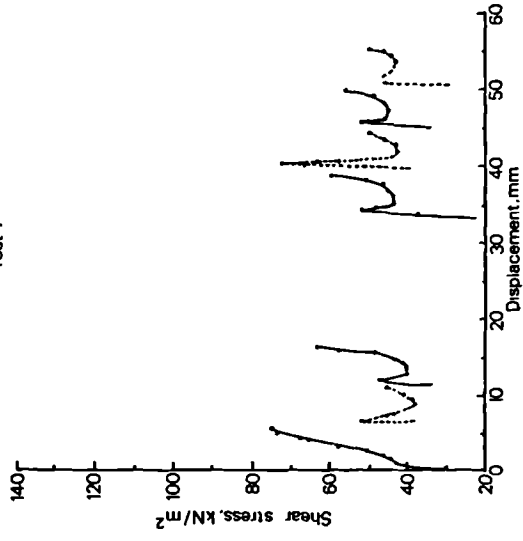
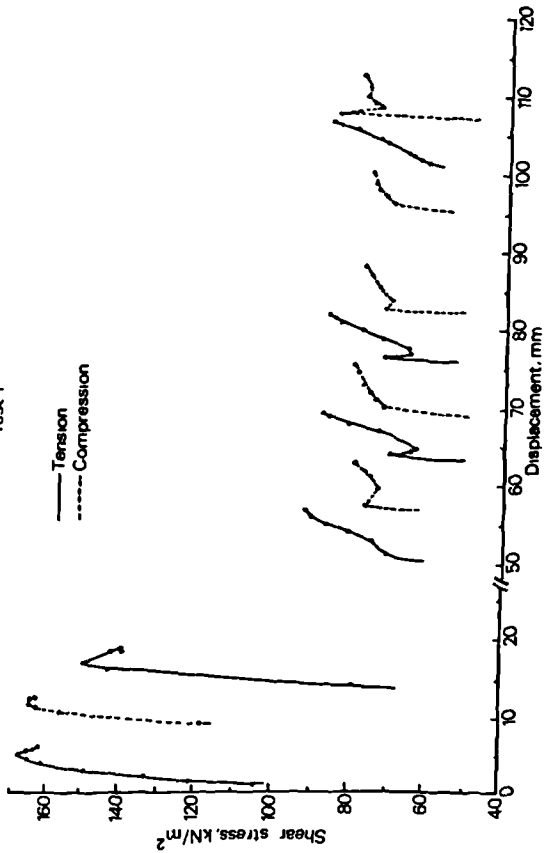


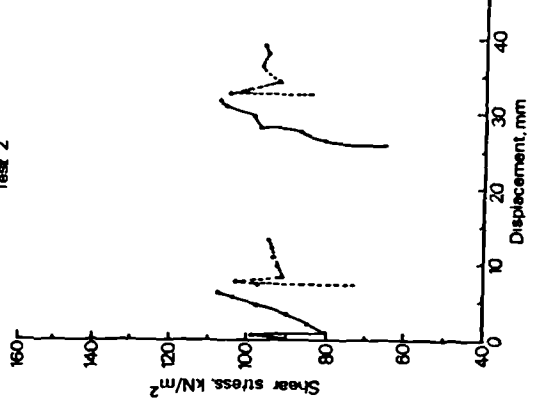
Fig. 5.8 Shear stress - displacement and displacement-vertical thickness relationships for shear box tests on remoulded tumbled and crushed sieved samples.

(h) CW1 CP200 sample

$\sigma_h = 313.3 \text{ kN/m}^2$
Test 1



$\sigma_h = 395.1 \text{ kN/m}^2$
Test 2



$\sigma_h = 490 \text{ kN/m}^2$
Test 3

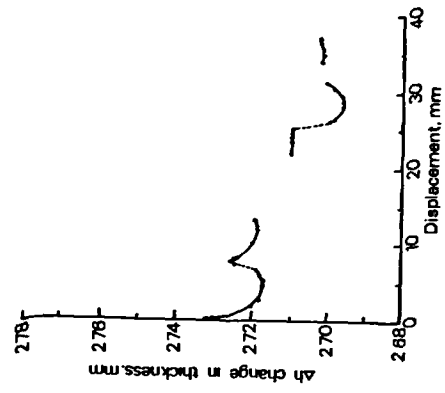
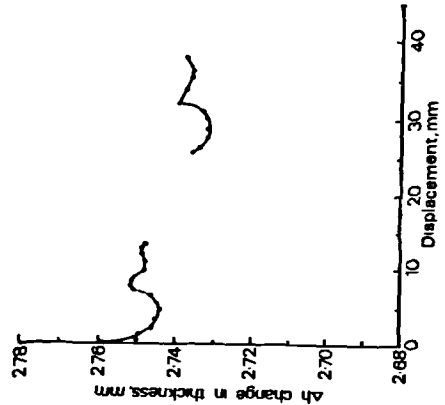
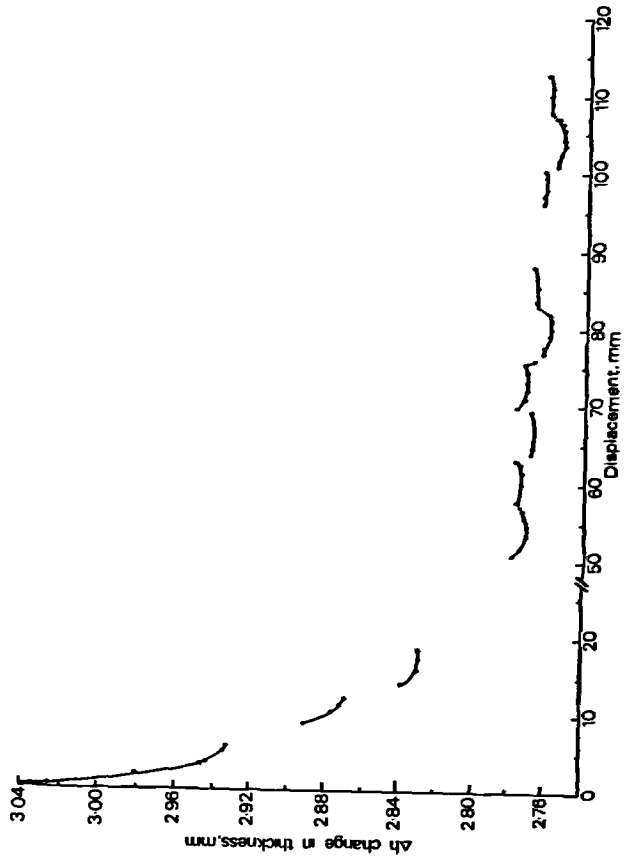
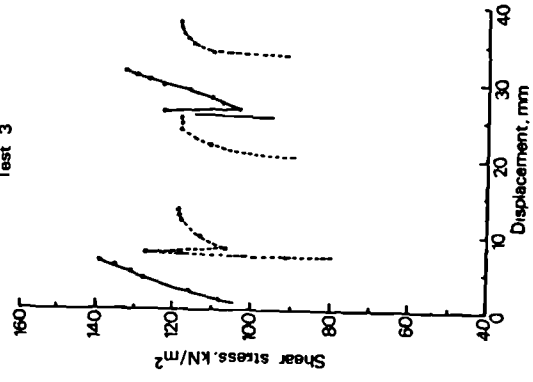


Fig. 5.8 Shear stress - displacement and displacement - vertical thickness relationships for shear box tests on remoulded tumbled and crushed sieved samples.

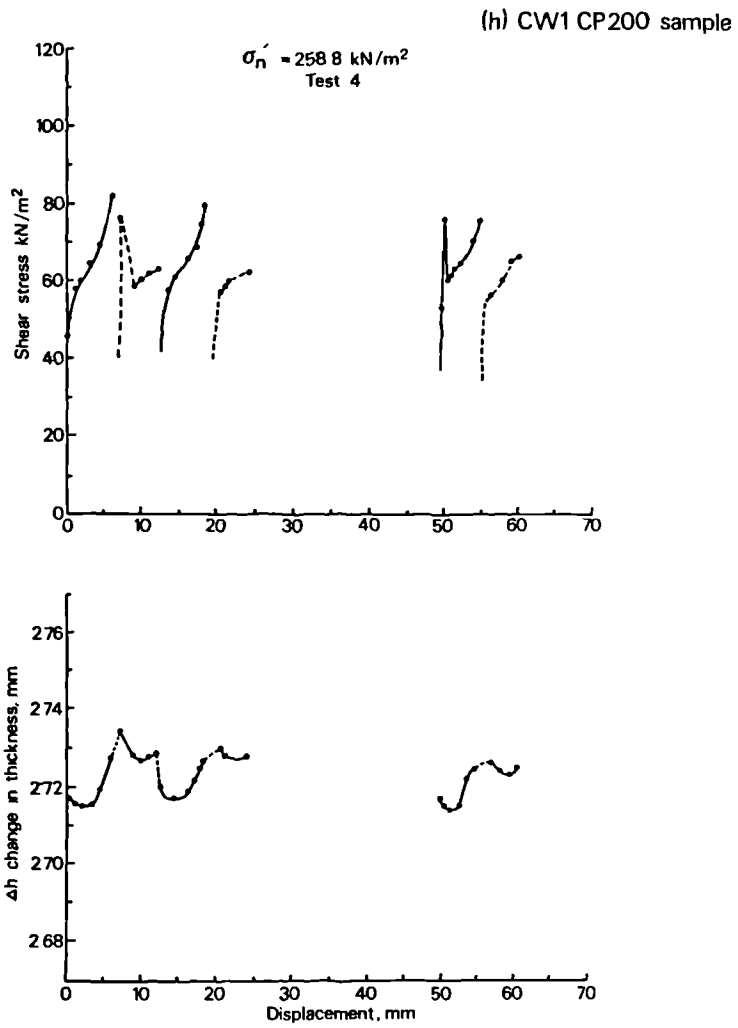


Fig. 5.8 Shear stress - displacement and displacement-vertical thickness relationships for shear box tests on remoulded tumbled and crushed sieved samples.

halves apart and disturbing the samples gives rise to an increase in shear strength. Reversal of the direction of shear allows the re-establishment of the mating position. The residual condition was assumed to correspond with the minimum shear stress which occur when two surface match. However, in some tests in Fig. 5.8 an increase occurs after the minimum value. In order to make the results systematic the residual condition was assumed to correspond with the terminal value of shear stress for compression. Mitchell (1976) makes the point that if irregularities are not orientated in the direction of shear a binding or a rotational effect is introduced. This may have happened in the case of sample CW1 (See Fig. 5.8b) and in fact the test was stopped to allow resetting of the sample. This explanation is supported by observation illustrated in Plates 5.5 to 5.11 since an increased degree of roughness of the post shear slip surface was observed for tests in which the difference between the tensional and compressional shear was greatest.

Sample thickness generally decreases with shear displacement but each reversal into the compression condition caused heave. This is attributed to the riding up of mismatched surfaces.

5.5.4 Variation in residual shear strength value

Following the literature review of Chapter 4, it may be concluded that a number of factors effect residual shear strength values. These will be considered with respect to variation in the normal effective stress, loading sequence, amount of displacement, rate of displacement, test method and sample preparation method.

i. Normal effective stress

The observation that residual shear strength varies with effective normal stress is not new (See Section 4.2.4) Tables 5.5, 5.6 and 5.7 together with Figs. 5.6 and 5.7 show the results of the residual shear



Plate No. 5.5 Slickensided shear surface - shear box test on sample SK.



Plate No. 5.6 Slickensided shear surface - shear box test on sample CW1CP200.

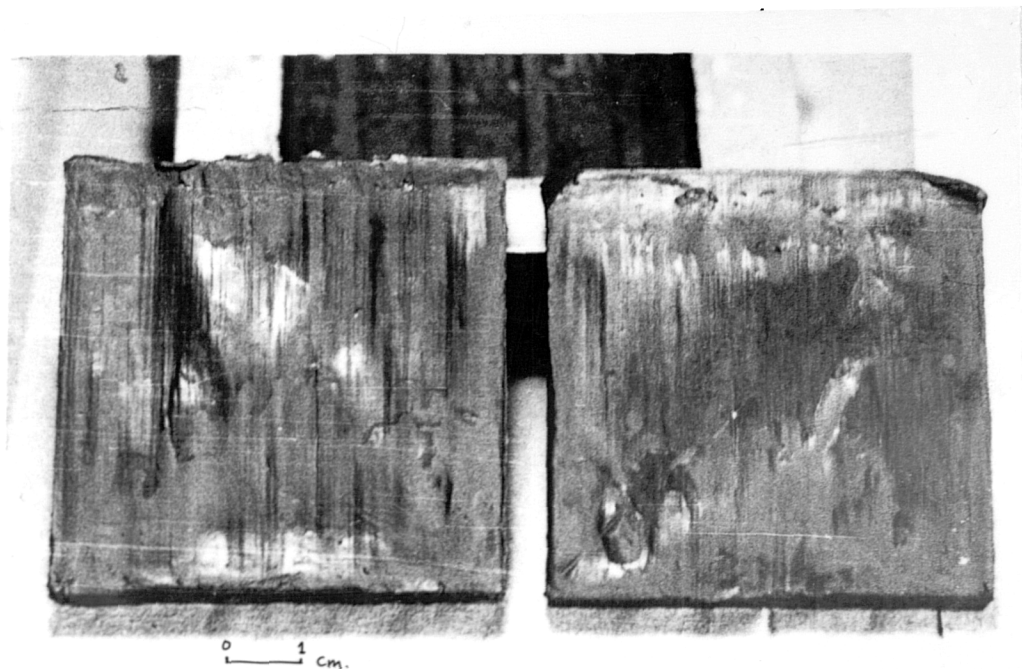


Plate No. 5.7 Slickensided shear surface - shear box test on sample CW1.



Plate No. 5.8 Slickensided shear surface - shear box test on sample MTBH.



Plate No. 5.9 Slickensided shear surface - shear box test on sample MT5.

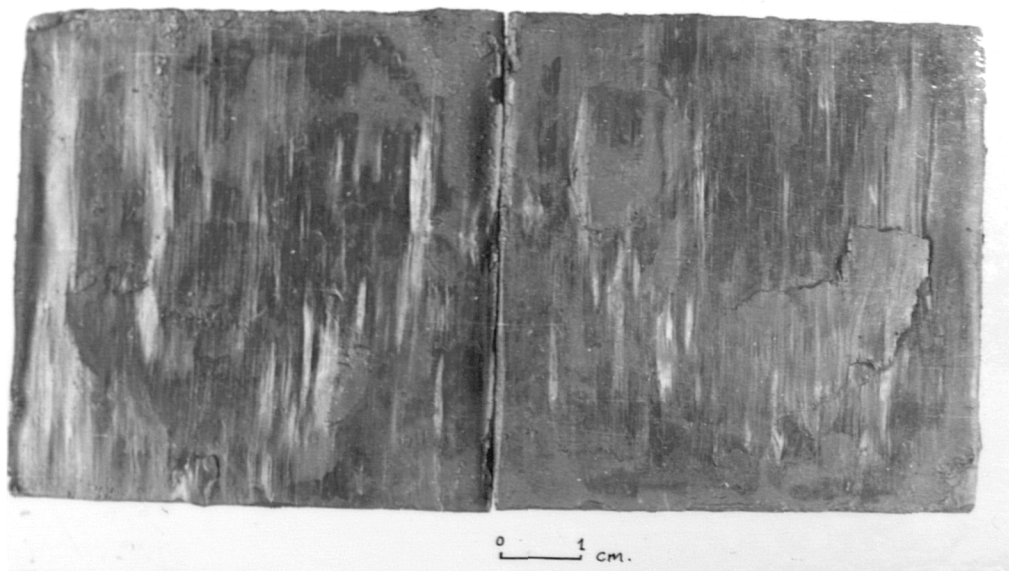


Plate No. 5.10 Slickensided shear surface - shear box test on sample AC.



Plate No. 5.11 Slickensided shear surface - shear box test on sample RP.

Table 5.5 Residual shear stress values, normal stress values and shear stress:
normal stress ratio for ring shear test on remoulded tumbled samples.

Sample	σ_n^1 kN/m ²	24.5	73.5	122.4	171.4	171.4	245.0	318.4	318.4	392.0	489.8	612.3	612.3	685.8
MTBH	τ_r N/m ²				⁵ 25.46		¹ 36.8	² 45.0		³ 54.2	⁴ 67.4			
	τ_r/σ_n^1				0.148		0.150	0.141		0.139	0.137			
	ϕ_{rr}^1 deg. c o				8.4		8.5	8.0		7.8	7.8			
CW1	τ_r kN/m ²				⁶ 25.22		⁵ 33.1	¹ 52.33	⁴ 42.6	² 53.3	³ 66.5			
	τ_r/σ_n^1				0.147		0.135	0.164	0.133	0.136	0.135			
	ϕ_{rr}^1 deg. c o				8.3		7.6	9.3	7.6	7.7	7.7			
CW2	τ_r kN/m ²				⁵ 33.61		¹ 46.44	² 60.00		³ 73.33	⁴ 92.18			
	τ_r/σ_n^1				0.196		0.189	0.188		0.187	0.188			
	ϕ_{rr}^1 deg. c o				11.0		10.7	10.6		10.5	10.6			
CW3	τ_r kN/m ²				⁵ 41.42		⁴ 58.15	¹ 77.86		² 90.29	³ 110.0	⁶ 140.0		
	τ_r/σ_n^1				0.241		0.237	0.224		0.230	0.226	0.228		
	ϕ_{rr}^1 deg. c o				13.5		13.3	13.7		12.9	12.7	12.8		
MT5	τ_r kN/m ²				⁵ 24.0		⁴ 33.8	¹ 45.45		² 49.09	³ 59.39			⁶ 84.24
	τ_r/σ_n^1				0.140		0.137	0.142		0.125	0.121			0.122
	ϕ_{rr}^1 deg. c o				7.9		7.8	8.1		7.1	6.9			7.00
MT6	τ_r kN/m ²				⁵ 26.2		¹ 40.0	² 46.5		³ 56.88	⁴ 71.2			
	τ_r/σ_n^1				0.152		0.163	0.146		0.145	0.145			
	ϕ_{rr}^1 deg. c o				8.6		9.2	8.3		8.2	8.2			
BUT	τ_r kN/m ²				⁴ 35.53			¹ 63.38		² 72.46	³ 89.07	⁵ 110.76		
	τ_r/σ_n^1				0.207			0.199		0.184	0.181	0.180		
	ϕ_{rr}^1 deg. c o				11.7			11.2		10.4	10.3	10.2		
CM	τ_r kN/m ²				⁵ 32.0		⁴ 44.0	¹ 58.93		² 65.33	³ 80.0			
	τ_r/σ_n^1				0.186		0.179	0.185		0.166	0.163			
	ϕ_{rr}^1 deg. c o				10.5		10.1	10.4		9.4	9.2			
RP	τ_r kN/m ²				⁶ 25.71	⁷ 27.14	⁵ 37.14	¹ 52.85	⁴ 44.28	² 54.0	³ 68.5	¹ 83.6	⁵ 85.0	
	τ_r/σ_n^1				0.150	0.158	0.151	0.165	0.139	0.137	0.139	0.135	0.138	
	ϕ_{rr}^1 deg. c o				8.5	8.9	8.6	9.4	7.9	7.8	7.9	7.7	7.9	
I AC	τ_r kN/m ²				⁵ 27.1		⁴ 36.4	¹ 47.8		² 52.8	³ 66.4			⁶ 88.5
	τ_r/σ_n^1				0.158		0.148	0.150		0.134	0.135			0.129
	ϕ_{rr}^1 deg. c o				8.9		8.4	8.5		7.6	7.7			7.3
BCL	τ_r kN/m ²			⁷ 33.77	⁵ 44.33		⁴ 60.37	¹ 80.75		² 90.37	³ 110.37			⁶ 158.7
	τ_r/σ_n^1			0.274	0.258		0.246	0.253		0.230	0.225			0.224
	ϕ_{rr}^1 deg. c o			15.4	14.5		13.8	14.2		12.9	12.6			12.6
CS	τ_r kN/m ²			⁷ 21.45	⁵ 27.77		⁴ 40.12	¹ 55.7		² 61.57	³ 74.84	⁶ 95.67		⁸ 104.93
	τ_r/σ_n^1			0.175	0.163		0.163	0.174		0.157	0.152	0.156		0.153
	ϕ_{rr}^1 deg. c o			9.9	9.2		9.2	9.9		8.9	8.6	8.8		8.6
KS	τ_r kN/m ²	⁹ 9.2	¹ 21.0	⁷ 33.4	⁵ 46.0		⁴ 64.0	¹ 87.0		² 96.0	³ 119.5			⁶ 160.5
	τ_r/σ_n^1	0.375	0.285	0.272	0.267		0.261	0.273		0.244	0.243			0.234
	ϕ_{rr}^1 deg. c o	20.5	15.9	15.2	14.9		14.6	15.2		13.7	13.7			13.1

No. 1,2,3----- load sequence.

Table 5.6 Residual shear stress values, normal stress values and shear stress : normal stress ratio for ring shear tests on remoulded crushed samples of Edale Shale from Hope Valley Cement Works.

Sample	σ_n' kN/m ²	171.4	245.0	318.4	3.92	489.8
CW1C	τ_r kN/m ²		²	¹	³	⁴
			49.66	67.8	77.0	94.6
	τ_r / σ_n'		0.202	0.212	0.196	0.193
	ϕ_{rr}' deg. c=0		11.4	12.0	11.1	10.9
CW2C	τ_r kN/m ²	² 56.0	¹ 79.2	³ 94.0		⁴ 120.0
	τ_r / σ_n'	0.326	0.323	0.295		0.244
	ϕ_{rr}' deg. c=0	18.1	17.9	16.4		13.7
CW3C	τ_r kN/m ²	⁴ 70.5	¹ 102.6	² 122		³ 180.1
	τ_r / σ_n'	0.411	0.418	0.383		0.367
	ϕ_{rr}' deg. c=0	22.3	22.7	20.9		20.1

No. 1,2,3-----is the load sequence.

Table 5.7 Residual shear stress values, normal stress values and shear stress : normal stress ratio for ring shear test on remoulded crushed sieved Edale Shale from Hope Valley Cement Works.

Sample	σ_n' kN/m ²	245	318.4	318.4	392.0	489.8
CW1CP200	τ_r kN/m ²	⁵ 48.5	¹ 67.16	⁴ 62.68	² 75.32	³ 94.0
	τ_r / σ_n'	0.198	0.210	0.196	0.192	0.191
	ϕ_{rr}' deg. c=0	11.1	11.9	11.1	10.8	10.8
CW1CR200	τ_r kN/m ²	⁴ 58.2	¹ 82.2		² 94.0	³ 115.0
	τ_r / σ_n'	0.237	0.258		0.239	0.234
	ϕ_{rr}' deg. c=0	13.3	14.4		13.4	13.2
CW1CR72	τ_r kN/m ²	⁴ 72.6	¹ 89.9		² 110.6	³ 133.6
	τ_r / σ_n'	0.296	0.310		0.282	0.272
	ϕ_{rr}' deg. c=0	16.5	17.2		15.7	15.2

No. 1,2,3---- is the load sequence.

strength ring shear tests for different normal effective stresses. From these results the initial effective stress used in each sample gives a residual shear strength higher than the values corresponding to latter normal stresses regardless of whether this is an increase or decrease in value. For example as indicated in Table 5.7 for sample CW1CP200 in which an initial σ_n' of 318.4 kN/m² gave $\phi_{rr}' = 11.9^\circ$, increasing σ_n' to 392 kN/m² reduces ϕ_{rr}' to 10.8°. Thus the difference in ϕ_{rr}' value for the initial σ_n' and the next σ_n' used is near to 1°. For all samples tested in the ring shear the difference ranges between 0.5 and 1.5° except for sample CW.2 shown in Table 5.5 for which the difference is much smaller. Bishop et al (1971) attributes this effect to the non-achievement of residual state in his tests on brown London Clay. However, in view of the fact that even for shear displacement in excess of 300 mm. (See Fig. 5.7d) the effect occurs, it seems likely that both consolidation and swelling of sample causes a reduction in ϕ_{rr}' .

The shear box results in Table 5.8 and Fig. 5.8 show that apart from sample CW1, the ϕ_{rr}' value for the first residual is higher than the latter ones. Again particle re-arrangement during consolidation is probably responsible for this effect.

ii. Loading sequence

The effect of loading sequence was investigated for all samples tested by the ring shear and shear box methods. These results are shown in Figs 5.9 and 5.10 for ring shear tests and Fig. 5.11 for shear box tests. Apart from the initial ϕ_{rr}' value a unique curve exists between τ_r/σ_n' values which depends only on the magnitude of the normal effective stress. So the loading sequence has no effect on residual shear strength which confirms the finding of many authors reviewed in Chapter 4.

iii. Amount of displacement

Table 5.8 Residual shear stress values, normal stress values, and shear stress : normal stress ratio for shear box tests on remoulded tumbled and crushed samples.

Sample	σ'_n kN/m ²	109.7	163.5	177.1	190.7	245.2	258.8	313.3	395.1	490.0	599.5	681.2
MT8H	τ_r kN/m ²		⁸ 36.5	⁴ 39.0		³ 49.0		¹ 65.0	² 72.5		⁵ 105	
	τ_r / σ'_n		0.220	0.220		0.199		0.207	0.183		0.175	
	$\phi_{rc=0}$ deg.		12.5	12.4		11.3		11.7	10.3		9.9	
CWI	τ_r kN/m ²					⁴ 59.0		¹ 71.5	² 90.0	³ 109.5		
	τ_r / σ'_n					0.240		0.228	0.238	0.223		
	$\phi_{nc=0}$ deg.					13.5		12.8	12.8	12.6		
AC	τ_r kN/m ²					⁴ 74.0		¹ 90.0	² 110.0	³ 135.0		
	τ_r / σ'_n					0.301		0.237	0.278	0.275		
	$\phi_{rrc=0}$ deg.					16.7		16.0	15.5	15.4		
RP	τ_r kN/m ²		⁵ 34.5		⁷ 39.0	⁴ 47.0		¹ 66.0	² 72.0	³ 85.0	⁶ 102.0	
	τ_r / σ'_n		0.211		0.204	0.191		0.210	0.182	0.173	0.170	
	$\phi_{rrc=0}$ deg.		11.9		11.5	10.8		11.9	10.3	9.8	9.6	
MT5	τ_r kN/m ²		⁵ 38.0			⁴ 50.0		¹ 65.0	² 75.0	³ 85.5		
	τ_r / σ'_n		0.232			0.204		0.207	0.189	0.174		
	$\phi_{rrc=0}$ deg.		13.0			11.5		11.7	10.7	9.9		
CM	τ_r kN/m ²			⁴ 43.0		¹ 60.0			² 82.0	³ 97.0	⁵ 108.0	
	τ_r / σ'_n			0.242		0.244			0.207	0.197	0.180	
	$\phi_{rc=0}$ deg.			13.6		13.7			11.7	11.2	10.2	
KS	τ_r kN/m ²	⁴ 46.0	⁵ 64.5				⁴ 88.0	¹ 101.0	² 120.0	³ 138.0		⁶ 175.0
	τ_r / σ'_n	0.422	0.394				0.340	0.322	0.303	0.231		0.256
	$\phi_{rc=0}$ deg.	22.8	21.5				18.7	17.8	16.9	15.7		14.4
CW1CP200	τ_r kN/m ²						⁴ 63.0	¹ 77.0	² 95.0	³ 118		
	τ_r / σ'_n						0.243	0.245	0.240	0.240		
	$\phi_{rc=0}$ deg.						13.6	13.8	13.5	13.5		

No. 1,2,3,-----is the load sequence.

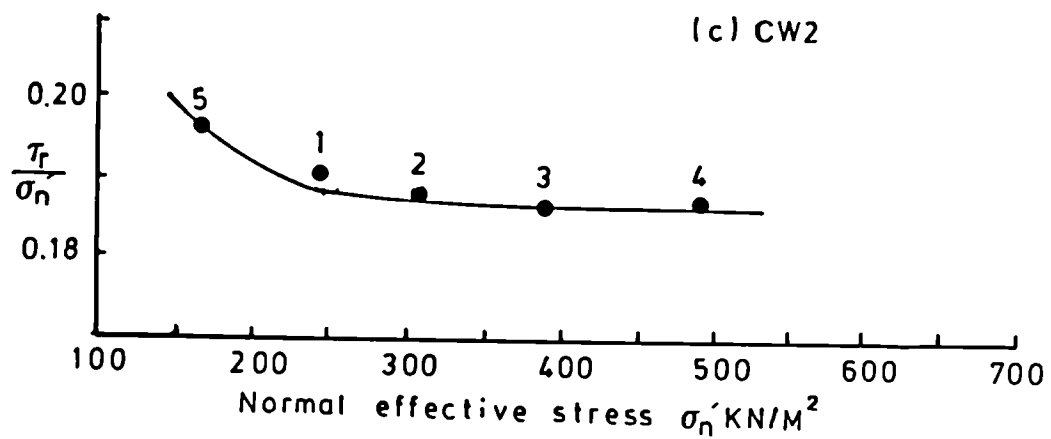
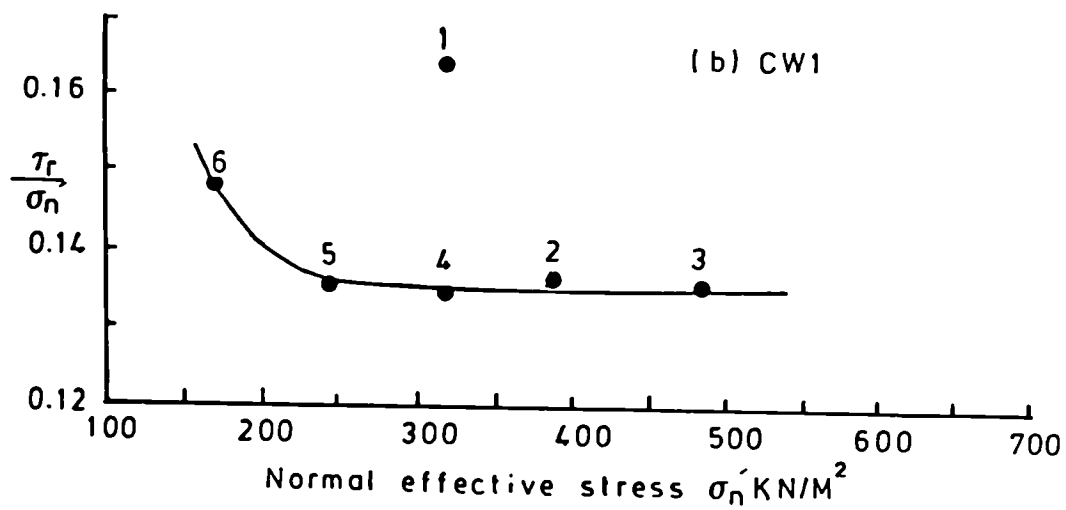
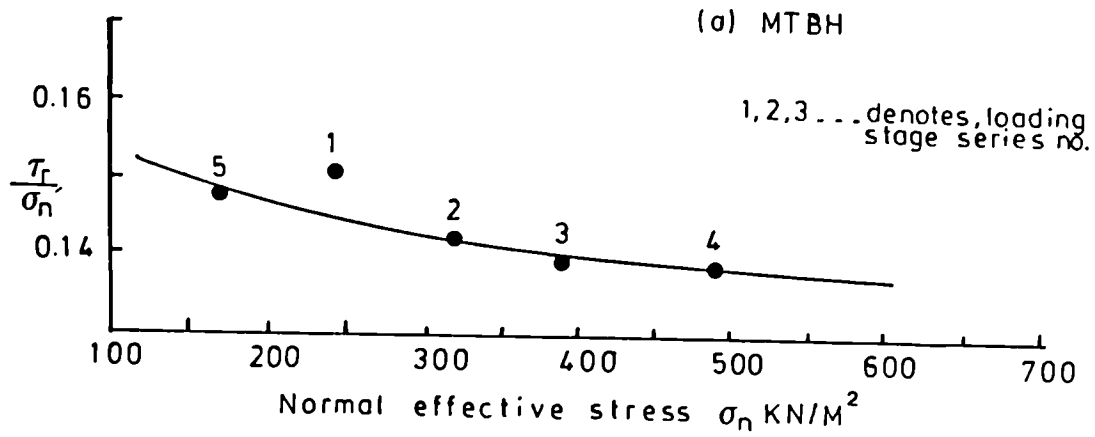


Fig. 5.9 Variation of residual shear stress ratio with normal effective stress for ring shear tests on remoulded tumbled samples.

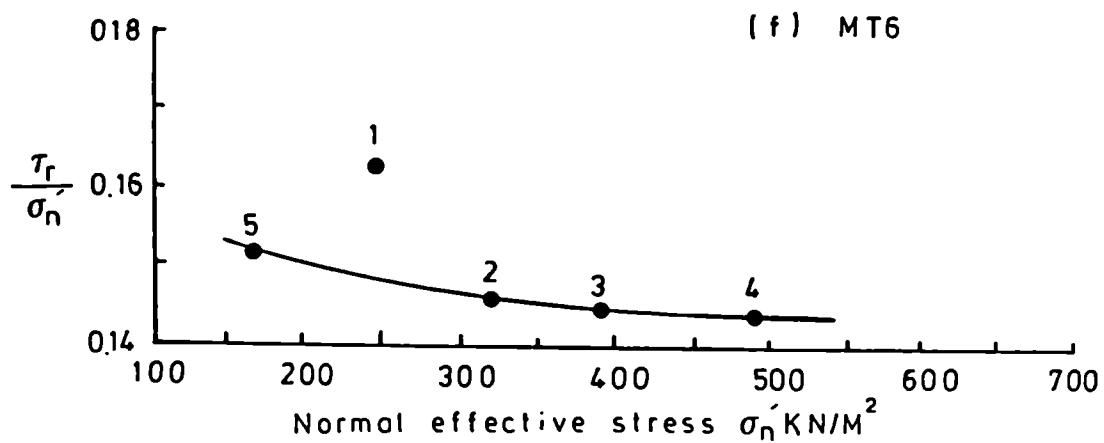
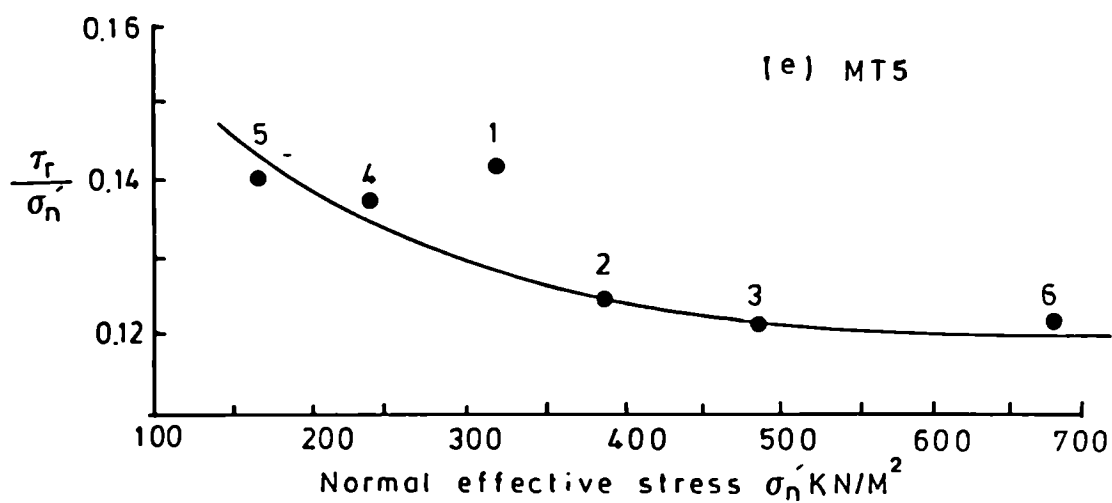
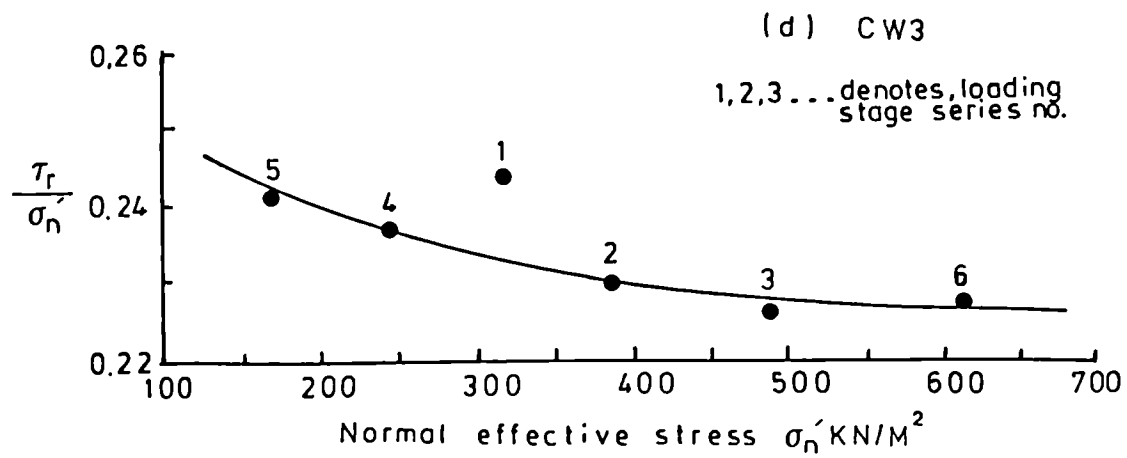


Fig. 5.9 Variation of residual shear stress ratio with normal effective stress for ring shear tests on remoulded tumbled samples.

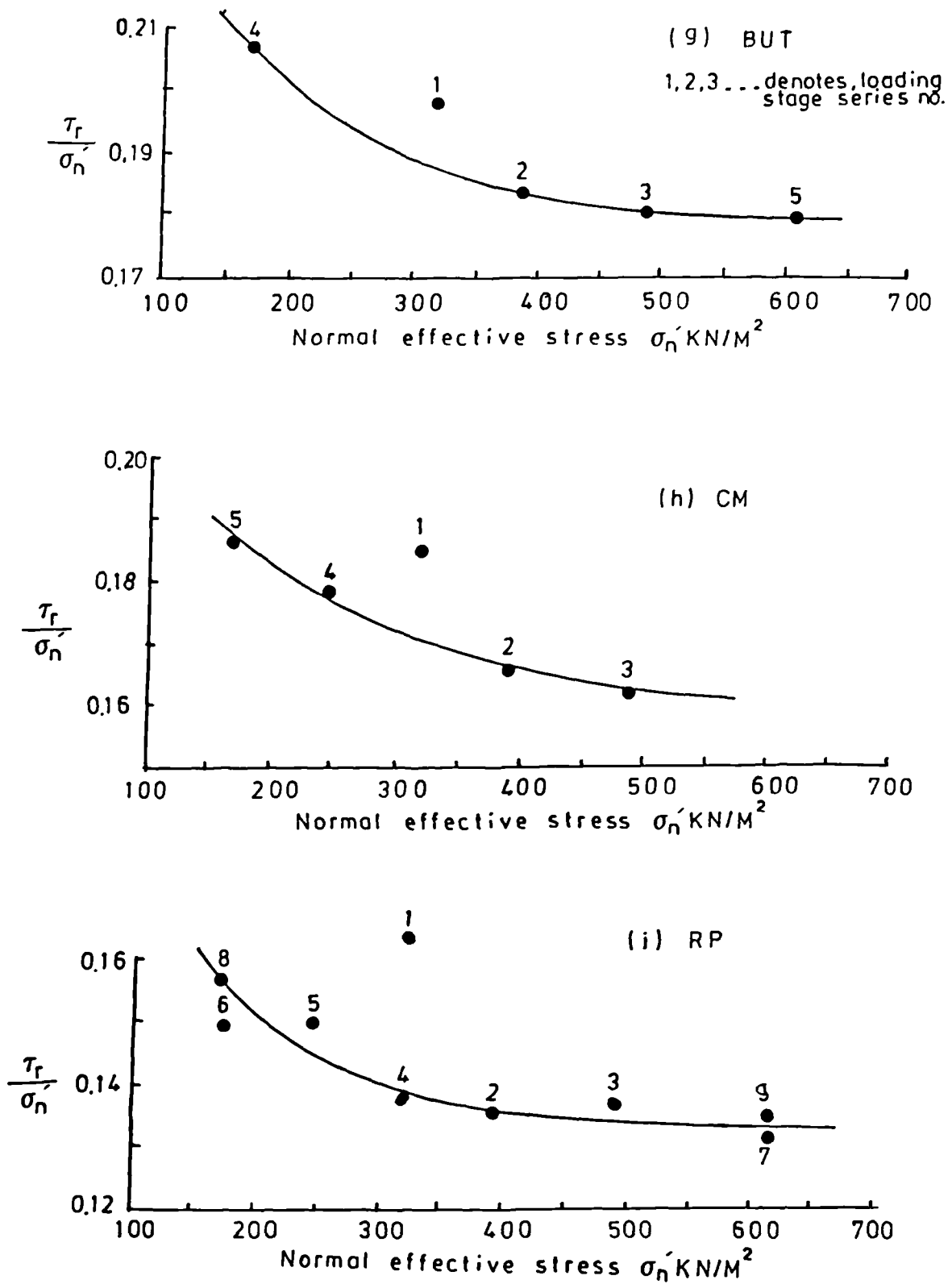


Fig. 5.9 Variation of residual shear stress ratio with normal effective stress for ring shear tests on remoulded tumbled samples.

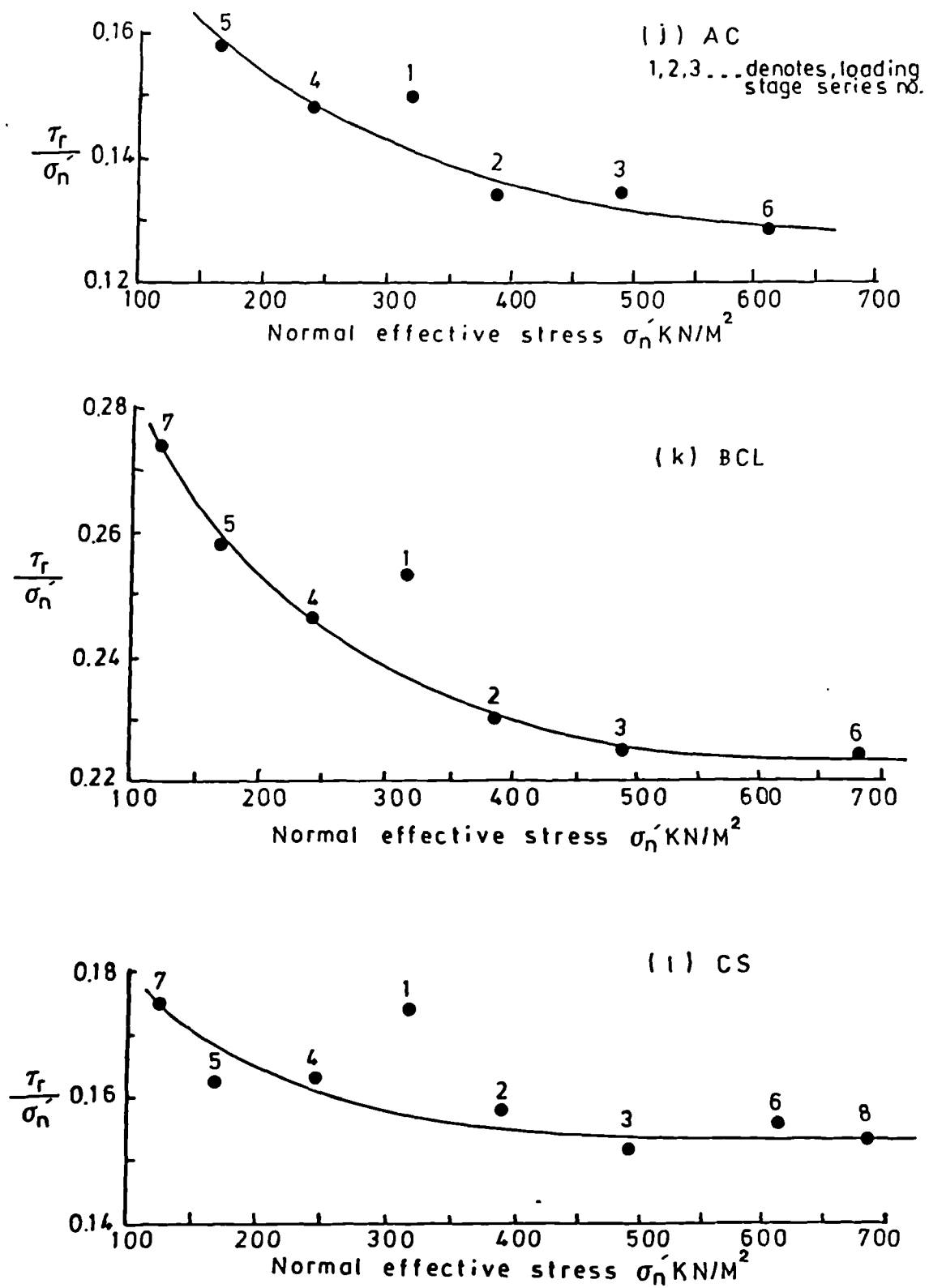


Fig. 5.9 Variation of residual shear stress ratio with normal effective stress for ring shear tests on remoulded tumbled samples.

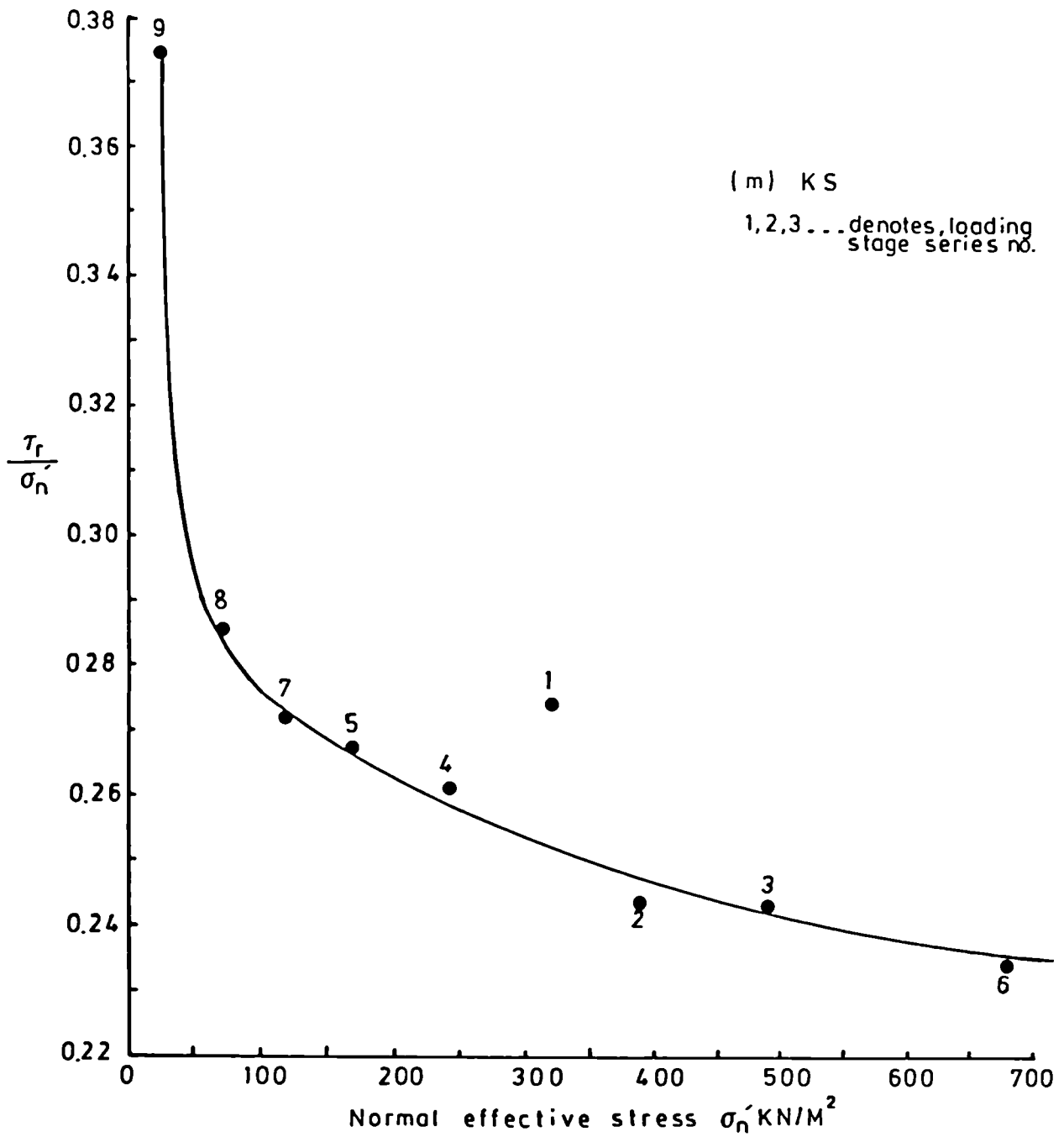


Fig. 5.9 Variation of residual shear stress ratio with normal effective stress for ring shear tests on remoulded tumbled samples.

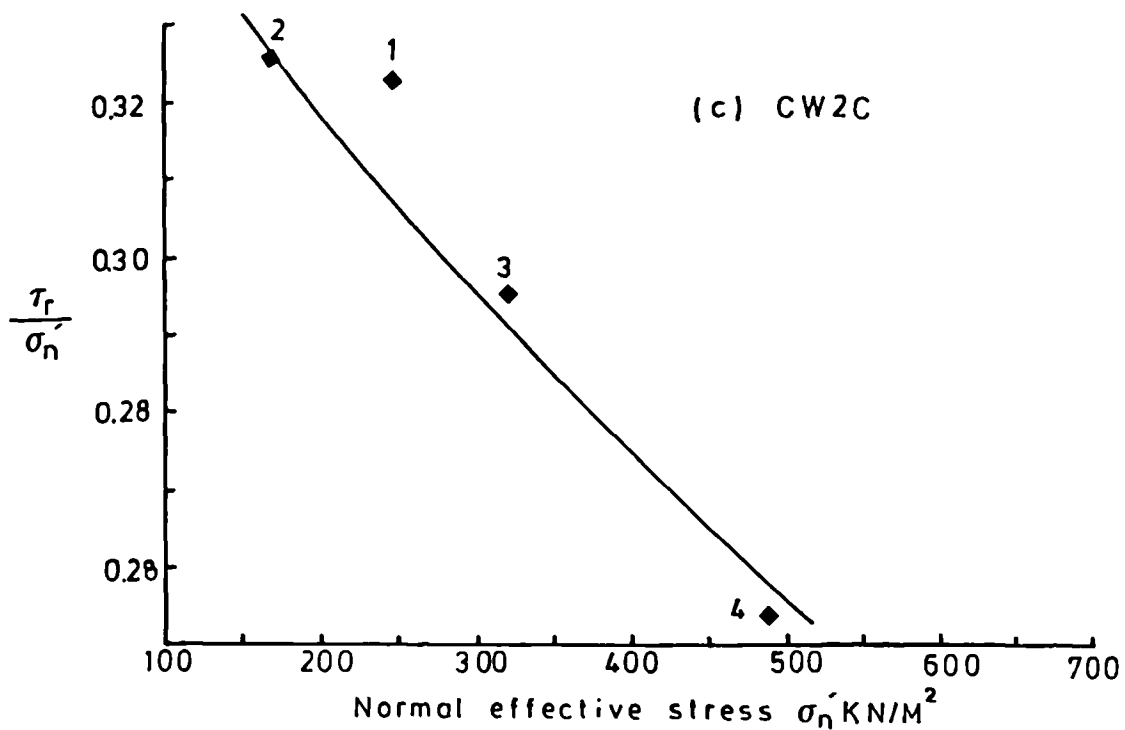
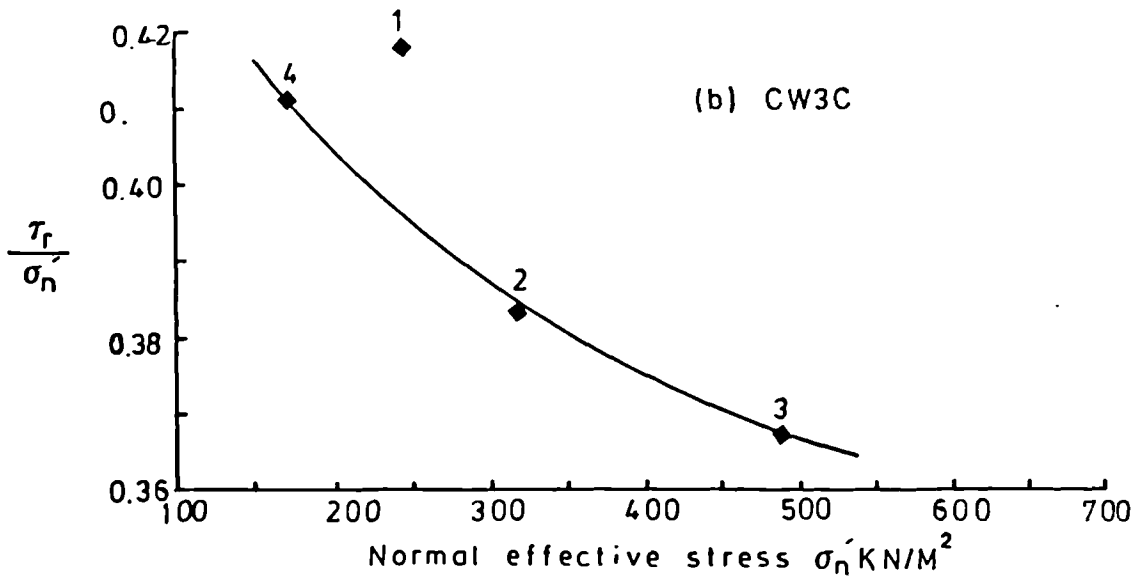
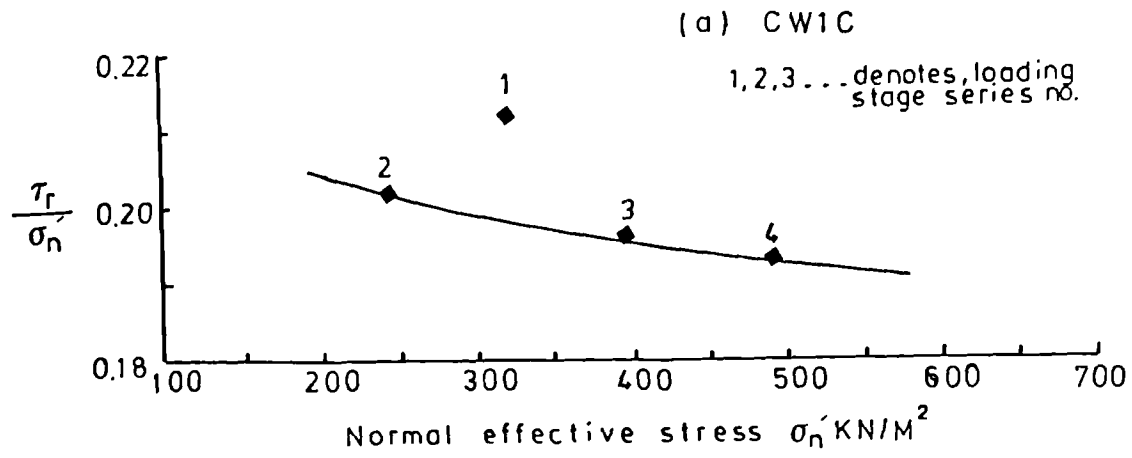


Fig. 5.10 Variation of residual shear stress ratio with normal effective stress for ring shear tests on remoulded crushed and crushed sieved samples.

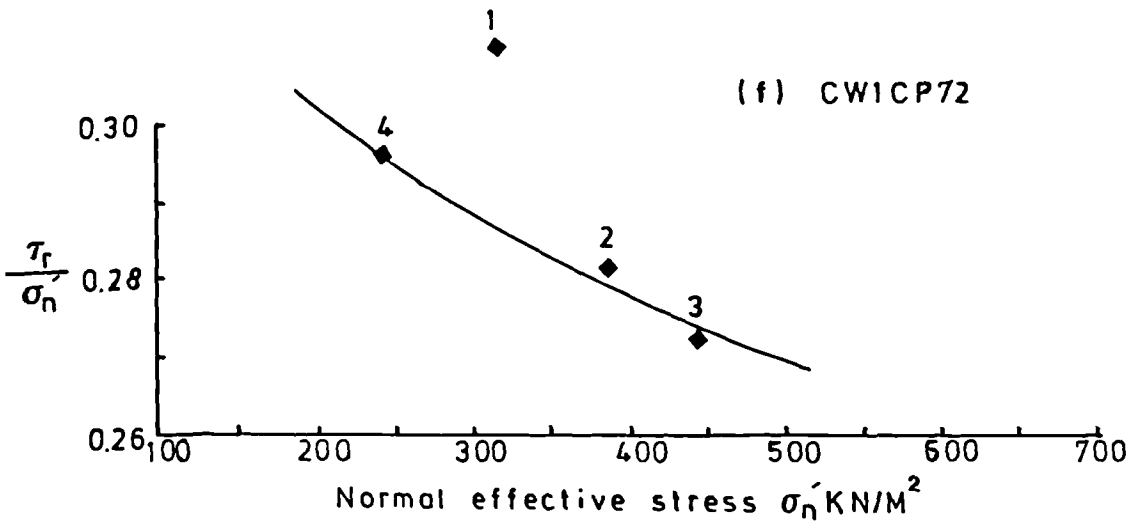
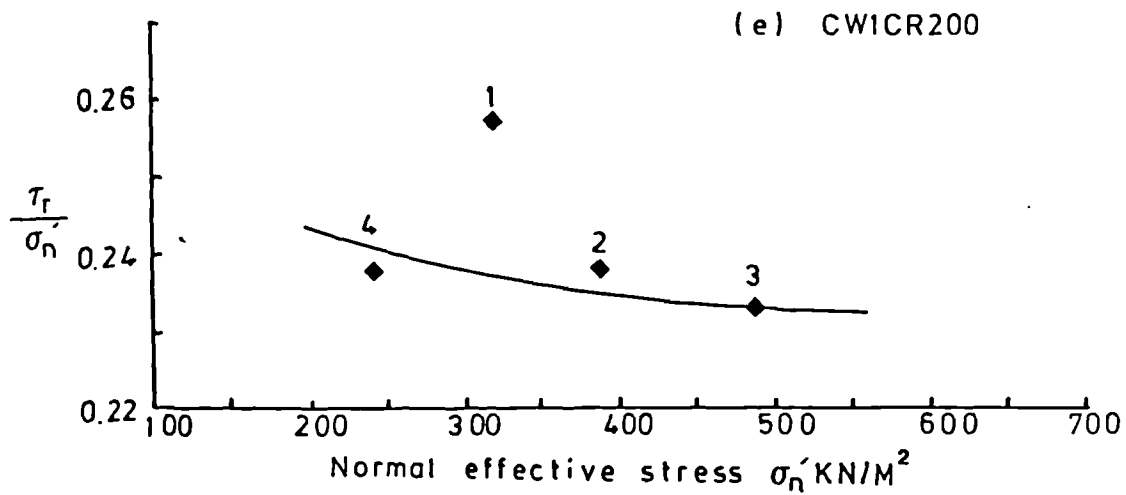
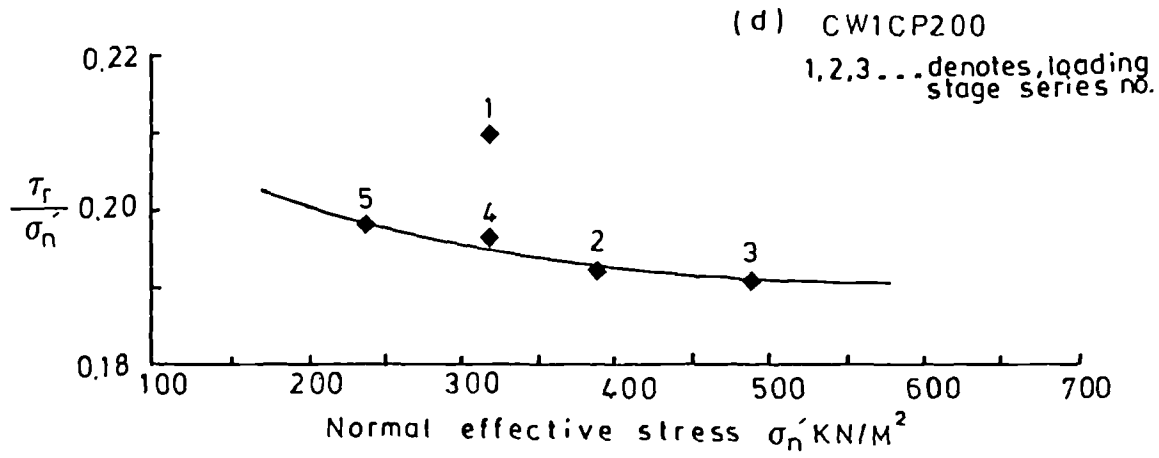


Fig. 5.10 Variation of residual shear stress ratio with normal effective stress for ring shear tests on remoulded crushed and crushed sieved samples.

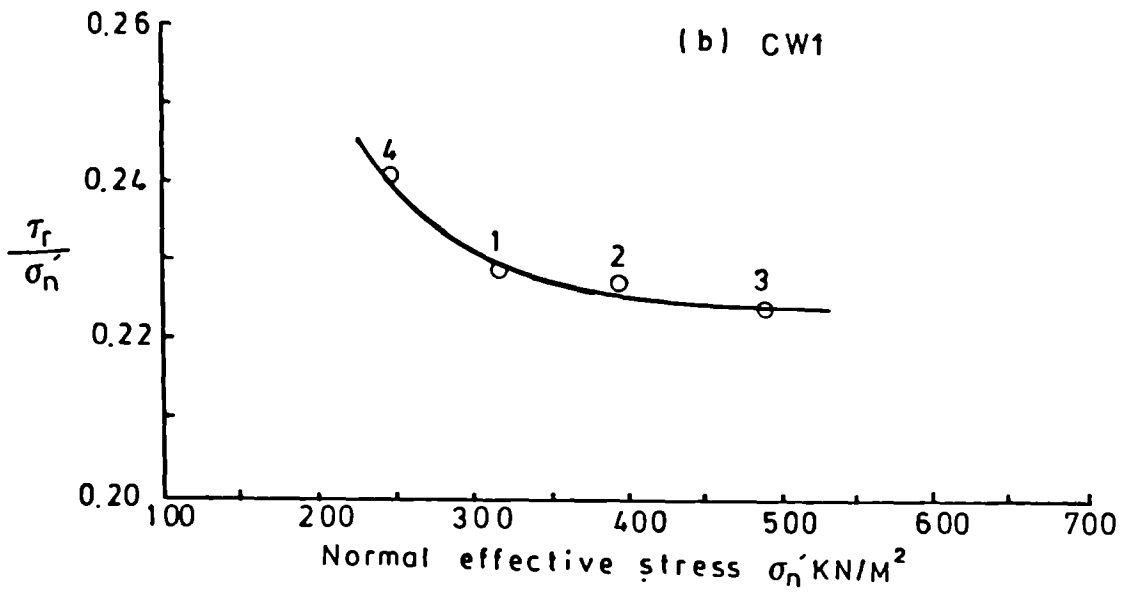
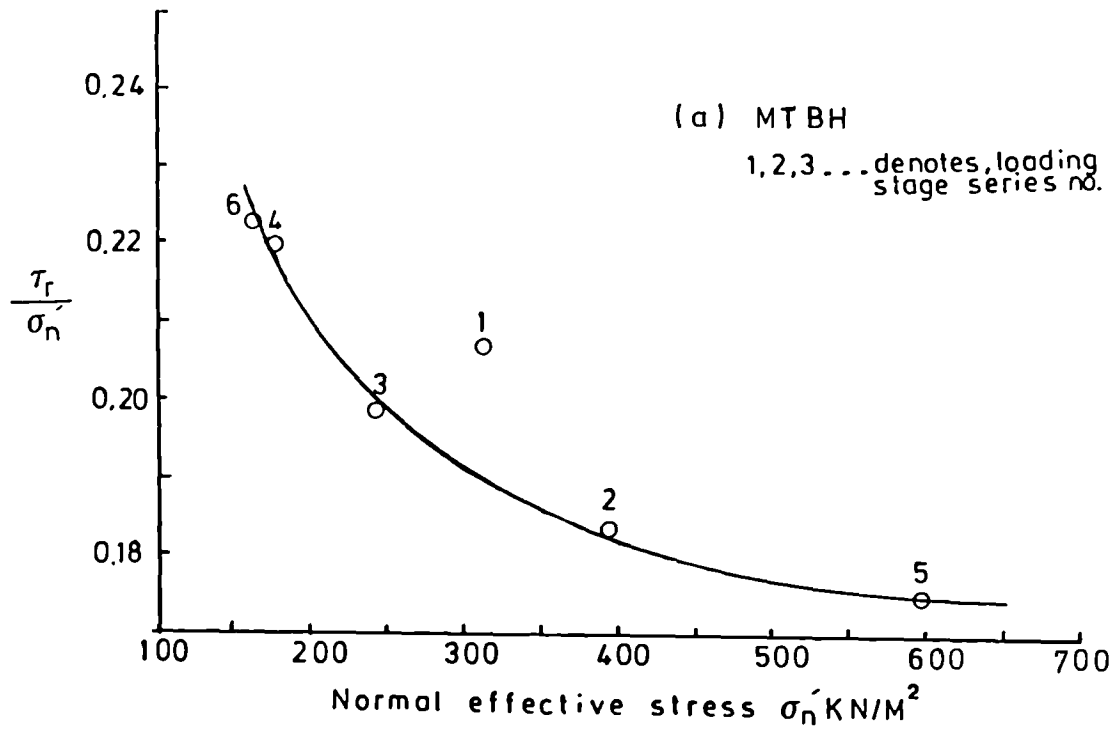


Fig. 5.11 Variation of residual shear stress ratio with normal effective stress for shear box tests on remoulded tumbled and crushed sieved samples.

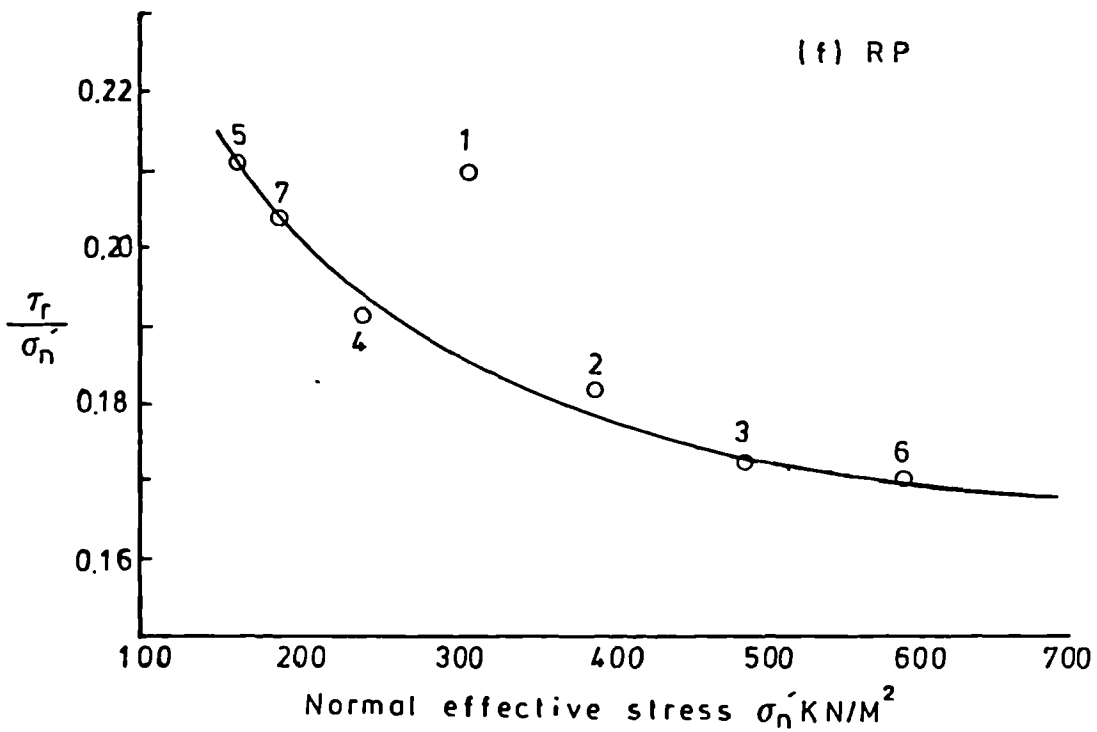
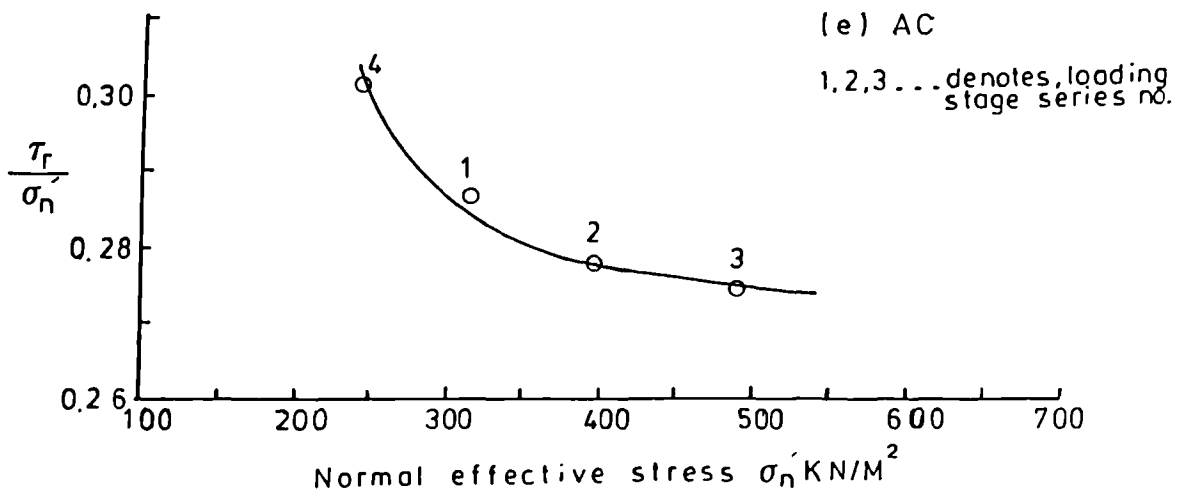


Fig. 5.11 Variation of residual shear stress ratio with normal effective stress for shear box tests on remoulded tumbled and crushed sieved samples.

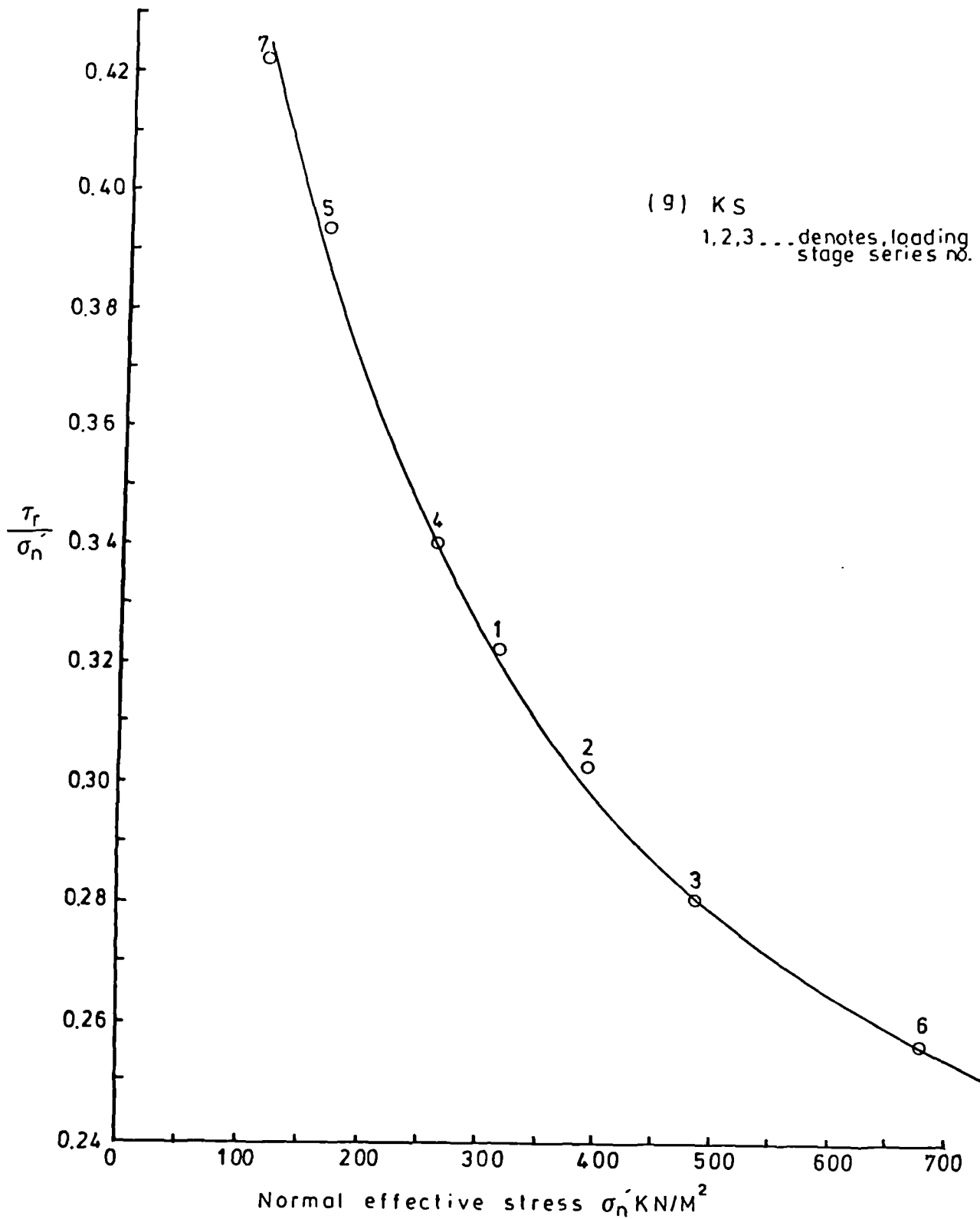


Fig. 5.11 Variation of residual shear stress ratio with normal effective stress for shear box tests on remoulded tumbled and crushed sieved samples.

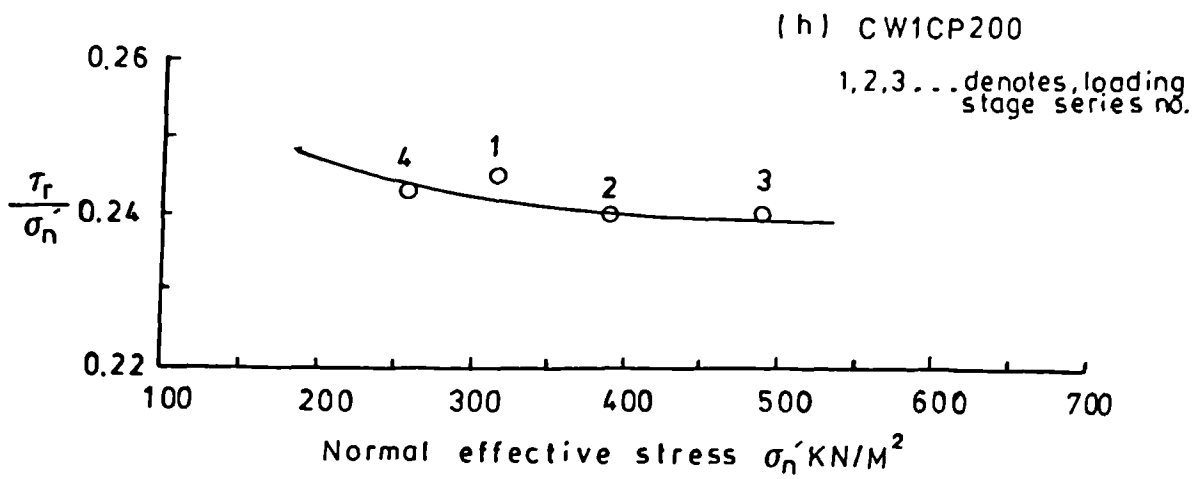


Fig. 5.11 Variation of residual shear stress ratio with normal effective stress for shear box tests on remoulded tumbled and crushed sieved samples.

As mentioned in Section 4.2.4, many authors, including Lagatta (1970), Bishop et al (1971) and Herrmann and Wolfskill (1966), have shown that the amount of shear displacement required to reach the residual state is reduced as σ'_n increases.

From the results of the present tests it is not possible to make definite conclusions regarding the effect of the amount of displacement. Most ring shear samples were tested at an initial σ'_n value of 318.4 kN/m² with few tests at an initial σ'_n equal to 245 kN/m² but there are no tests in which the same sample was tested at more than one initial σ'_n value. Therefore it is not possible to compare the initial displacements with each other since any differences in the amounts to produce the residual condition could be due to differences between the samples. In the case of the shear box all the tests were carried out at an initial σ'_n of 313.3 kN/m² except one test at 245.2 kN/m².

iv. Rate of displacement

Investigations of the effect of changing the rate of displacement were carried out on two samples, tumbled sample (MT6) and crushed sample (CW2C). The results are given in Fig. 5.12A and B and the residual shear strength parameters (obtained from individual graphs plotted for each test) are presented in Tables 5.9 and 5.10.

The test on sample MT6 with rates between 0.8 and 0.024 degree/minute was carried out after a normal series of tests (rate 0.120 degree/minute) at a different normal effective stress values. Table 5.9 shows that increasing the rate from 0.12 to 0.8 deg/minute causes an increase in ϕ'_{rr} of about 1.3°. Since subsequent decreases in rate down to values as small as 0.024 deg/minute caused reduction of ϕ'_{rr} to a minimum of 9.6° it seems probable that increasing the rate over this range causes only a slight increase in ϕ'_{rr} value. These values are all greater than $\phi'_{rr} = 8.6^\circ$ established for a rate

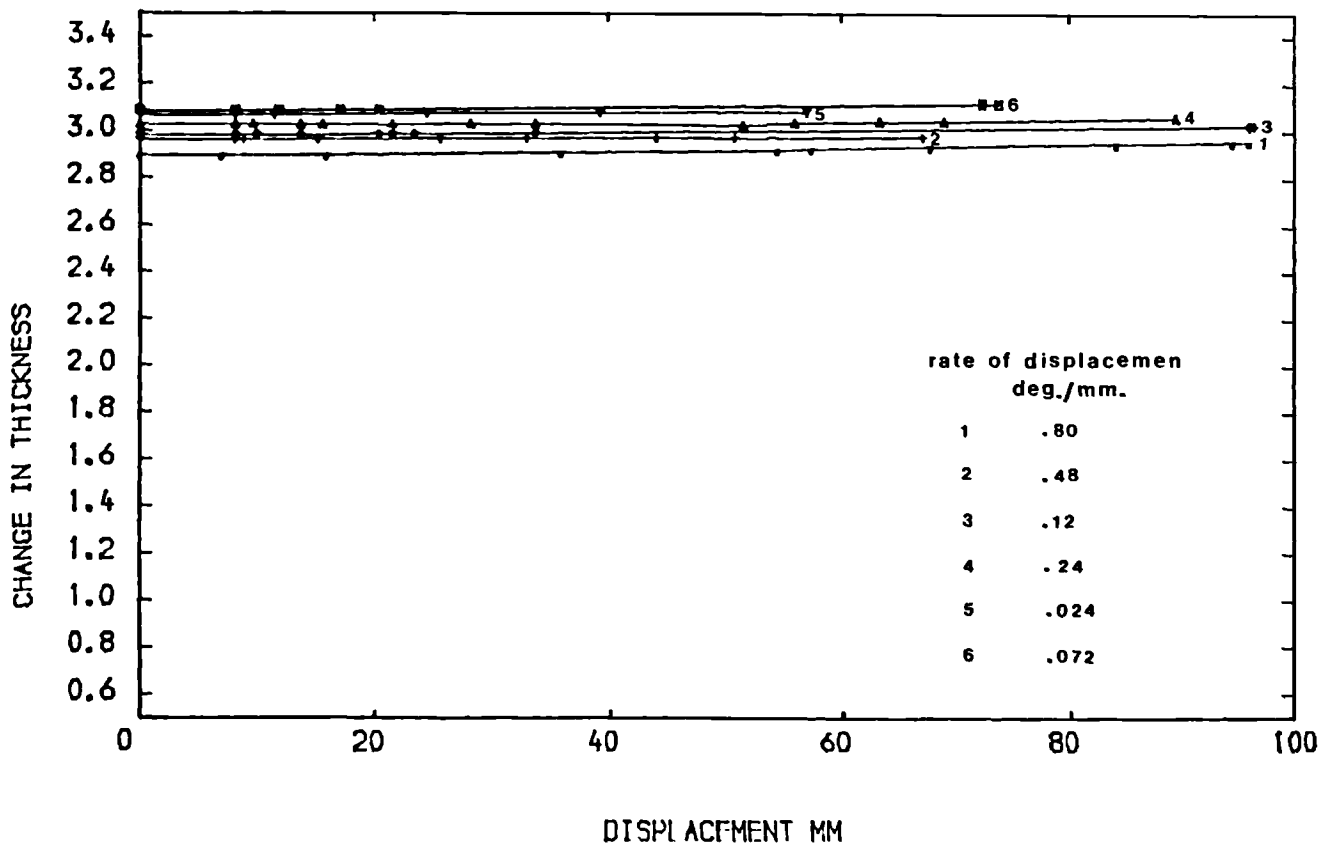
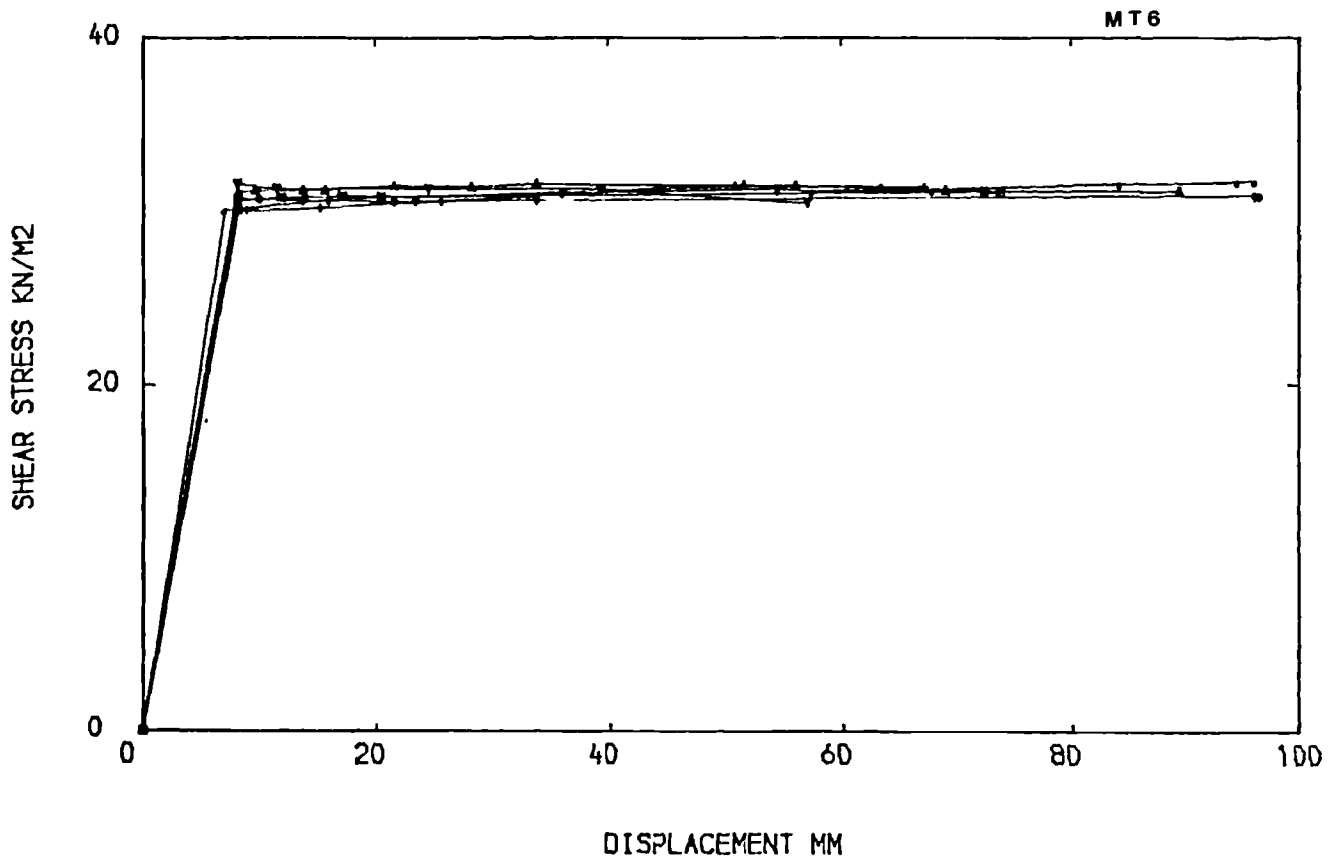


Fig. 5.12 A Effect of rate of strain on residual shear stress and vertical thickness of remoulded tumbled sample.

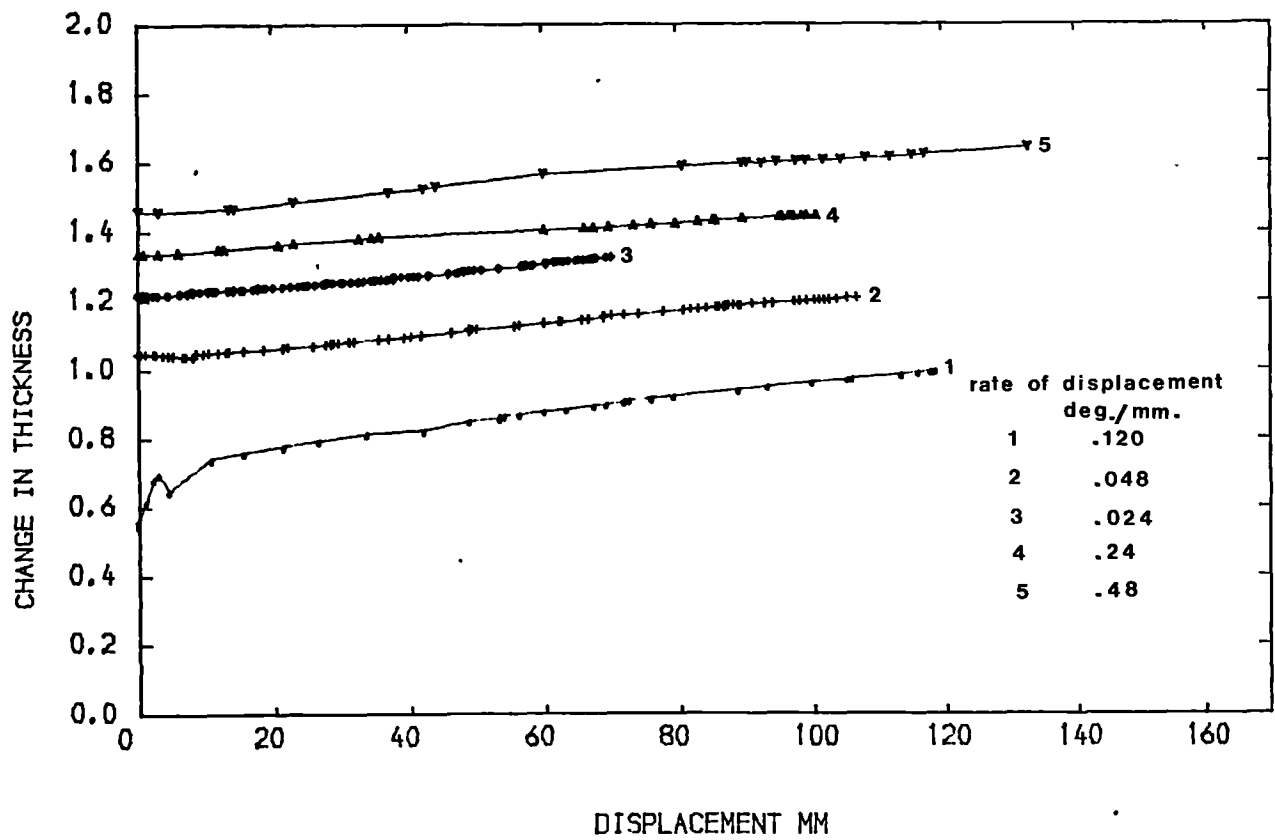
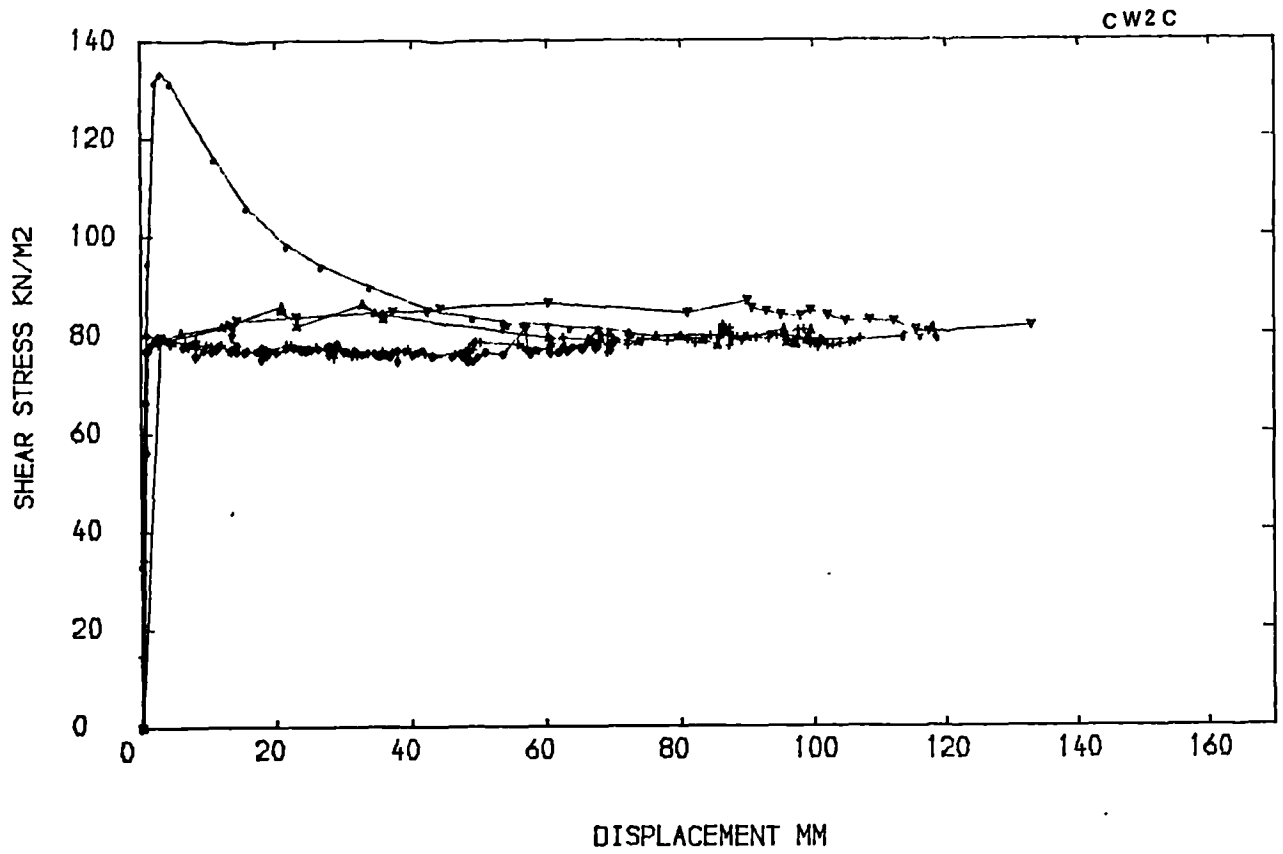


Fig. 5.12 B Effect of rate of strain on residual shear stress and vertical thickness of remoulded crushed sample.

Table 5.9 The effect of rate of displacement on residual shear strength for ring shear tests on remoulded tumbled sample.

rate deg/min	σ_n' kN/m ²	τ_r kN/m ²	ϕ_{rr}' degree
0.120	171.4	26.2	8.6
0.80	171.4	30.06	9.9
0.48	171.4	29.47	9.7
0.120	171.4	29.30	9.7
0.24	171.4	29.68	9.8
0.024	171.4	29.26	9.6
0.072	171.4	29.43	9.7

MT6 Sample

Table 5.10 The effect of rate of displacement on the residual shear strength for ring shear tests on remoulded crushed sample.

rate deg/min	σ_n' kN/m ²	τ_r kN/m ²	ϕ_{rr}' degree
0.120	245	79.33	17.9
0.048	245	77.77	17.6
0.024	245	76.22	17.2
0.24	245	78.55	17.7
0.48	245	79.8	18.0

CW2C Sample

of 0.120 deg/min. in the standard tests but this is probably due to the fact that the original shear surface was disturbed during the very rapid first shear which introduced coarser material onto the shear surface. In Fig. 5.13 the relative change in ϕ_{rr}' is small over rates spanning more than an order of magnitude. The effect of changing the rate of displacement was also determined for crushed sample CW2C which was consolidated under a normal effective pressure of 245 kN/m². As shown in Table 5.10 a slight decrease in ϕ_{rr}' occurred with rate of displacement reduction. The results of this series of tests support the comments made with regards to the effect of changes in the rate of displacement for the tumbled sample. Again, as shown in Fig. 5.14 there is a slight reduction in ϕ_{rr}' amounting to about 0.8° as the rate decreases from 0.48 deg/min. to 0.024 deg/min. However, disturbance to the sample was avoided by shearing at rates slower than the standard one of 0.120 deg/min. before the very rapid ones were used.

5.5.5 Failure envelopes for residual condition

The shear stress - normal effective stress relationship expressed conventionally in terms of ϕ_{rr}' and c_{rr}' are linear to a good approximation and the shear strength parameters have been derived by the least squares method. Fig. 5.15 and 5.16 represent the failure envelopes for the ring shear tests, while Fig. 5.17 displays the corresponding graphs for the shear box tests. The values of ϕ_{rr}' and c_{rr}' are assembled in Table 5.11. Examination of this tables reveals that the residual shear strength values are lowest for the tumbled ring shear samples and increase in the order crushed ring shear, shear box tumbled and, crushed sieved ring shear.

These trends can be demonstrated by considering individual group of results for different tests on the

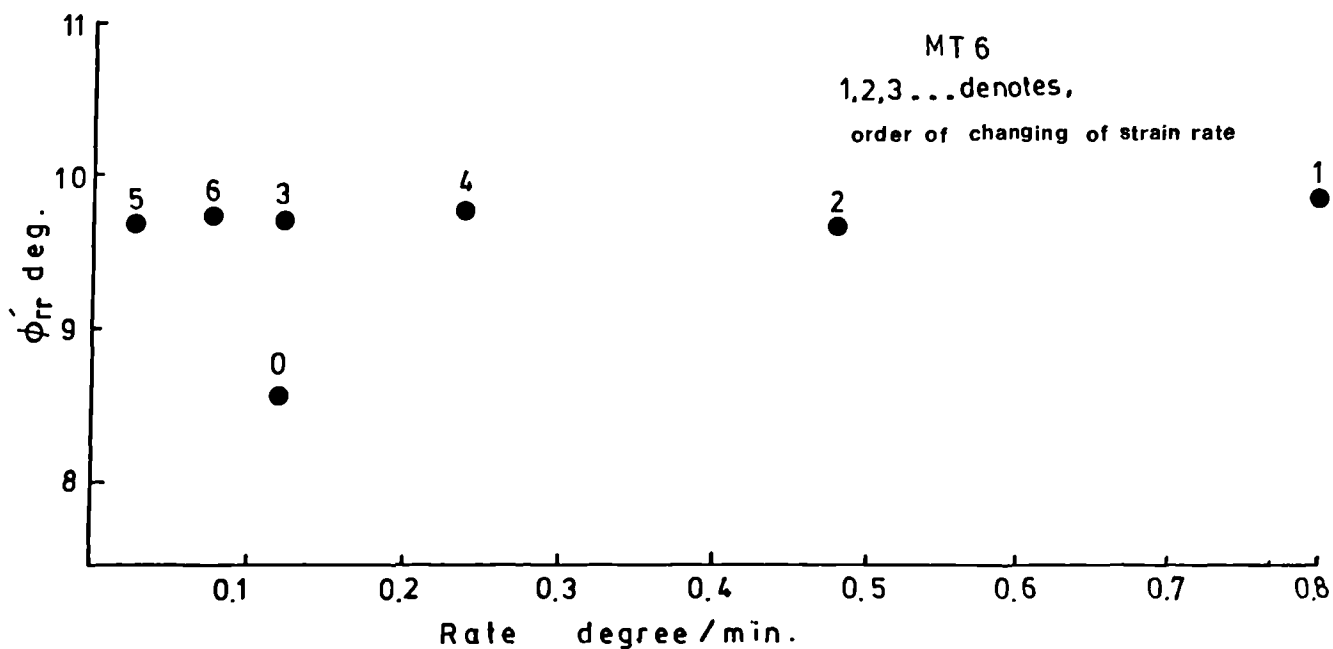


Fig. 5.13 Effect of rate of strain on tumbled sample.

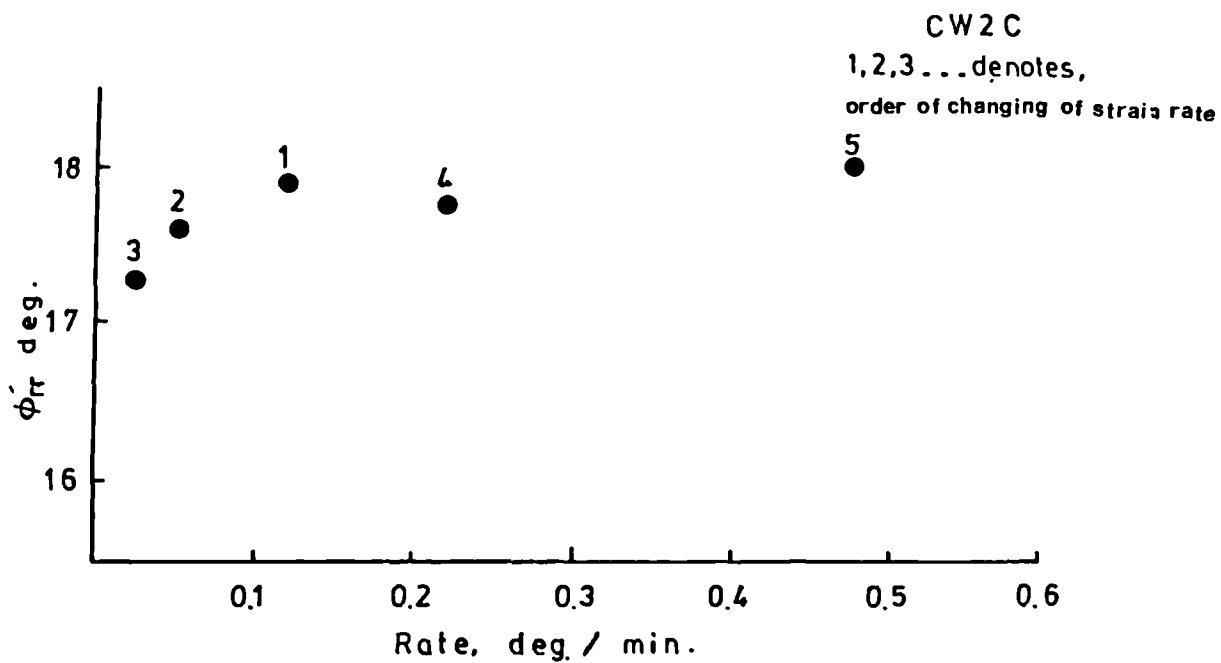


Fig. 5.14 Effect of rate of strain on crushed sample.

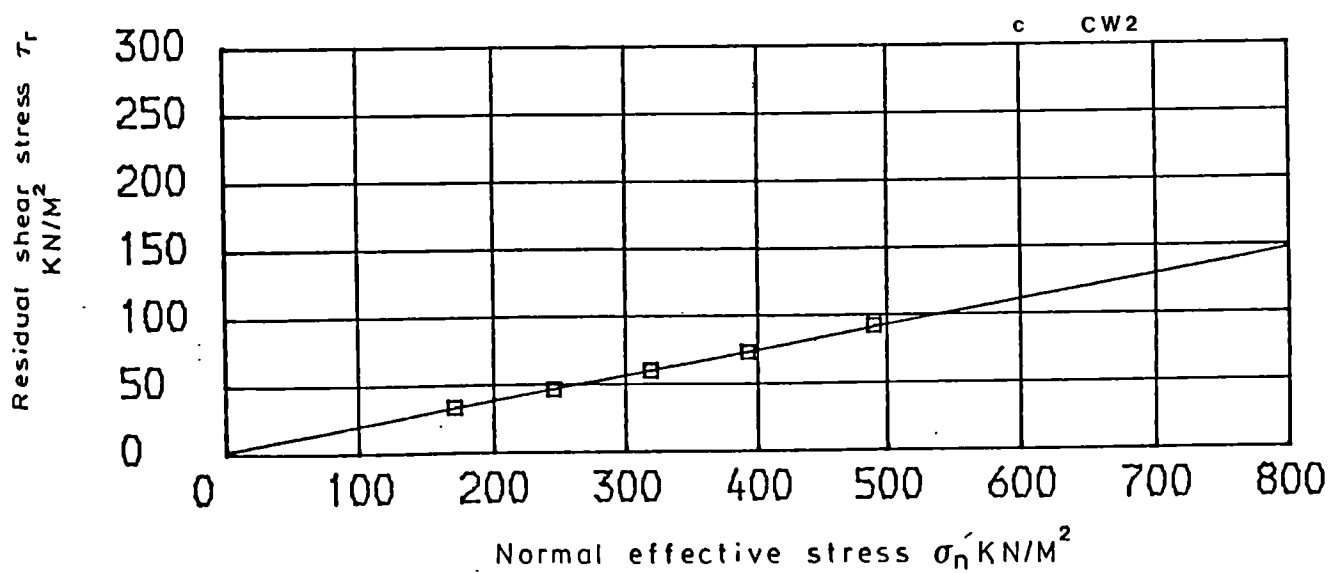
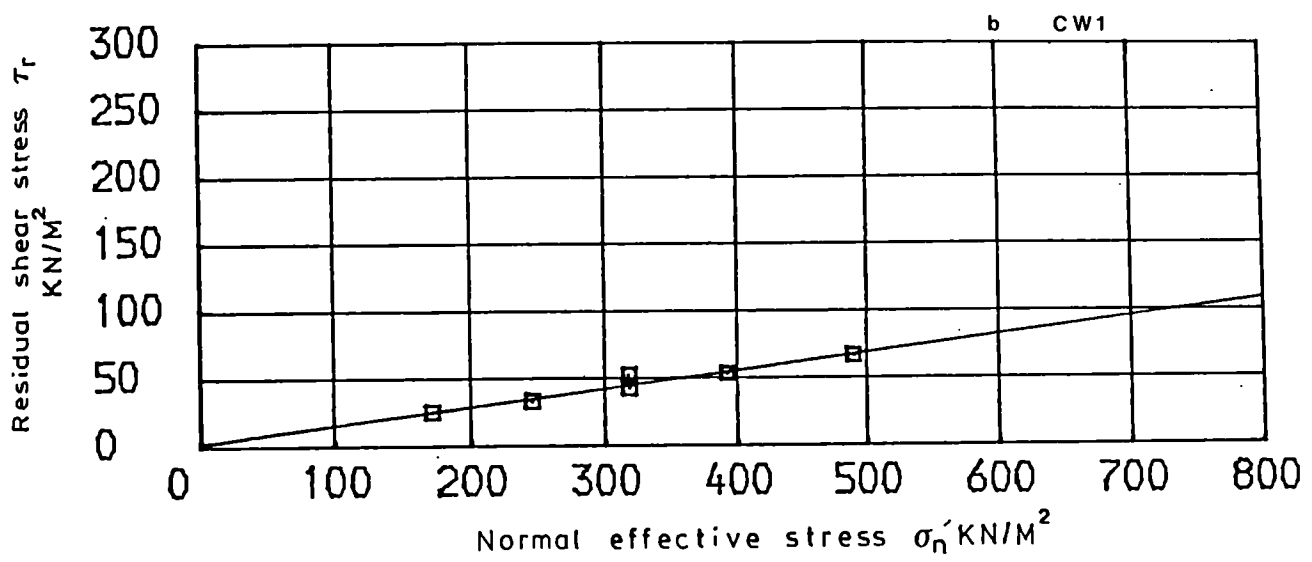
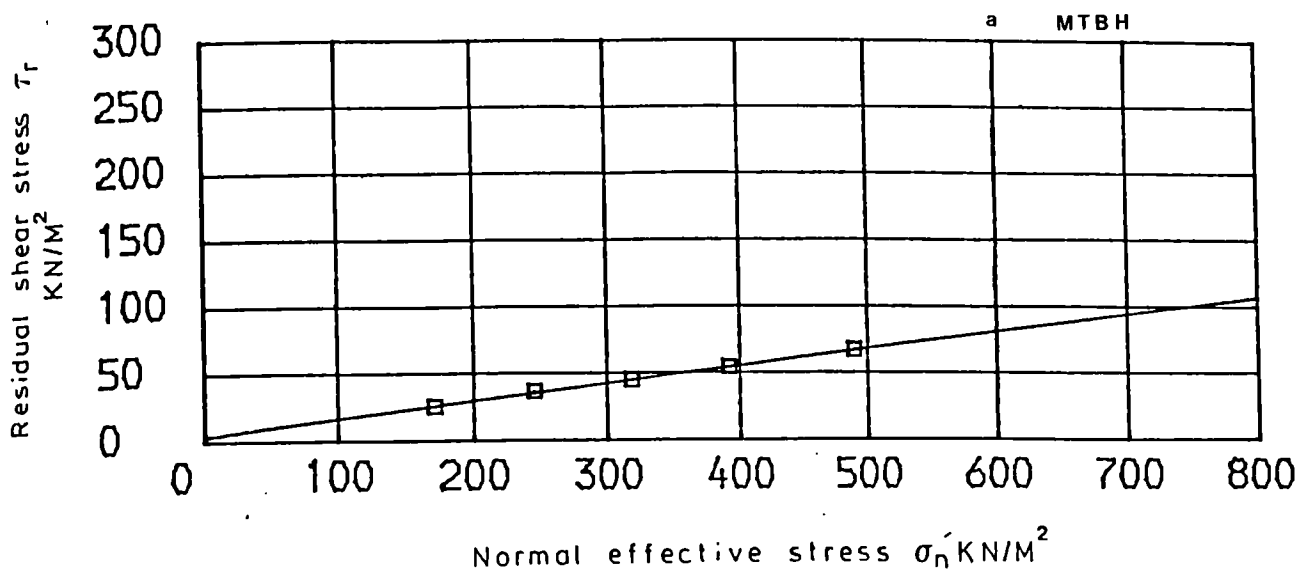


Fig. 5.15 Residual shear stress - normal effective stress relationship for ring shear test on remoulded tumbled samples.

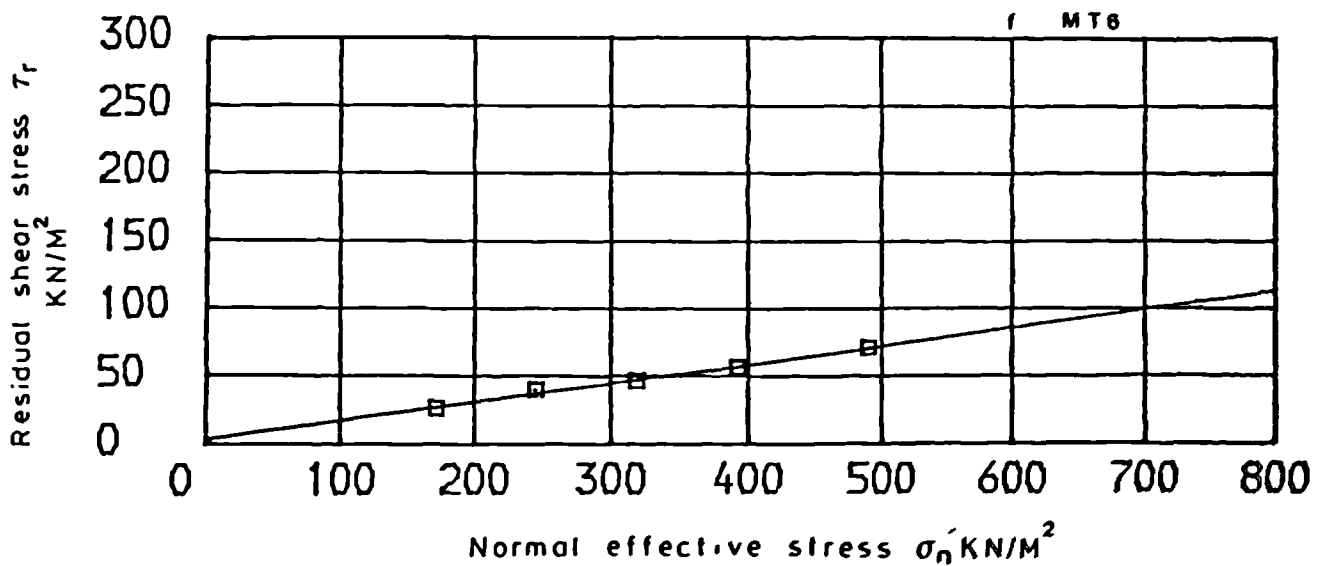
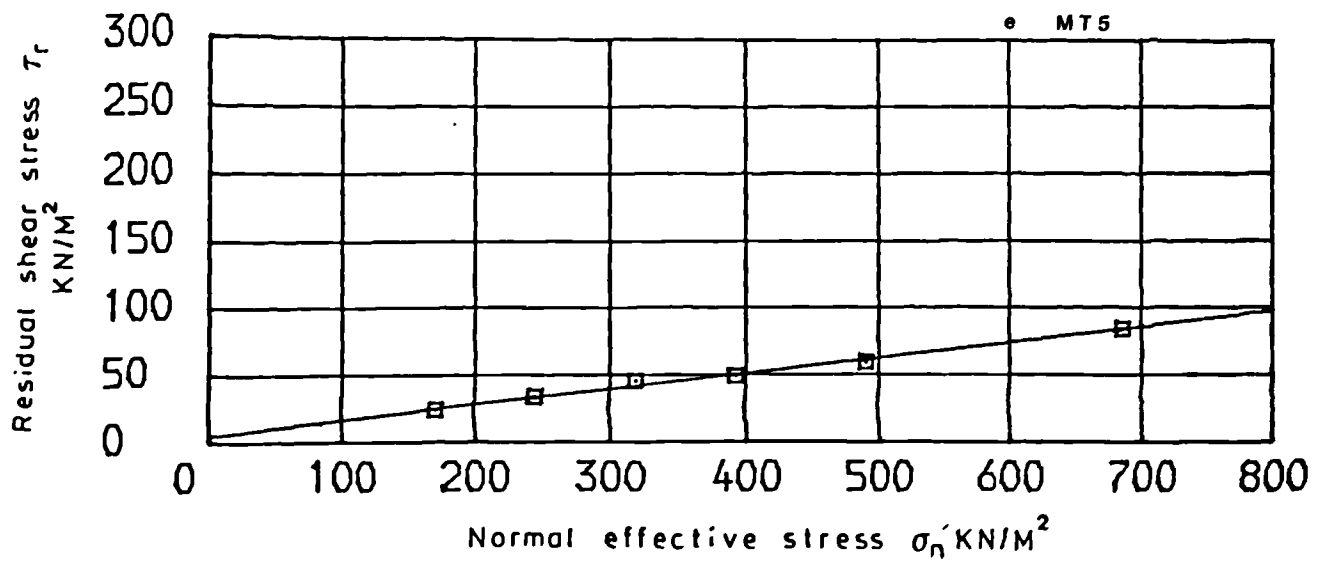
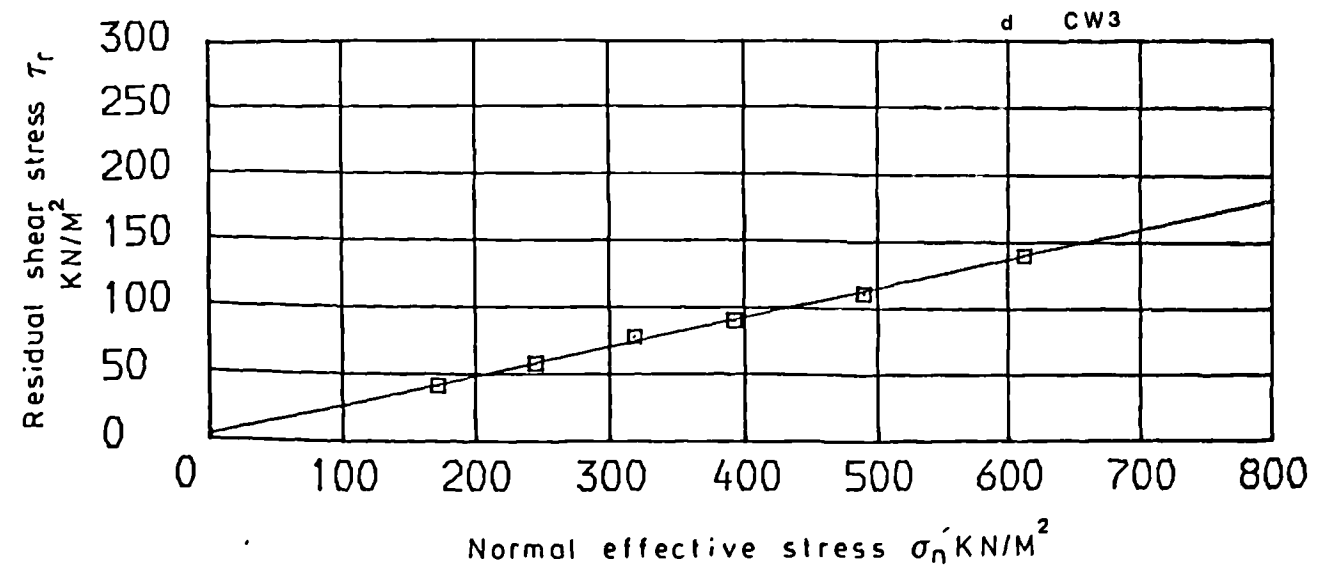


Fig. 5.15 Residual shear stress - normal effective stress relationship for ring shear test on remoulded tumbled samples.

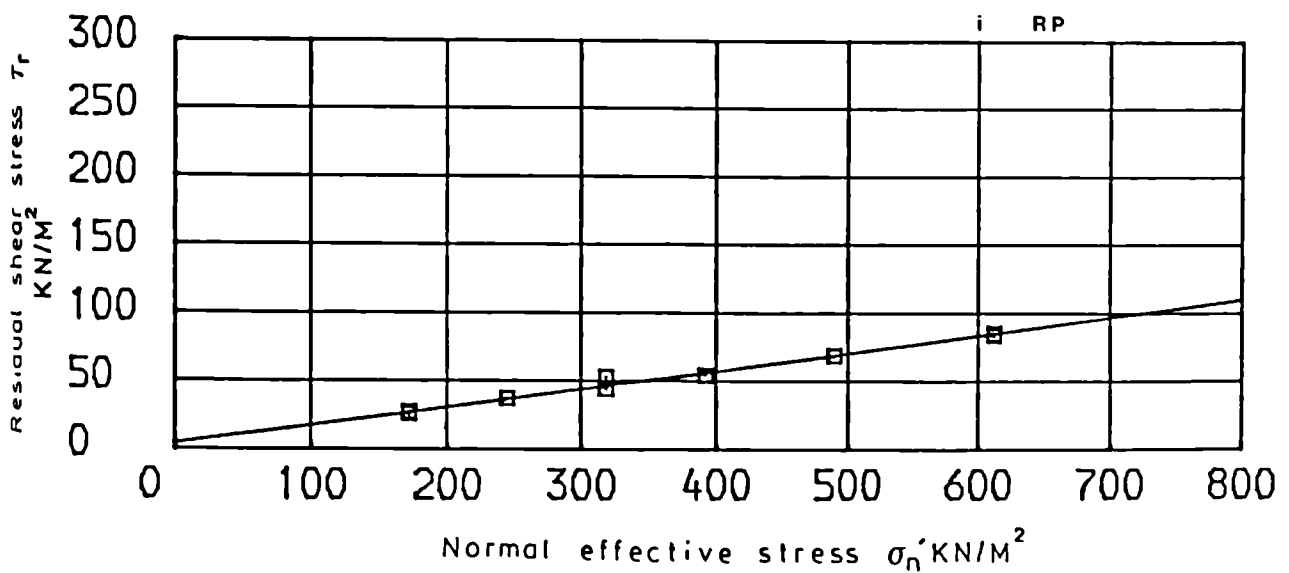
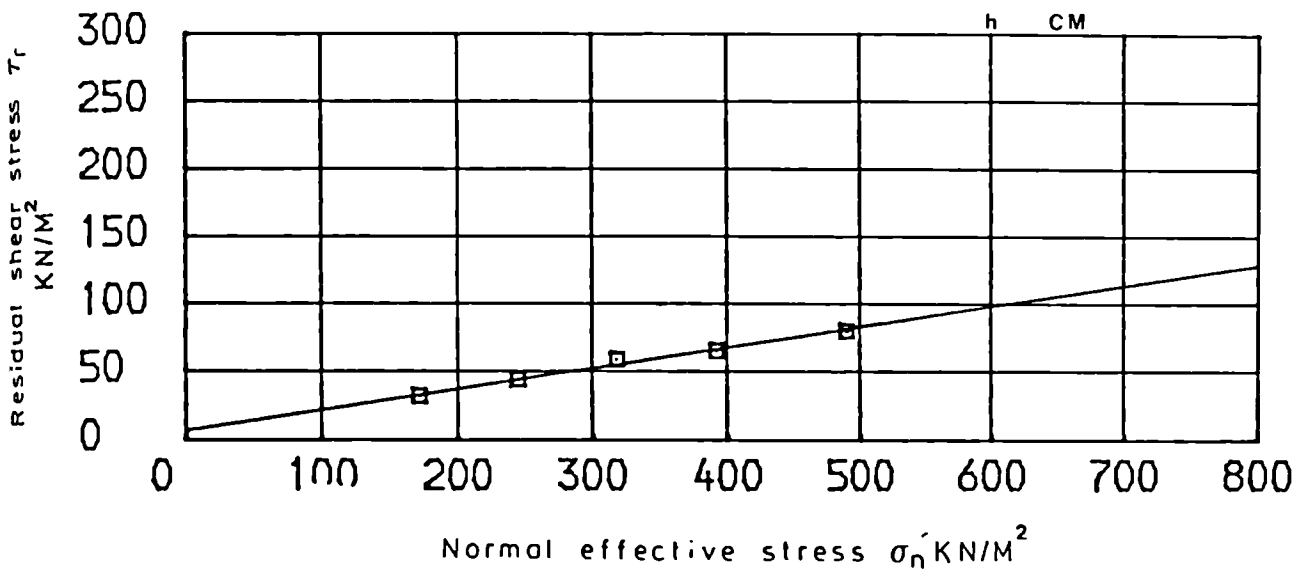
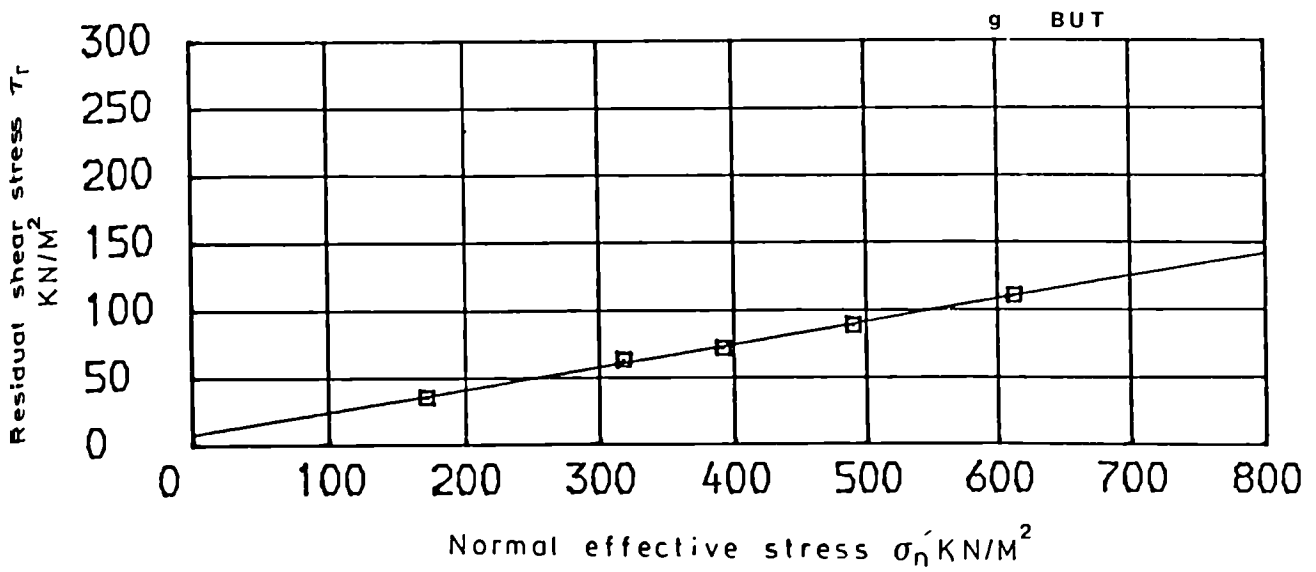


Fig. 5.15 Residual shear stress - normal effective stress relationship for ring shear test on remoulded tumbled samples.

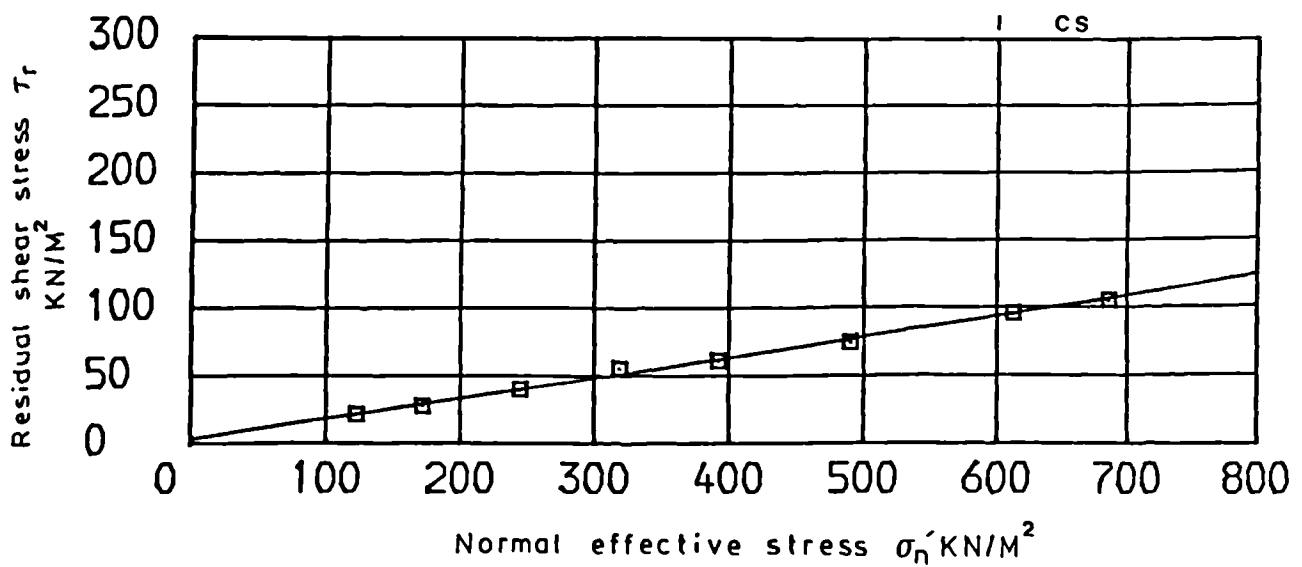
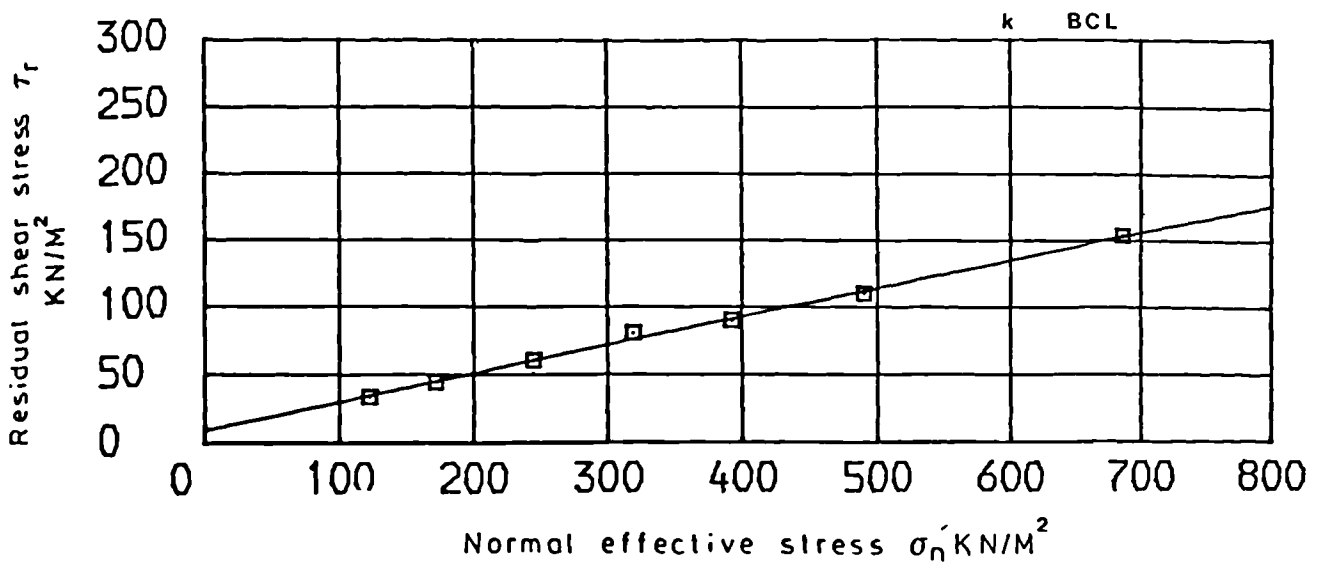
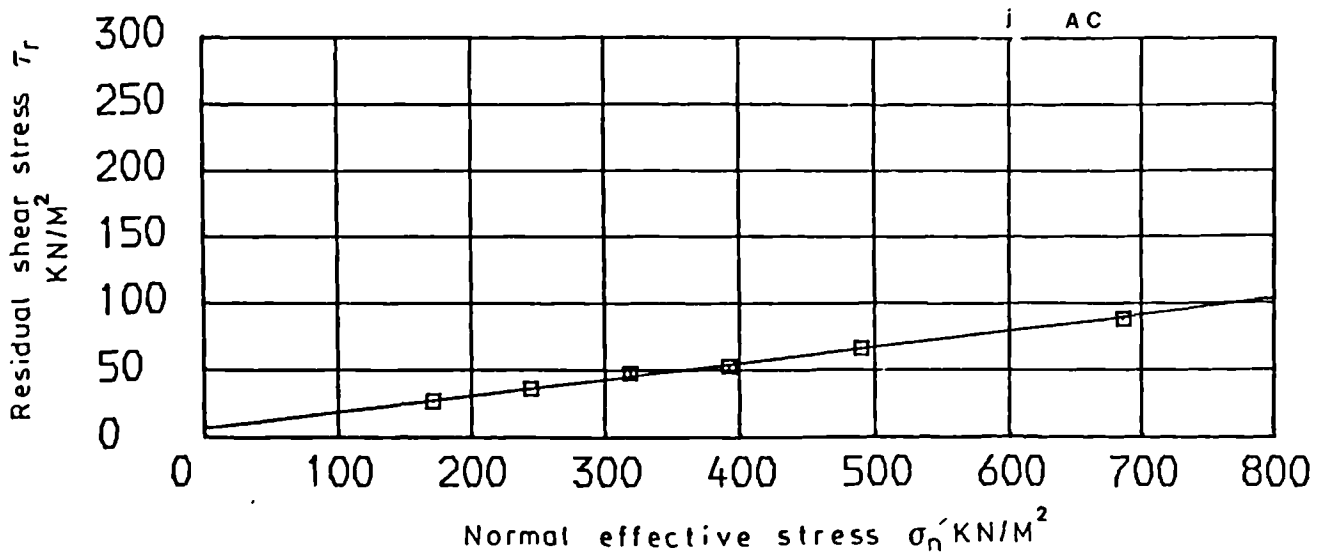


Fig. 5.15 Residual shear stress - normal effective stress relationship for ring shear test on remoulded tumbled samples.

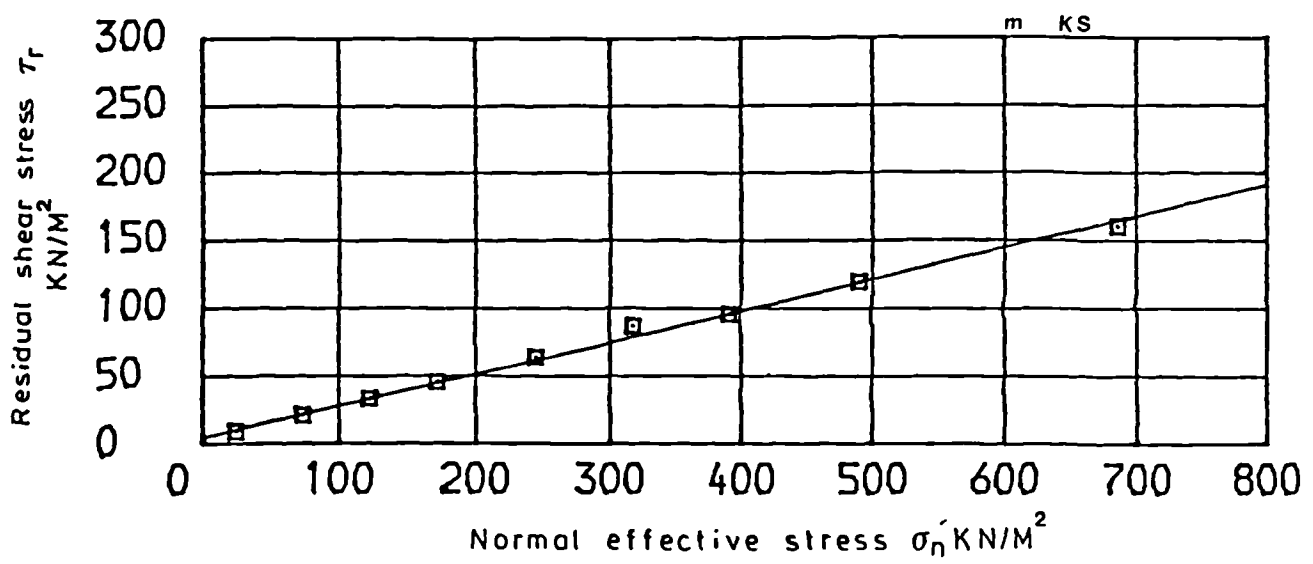


Fig. 5.15 Residual shear stress - normal effective stress relationship for ring shear test on remoulded tumbled samples.

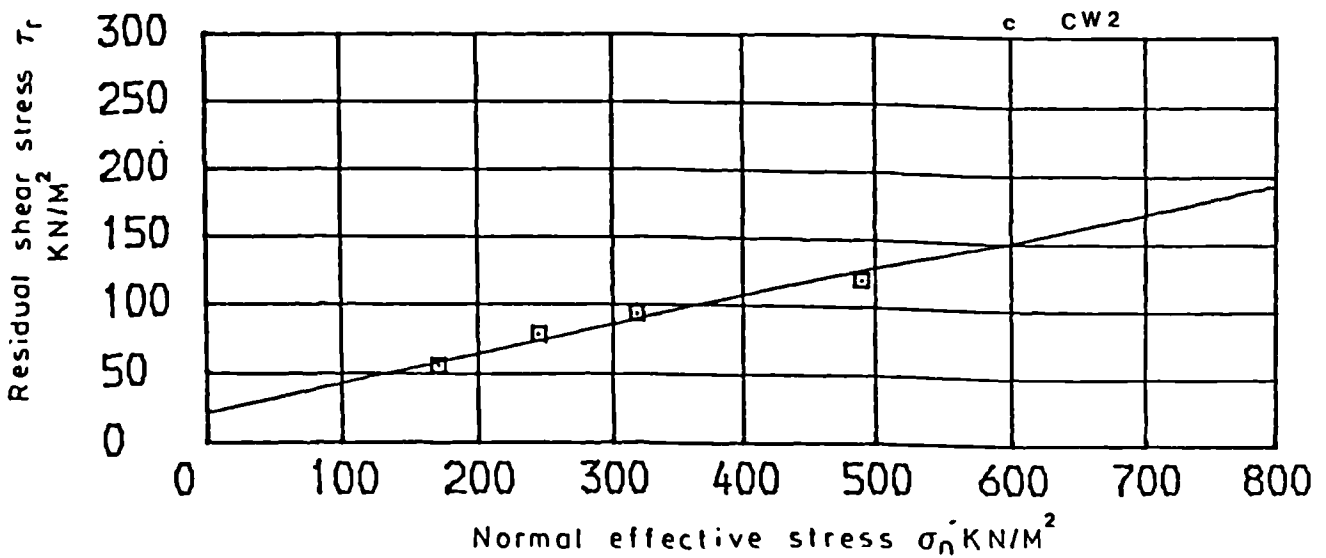
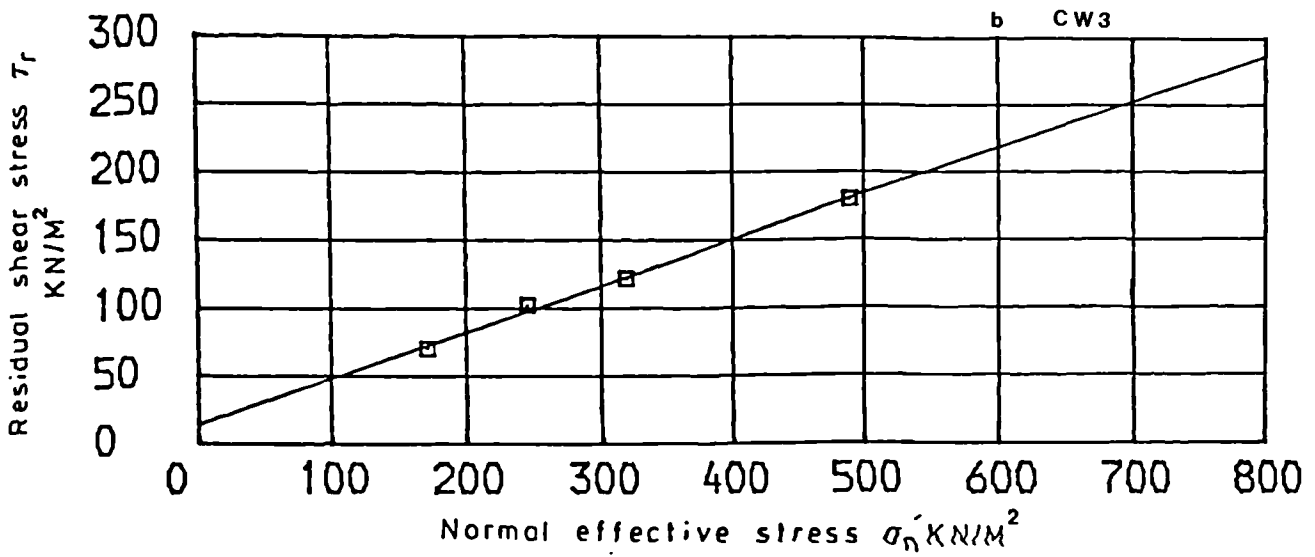
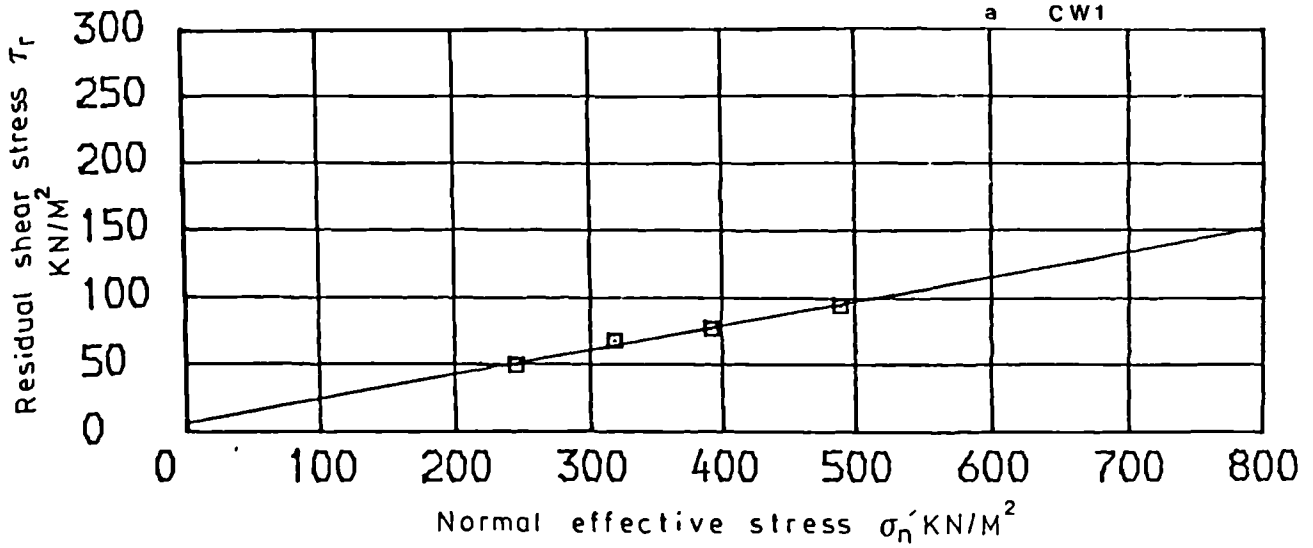


Fig. 5.16 Residual shear stress - normal effective stress relationship for ring shear tests on remoulded crushed samples.

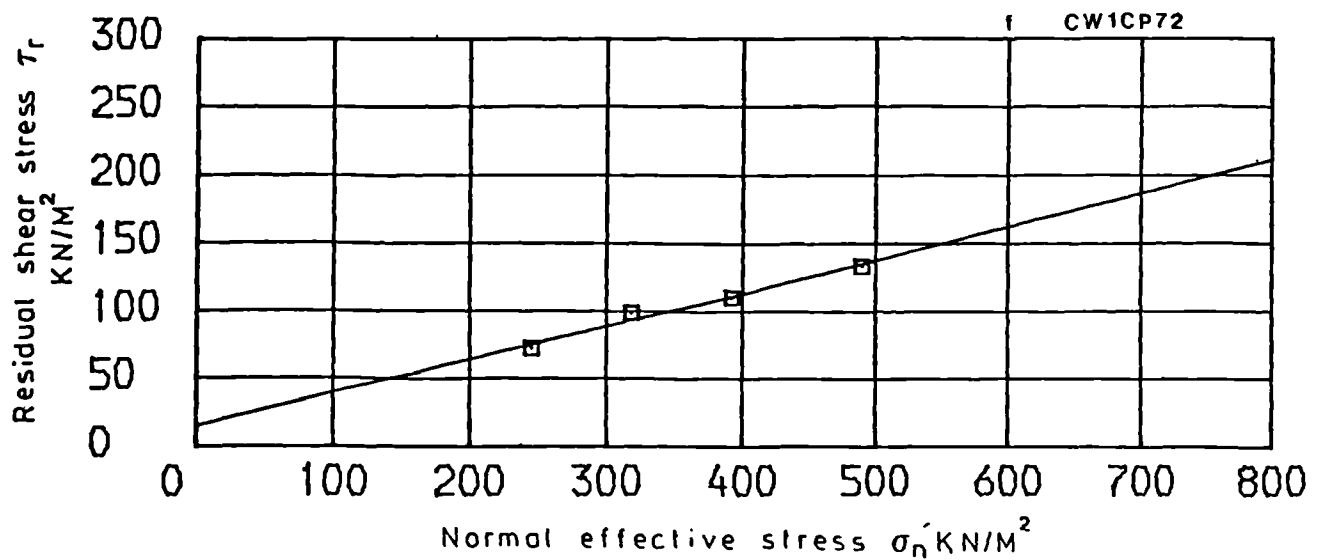
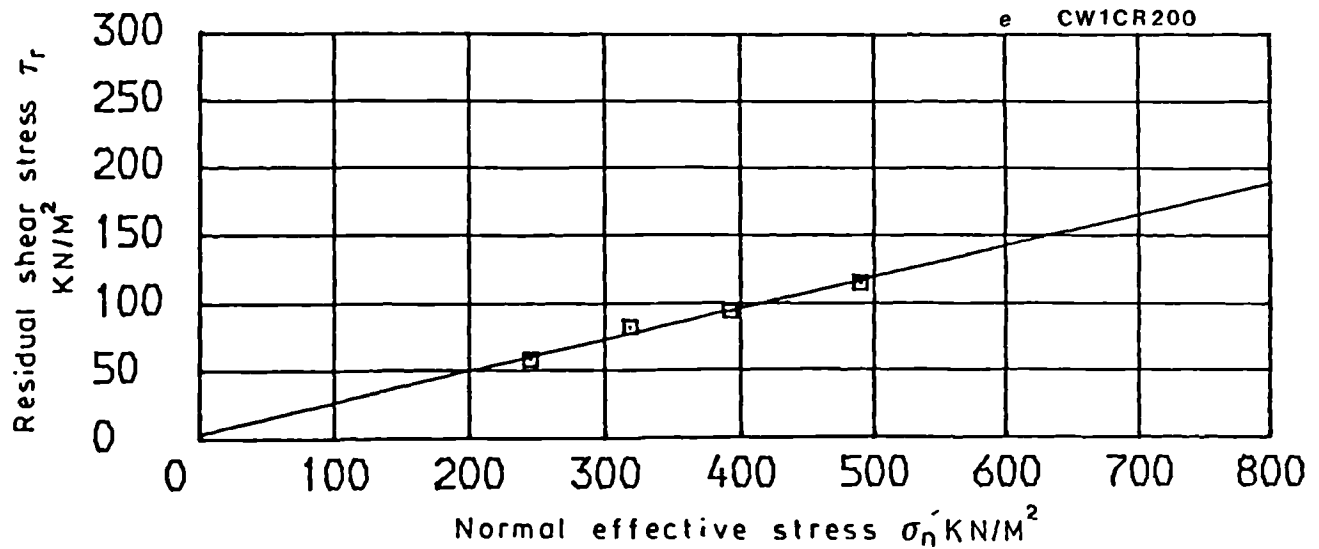
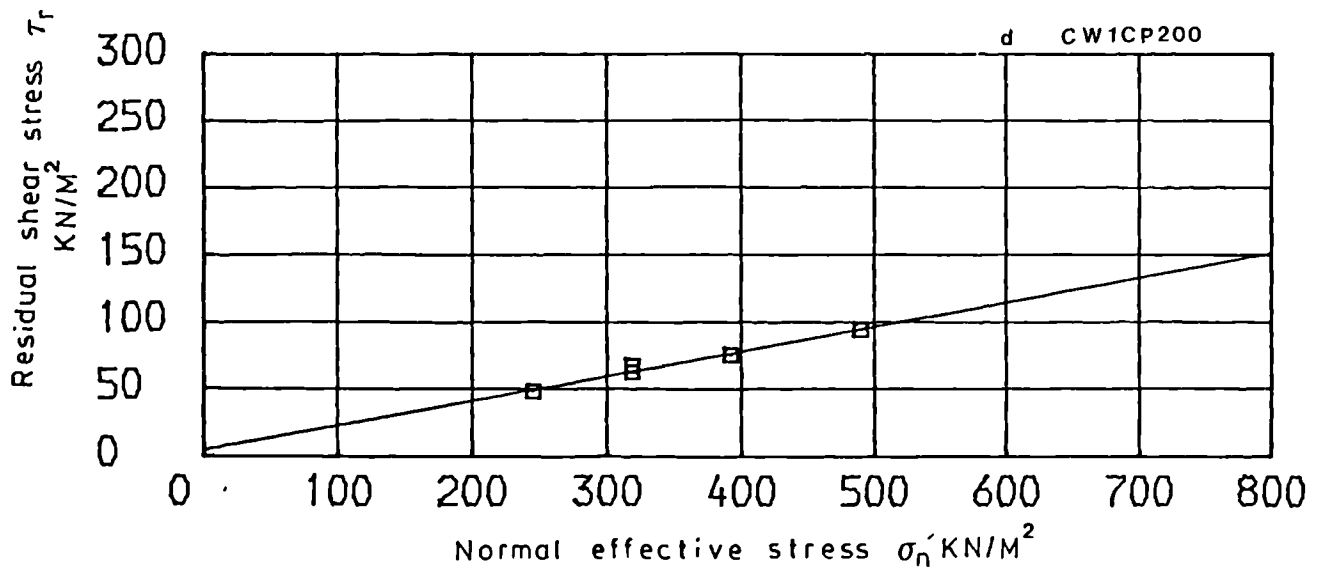


Fig. 5.16 Residual shear stress - normal effective stress relationship for ring shear tests on remoulded crushed samples.

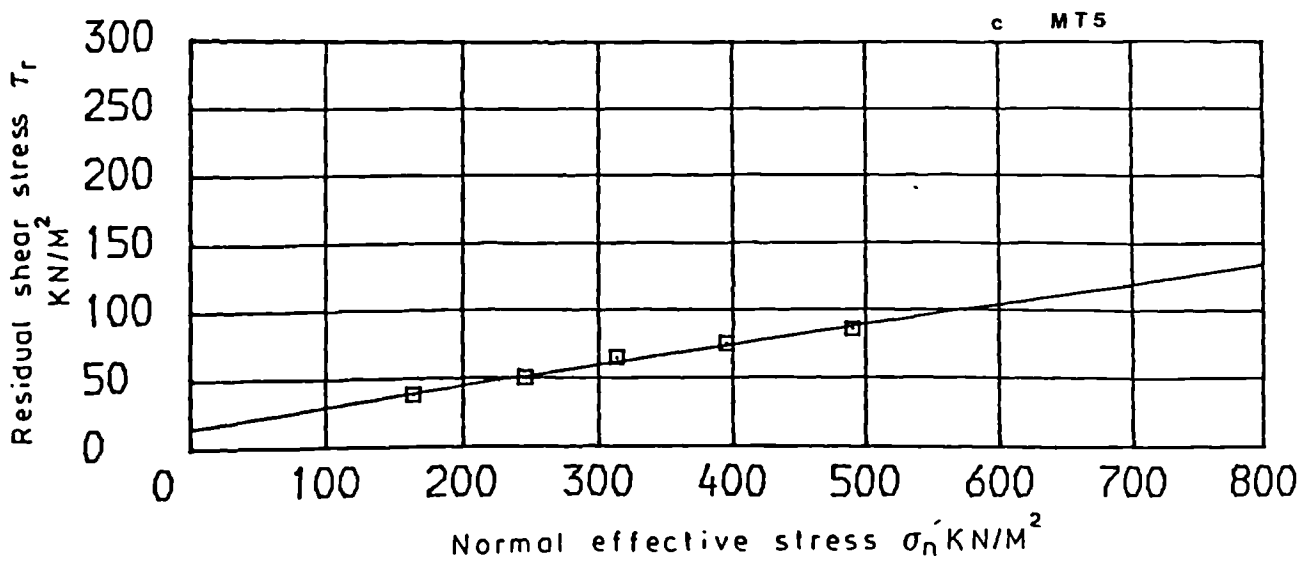
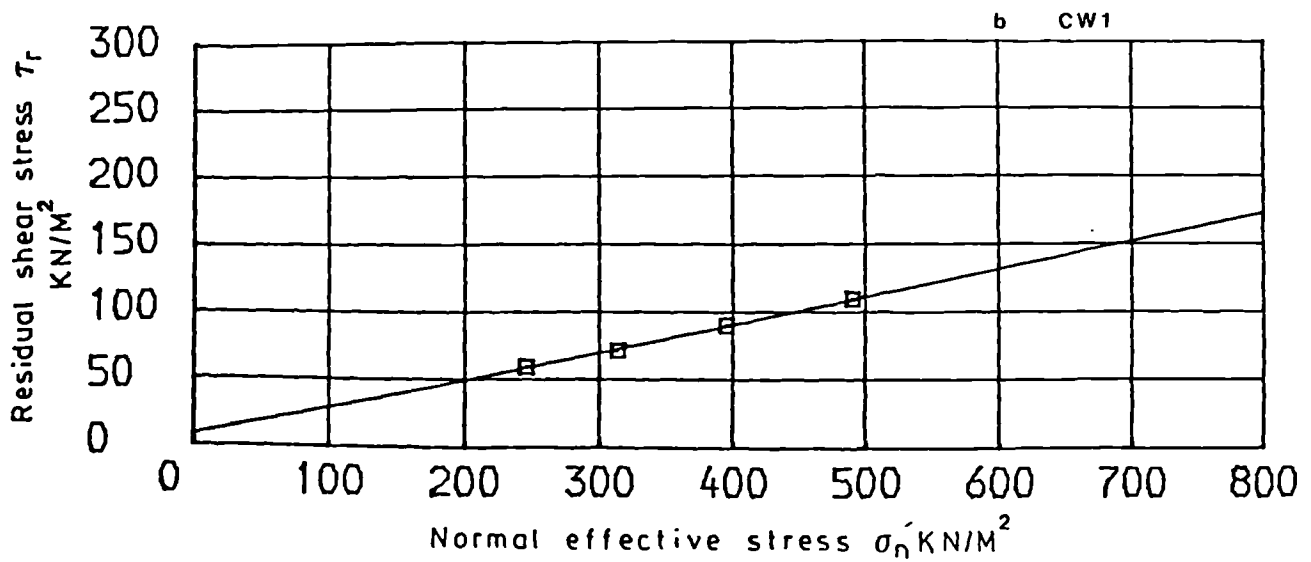
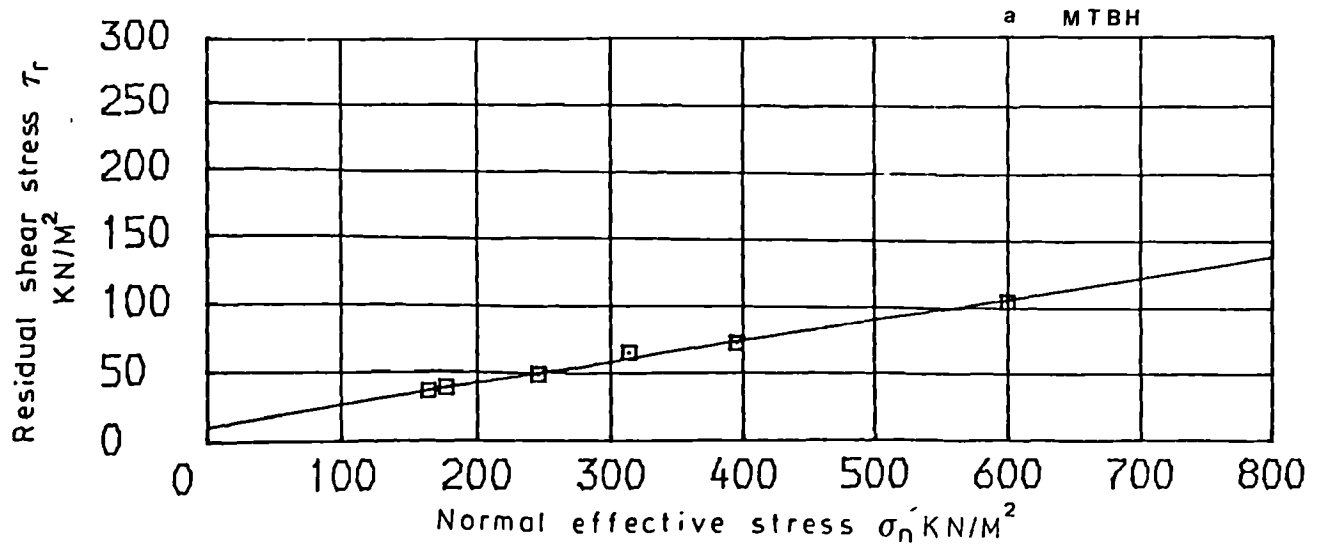


Fig. 5.17 Residual shear stress - normal effective stress relationship for shear box tests on remoulded tumbled and crushed sieved samples.

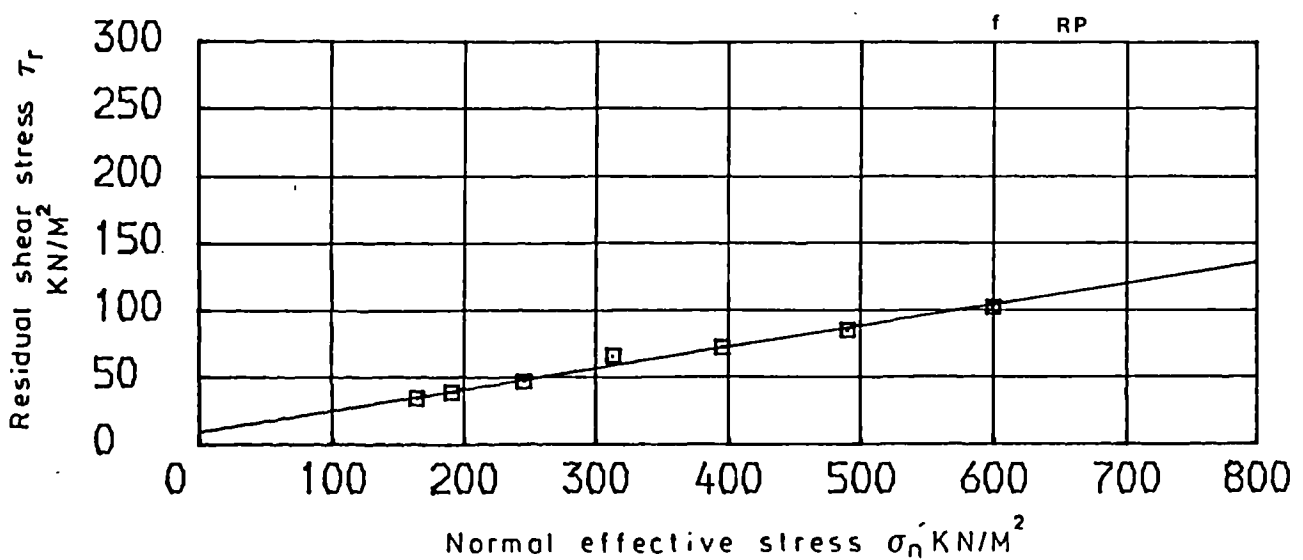
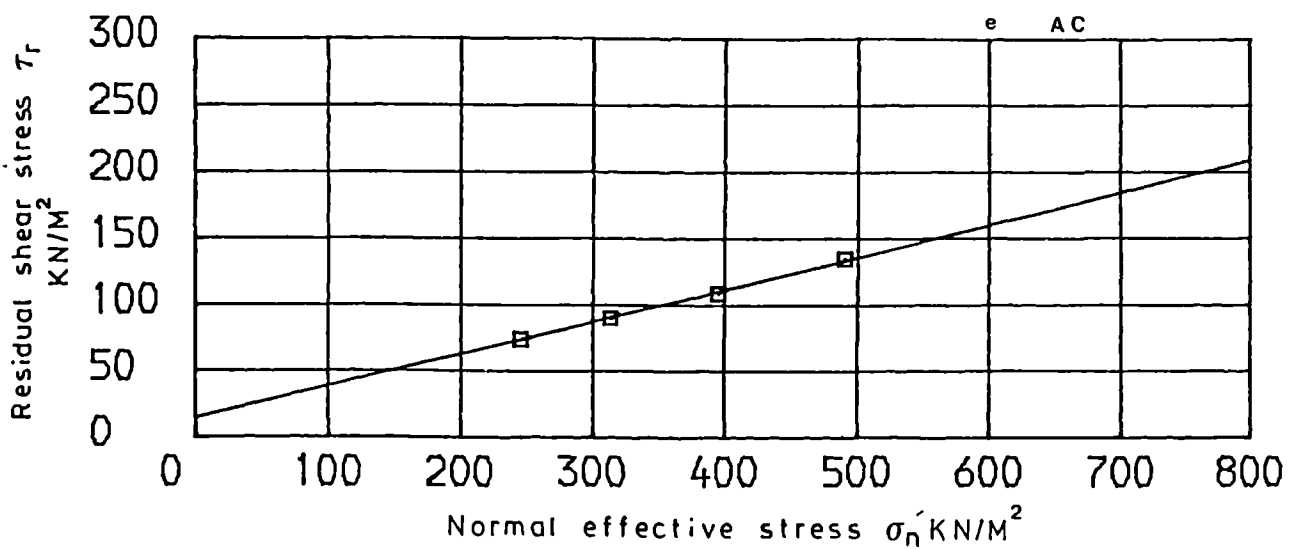
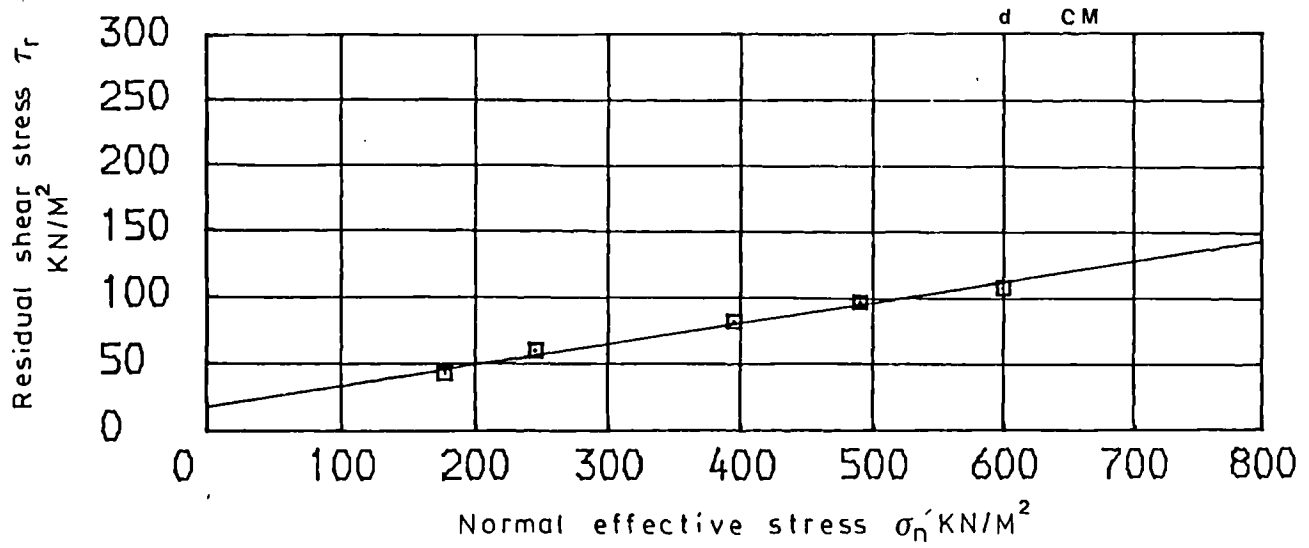


Fig. 5.17 Residual shear stress - normal effective stress relationship for shear box tests on remoulded tumbled and crushed sieved samples.

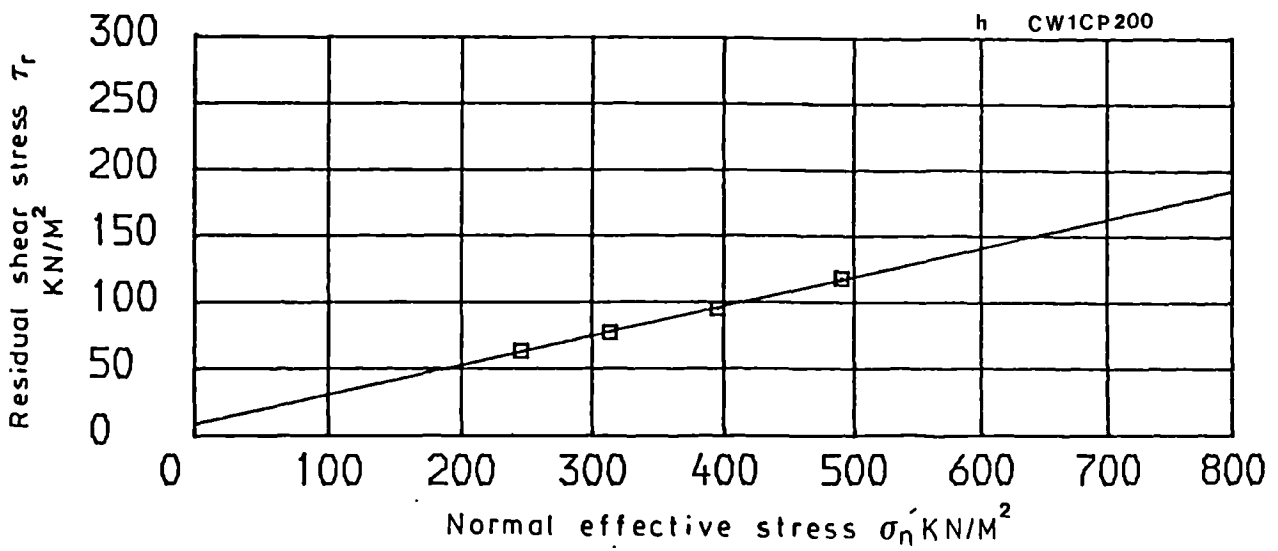
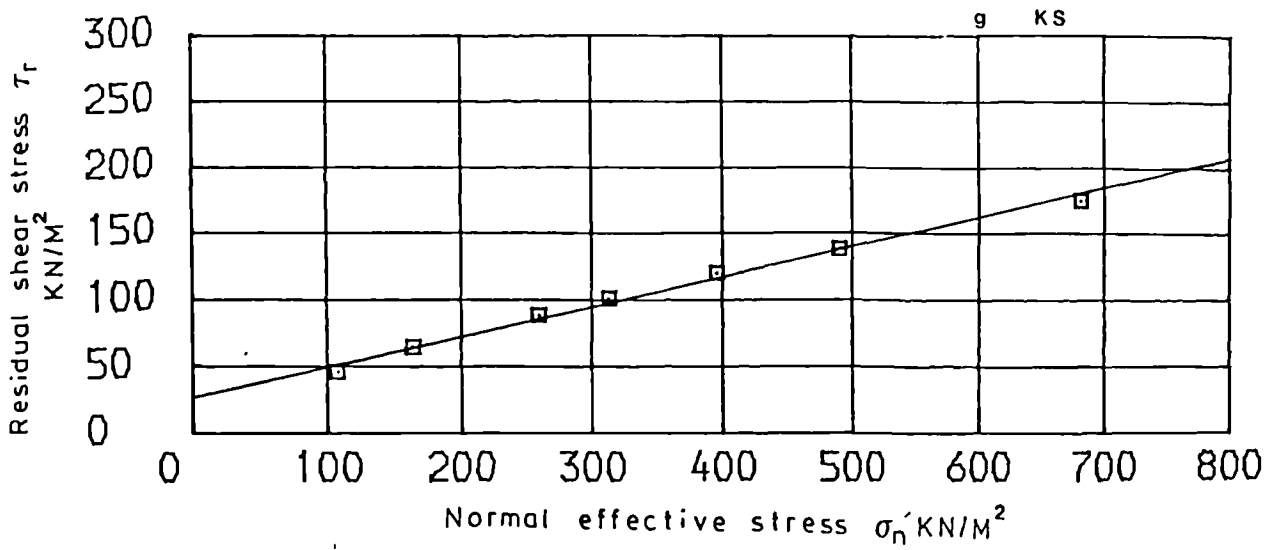


Fig. 5.17 Residual shear stress - normal effective stress relationship for shear box tests on remoulded tumbled and crushed sieved samples.

Table 5.11 Strength values for ring shear and shear box tests on tumbled, crushed, crushed and sieved remoulded samples.

Test	Ring shear						Shear box						
	tumble		crushed 36		crushed and sieved		tumbled		crushed and sieved		crushed and sieved		
Preparation	ϕ_{rr}^i deg.	c_{rr}^i kN/m ²	ϕ_{rr}^i deg.	c_{rr}^i kN/m ²	ϕ_{rr}^i deg.	c_{rr}^i kN/m ²	ϕ_{rr}^i deg.	c_{rr}^i kN/m ²	ϕ_{rr}^i deg.	c_{rr}^i kN/m ²	ϕ_{rr}^i deg.	c_{rr}^i kN/m ²	mesh size
MTBH	7.5	4.1					9.0	10.5					
			10.5	5.0	< 200				8.5	12.4			< 200
CW1	7.5	2.5	10.5	6.1	> 200		11.5	8.2					
			13.0	3.6	> 72								
			13.5	15.4	> 72								
CW2	10.5	2.4	12.0	21.3									
CW3	12.5	3.8	19.0	14.5									
MT5	6.5	4.9					8.5	14.5					
MT6	8.0	3.8											
CM	8.5	6.8					9.0	17.8					
BUT	9.5	7.6											
AC	7.0	6.5					13.5	14.3					
RP	7.5	4.3					9.0	9.5					
CS	8.5	3.1											
BCL	12.0	8.9											
KS	13.0	4.9					12.5	27.0					

same rock specimen subjected to differing styles of preparation. In the case of sample CW, the undifferentiated crushed (< 36 mesh) sample gives the same ϕ'_{rr} value as the fine (< 200) fraction differentiated crushed material (See Table 5.2). Apparently the fine fraction dominates the behaviour of the undifferentiated material. Consideration of the differences between the differentiated crushed samples indicates that ϕ'_{rr} is increased by approximately 3° when comparing the fine (< 200) fraction with the coarser (< 36, > 72) fraction. This is probably explained by the presence of aggregated strong grains of clay minerals and quartz particles. In the case of the sieved (< 200) sample, in fact ϕ'_{rr} is some 2° lower for the shear box than for the ring shear although c'_{rr} is more than 7 kN/m^2 greater. The higher cohesion values for the crushed material are probably due to interlocking between aggregated grains. The lower value obtained for the more disaggregated tumbled and finely crushed samples supports this view.

Sample KS yields results which lie outside this general trend in that ϕ'_{rr} for the ring shear tumbled sample is 0.5° more than the corresponding shear box result although the c'_{rr} value is considerably higher in the latter test.

The fact that the shear stress-displacement curves of sample CW1CR72 in Fig. 5.7 shows a fluctuating τ'_r value after displacements of 130 mm. suggests that incomplete disaggregation is responsible for the higher strengths of the coarser samples. The presence of rotund aggregated particles would be significant since these do not become orientated in the direction of shearing. Presumably lower values of shear stress occur when a proportion of these particles have been comminuted and or removed from shear surface.

It would be anticipated that the grinding of grains during shear would lead to comminution of clay aggregates so that with sufficient displacement all samples would have the same shear strength. If quartz and other rotund

minerals are preferentially removed during sieving then the coarser ones would be stronger. However, it seems probable that grains passing 72 mesh B.S. will be predominantly clay aggregates rather than quartz and other 'hard' rotund minerals. Clearly, if this is the case, then it follows that condition on the shear surface are not conducive to the complete break up of aggregated clay particles. Since, in the tests, the shear stress was at a minimum value, it seems unlikely that further displacement would have reduced the strength to the extent achieved by disaggregation prior to testing.

Actually this leads on to the interesting argument that the value of residual measured depends on the disaggregation possible on the shear plane. Obviously under normal laboratory test conditions insufficient breakdown occurs. In natural slip surface the displacement may be much greater and weathering solutions can cause disaggregation of the clay aggregate. However, whether complete disaggregation would then occur is still unknown.

5.5.6 Statistical analysis

The observations suggest that there are significant difference between the results of the ring shear and shear box tests. In fact, in view of the large number of tests which have been performed using both apparatus, it is possible to use a statistical method to determine the consistency of the results for a particular test type, and also determine whether the apparent differences between the tests types are supported statistically. The method of the analysis is discussed in Appendix D.

The analysis shows in Tables D1 to D5 that for a particular type of test (shear box or ring shear) there is no significant difference at 5% level between samples tested. This is because the samples were prepared in a systematic way and there is no bias in the manner of sample preparation. This result occurs in all analysis.

However, the ring shear and the shear box produce different results significant at 5% level. Hence the conclusion that the ring shear produces lower residual shear strength values than the shear box is valid statistically.

The analysis also shows a significant difference at the 5% level for the results obtained from the ring shear apparatus and a non-significant difference at this level for the shear box results. This observation requires the influence of an effect external to the experiment since if it is assumed that the two apparatus work properly, the results of the analysis should show either a significant or a non-significant difference for both set of results. So significant differences in ϕ'_{rr} and c'_{rr} are probably due to constitution of the sample but the non-significant results must be due to external effects. Since the actual analysis is contradictory it is suggested that factors other than the composition of the samples tested or the test conditions are responsible for the non-significant shear box results. One explanation for this would be the presence of dislodged grains in the gap between the two halves of the box.

5.6 Relationship between (ϕ'_{rr} , c'_{rr}) and other engineering properties.

From the discussion in Section 4.2 relating to the literature on residual shear strength, various factors are expected to influence ϕ'_{rr} . The opportunity is taken to consider those which can be attributed to the properties of the materials tested with respect to grading, composition, classification and water content. The relationship between c'_{rr} and various engineering properties is also considered.

5.6.1 Grading and composition

The particle size distribution of all tumbled ring shear samples from which shear strengths are given in Table 5.11 are presented in Fig. 5.5.A and B. The samples

can be considered in terms of their clay contents ($< 2 \mu\text{m}$ fraction) and further distinguished with reference to silt content ($< 0.06 \text{ mm.}$ fraction). It is also useful to consider Fig. 5.18 which is a plot of clay content versus laboratory residual friction value for tumbled ring shear samples. It is noticeable that the coarser samples, including CW2 and CW3 with about 30% of clay, 60-63% of silt and respectively KS and BCL with 23-27% of clay, 71-76.5% silt have the higher ϕ_{rr}' values. On the other hand, MTBH and MT5 produce lower ϕ_{rr}' values at $6.5-7.5^\circ$ for clay contents of 61.5% and 50% respectively.

Although in general, the greater the quantity of clay sized material the lower is ϕ_{rr}' for clay fraction above about 40%, further increases in clay do not appear to have an effect on ϕ_{rr}' value. Within the data for clay content between about 25 and 40% there is a general trend of decreasing ϕ_{rr}' , but the data shows much scatter. This variability probably arises since the different samples have dissimilar mineralogies. In particular, sample MT5 which has clay size content of 50% and ϕ_{rr}' of 6.5° should be compared with sample MTBH, with clay size fraction of 61.5% and a higher ϕ_{rr}' value of 7.5° . This difference is explained by a higher quartz content of 21% in MTBH. Similar remarks are appropriate in the case of samples CS and BUT. The present determinations are considered in the light of the clay size fraction and amount of quartz present in the samples together with clay: quartz ratio in Fig. 5-18 which shows the decrease of ϕ_{rr}' value with increasing amount of clay sized material. This is the same relationship as that of Fig. 4.13 found by Lupini et al (1981). Although the relationship between ϕ_{rr}' value and the amount of quartz in Fig. 5.19 shows some scattering, a general trend of ϕ_{rr}' increase with increasing the quartz percentage occurs. The scattering of the points may be related to the grain size of the quartz present in the samples, for example the percentages of the quartz from sample KS and BCL are

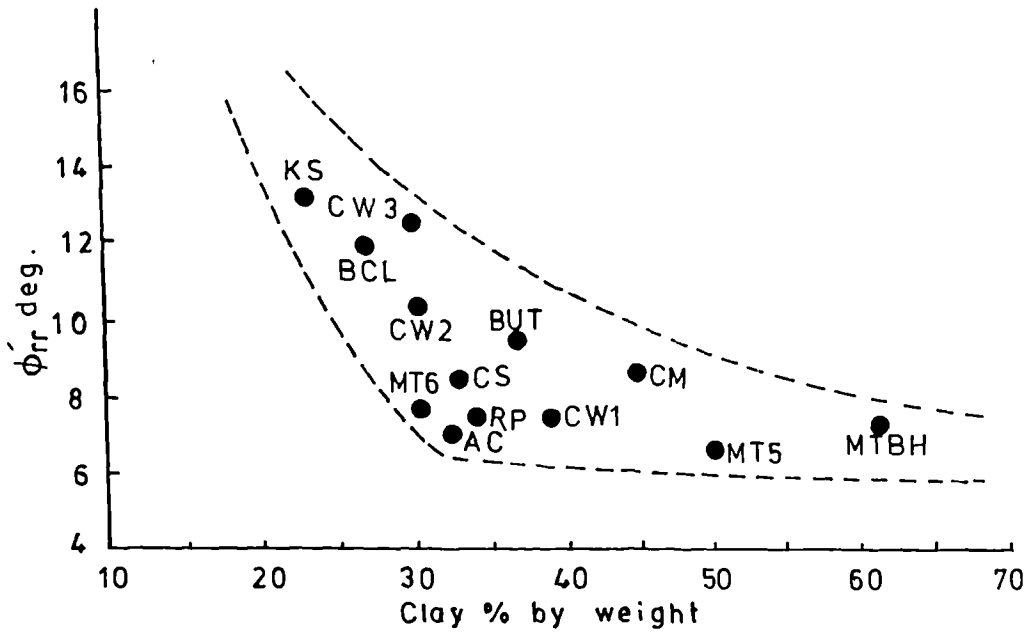


Fig. 5.18 Relationship between clay fraction and residual shear strength for ring shear tests on remoulded tumbled samples

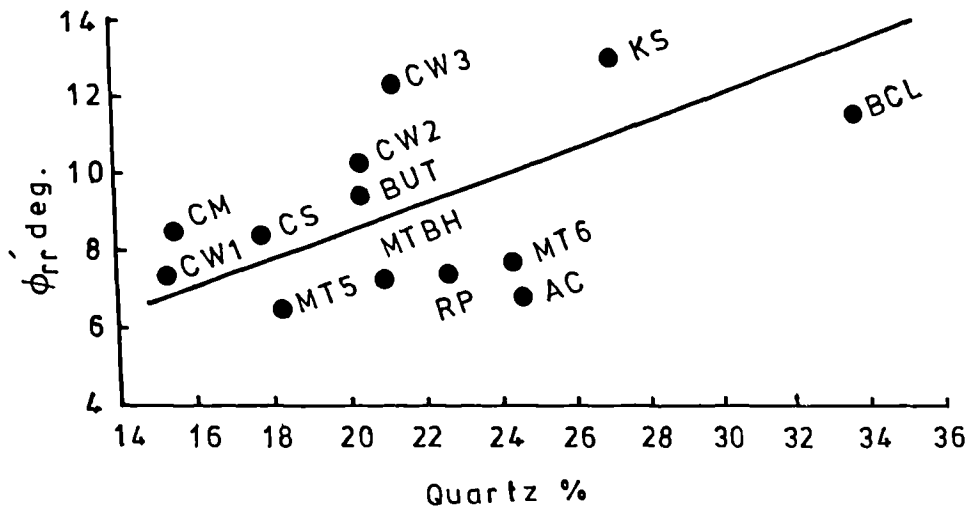


Fig. 5.19 Relationship between quartz and residual shear strength for ring shear test on remoulded tumbled samples

27.5 and 34% respectively. In fact the grain size analysis shown in Fig. 5.5B indicates that the grading is coarser for sample KS than BCL. Although the percentage of quartz in sample BCL is 12% higher than that for sample CW3 the ϕ_{rr} value is 0.5% less. Again the upper part of the grain size distribution Fig. 5.5A and B shows that sample CW3 is a coarser grained material which was confirmed by a visual identification to be quartz.

Cripps and Taylor (1981) consider that a useful way demonstrating the influence of clay fraction on residual shear strength is to express it in terms of the ratio of clay minerals to massive minerals (See Section 4.2). In the present materials by far the greatest proportion of massive minerals would be quartz and so in Fig. 5.20 the ϕ_{rr} values is plotted against the clay: quartz ratio for comparison with data summarized by Cripps and Taylor (1981). The results of the ring shear and shear box tests on tumbled samples were plotted against the clay: quartz ratio in which as expected ϕ_{rr} is reduced with increasing the ratio of clay: quartz, but the amount is rather lower than for the published data shown in Fig. 5.20. It is suggested that may be due to the method of preparation of samples. In the published data Coal Measures samples were prepared by cut-plane tests on undisturbed samples with no disaggregation preparation. Also, Taylor (personal communication) found that ultrasonic disaggregation of colliery spoil reduced ϕ_r from 29° to 13°. In present study only quartz was taken as being diagenetic and the data are concentrated towards the left hand side of the diagram. Also the ring shear test results which produce lower strength values are dominant.

The method of semi-quantitative determination of clay mineralogy by X-ray diffraction is described in Appendix C. Briefly the $< 2 \mu\text{m}$ size fraction of powdered rock was smear mounted for analyses in air dried, ethylene glycolated, heated to 300°C and heated to 550°C conditions. The peak areas were determined by Schultz (1960) method.

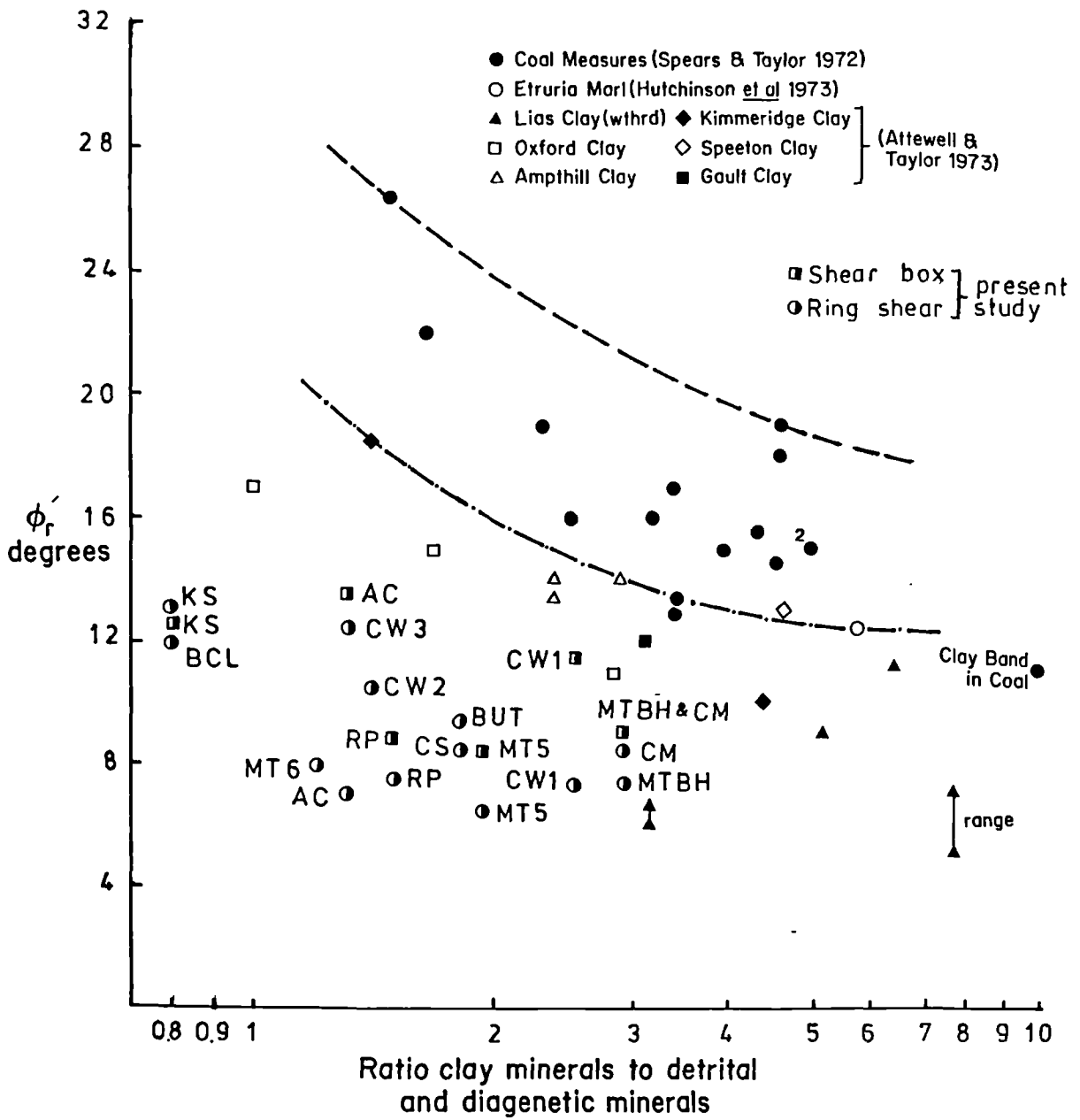


Fig. 5.20 Comparison between published and present relationship between residual shear strength and ratio of clay minerals to detrital minerals.

As shown in Table 5.4 the main clay constituents are kaolinite and mixed layer clay, illite is present in small amounts together with chlorite. These data are compared with ϕ_{rr}' for tumbled ring shear tests in Fig. 5.21. Clearly there is a good deal of scatter, but some tentative trends are discernable. In particular, increases in the amount of mixed layer clay, kaolinite and perhaps illite would appear to be accompanied by some reduction in the laboratory ϕ_{rr}' value and quartz grain size and the total clay: quartz ratio have already been considered in this context.

The ratios of each clay mineral type to the XRD quartz amount for the whole rock scan are also given in Table 5.4. These data are plotted against laboratory ϕ_{rr}' for tumbled ring shear tests in Fig. 5.22. Again, the data show much scatter, but some trends may be apparent. Rather tentative ones are suggested for illite and kaolinite but a much clearer one occurs in the case of mixed layer clays.

Clearly the relationship between laboratory ϕ_{rr}' and clay size fraction, amount of quartz, type of clay minerals and ratio clay minerals: quartz all show some scattering. It is believed that the main cause of this scattering is the effect of relative percentages of clay and quartz minerals, relative grain size distribution and also the relative percentages of types of clay minerals in each sample.

5.6.2 Classification and water content

The plasticity data in terms of liquid limit and plasticity index presented in Table 5.3 are plotted against laboratory ϕ_{rr}' values for tumbled ring shear samples in Fig. 5.23. These graphs confirm the general trends anticipated in review Section 4.2 and may be compared with published data in Fig. 5.24. It is interesting to note that the present data plot towards the lower ϕ_{rr}' end of the diagram and coincide with lower limit

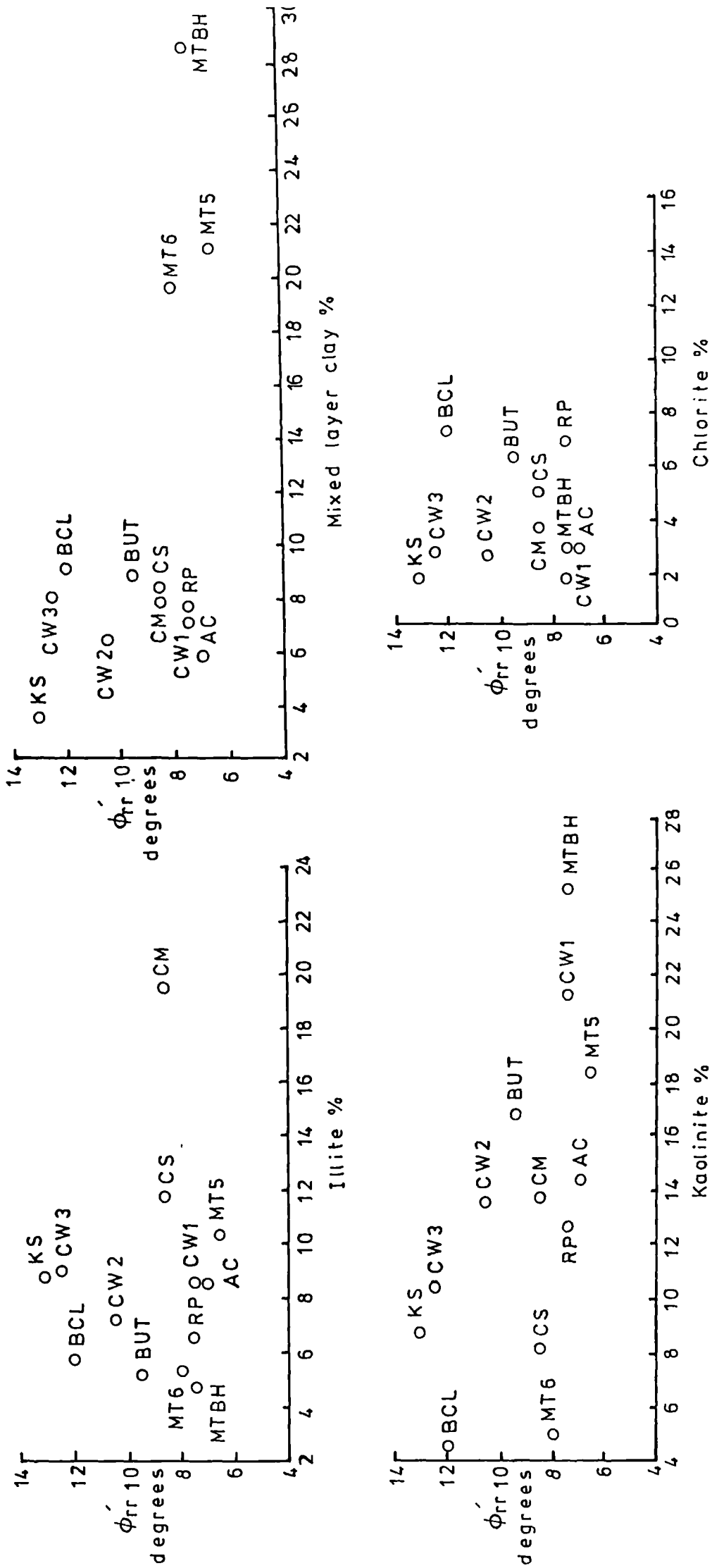


Fig. 5.21 Relationship between residual shear strength for ring shear tests on tumbled samples and amount of clay.

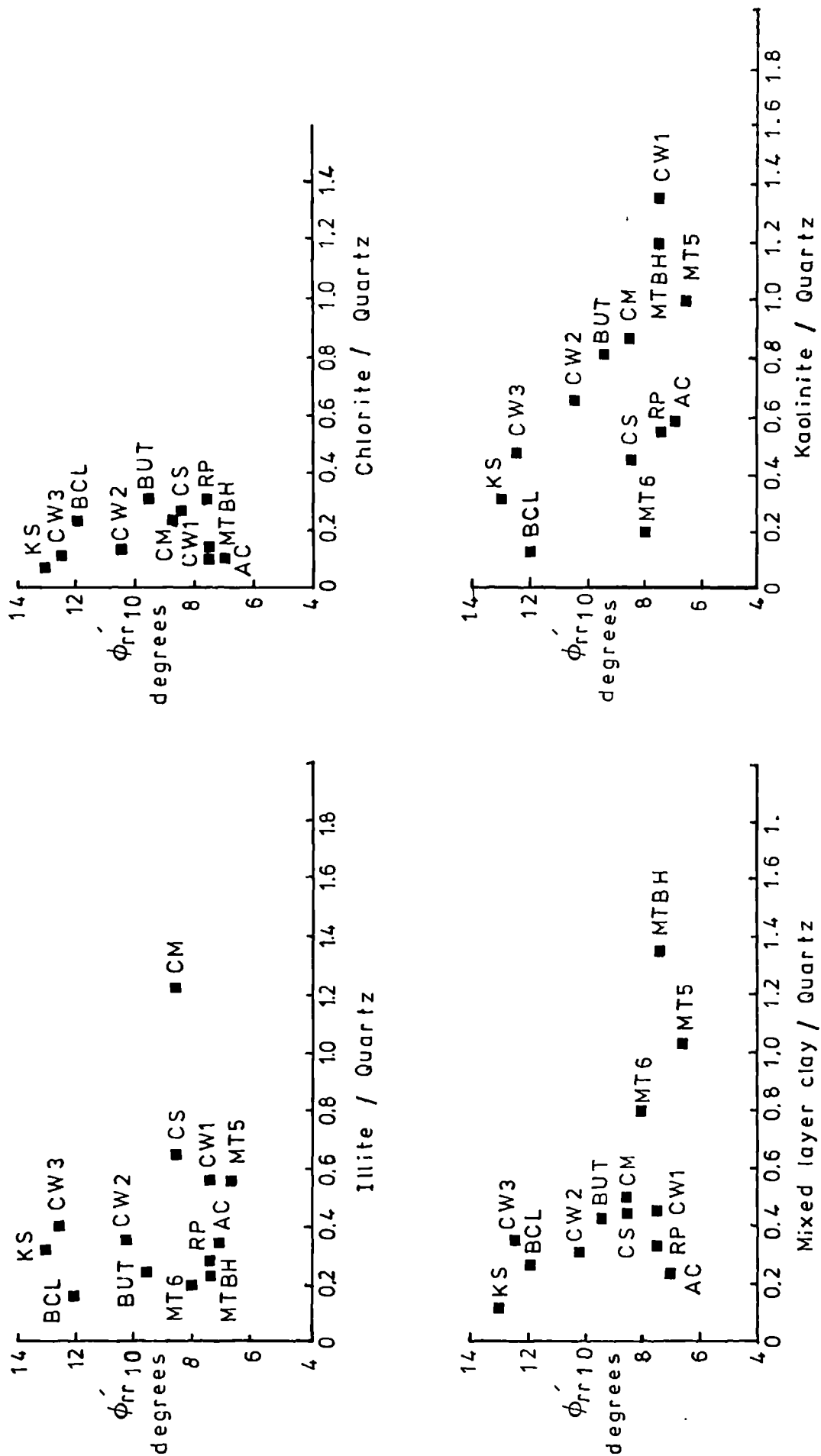


Fig. 5.22 Relationship between residual shear strength for ring shear tests on remoulded tumbled samples and clay minerals: quartz ratio.

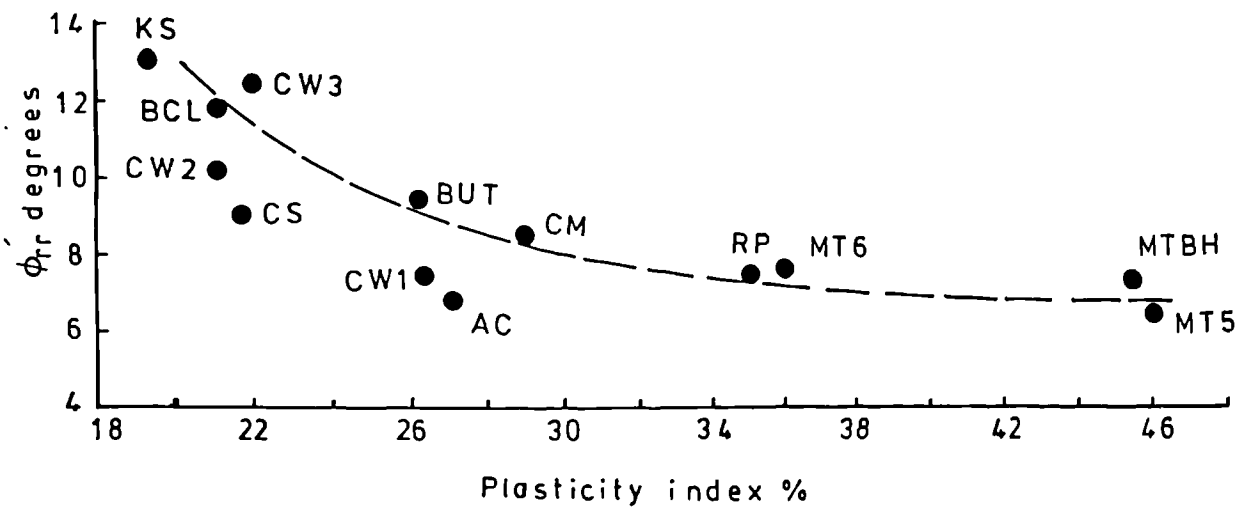
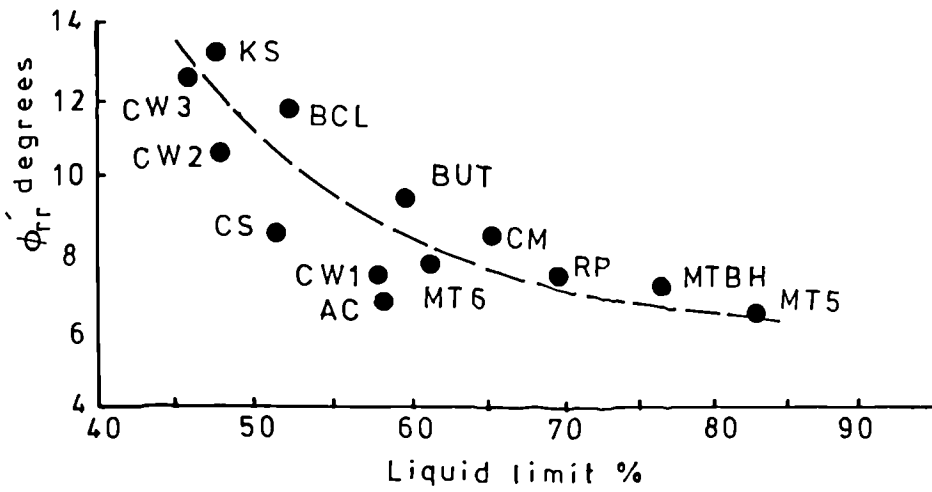


Fig. 5.23 Relationship between residual shear strength for ring shear tests on reoulded tumbled samples and liquid limit or plasticity index.

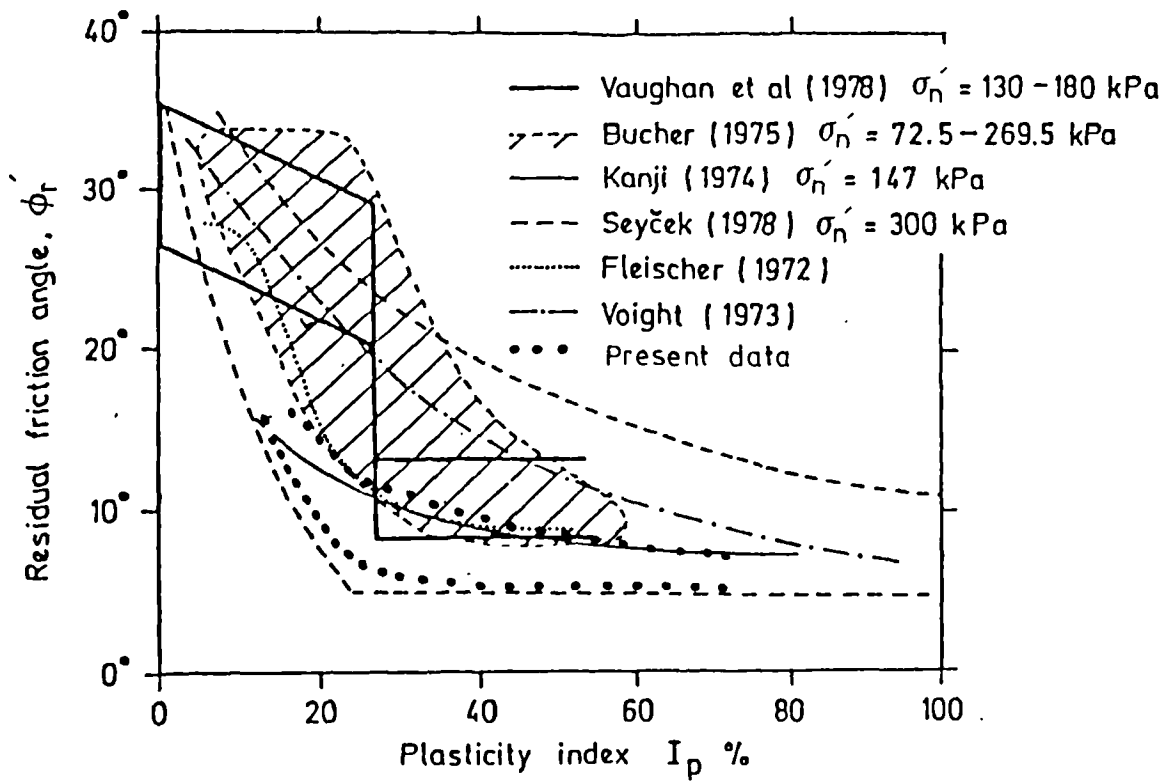


Fig. 5.24 Published and present relationships between residual shear strength and plasticity index.

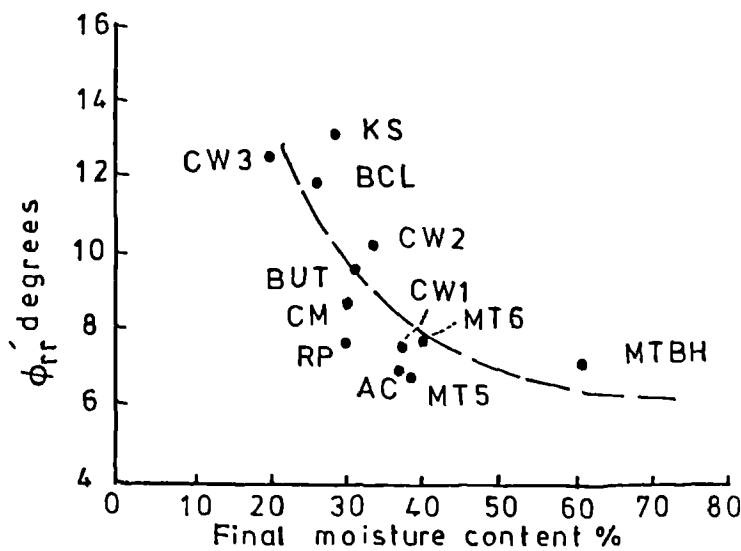


Fig. 5.25 A Relationship between residual shear strength for ring shear tests on remoulded tumbled samples and final moisture content.

of Fleiscter's (1972) results. This feature is attributed to the superior disaggregation achieved by tumbling compared with other methods of sample preparation. If laboratory ϕ_{rr}' values for crushed ring shear samples are included the difference is apparent and it should also be remembered that although the data in Fig. 5.24 are for ring shear and shear box apparatus, the methods of sample preparation are not exactly known.

It was noted in Section 4.2.2 that little data regarding the final water content of samples appears in the literature. However, in view of the fact that this parameter is expected to be a function of grain size and mineralogy, a correlation would be anticipated. In fact the graphs of final moisture content (See Table 5.12 and 5.13) and laboratory ϕ_{rr}' values for both tumbled ring shear and tumbled shear box samples plotted in Fig. 5.25 A and B display reasonably good correlation. In fact the scatter of data points is produced compared with those for grain size and mineralogy. Unfortunately it is not possible to relate these data for Namurian shale to other mudrocks, but clearly final moisture content could be a useful parameter in the consideration of these data.

In fact the final water content is probably a function of the last normal stress used in the test. Notwithstanding probable changes in value due to air or water uptake upon load removal and dismantling of the equipment at the end of the test. Although the sample container was drained of water before the load was removed, water could have been drawn from the porous plates. However, it is possible that if the final normal stress were normalized the scatter of the point in Fig. 5.25A and B would be reduced.

As indicated in Table 5.3 the samples tested contain between 1.4 - 2.9% organic carbon. Jackson and Fookes (1974) attribute lower plasticity values to the presence of more organic matter. Since Fig. 5.24 shows that ϕ_{rr}' decreases with increasing plasticity index a correlation would be expected in which ϕ_{rr}' decreases with decreasing

Table 5.12 Initial and final moisture contents of ring shear samples.

Sample No.	Initial m.c. %	Final m.c. %
MTBH	71.51	62.60
CW1	49.94	38.86
CW2	45.66	34.67
CW3	37.37	20.57
MT5	65.84	39.94
MT6	59.29	40.76
CM	53.55	30.21
BUT	47.97	32.48
AC	42.37	37.79
RP	53.92	30.17
CS	51.41	-
BCL	39.99	27.57
KS	36.14	29.43

Table 5.13 Initial and final moisture contents of shear box sample.

Sample	Initial m.c. %	Final m.c. %
MTBH	56.63	36.92
CM	51.92	30.69
RP	52.23	37.69
CW1	52.95	30.54
KS	39.36	22.75
MT5	65.83	33.83
AC	43.86	27.11
CW1CP200	31.08	20.43

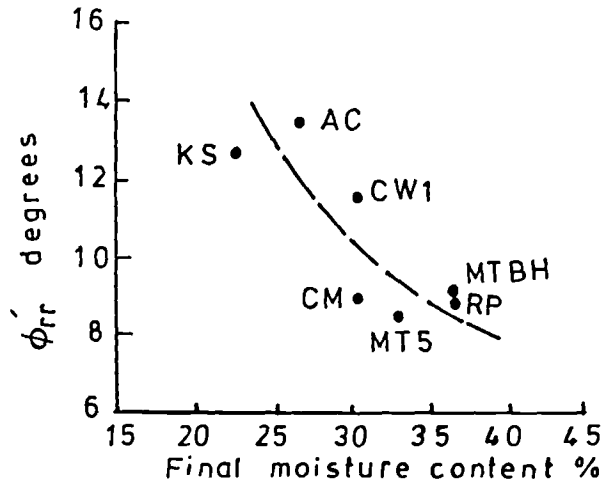


Fig. 5.25 B Relationship between residual shear strength for shear box tests on remoulded tumbled samples and final moisture content.

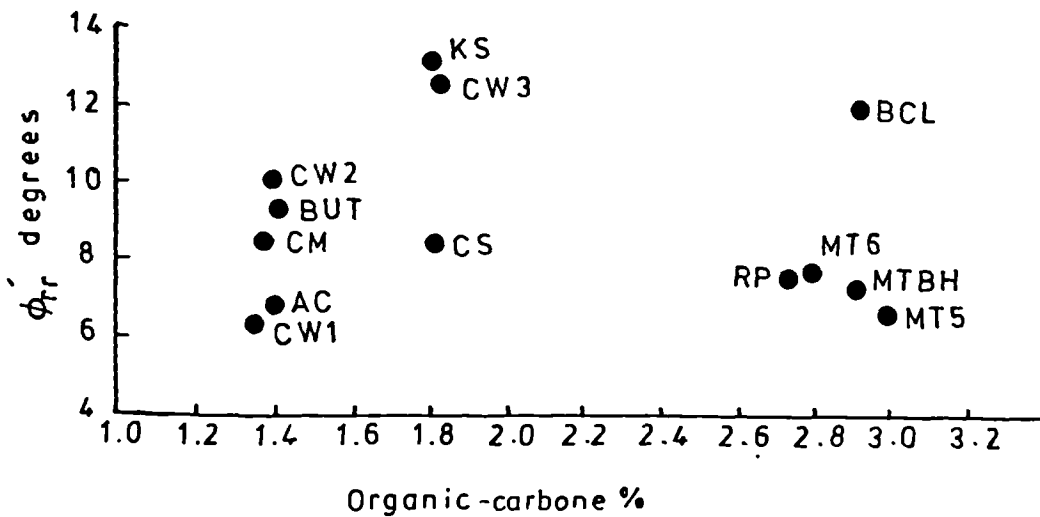


Fig. 5.26 Relationship between remoulded residual shear strength for ring shear tests on remoulded tumbled samples and amount of organic carbon .

organic -carbon content. The data presented in Fig. 5.26 are inconclusive in this respect although the mineralogy, grain size, quartz content and other effects may also affect this relationship. No correlation appears to occur between soluble carbonate and laboratory ϕ_{rr} value.

5.6.3. Relationship of c_{rr} to engineering properties

The remoulded cohesion values, c_{rr} obtained from shear stress-normal effective envelopes of Fig. 5.15 are shown in Table 5.11. These are plotted against various engineering properties including clay fraction, percentage of silt size grains, quartz content, clay: quartz ratio and amount of organic-carbon in Fig. 5.27. The data show some scattering but some trends are also present. In particular the remoulded c_{rr} value would appear to decrease with increasing clay content while it decreases with *decreasing* amounts of quartz. The silt size fraction in Table 5.3 would appear to consist of clay aggregates and it is believed that the cohesion values increase with increased amount of these aggregations. However, the relationship shown in Fig. 5.27 shows scattering. Sample MTBH, which contains a high clay fraction of 61.5% lies outside the general trend. The ratio of clay:quartz also displays scattering but there is a general trend of decreases in c_{rr} value with increasing clay: quartz ratio. As shown in Fig. 5.27, no particular relationship would appear to occur between c_{rr} value and liquid limit, plasticity index or organic-carbon content.

5.6.4 Remoulded peak shear strength

During the course of this study it is intended that assessments should be made of the initial instability of various landslips which occur in North Derbyshire. In order to carry out the analysis described in Chapter 8, it is necessary to determine values of the shear strength of the affected shales in a fully softened

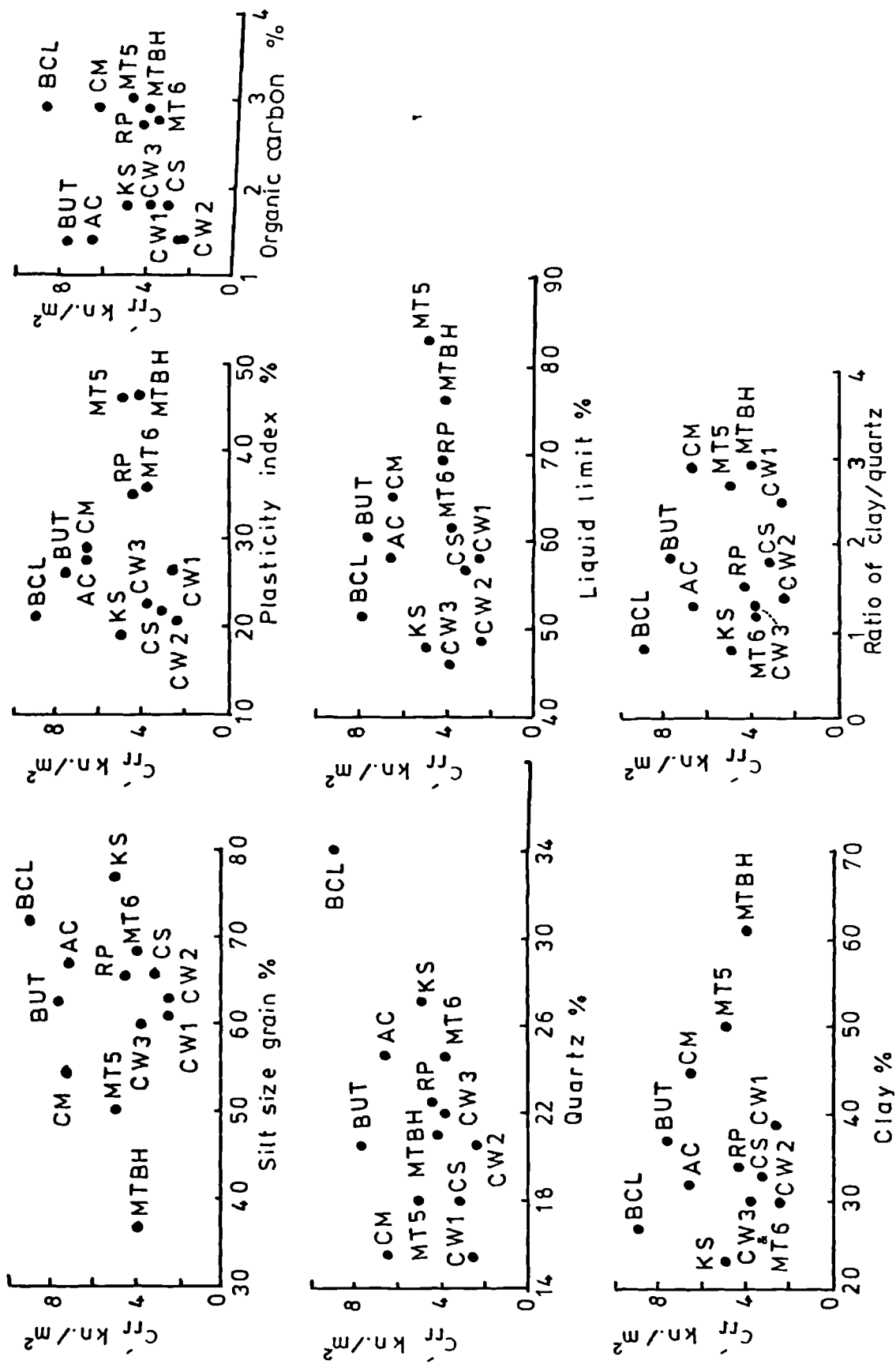


Fig. 5.27 The relationship between C_{rr} and various engineering properties for remoulded tumbled ring shear tests.

condition. Hence the peak remoulded strength of certain samples was measured by ring shear tests. The results of these tests are shown in Table 5.14 and the relevant shear stress-displacement curves appear in Fig. 5.28. The shear stress-normal effective stress envelopes are reproduced in Fig. 5.29 and finally the remoulded peak shear strength values in terms of c_{rp} and ϕ_{rp} appear in Table 5.15.

5.7 Conclusion

The laboratory ring shear residual shear tests on samples of Namurian shale obtained from outcrop samples in landslip areas, a borehole and the quarry at the Hope Valley Cement Works, give remoulded ϕ_{rr} values ranging between 6.5 and 13°. The corresponding remoulded cohesion c_{rr} values lie between 2.4 and 8.9 kN/m². The average values are $\phi_{rr} = 9^\circ$ and $c_{rr} = 4.5$ kN/m². The corresponding ranges for the laboratory shear box tests are little higher with ϕ_{rr} range between 8.5 and 13.5° with c_{rr} from 8.2 to 27 kN/m².

The variation in the residual shear strength parameters are largely explained by differences in the relative percentages of mineral constituents and grain sizes of the samples. The statistical analysis carried out on these data indicates that the shear box results are more erratic than the ring shear ones in that apparent differences between individual samples could be explained by variation in the test results engendered by the equipment rather than the sample. Since significant differences are found between the different samples in ring shear tests it would appear that the shear box is insufficiently accurate to detect these differences with confidence. Probably the presence of grains of soil in the join between the boxes accounts for this problem. The statistical analysis supports the conclusion that lower shear strength is obtained by ring shear testing compared with the shear box. The roughness or the degree of irregularity of the slip surface in the shear box would appear to have a direct effect on the results. In particular, the shear

Table 5.14 Remoulded peak shear stress, values, normal stress values for ring shear tests on remoulded tumbled samples.

Sample	σ'_n kN/m ²	171.4	245	318.4	367.4	392
MTBH	τ kN/m ²		¹ 75.5	² 95.0		³ 111.0
	ϕ'_{rp} deg.		17.1	16.6		15.8
BUT	τ kN/m ²		¹ 99.5	² 125.0		³ 153
	ϕ'_{rp} deg.		22.1	21.4		23.3
AC	τ kN/m ²	¹ 63.5	² 84.0			³ 133.0
	ϕ'_{rp} deg.	20.3	18.9			18.7
RP	τ kN/m ²		¹ 90	² 119	³ 128.5	
	ϕ'_{rp} deg.		20.1	20.4	19.2	
KS	τ kN/m ²		¹ 116.5	² 151.0		³ 181.5
	ϕ'_{rp} deg.		25.4	25.3		24.8

No. 1,2,3 is the load sequence.

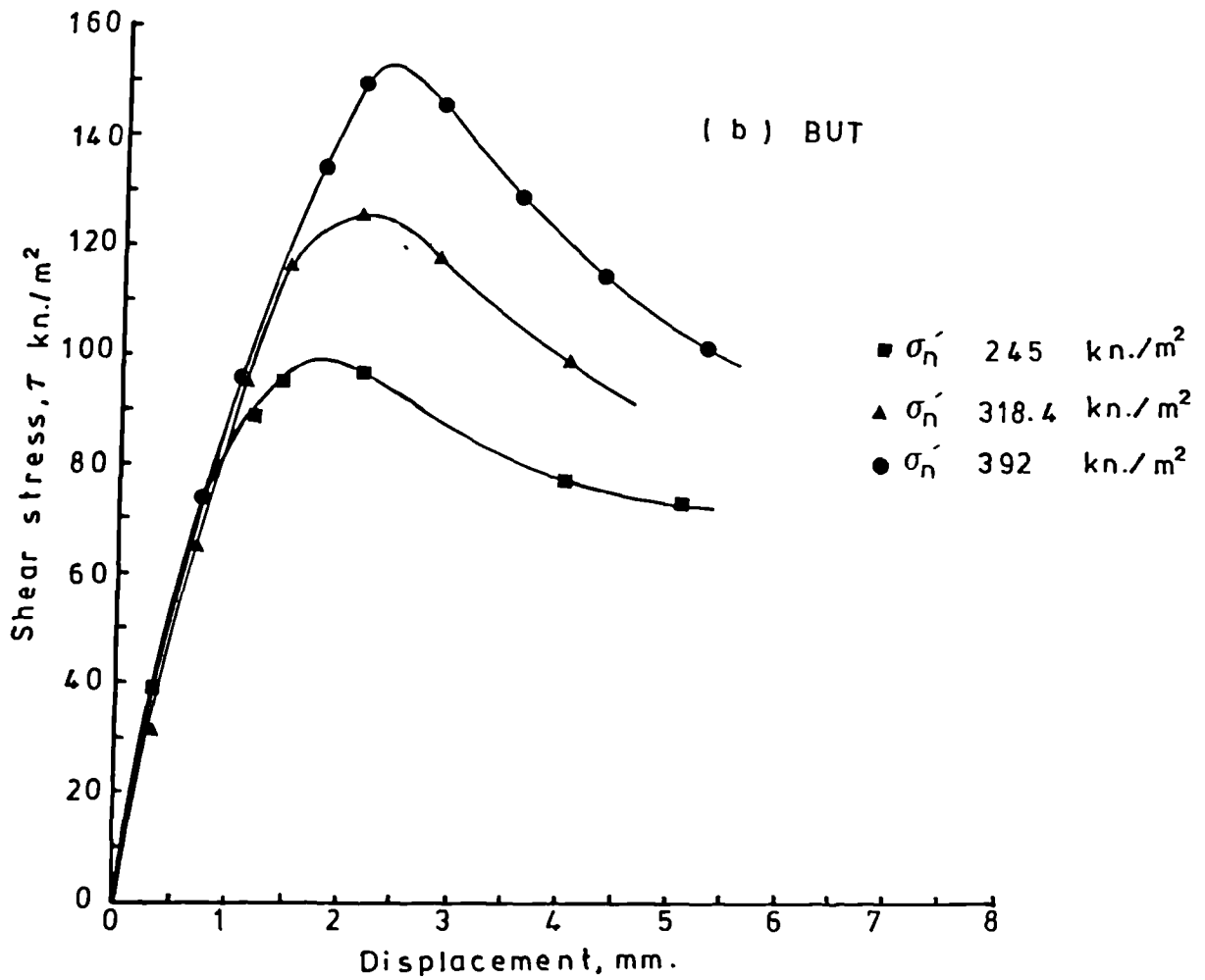
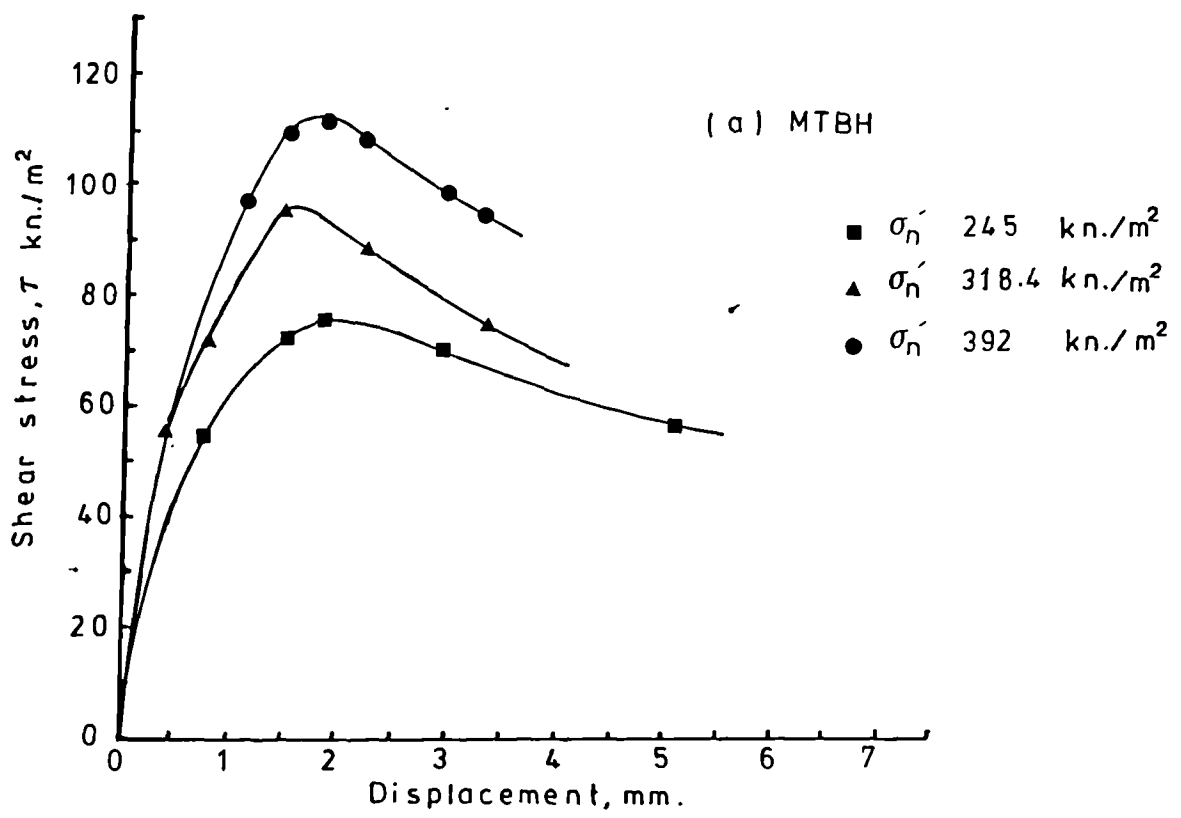


Fig. 5.28 Displacement shear stress curves for ring shear on remoulded tumbled samples.

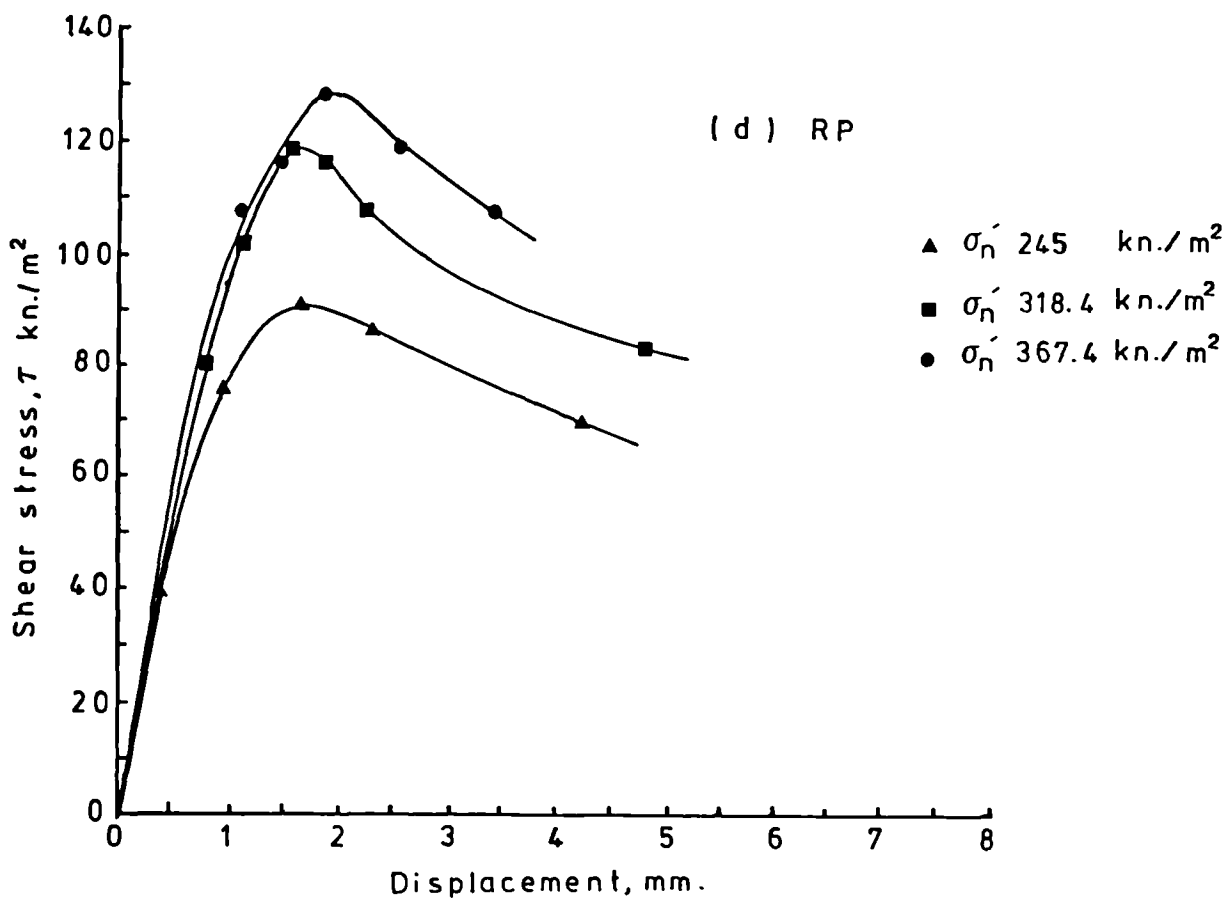
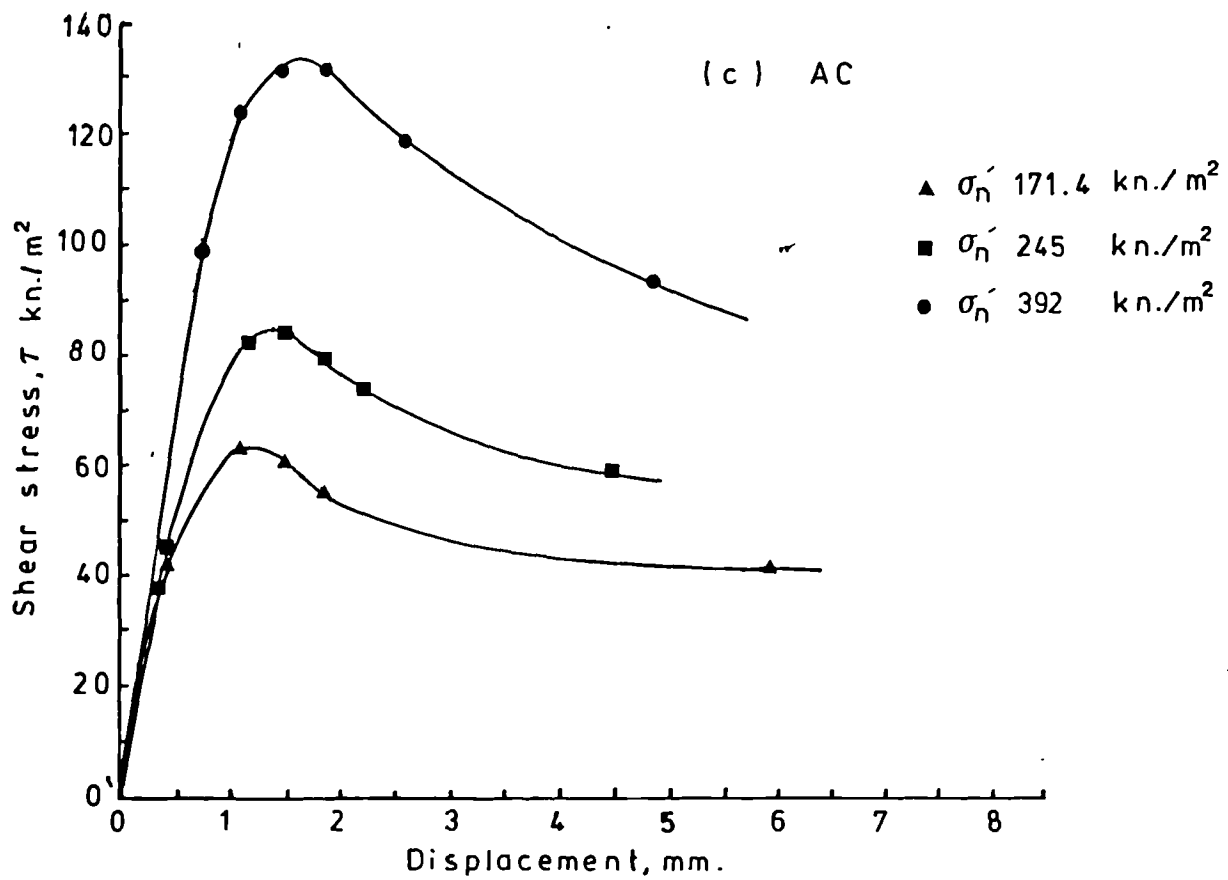


Fig. 5.28 Displacement shear stress curves for ring shear on remoulded tumbled samples.

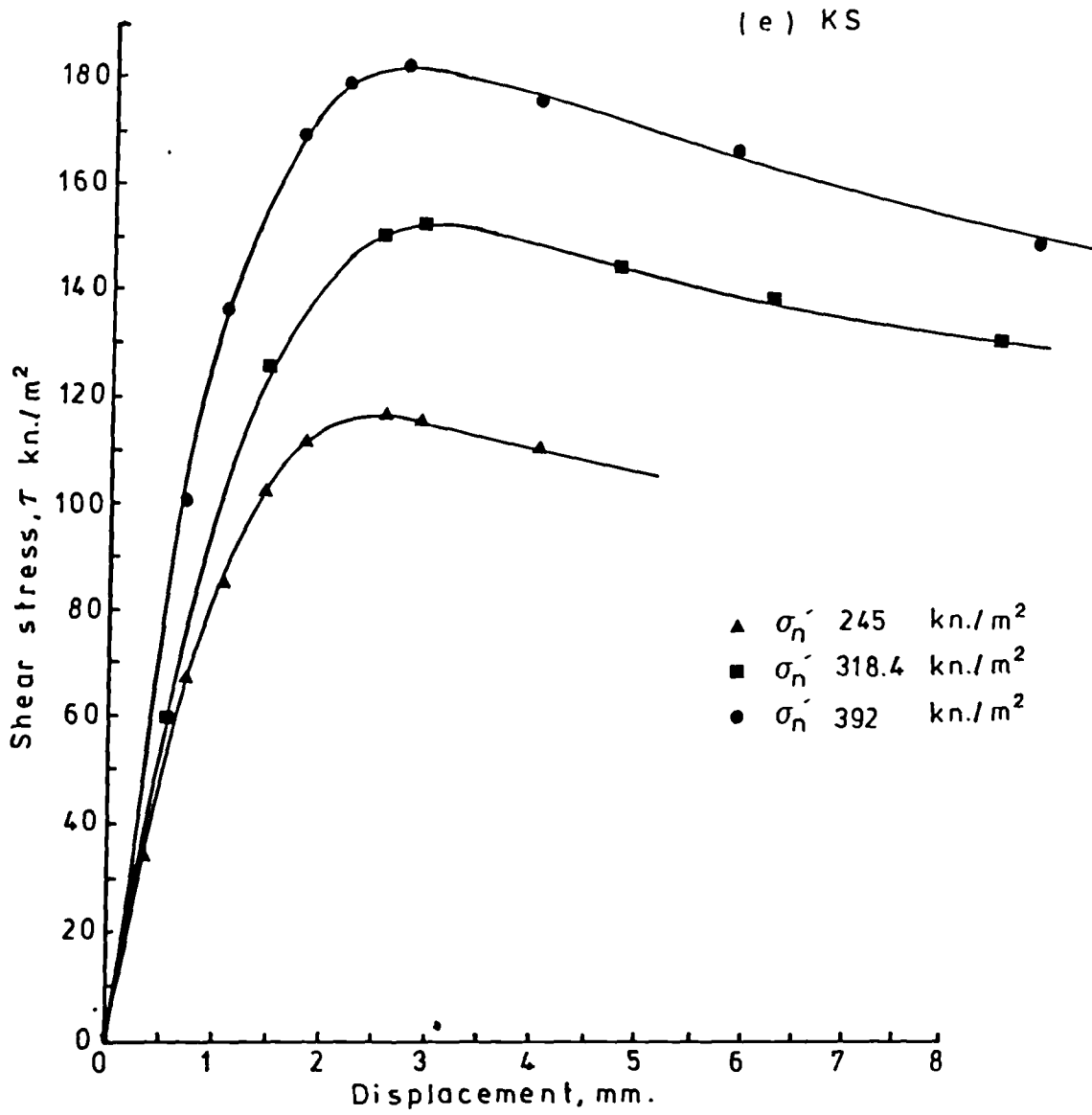


Fig. 5.28 Displacement shear stress curves for ring shear on remoulded tumbled samples.

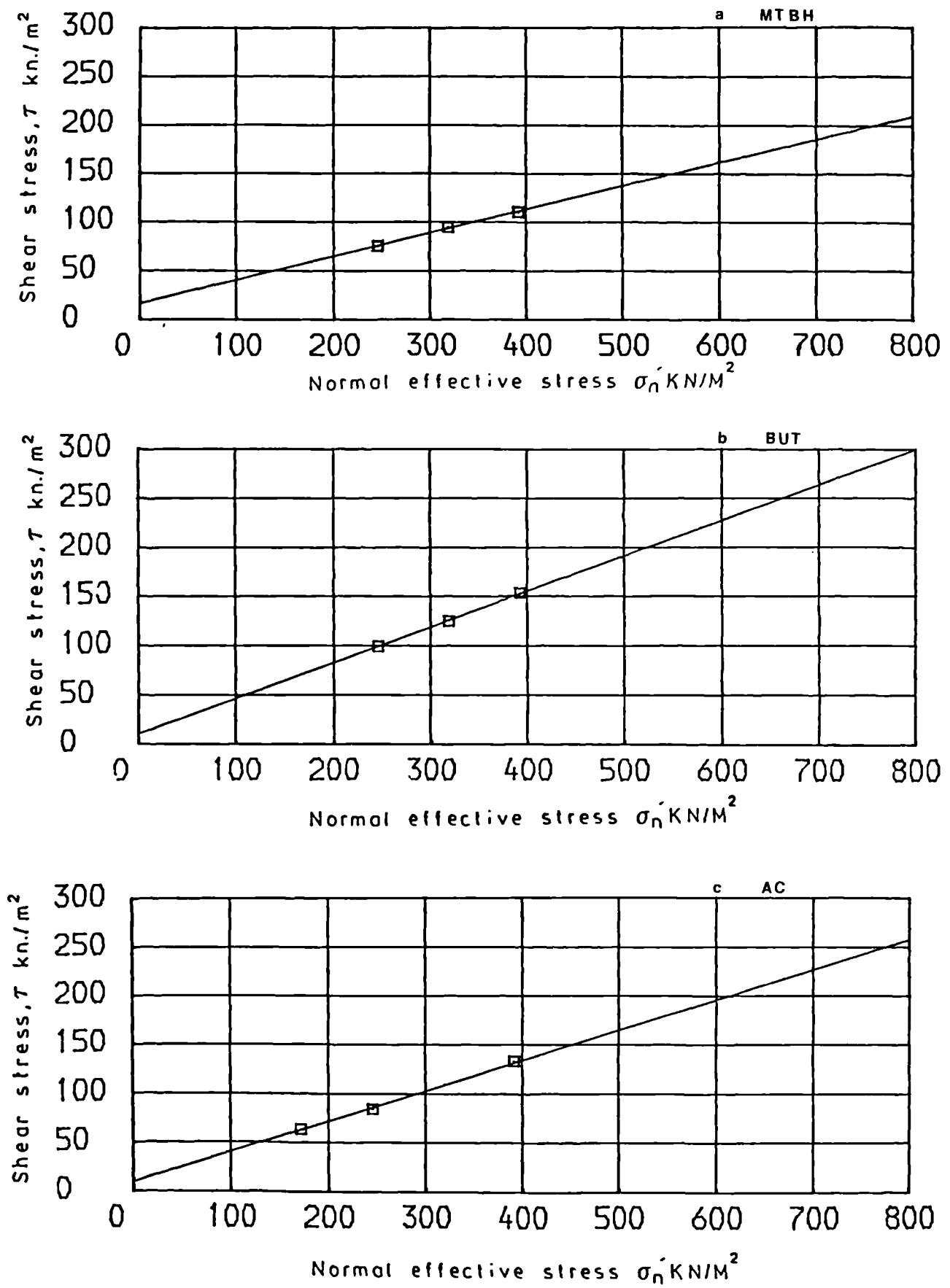


Fig. 5.29 Remoulded peak shear stress - normal effective stress relationship for ring shear test on remoulded tumbled samples.

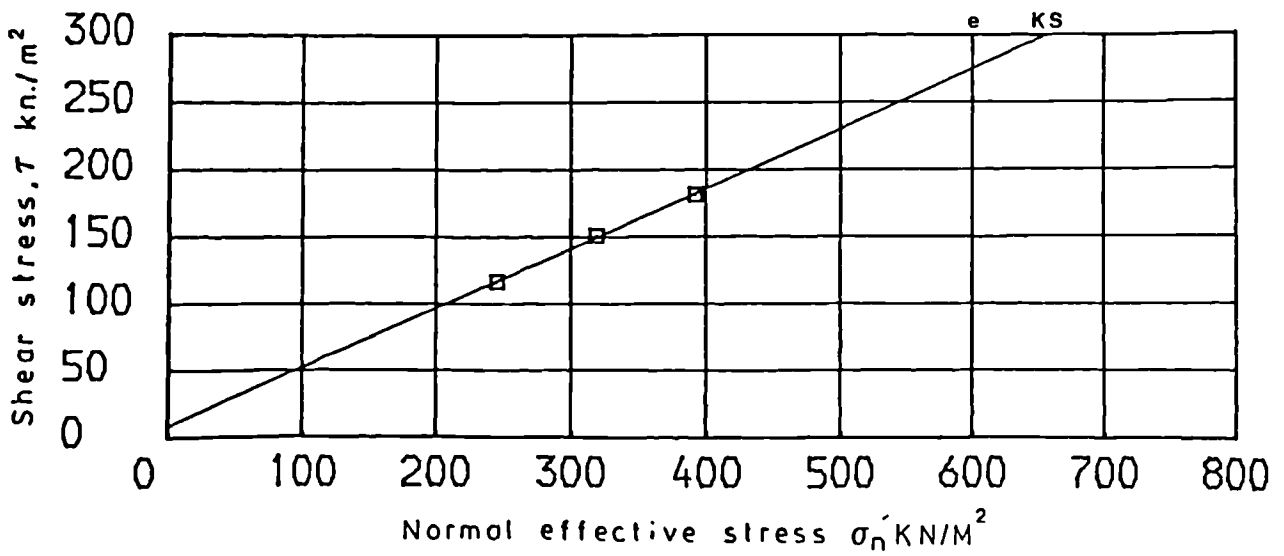
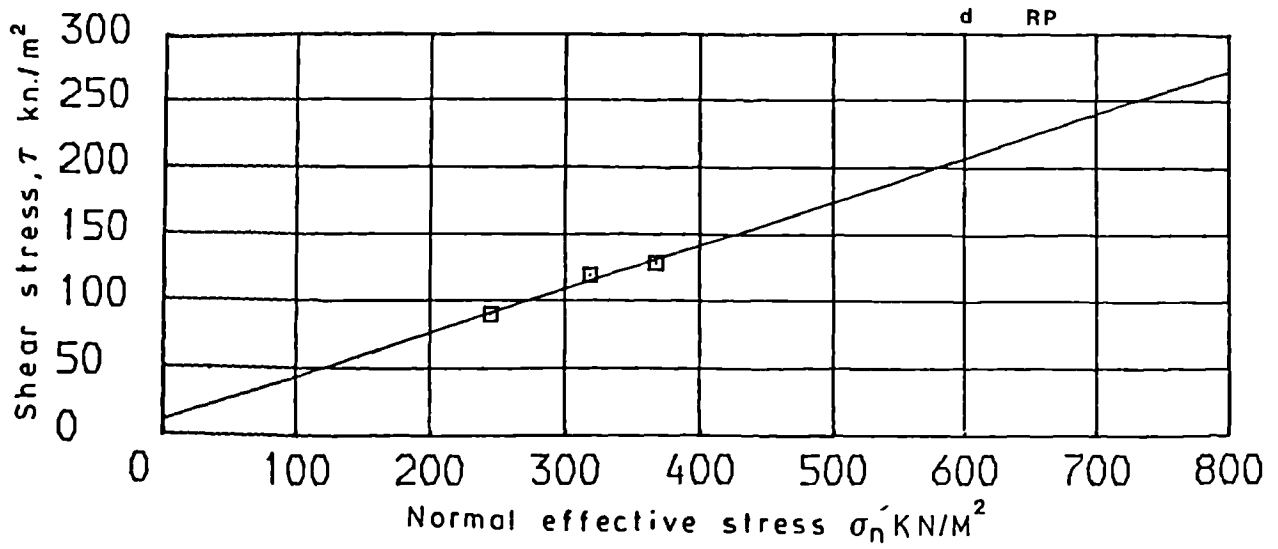


Fig. 5.29 Remoulded peak shear stress - normal effective stress relationship for ring shear test on remoulded tumbled samples.

Table 5.15 Peak shear strength values for ring shear test on tumbled remoulded samples.

Sample	ϕ_{rp} degree	c_{rp} KN/m ²
MTBH	13.5	16.6
BUT	20.0	10.6
AC	17.0	9.8
RP	18.0	10.9
KS	24.0	7.9

stress is always higher in the tensional stroke when mismatched irregularities are being forced out of their mating position.

Tumbled samples always produce a lower residual shear strength (ϕ_{rr}' and c_{rr}' values) than the crushed ones owing to the superior break up of clay aggregations. It would appear from these differences in ϕ_{rr}' and c_{rr}' that disaggregation during shearing in tests is not as effective as that due to tumbling.

Using different sieved fractions of the crushed samples has little effect on the remoulded residual friction angle ϕ_{rr}' with quite similar results being obtained for various sizes. In fact some crushed samples yield a relatively high cohesion (c_{rr}') value but this may be due to cohesive forces between the larger clay aggregations.

As expected the normal effective stress value used in the tests has a direct influence on the residual shear strength. If c_{rr}' is assumed to equal zero apparently ϕ_{rr}' decreases with increasing σ_n' . But drawing the envelope in Fig. 5.15^M produces a straight line for even a very low normal effective stress values. In the case of blue London Clay Bishop et al (1971) report a nearly constant value of ϕ_r' for various σ_n' values with a linear stress envelope which passes through the origin. The present tests on Namurian shale also give a straight envelope but with a positive cohesion intercept. It is noticeable that the test using the initial normal stress value produces a relatively higher shear stress compared with succeeding normal stresses. This effect is attributed to consolidation due to the imposition of the second load. Apart from the observation that the first load gives a relatively high value, the loading sequence does not effect the residual shear strength value.

The rate of displacement would appear to have little effect on residual shear strength. Over a range of more one order of magnitude, the value of ϕ_{rr}' changes by less than one degree.

A good correlation exists between ϕ_{rr}' and the moisture content at the end of the test. This is probably a reflection of grading and mineralogy. The residual shear strength has also been shown to increase with decreasing clay fraction, increasing amount of quartz, decreasing proportion of mixed layer clay, decreasing liquid limit and decreasing plasticity index. The value of c_{rr}' also decreases with increasing clay content clay:quartz ratio, and decrease of quartz content and amount of silt size clay aggregates, but although the data display are somewhat scattered. No correlation could be found between c_{rr}' and liquid limit, plasticity index or amount of organic-carbon.

CHAPTER 6

STABILITY OF SLOPES

6.1 Introduction

6.1.1 Purpose and philosophy

The problem of the instability of both natural and excavated slopes has to be faced in many fields of human activity, landslips can be responsible for much damage and even loss of life so reliable methods for the observation, measurement and prediction of slope instability are necessary to prevent slope movement and control or correct landslip events.

6.1.2. Classification

Mass movements may be classified from various points of view. For present purposes the most useful form of classification is probably of Skempton and Hutchinson (1969) based on the mode of failure. Styles of instability are then grouped according to appropriate method of analysis. Some authors have used other criteria for their classifications including the mode and the rate of movement, the shape of the slip surface and the type of material involved.

According to Zaruba and Mencl (1982), Sharp (1938) classified slides according to the type of material and the rate of movement. The chief criteria used in the classification by Varnes (1958) and (1978) shown in Table 6.1 are the type of movement with the type of material of secondary importance. Thus, movements are divided into main five groups, respectively: falls, topples, slides, spreads and flows. A sixth group of complex slope movements includes combinations of two or more of the other five types. Materials are divided into two classes of rock, and engineering soil is further divided into debris and earth flow.

Table 6.1 Abbreviated classification of slope movement (after Varnes, 1978).

TYPE OF MOVEMENT	TYPE OF MATERIAL	
	Bedrock	Engineering soils
Falls	rockfall	predominantly coarse debris fall earth fall
Topples	rock topple	debris topple earth topple
	rotational	debris slump earth slump
Slides	rock block slide	debris block slide earth block slide
	rock slide	debris slide earth slide
Lateral spreads	rock spread	debris spread earth spread
Flows	rock flow (deep creep)	debris flow earth flow (soil creep)
Complex	combination of two or more principal type of movement.	

A classification shown in Table 6.2 based chiefly on the mechanism and morphology of movement with some consideration of the rate of movement and type of material involved has been proposed by Hutchinson (1968). In this, mass movements are divided into three principal groups. Creep, frozen ground phenomena and landslides.

Classification and terminology of slope movement by Nemcok et al (1972) groups them according to mechanism and rate of movement into four basic categories which are called creep, flow, slide and fall. Creep involves a wide range of slow movements (a few centimetres per year), including talus creep. Flow refers to long term gravitational deformation of mountain slopes where the sliding mass contains so much water, that the movement has the character of a flow: an earth flow, or mud flow. The third category involves relatively rapid movements along a definite slide surface. Abrupt movements of solid rocks in which tree falls is a major feature are placed in the fourth group.

Zaruba and Mencl (1969, 1982), classify the sliding phenomena according to regional conditions. Their proposed classification is as follows:

- i. Slope movement of superficial deposits (slope detritus or weathered materials produced mainly by sub aerial agents. This group includes talus creep which causes terminal bedding of strata, sheet slides, earth flows and debris flows or muren which is a local Alpine name of mountain debris flows liquification of sand.
- ii. Slide rocks including clays, marls, clay shales and claystone . These are subdivided according to the style of movement where this can be a long cylindrical surface, a composite sliding surface or caused by squeezing of soft underlying rocks.
- iii. Slope movements involving solid rocks. Again the style of movement is used to further subdivide these forms of instability into rock slides on predisposed surfaces including bedding planes, schistosity

Table 6.2 Hutchinson's (1968) classification of mass movement.

Principal group	Type of mass movement
I Creep	shallow soil and talus creep
	deep seated and continuous creep
	progressive creep
II Frozen ground phenonema	solifuction, cambering, bulging and stone streams
III Landslides	translational slides
	rotational slips
	falls
	subaquous slides

jointing or faults planes, long term deformation of mountain slopes and rock falls.

- iv. Special kinds of slope movement which constitute important geological phenomena in particular places. These include instability due to solifluction processes, that is very sensitive or quick clays and subaqueous slides.

Skempton and Hutchinson (1969), also Skempton (1953a and b) offer a more restricted morphological classification of clay slopes, in which the length, breadth and depth of the unstable zone are utilised. These dimensions are defined in Fig. 6.1. Clearly such a classification does not take cognizance of the nature of the material affected or necessarily the style of movement. However, their classification does aid the choice of an appropriate analysis method. This classification is shown in Fig. 6.2 and may be summarized as follows:

- i. Falls

Movement of material due to *detachment* along a vertical or near vertical discontinuity (usually a tension crack or joint). Instability of this type is commonly short term in character and is liable to occur in steep slopes including river banks or sea cliffs subject to base erosion.

- ii. Rotational slides

Rotational slips or slumps are characteristic of slopes less steep than those subjected to falls. They commonly occur in fairly uniform weathered clay or shale and colluvial clay. Generally movement occurs along a deep seated shear rupture surface and these slides may be further subdivided according to the shape of the failure surface:

- a. Circular rotational slips

These occur in cut slopes of relatively uniform clays and natural slopes in over-consolidated clay.

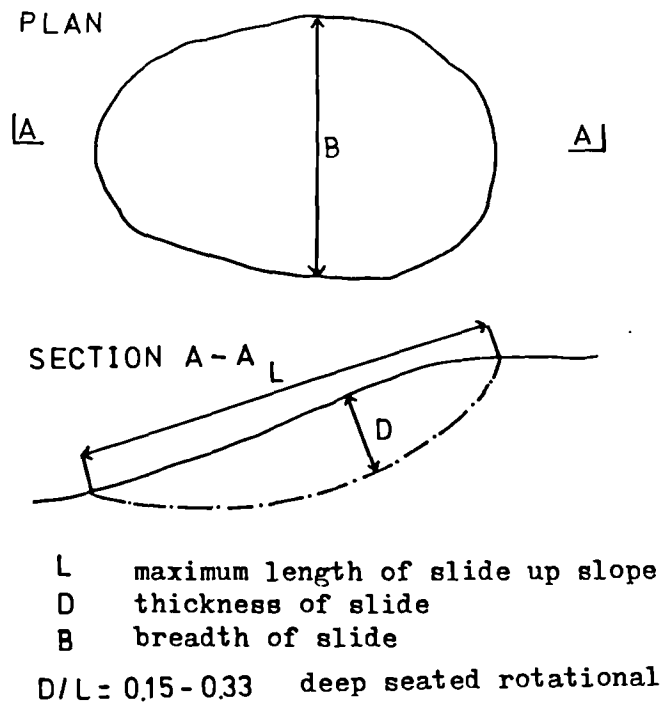


Fig. 6.1 Landslide properties (After Skempton, 1953 a and b).

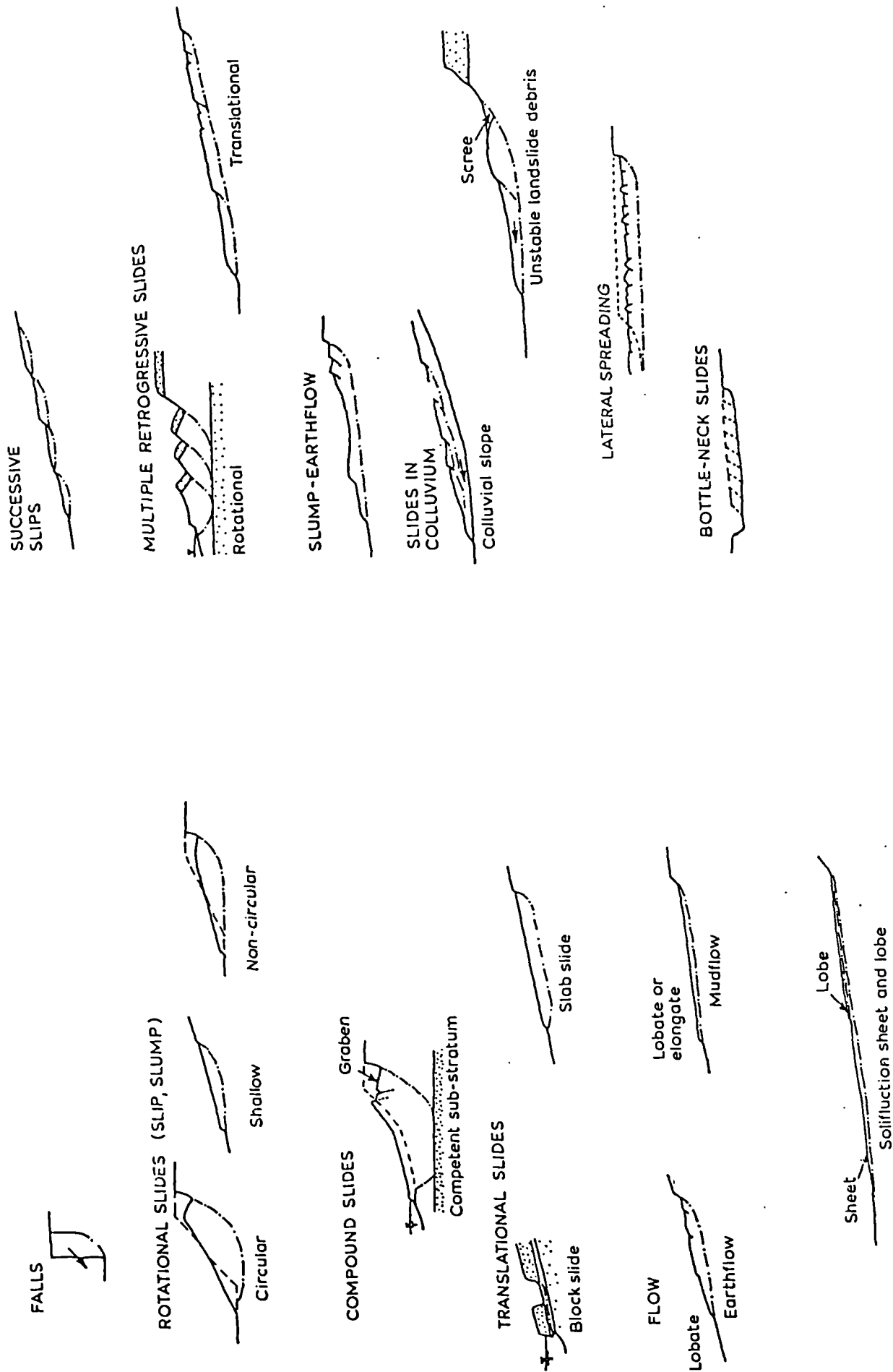


Fig. 6.2 Some basic types of mass movement, multiple and complex landslides in clay slopes. (After Skempton and Hutchinson, 1969).

b. Non-circular rotational slips

These slides are usually associated with slope instability in over-consolidated clay in which a degree of non-homogeneity has been produced by weathering processes. Anisotropy due to stratification also influences the form of these slips.

iii. Translational slides

Translational slides occur due to displacement along a relatively shallow planar surface which may be a bedding plane, the base of the weathered zone or other discontinuity. Translational slides may be further subdivided:

a. Block slide

More lithified jointed rock masses are subject to block slide activity in which joint bounded blocks of rock, separate from the rock mass and slide as units on well-defined bedding planes, joints or faults.

b. Slab slides

Slab slides are a variety of translational failure characteristic of weathered clayey soil overlying relatively fresh material in which detachment occurs along the interface and mass movement causes little internal distortion of the moving material.

iv. Compound slide

Some slides combine elements of both rotational and translational failure. These occur where full rotation of the moving mass and curvature of the rupture surface are inhibited by an underlying planar feature. Generally, the failure surface occurs at a greater depth in compound slides compared with translational types.

v. Flows

Skempton and Hutchinson (1969) point out that flows are a rather neglected and little understood variety of slope instability, with corresponding confused terminology. Although, in true flows the individual particles act independently of one another, flows

are generally regarded as slope instability styles in which the moving material does not behave in a coherent manner giving rise to large distortions. Skempton and Hutchinson (1969) subdivided flows as follows:

a. Earthflow

An earthflow is defined as slow movements of softened, weathered debris or colluvium which often develop in material forming the toe of a slide.

b. Mudflow

Mudflows are glacier like in form and usually affect surfaces with inclination varying between about 5° and 15°. The rates of mudflow movement vary widely and can be highly seasonal in character depending on water content. Mudflows commonly develop where a mass of argillaceous debris becomes softened by water giving rise to an ill sorted mixture of remnant debris in a soft clay matrix.

vi. Solifluction lobes and sheets

Solifluction is associated with periglacial conditions where movements occur in an upper active layer above a permafrost horizon. Movement may be slow, as the cumulative effect of many freeze-thaw cycles, or more rapid as a mudflow of thawed saturated debris.

According to Chandler (1972) the term solifluction was originally defined by Anderson (1906) as the slow flowing from higher to lower ground of masses of surface material saturated with water. More recently the term has been used by Skempton and Petley (1967), Skempton and Hutchinson (1969) and Weeks (1969) to describe the results of a periglacial process, as defined above, which has resulted in the formation of shear surfaces in clay slopes. Chandler (1972) suggests that the sheet movement of clayey sediments generally occurs on slopes for which the slope angle exceeds about 7° to 8° for

some distance. These slides are the result of periglacial climatic conditions in which down slope movements may be attributed to landslide processes that do not require higher pore water pressures than that provided by the water table at the ground surface. Skempton and Hutchinson (1969) have found that the lobes consist of angular rock fragments in a matrix of sand silt and clay and are typically 3-5 m. thick.

vii. Successive slips.

Successive slips may develop upwards from the foot of a slope. Shallow rotational shears become linked together in a regular or an irregular manner to form step like features. If a sufficiently large number of slips occur within a particular area the surface morphology could be confused with that for translational sliding.

viii. Multiple retrogressive slides.

Multiple retrogressive slides occur most frequently in actively eroding high relief in which a thick stratum of overconsolidated fissured clay or clay shale is overlain by a thick bed of more competent rock.

ix. Slump-earthflow

The slump earthflow is a variety of compound slide which develops as a continuation of long rotational slides in which the over-ridden toe of the disturbed mass becomes softened by water ingress and develops into an earthflow.

x. Colluvium slides

Inherently unstable material such as landslip debris may be subject to colluvial slides which can also involve the regeneration of older slide surfaces rather than the initiation of first-time slides in the accumulated collovium.

xi. Spreading failure

Sudden and generally very rapid lateral spreading of a retrogressive translational slip on quite gentle slopes can produce graben and horst structures.

This type of failure is attributed to the presence of elevated pore water pressures in a previous basal layer. Dissipation of these pressure is at the expense if fluidisation of the superincumbent clay mass.

xii. Bottle neck slides

Bottle neck slides are peculiar to quick clays in which they form retrogressive, multiple, rotation failures. They take place as an initial rotational failure of stiffer material forming a crust above sensitive clay. The banks of incised streams are particularly susceptible to instability initiated by erosion which is followed by initial failure and very rapidly spreading of instability into less weathered material.

The recognition of the presence of instability depends on detailed observation of changes in geometry, changes in attitudes of beds, trees, and fences, also the morphology of the surface, the position of shear surfaces on the surface and the nature of sliding material. In the case of rotational and translational slides, the shape and the position of upper surface are influenced principally by the distribution of pore water pressure and, the variation of shearing strength within the rock or soil mass. It is usually convenient to analyse slopes in which the shape of the rupture surface is assumed to be identical at all cross sections. In addition, shearing stresses and shearing strength are assumed to be uniformly distributed along the slip surface.

6.1.3 Factors contributing to slope failure

The susceptibility to sliding is determined by the geological structure, lithology, hydrogeological conditions and the stage of morphological development of the area. According to Zaruba and Mencil (1982) and Jumikis (1965), the most important factors that may disturb slope stability are as follows:

- i. Changes in the slope gradient, these may be caused by natural or artificial influences, including stream erosion at foot of slope or by excavation. An increase in slope gradient produces a change in the internal stress of the soil or rock mass, equilibrium conditions are disturbed by increases in shear stress.
- ii. Changes in the slope heights as a result of excavation or artificial filling.
- iii. Overloading by the construction of embankments, filling and other forms of loading which produce and increase in shear stress. Increases in pore water pressure in clayey soils also decrease shear strength.
- iv. Vibration and earthquakes which produce sudden transient overloading and more gradual changes of density and water pressure.
- v. Changes in water content in which the penetration along joints of run-off which increases hydrostatic pressures and reduces shear strengths. (See Section 6.2.1.) Also loading may change since wet soil is heavier than dry soil.
- vi. Effect of the movement of ground water, which may be considered under three headings.
 - a. Flowing ground water exerts a pressure on soil particles.
 - b. Ground water which removes soluble cementing substances causing a weakened of soil or rock.
 - c. Internal erosion of rock or soil.
- vii. Frost effects the stability of slopes mainly through the freezing of water in rock fissures. Also the freezing surface water can impede drainage is giving rise to elevated pore water pressures.

- viii. Mechanical and chemical weathering generally reduce the shear strength of soil and rocks.
- ix. The roots trees and other form of vegetation can contribute to the stability of slopes by mechanical binding effects and also due to the removal of moisture from the ground.

6.2 Stability Analysis

The analysis of the stability of slopes by mathematical procedures is applicable to the evaluation of failure due to sliding along a definable surface. Slide failure occurs when the shear resistance mobilised along the failure surface is exceeded by shearing stresses imposed on that surface. Static analysis of sliding requires knowledge of the location and shape of the potential failure surface, the shear strength along the failure surface and the magnitude of the driving forces. Failures can begin at any point along the failure surface, where the stress exceeds the strength, Hunt (1984) points out that it usually occurs at a value of shear strength which can be considerably less than the peak strength measured by conventional testing techniques.

The methods of analysis are based on the assumption that the shearing resistance of the soil along a potential failure surface is developed to the same extent at every point. This implies that the factor of safety along the potential slip surface everywhere is the same. Parcher and Means (1968) argues that this is not the same as saying that the shearing stresses are uniformly distributed along the surface because the normal stresses are not necessarily constant. In fact, the true stress-strain curve of a typical soil deviates to a considerable extent from this ideal so that the ratio of strength to shear stress will not be uniform along the entire length of a potential slip surface. Hence in real situations such as those considered by Peck (1967) and Hunt (1984) the state of limiting equilibrium is associated with a non-uniform mobilization of shearing resistance along the

rupture surface. Parts subjected to high values of shear stress will fail before less highly stressed parts. The redistribution of stresses due to initial failure may then cause other parts to become over-stressed and thus failure occurs elsewhere. By this process the soil undergoes progressive failure during the establishment of a continuous rupture surface. Accordingly Terzaghi and Peck (1948) and Taylor (1948) have associated progressive failure with non-uniform stress-strain conditions and the redistribution of shear along a potential sliding force.

Simons and Menzies (1978) and Bromhead (1984) explain that the process of progressive failure occurs when an element within the soil is in a state of local overstress and sheared beyond peak failure strain so that it sheds part of its stress. This stresses must carried out to neighbouring elements until equilibrium is re-established. It may be that equilibrium cannot be achieved, in which case the shear zone grows until it is continuous through the whole mass. Further deformation occurs until the sliding mass moves into equilibrium, with a strength approaching residual acting all around sliding surfaces. Since the stresses are usually highest at the toe of slope, Hunt (1984) notes that failure often begins there and progresses up slope. Myslivec (1976) has approximated progressive failure by using the residual shear strength value along the upper portion of failure and the peak strength in the lower zone. See also Parry (1972).

Early in the history of the analysis of the stability of slopes peak undrained shear strength values were used but it was found that much higher factors of safety than those apparently operating were obtained. Peak effective shear strength also yields values too high but, on the other hand, residual shear strength values apparently underestimate the value. Fully softened peak shear strength defined by Skempton (1970) (See Section 8.2) would appear most appropriate in the analysis of first time slides. For pre-existing failure surfaces residual

shear strengths were suggested by Deer and Patton (1971) and Skempton (1970) to be the best values.

In Chapter 8 of the present study a fully softened remoulded peak shear strength has been used in the analysis of slopes to aid with locating the most probable slip surface for first time sliding. Then a remoulded residual shear strength was used for calculating the stability of the landslips with respect to subsequent movement.

6.2.1 Effective and total stress conditions

As mentioned in Section 4.1, the generation of pore water pressures modifies the stresses acting within soil masses and affects the shear strength characteristics of the material. Hence when analysis the stresses acting on, and within, a soil mass, it is necessary to take into account forces produced by the pore water pressure.

Work by Skempton (1964) indicates that for cuttings in clay, the pore water pressure at any point depends not only on the position of the water table, but also to an important extent on the response of the clay to changes in stress which took place during unloading. In the course of time, however, the pore water pressures throughout the material gradually adjust until finally everywhere in hydrostatic equilibrium with the prevailing ground water regime. This equilibration time depends on the permeability of the medium. In the case of clay, Bromhead (1984) suggests that the period may be years and decades, but it may take centuries for some large slopes. At the end of this period, all excess pore water pressure introduced upon the excavation of the slope will be dissipated so that this long-term condition contrasts with the short-term, or end of the construction, condition, unless modified by applied stress or sources of water pressure.

Mogenson and Sangrey (1978) confirms that fully saturated soils behave as purely cohesive materials (i.e.

$\phi = 0$) where sheared to failure without permitting drainage. These results are interpreted in terms of total stresses, so undrained total stress analyses are limited to slopes where the pore water pressures are governed by total stress changes and no significant dissipation of pore water pressure has occurred. Where pore water is governed by steady seepage conditions stability analysis should be performed in terms of effective stresses. This is the usual condition of natural slopes in both soil and rock.

Generally speaking a purely cohesive analysis or $\phi = 0$ analysis requires knowledge of only the undrained shear strength of the medium while for an effective stress analysis, the effective shear strength parameters (ϕ' , c') and the pore water pressure *distribution must* be known. In other words, under total stress conditions, the measured stress includes both the pore water pressures and the grain-to-grain contact stresses. In the effective stress condition grain-to-grain contact stresses increase as the pore pressure dissipates.

6.2.2 Limit equilibrium analysis

Analytical methods applied to evaluate slope stability are based on the concepts of limiting equilibrium. It is assumed that once a slope has failed, the factor of safety is unity, and back analysis can be used to estimate, the average shearing resistance along the failure surface. Other variables may also be determined where the shear resistance is already known. A factor of safety against instability (F) is defined as the ratio of the forces restraining movement to those causing movement. In practice for slopes in which only body forces are significant, and where movement along a particular surface is being considered, this means that $F = \frac{S}{\tau}$ in which S=shear strength and τ = shear stress. Thus if the resistive forces are equal to the driving forces the factor of safety equal unity and the slope is just stable but

on the point of failure, values less than unity denote slopes which are unstable and values greater than unity correspond with stable slopes.

According to Morgenstern and Sangrey (1978) the following principles are common to all methods of analysis:

- i. A slip mechanism is postulated in which the slopes are assumed to fail along the planar or circular sliding surfaces. Where the ground conditions are non-uniform, sliding surfaces of more complex shape may occur. So methods have also been developed to handle surface of arbitrary shape.
- ii. The shearing resistance required to equilibrate the intendant static forces propagating slip are calculated where the potential slip mass is in a state of limiting equilibrium, and the failure criteria of the soil or rock is satisfied everywhere along the proposed failure surface. The various methods of analysis differ in the degree to which the conditions for equilibrium are satisfied and some common methods violate the conditions for static equilibrium.
- iii. The calculated shearing resistance required for equilibrium is compared with the potential shear strength of the failure surface in terms of the factor of safety.
- iv. The mechanism with the lowest factor of safety is found by iteration.

The shearing force results from gravity forces and internal pressures acting on, and within, the mass bounded by the failure surface. Those forces are a function of the weight of the material, slope angle, depth to the failure surface, and pressures developed in joints due to the freezing of water or the swelling of particular materials. The resisting forces are provided by the shear strength mobilized along the failure surface and gravitational forces. The former type may be reduced by increases

in pore water pressures along the failure surface, lateral strains in overconsolidated clays and clayey shales, the dissolution of cementing agents, leaching and the development of tension cracks.

6.3. Locating the slip surface

In order to carry out a stability analysis the slip surface must be located. Slip surfaces are located by a variety of methods in which detailed morphological studies, boreholes, trail pitting and a variety of types of instrumentation may all be important. Hutchinson (1982) describes the use of trail pits for locating slip surfaces down to depths of 3 to 6m. At least two adjacent faces of the pit should be carefully logged to a reasonably large scale noting the attitude of any slip surfaces, changes in lithology and orientation fluting and striations. Four trial pits were excavated by Chandler (1970) to locate the slip surface of a shallow slabslide in Lias Clay near Uppingham, Rutland. The principal shear surfaces encountered in each trail pit were highly polished, light grey, sub-planar surfaces without striation. Early and Skempton (1972), also photographed polished and striated slip surfaces from Waltons Wood, Staffordshire.

Since the actual slip surfaces are generally only paper thin, Hutchinson (1982) suggests that continuous borehole samples would be required with high degree of recovery and no sample disturbance. Naturally, the existence of zone of disturbance at the ends of each sample gives gap in the sequence. Hutchinson overcame this problem by putting down a second borehole close to first and sampling on a staggered pattern. Early and Skempton (1972) noticed the position and the inclination of the slip surface of the landslide at Walton's Wood in the core samples. Changes of lithology were noted by Hutchinson (1982) to correspond with the position of the shear surface when a landslip as overridden a contrasting material. Similar effects may also be significant where

the slip surface is inclined with respect to the bedding, that is in rotational, rather than translational slides.

Geophysical methods are being used increasingly in the landslide investigations. It is often advantageous to use several methods in combination but most geophysical methods require calibration with boreholes.

According to Hutchinson (1982), seismic refraction is the most widely used of geophysical methods. Providing there is a seismic contrast between the landslip material and underlying soil or rock, the base of the landslide can be established. geophysical methods are particularly suitable for establishing the height of water table.

Seismic reflection investigations are also used but these involve considerably more field and processing work compared with refraction studies. The technique is also difficult to apply at shallow depths and on land because high energy surface wave arrivals tend to obliterate relatively small amplitude reflections. Recent improvements in the equipment and techniques, however, have increase the usefulness of this method. Electrical resistivity surveys operate according to the ground and ground water conditions. The electrical resistivity of the landslide material may be greater or less than that of the adjacent strata.

Morphological methods rely on observation relating to shape of the ground surface; the details of these methods are given in Chapter 8.

6.4 Determination of Factor of Safety

Various methods of analysing the stability of slopes have been proposed. In many respects the principles of these methods are similar. According to Suklje (1969), the method of stability analysis using potential failure surfaces was first introduced by Paterson (1916) and Hultin (1916) and later supplemented by Fellenius (1927). Extensive work by Swedish workers has lead to the establishment of the so called Swedish method of slip analysis

(Attewell and Farmer, 1975). This method, which assumes a circular rupture is also known as the conventional method of slices. It was first proposed by Fellenius (1936) and was originally applied in terms of total stress. The analysis is carried out by determining the stability along a typical longitudinal cross section or several sections in the case of wide slips, or for variable conditions. A particular section is analysed by dividing it into a series of vertical slices of convenient width as shown in Fig. 6.4. The forces due to body weight of each strip are calculated separately and then the components causing instability and those promoting stability are summed for all strips and expressed as a ratio.

Within the context of this research, it is useful to analyse the condition stability for two modes of failure.

- i. Translational failure on a planer surface for an infinite slope whose length is much greater than the depth of the failure surface.
- ii. Rotational failure on non-circular failure surface for a finite slope which involves movement along a surface limited in extent.

The following sections are dedicated to the derivation of formula appropriate to the determination of the factor of safety against movement for these two modes of failure. These derivations follow closely the practice of Craig (1982) Skempton and Delory (1957) and Smith (1977).

A number of methods have been proposed for analysing the stability of soil masses subject to rotational failure. The more important ones are compared with each other by Skempton and Hutchinson (1969).

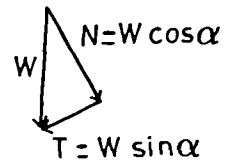
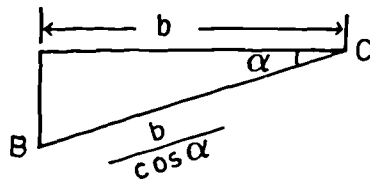
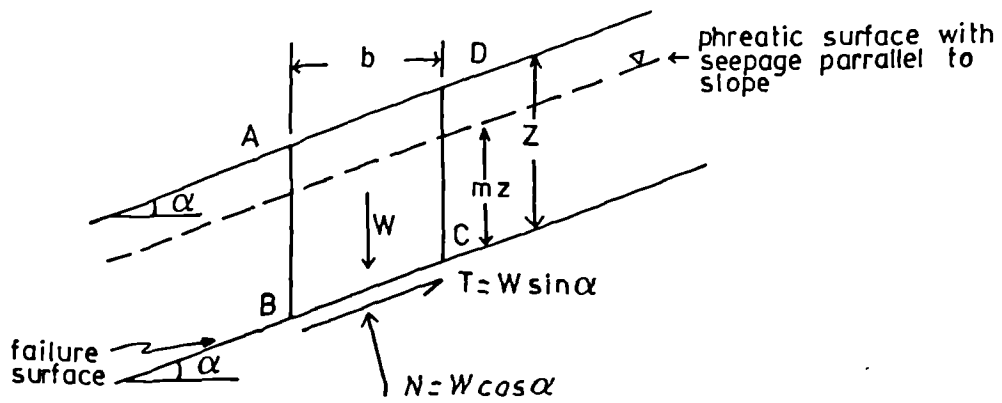
- a. Bishop simplified
- b. Morgenstern and Price
- c. Janbu
- d. Conventional method of slices.

The Bishop simplified method is appropriate only in the case of circular slips, whereas the slip surfaces of present interest are markedly non-circular slips, (See Chapter 7). For non-circular slips the sliding mass is divided into series of slices the stability of each one of which is analysed independently and then summed for all slices. Figure 6.4 shows a slip divided into slices together with the forces acting on each of these elements. The forces affecting the slice are the shear and normal forces acting on each of the surfaces, that is the base together with interslice forces. (See Fig. 6.4). In the case of the conventional method of slices, it is assumed that the interslice forces cancel out each other whereas in the other methods they are taken into account. Skempton and Hutchinson (1969) have demonstrated that the effect of this simplification depends on the ratio between the depth below ground level of the slip surface and the length of the sliding mass. (D/L ratio). Thus, the error is most severe for the near-circular slips and it disappears in the case of planar slides. Table 8.6 indicates that the slips in the study area display D/L ratios in range 0.08 to 0.17 for which Skempton and Hutchinson (1969) report that the conventional method of slices produces a value of factor of safety 2% to 8% for D/L ratios of 0.06 - 0.17 respectively, lower than the Morgenstern and Price or Janbu methods. The conventional method used in this study for the following reasons.

- i. It is simple and rapid method, easy to apply.
- ii. It gives a remarkably successful results if applied to non-circular surfaces.
- iii. Reasonably simple to analyse multi-layer problems.
- iv. Reasonably simple to vary position of water table, change the angle of slope or change the shape of the slip surface.
- v. Easily performed using a desk calculator in which a greater 'feel' for the model being analysed is gained, compared with more automated styles of analysis.

6.4.1. Infinite slope-planar slide

Fig. 6.3 shows part of an infinite slope of angle α in which the failure surface BC is at a constant depth, z and the phreatic surface occurs at constant height of mz above the failure surface.



$$BC = \frac{b}{\cos \alpha}$$

- W weight of slice
- Z vertical depth
- mz vertical height of water table
- b breadth of slice

Fig. 6.3 Forces in planer slide analysis.

It will be assumed that the factor of safety for the slope will be the same as that for elemental slice ABCD. Now the forces acting on this slice comprise those due to its weight W as well as shear and normal forces acting on the failure surface BC.

The weight of slice per unit width is given by

$$W = \rho b z \dots\dots\dots(6.1)$$

where ρ is the density of the soil, and b is the horizontal breadth of the slice.

The weight can be resolved into normal and tangential forces acting on BC, the base of element:

$$N = \rho b z \cos \alpha \dots\dots\dots(6.2)$$

$$T = \rho b z \sin \alpha \dots\dots\dots(6.3)$$

Now in terms of the horizontal breadth of the slice, the length of BC is $b/\cos \alpha$ and so, normal and tangential stresses per unit width of the failure surface are respectively:

$$\sigma_n = \frac{\rho b z \cos \alpha}{\frac{b}{\cos \alpha}} = \rho z \cos^2 \alpha \dots\dots\dots(6.4)$$

$$T = \frac{\rho b z \sin \alpha}{\frac{b}{\cos \alpha}} = \rho z \sin \alpha \cos \alpha \dots\dots\dots(6.5)$$

The effective normal stress is $\sigma_n' = \sigma_n - u$..(6.6) where u is the pore water pressure. So

$$\sigma_n' = (\rho z \cos^2 \alpha - u) \dots\dots\dots(6.7)$$

The force opposing motion is mobilized on surface BC and from the Coulomb equation (See Section 4.1) it is:

$$\tau = c' + \sigma_n' \tan \phi' \dots\dots\dots(6.8)$$

The factor of safety, $F = \frac{\text{Resisting force}}{\text{Disturbing force}}$

$$\text{so } F = \frac{c' + (\rho z \cos^2 \alpha - u) \tan \phi'}{\rho z \sin \alpha \cos \alpha} \dots\dots\dots(6.9)$$

If the water table creates a hydrostatic component of pressure on the slip surface with flow out of the slope

$$u = \rho_w m z \dots\dots\dots(6.10)$$

where ρ_w is the density of water.
From equation 6.9

$$F = \frac{c' + (\rho \cos^2 \alpha - m \rho_w) z \tan \phi'}{\rho z \sin \alpha \cos \alpha} \dots\dots\dots(6.11)$$

If the water table is maintained at a constant depth below the ground surface with seepage parallel to the slope then

$$u = \rho_w m z \cos^2 \alpha \dots\dots\dots(6.12)$$

and

$$F = \frac{c' + (\rho - m \rho_w) z \cos^2 \alpha \tan \phi'}{\rho z \sin \alpha \cos \alpha} \dots\dots\dots(6.13)$$

6.4.2 Finite slope - rotational slide

Fig. 6.4 shows the sliding mass divided in to n slices each of which are subjected to forces shown in fig. 6.4.b.

The factor of safety F against failure of any slice i is given by

$$F = \frac{\tau_i}{T_i} \dots\dots\dots(6.14)$$

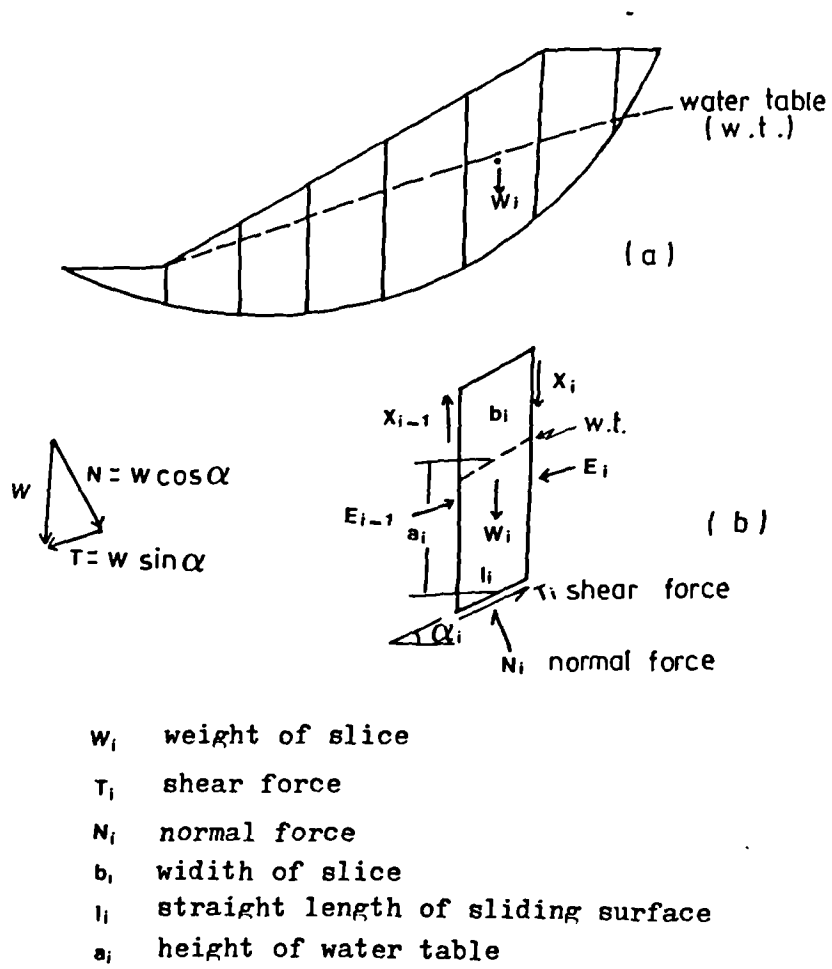


Fig. 6.4 Forces acting on single slice in sliding mass.

where τ_i , is the strength mobilized on the failure surface and T_i is the component of weight promoting failure. For the whole slope

$$F = \frac{\sum_{i=1}^n T_i}{\sum_{i=1}^n T_i} \dots\dots\dots(6.15)$$

The total weight of each slice W_i can be resolved into normal and tangential forces:

$$N_i = W_i \cos \alpha_i \dots\dots\dots(6.16)$$

$$T_i = W_i \sin \alpha_i \dots\dots\dots(6.17)$$

The total normal force on the base is N (equal to $\sigma_n l$). In general this force has two components: the effective normal force N' (equal to $\sigma'_n l$) and boundary water force U (equal to $u l$) where u is the pore water pressure at the centre of base and l is the length of the base. In this solution it is assumed for each slice that the resultant of the interslice forces is zero.

The force on each slice normal to its base is

$$N_i = W_i \cos \alpha_i - u_i l_i \dots\dots\dots(6.18)$$

The force opposing motion is mobilized on surface which from Coulomb equation is (See Section 4.1) given by:

$$\tau_i = c + \sigma_n \tan \phi \dots\dots\dots(6.19)$$

The factor of safety $F = \frac{\text{Resisting force}}{\text{Disturbing force}}$

$$\text{So } F = \frac{\sum_{i=1}^n (c_i + \sigma_n \tan \phi) l_i}{\sum_{i=1}^n W_i \sin \alpha_i} \dots\dots\dots(6.20)$$

or

$$F = \frac{\sum_{i=1}^n (c_i l_i + N_i) \tan \phi}{\sum_{i=1}^n W_i \sin \alpha_i} \dots\dots\dots(6.21)$$

From equation 6.18 this becomes:

$$\text{Factor of safety } , F = \frac{c_i l_i + \sum (W_i \cos \alpha_i - u_i l_i) \tan \phi}{\sum W_i \sin \alpha_i} \dots\dots\dots(6.22)$$

In the present research the analysis of the ten landslips in case of the first time slide and post failure stability, were carried out using the equation 6.22 (See Chapter 8).

6.5 Summary

The classification of slope instability is most usefully carried out in a way which describes the mode of movement of the failed mass. In terms of the problems experienced in the area of interest, slips with a curved arc or circular failure are most important. Clearly, the geological conditions, particularly in respect of strength, homogeneity and isotropy together with the presence of discontinuities and the water conditions exert significant controls.

The stability of slopes is controlled by the shearing resistance of the material and factors affecting loading and body forces. In natural slopes, stability is controlled by the interaction of topography and shear strength with the hydrological conditions influencing both body forces and strength. The attainment of stability of a sliding mass implies a factor of safety just in excess of unity. Further instability requires a reduction in shear strength, changes in hydrological conditions

or changes in external loading due to either unnatural or natural causes including the accumulation of scree. Within the consideration of changes in shear strength, progressive failure of material results in a non-uniform factor of safety along the slip surface. The term progressive failure as defined by Bishop (1967) indicates the spreading of the failure over the potential surface of sliding from a point or line towards the boundaries of the surface. The stresses in the clay near the periphery of this surface approach the peak value while the shearing resistance of the clay in the area of failure initiation is nearer the much smaller ultimate value. The total shearing force acting on a surface of sliding at the instant of complete failure is considerably smaller than the shearing resistance computed on the basis of peak values.

The available methods of analysis depend on limiting equilibrium theory from which a factor of safety against failure is calculated. One major difficulty with accurate determination of the factor of safety is that the analysis can only be carried out if the position of the slip surface is known. In some other methods of analysis such difficulties are overcome, but other assumptions are introduced instead. The method described by Fellenius (1936) for instance is appropriate to circular slips in which the position of the intersection of the slip surface with the ground surface is used to define a series of circles so that the most critical one is found by iteration. Morphological studies described in Chapter 7 indicate that assumption of this type would not be appropriate in the landslides studied. However, since it is possible to use morphological and other evidence to establish a likely failure surface, the method of slices for translational infinite and finite rotational slides can be used in this study.

Obviously, direct measurement of the slip surface position by observation of borehole cores, the use of slip detectors as described by Chandler (1970) and trial

pits as described by Early and Skempton (1972) albeit widely spaced in some cases, provide positive data. In situations in which insufficient measurements are available a more subjective approach may be adopted in that a slip surface commensurate with the degree of rotation, geological structure, post-slip topography and pre-slip topography is assumed. Iteration is then used to establish the most critical slip surface within a family of possible surfaces conforming with the observation where the data are ambiguous.

Chapter 8 includes detailed analysis to determine the position of slip surfaces for first time slides and the post failure stability. Appropriate values of shear strength for first time sliding and post failure sliding are used which indicate appropriate water condition. From this it is possible to compare back analysed shear strength values with laboratory ones.